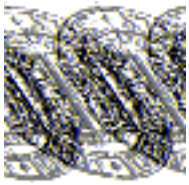

# UNIVERSITA' DEGLI STUDI DI PADOVA

Sede Amministrativa: Università degli Studi di Padova

Dipartimento di Neuroscienze

SCUOLA DI DOTTORATO DI RICERCA IN:

*SCIENZE MEDICHE, CLINICHE E SPERIMENTALI*

INDIRIZZO: *NEUROSCIENZE*

*CICLO XX*

# MITOCHONDRIAL DNA HETEROPLASMY IN MUSCLE CYBRIDS HARBOURING A3243G MELAS MUTATION

**Direttore della Scuola:** Ch.mo Prof. Silvano TODESCO

**Supervisore:** Dott.ssa Lodovica VERGANI

**Dottorando:** Adriana MALENA

Gennaio 2008

# INDEX

# ABBREVIATIONS

| | |
|---|---|
| $^{32}$P-dCTP | Cytidine 5'-[$\alpha$-$^{32}$P] triphosphate |
| AA | Aminoacids |
| ANT | Adenine Nucleotide Translocator |
| APS | Ammonium persulfate |
| BSA | Bovine Serum Albumin |
| CoQ | Co-enzyme Q |
| COX | Cytochrome c oxidase |
| DMEM | Dulbecco's Modified Edge Medium |
| DMSO | Dimethyl Sulfoxide |
| dNTP | Deoxyribonucleotide triphosphate |
| DTNB | 5,5'-Dithiobis(2-nitrobenzoic acid) |
| DTT | 1,4-dithio-DL-threitol |
| EDTA | Ethylenediaminetetraacetic acid |
| EGF | Epidermal Growth Factor |
| EtBr | Ethidium Bromide |
| ETC | Electron Transport Chain |
| $FADH_2$ | Reduced Flavin Adenine Dinucleotide |
| FCCP | Carbonyl Cyanide P-(Trifluoromethoxy) Phenylhydrazone |
| FCS | Foetal Calf Serum |
| FGF | Fibroblast Growth Factor |
| GPx | Glutathione peroxidase |
| GR | Glutathione reductase |
| GSH | Reduced glutathione |
| GSSG | Oxidized glutathione |
| IMP | Isoleucine Methionine Phenylalanine |
| LC-PCR | Last Cycle Hot PCR |
| LHON | Leber Hereditary Optic Neuropathy |
| MELAS | Mitochondrial encephalomyopathy, lactic acidosis, strokes-like episodes |
| MERRF | Myoclonus Epilepsy Associated with Ragged - Red Fibers |
| mtDNA | Mitochondrial DNA |
| NAC | N-Acetyl-Cysteine |
| NADH | Nicotinamide Adenine Dinucleotide |
| NARP | Neuronal Ataxia Retinitis Pigmentosa |
| O.D. | Optical Density |

| | |
|---|---|
| OXPHOS | Oxidative phosphorylation |
| PBS | Phosphate Buffered Saline |
| PCR | Polymerase Chain Reaction |
| PFA | Para-formaldehyde |
| POD | Peroxidase |
| PS | Penicillin and Streptomycin |
| RD | Rhabdomyosarcoma |
| RFLP-PCR | Restriction Fragment Length Polymorphism PCR |
| RT-PCR | Real Time PCR |
| SDS | Sodium dodecyl sulfate |
| SOD | Superoxide dismutase |
| TAE | Tris-Acetate-EDTA |
| TBE | Tris-Borate-EDTA |
| TE | Tris-EDTA buffer |
| TEMED | N,N,N',N'-Tetramethylethylenediamine |
| VIT | Vitamins |

# ABSTRACT

The maternally inherited mitochondrial DNA (mtDNA) A3243G point mutation, in $tRNA^{Leu(UUR)}$ gene is associated with mitochondrial encephalomyopathy, lactic acidosis and stroke-like episodes (MELAS), but it has also been detected in other pathologies, such as cardiomyopathy, maternally inherited diabetes with deafness (MIDD) and progressive external ophtalmoplegia (PEO). Despite the knowledge of the genetic defect that impairs mitochondrial protein synthesis and thereby compromises respiration, a complete understanding of the pathogenesis of MELAS remains elusive. Every cell contains multiple copies of mtDNA and in cells and tissues of patients with this syndrome, mutant and wild-type mtDNA molecules coexist (heteroplasmy).

Clinical status of human mitochondrial disorders associated with heteroplasmic mtDNA mutations is greatly dependent on the residual amount of wild-type mtDNA molecules. No clinical symptoms or biochemical respiratory chain defects are detected above a relatively low threshold of wild-type mtDNA proportion [1]. A "selective advantage" or "dominant factor" of mutant mtDNA molecules is known. In this work we aimed to: i) verify different conditions able to modify the percentage of mutant mtDNA in vitro; ii) try to understand why mutant mtDNA molecules had a selective advantage in cultured muscle cells.

At first heteroplasmic cybrids with a muscular nuclear background harbouring MELAS mutation (RD cybrids) have been established. Different growth regimes (antioxidant supplementation, creatine, uridine, low glucose) were tested to verify an influence on percentage of MELAS mutation, but all failed.

In this work we substantiated the greater survival of muscular heteroplasmic 83% and 92% MELAS cybrids compared to homoplasmic 0% and 99% cells, in energetic stress conditions (5mM glucose instead of 25mM glucose). Physiological, biochemical and molecular analysis indicated that cells with an intermediate mutant load presented an increase of their bioenergetic anaerobic and aerobic pathways. This probably helps the cells to better survive in energetic stress as shown by growth rate and RCR values, concomitant to a reduced ROS generation.

Mitochondrial fusion was favoured through the downregulation of Drp1 and hFis1, proteins involved in mitochondrial fission, using RNAi method. Surprisingly mitochondrial fusion determined the increase of mutant mtDNA molecules in some clones. This result shows that mitochondrial fusion favours mutant mtDNA molecules that are dominant on wild-type in a muscle nuclear background.

# RIASSUNTO

La mutazione A3243G nel gene $tRNA^{Leu(UUR)}$ del DNA mitocondriale (mtDNA) è associata ad una varietà di sindromi, la più comune è la sindrome MELAS (mitochondrial encephalomyopathy, lactic acidosis and stroke-like episodes), ma in certi casi la stessa mutazione è associata a diabete con sordità, cardiopatia o oftalmoplegia esterna progressiva. È noto che il difetto genetico altera la sintesi proteica e di conseguenza compromette la respirazione cellulare, però non è ancora chiara la patogenesi della sindrome MELAS. Ogni cellula contiene molte copie di mtDNA e nelle cellule e tessuti dei pazienti affetti da questa sindrome si osserva la coesistenza di molecole di mtDNA wild-type e mutate, condizione nota come eteroplasmia.

In particolare non si conosce la modalità che porta all'aumento delle molecole di mtDNA con mutazione MELAS rispetto alle molecole di mtDNA normali, aumento che determina l'insorgenza del fenotipo clinico, quando queste raggiungono un valore soglia. Da anni è noto un "vantaggio selettivo" o "fattore dominante" delle molecole di mtDNA mutato. Lo studio svolto ha avuto come obbiettivi: i) verificare condizioni in vitro che potessero modificare la percentuale di mtDNA mutato; ii) capire in che cosa poteva consistere il vantaggio selettivo delle molecole di mtDNA mutato in cellule simil-muscolari.

Prima di tutto sono stati ottenuti cibridi simil-muscolari eteroplasmici per la mutazione MELAS. Vari regimi di crescita (presenza di antiossidanti, uridina, creatina, riduzione di glucosio) sono stati testati per verificare una possibile influenza sulla percentuale di mutazione MELAS, ma nessuno ha dimostrato di modificare significativamente la quantità di mtDNA mutato.

Si è dimostrato che in condizioni di stress energetico (riduzione di glucosio da 25mM a 5mM) cibridi eteroplasmici, con 83% e 92% di mtDNA mutato, hanno una maggiore capacità di sopravvivenza rispetto ai cibridi omoplasmici con 0% e 99% di mtDNA mutato. Analisi fisiologiche, biochimiche e molecolari hanno indicato che le cellule eteroplasmiche hanno un potenziamento dei pathways bioenergetici anaerobici e aerobici. Questo probabilmente aiuta le cellule a sopravvivere meglio in condizioni di stress energetico, come dimostrato da rate di crescita e valori di RCR, insieme ad una ridotta generazione di ROS. La fusione mitocondriale è stata favorita mediante tecniche di RNAi con downregolazione di Drp1 e hFis1, proteine che favoriscono la fissione mitocondriale. Sorprendentemente la fusione ha determinato in alcuni cloni l'aumento di mtDNA mutato, indicando che la fusione favorisce le molecole mutate di mtDNA, risultate dominanti rispetto alle wild-type in un background nucleare di muscolo.

# 1 INTRODUCTION

## 1.1 Mitochondria

### 1.1.1 Structure

Mitochondria provide a myriad of service to the cell, including energy production, calcium buffering and regulation of apoptosis. They also have an important role in metabolism of lipids, nucleotides, folate, heme and urea.

Most cells contain hundreds of mitochondria. How these diverse functions are coordinated among the hundreds of mitochondria in a given cell is largely unknown, but is probably dependent on the dynamic nature of mitochondria.

These organelles range from 0,5–1 μm in size. A mitochondrion contains inner and outer membranes composed of phospholipid bilayers and proteins. Because of this double-membraned organization, a mitochondrion has five distinct compartments: the outer mitochondrial membrane, the intermembrane space (the space between the outer and inner membranes), the inner mitochondrial membrane, the cristae space (formed by infoldings of the inner membrane), and the matrix (space within the inner membrane) (fig.1.1) [1-4].

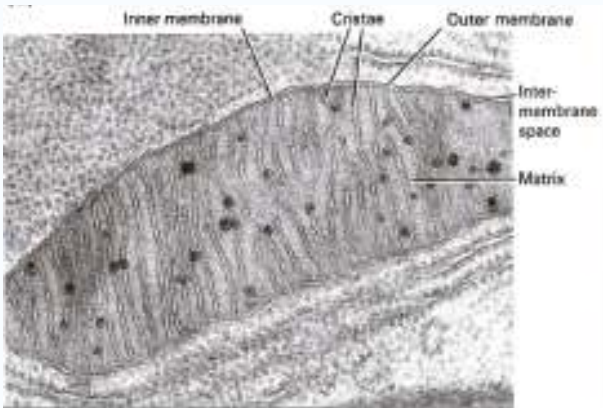


**Figure 1.1:** Electron microscopy image of a mitochondrion.

The outer mitochondrial membrane, which encloses the entire organelle, contains numerous integral proteins called porins. These porins form large aqueous channels that permit the passage of molecules 5000 Dalton or less in molecular weight. Larger proteins can also enter the mitochondrion via an N-terminal signaling sequence which permits translocation by a large multisubunit protein known as TOM (translocase of the outer membrane).

The intermembrane space is the space between the outer membrane and the inner membrane. Because the outer membrane is freely permeable to small molecules but not to proteins, the intermembrane space is chemically equivalent to the

cytosol with respect to small molecules, but not to protein composition. This space is home to cytochrome c [5].

The inner mitochondrial membrane contains hundreds of proteins involved in the respiratory chain, ATP synthesis and specific transport across the membrane. The inner membrane is rich in an unusual phospholipid, cardiolipin, that helps to make the inner membrane impermeable; in fact the inner membrane does not contain porins and is highly impermeable to all molecules. Almost all ions and molecules require special membrane transporters to enter or exit the matrix. Proteins are ferried into the matrix via the translocase of the inner membrane (TIM) complex. In addition, there is a membrane potential across the inner membrane formed by the action of the enzymes of the electron transport chain.

The inner mitochondrial membrane is compartmentalized into numerous cristae, which expand the surface area of the inner mitochondrial membrane, enhancing its ability to produce ATP. These are not simple random folds but rather invaginations of the inner membrane which can affect overall chemiosmotic function. Mitochondria of cells that have greater demand for ATP, such as muscle cells, contain more cristae.

From 3D images of “electron microscopy tomography” (fig.1.2a) cristae appear polymorphous and tubular. Cristae are like swollen bags with narrow tubular junctions to the inner membrane. Formation of tubular cristae and cristae junctions is a dynamic process and might be sensitive or controlled by matrix volume and the energetics of protein-lipid membrane folding. There are evidences that the mitochondrial inner membrane is a dynamic structure able to change shape rapidly in response to alterations in osmotic and metabolic conditions. The hypothesis is that these conformational changes are an integral part of feedback mechanism by which mitochondria respond to environmental perturbations. In fact in mitochondria from patients with mitochondrial myopathy, it was observed that many cristae lacked connection with the inner membrane (fig.1.2b). The disruption of the tubular connections can explain the altered activity of pathologic mitochondria [6].

The matrix is the space enclosed by the inner membrane. It is important in the production of ATP with the aid of the ATP synthase contained in the inner membrane. The matrix contains hundreds of enzymes with a lot of functions such as oxidation of pyruvate and fatty acids and the citric acid cycle. It also contains mitochondrial ribosomes, tRNA, and several copies of the mitochondrial DNA genome.

The endosymbiotic hypothesis for the origin of mitochondria suggests that

mitochondria descended from specialized bacteria (probably purple non-sulfur bacteria) that were incorporated into the cytoplasm of another cell by endocytosis. The ability of symbiont bacteria to conduct cellular respiration in host cells that had relied on glycolysis and fermentation would have provided a considerable evolutionary advantage. This symbiotic relationship probably developed 1.7-2 billion years ago [7].

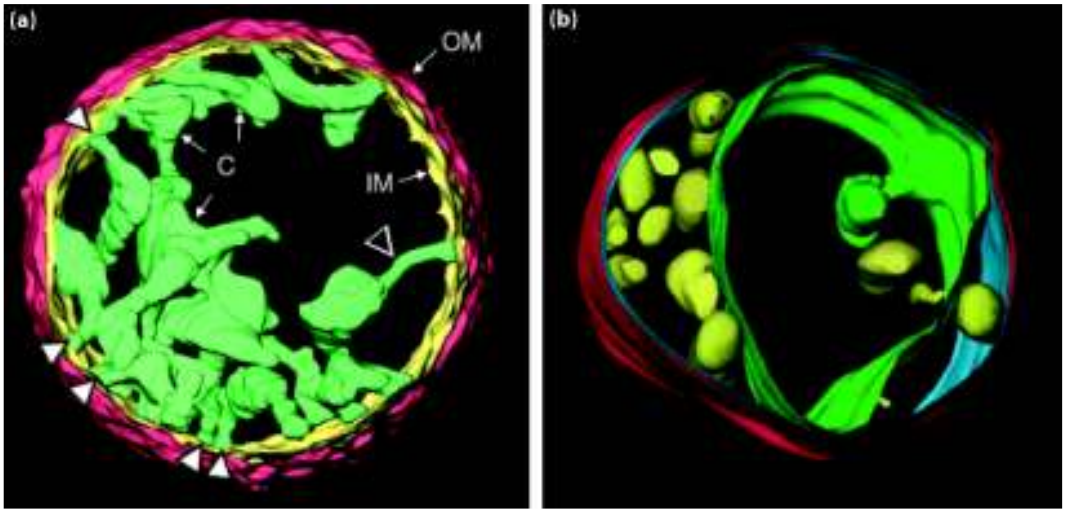


**Figure 1.2: a)** 3D electron microscopy tomography reconstruction of an isolated normal mitochondrion from rat-liver (Mannella C.A.). C, cristae; IM, inner boundary membrane; OM, outer membrane. Cristae (green) are swollen cisterns or sacs with multiple, tubular connections (arrows) to the peripheral surface of the inner membrane and to each other. **b)** Pathological mitochondrion (M. Huizing) from a patient with mitochondrial myopathy, containing numerous small vesicles (luminous green) that do not connect to the inner membrane (blue). There is a second large internal membrane (green), which has a vesicle-like protrusion, suggesting either that this unusual membrane is formed by fusion of the vesicles or, conversely, that the vesicles are formed by budding from it.

### 1.1.2 Mitochondrial respiratory chain

Oxidative phosphorylation (OXPHOS) is carried out in the inner mitochondrial membrane by four enzymatic complexes of the respiratory chain (complexes I-IV) and by the ATP-synthase (complex V). Coenzyme Q (a quinone) and cytochrome c are also involved in mitochondrial respiration, serving as 'electron shuttles' between the complexes [1].

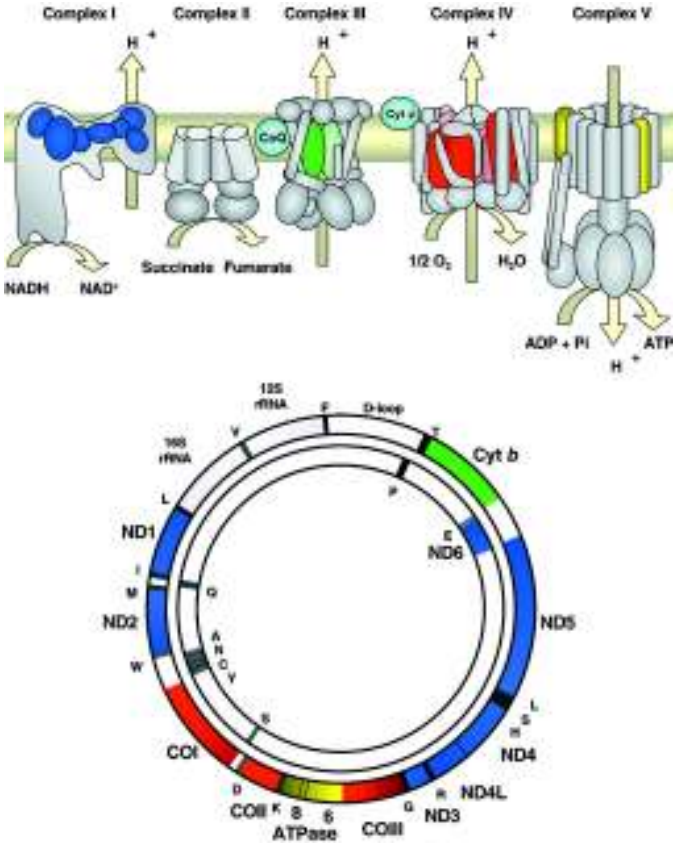


**Fig. 1.3** Creative drawing of the respiratory chain and human mitochondrial DNA. Top: respiratory chain complexes. Mitochondrially encoded subunits, embedded in the midst of nuclear-encoded subunits, are shown in different colours: complex I subunits = blue; complex III subunit = green; complex IV subunits = red; complex V subunits = yellow. Pi = inorganic phosphate; Cyt c = cytochrome c; CoQ = coenzyme Q. Bottom: mtDNA. myt genes: complex I genes = blue; complex III cytb gene = green; complex IV genes = red; complex V genes = yellow. syn genes: tRNA genes = grey; rRNA genes = purple. Cyt b = cytochrome b; COI = complex I; COII = complex II; COIII = complex III [8].

In humans, complex I or NADH-ubiquinone oxidoreductase, which accomplishes the oxidation of NADH derived by the oxidation of fatty acids, pyruvate and amino acids, contains seven subunits which are encoded by the mtDNA (subunits ND1-ND6 and ND4L), plus at least 39 nuclear-encoded subunits [9, 10].

Complex II or succinate-ubiquinone oxidoreductase, which accomplishes the oxidation of $FADH_2$ derived from fatty acid and Krebs' cycle, is composed of only four subunits, all encoded by the nuclear genome.

Complex III or ubiquinol-ferricytochrome c oxidoreductase holds one subunit,

cytochrome b, encoded by the mitochondrial genome and 10 subunits encoded by the nuclear genome.

Complex IV or cytochrome c oxidase (COX) is composed of 13 subunits, three of which are encoded by mtDNA (COX I-III) and the other 10 by nuclear DNA.

In addition, the mitochondrial electron transport chain (mETC) contains highly mobile, small electron carriers, one hydrophobic, coenzyme Q10 and the protein cytochrome c, synthesized by nuclear genes. In substance the mETC is especially built to accept electrons from NADH and $FADH_2$, transfer them through a series of oxidation-reduction reactions to molecular oxygen to produce water and to simultaneously coupling this exergonic reaction to the translocation of protons across the inner membrane [11, 12].

Synthesis of ATP from ADP is the second fundamental reaction of the mitochondrial respiratory chain, a process performed by complex V or ATP synthase.

ATP synthase is composed of two mtDNA-encoded subunits (ATPase 6 and 8), and at least 14 nuclear DNA-encoded subunits.

The proton electrochemical gradient generated at the mETC level during electron transfer to oxygen creates a polarization of the inner membrane which is changed back by the proton flux through a proton channel which resides in the $F_0$ component of ATP synthase. The proton flux drives the condensation of ADP and inorganic phosphate into ATP. Electron transfer across the mETC and ATP synthesis are coupled, or linked. In fact, the respiratory chain works as proton pump which generates a proton gradient and a membrane potential of about 180mV across the inner membrane with a negative polarity at the matrix side of the inner membrane. The proton gradient is utilized by the ATP synthase to phosphorylate matrix ADP. During this process the proton gradient is decreased and this activates respiration.

Notably, energy production in mitochondria requires not only a full assembly of functional protein at the level of the inner mitochondrial membrane, but also a bidirectional flow of information between the nuclear genome and the mitochondrial genome to adjust energy production in tissues to different energetic demands [13].

Accordingly, many different mutations in mtDNA and nuclear DNA encoding subunits, components or regulators of the respiratory chain function can produce a wide range of OXPHOS diseases [8].

### 1.1.3 Mitochondrial DNA

The first description of a circular DNA structure located in the mitochondria dates from 40 years ago [14]. Several unique characteristics discriminate mitochondrial from nuclear DNA.

Mitochondria are polyploid, in fact the mitochondrial DNA (mtDNA) is a multycopy genome. A cell contains hundreds of mitochondria, and each mitochondrion contains five to ten copies of mtDNA [15]. Dependent to the tissue and energy demand, each cell contains between 500 and 10000 mtDNA molecules, except for mature oocytes which contain between 100000 and 600000 mtDNA molecules [16]. At cell division, mitochondria and their genomes are randomly distributed to daughter cell.

Human mtDNA is a 16569 bp circular minichromosome, composed of two complementary strands, the heavy and light strands, with a genetic code different from the nuclear DNA [17] and it is transmitted entirely through the maternal line. mtDNA codes for a total of 37 genes. They are 13 genes encoding key-protein subunits of the OXPHOS complexes (complex I, III, IV and V) and 22 transfer RNAs (tRNA) and 2 ribosomal RNAs, genes involved in their in-situ translation. Approximately 6% of the mtDNA is non-coding, located predominantly in the D-loop, a region of 1kb, which contains the promoters for light and heavy strand transcription. The mtDNA is compact, it contains no introns, several overlapping genes and incomplete termination codons [18].

mtDNA molecules are packed in somatic cells as nucleoids in which six to ten molecules form a group with several different proteins. About 30 proteins from different species have been identified as potential components of mt-nucleoids. These nucleoids are not static entities, and mtDNA molecules exchange between nucleoids. The nucleoids are attached to the inner mitochondrial membrane near the OXPHOS system, where reactive oxygen species (ROS) are produced. Because of the lack of histones and other protective proteins and an ineffective repair mechanism, the mtDNA mutates 10-16 times more frequently as the nuclear DNA, and because of the lack of introns the mutations have a high probability of affecting genes and being pathogenic [19].

## 1.2 Heteroplasmy and Segregation of mtDNA

Unlike nuclear DNA, in which there are only two copies of each gene per cell, thousands of copies of mtDNA are present in every nucleated cell. As compared with nuclear genomic DNA, mtDNA accumulates oxidative lesions at a higher rate due to damage by reactive oxygen species, which are byoproducts of oxidative phosphorylation, and as a consequence, exhibits a higher spontaneous mutation rate [20, 21]. In contrast to the expected heterogeneity from the higher copy number and mutation rate, as a basic state, all copies of mtDNA are genetically identical within a cell and within individual higher eukaryotes, including humans. This genetic state is called “homoplasmy”. Mutations and mating generate mtDNA heterogeneity, which is called “heteroplasmy” [22]. Normal individuals are homoplasmic. Heteroplasmy occurs within cells (and probably within mitochondria) as well as within and between tissues, and so could be considered to be the polyploid version of what for diploid genomics is termed heterozygosity. Heteroplasmy, the presence of both normal and mutant mtDNA in a single individual, is present in most mitochondrial diseases, so that the proportion of mutant mtDNA in any cell or tissue may range from 0% to 100%.

There appears to be a threshold effect that dictates the phenotypic expression of a mtDNA associated character, and symptoms arise only from tissues with a high amount of mutant mtDNA. In fact, for a given heteroplasmic mutation, only when mutated gene copies accumulate over a certain threshold, the deleterious effects of the mutation will no longer be complemented by the co-existing wild-type mtDNA, and will be expressed phenotypically as a cellular dysfunction leading to disease. Accumulation of mutant mtDNAs in affected tissues is an explanation for the progressive nature of these disorders [23].

Particular characteristic of mtDNA is the maternal inheritance. When the oocyte is fertilized the same amount of genetic nuclear information is given by oocyte and by spermatozoon but all mitochondria and all mtDNA derive from oocyte. For this reason the mtDNA transmission differs from Mendelian inheritance. Normally if a mother bears a point mutation, she can transmit it to all her children but only daughters will transmit the mutation to their progeny. Heteroplasmy, threshold expression and stochastic segregation are characteristic of maternal, non-Mendelian genetics of mtDNA [24].

Battersby et al. [25] used a heteroplasmic mouse model to investigate the genetic basis for the tissue-specific segregation behaviour of mtDNA.

Unlike nuclear DNA, the replication of mtDNA is not strictly linked to the cell cycle and there is no strict control of partitioning of mtDNAs at cytokinesis. The

rate of segregation of mtDNA sequence variants is thus a function of mtDNA copy number and turnover rate, and in the absence of selection, the process can be modeled as a random walk. However, most pathogenic mtDNA mutations are heteroplasmic, and the segregation of mutated and wild-type mtDNAs often deviates from this random pattern, suggesting that the dysfunction caused by the mutation influences the process of segregation. The same mutation can also produce distinct clinical phenotypes in different pedigrees, a result of non-random distribution of mutated and wild-type mtDNAs, suggesting that nuclear background can influence mtDNA segregation [25].

The segregation pattern of pathogenic mtDNA mutants is an important determinant of the nature and severity of mitochondrial disease, but it varies with the specific mutation, cell type and nuclear background.

Yoneda et al. observed a shift in the proportion of the two mitochondrial genotypes in a number of cybrids clones, generated in bone nuclear background. In all the case where a shift was observed, there was an increase in the proportion of mutant mtDNA [26]. A novel finding observed by Dunbar et al., was that nuclear genetic background can influence the segregation of mutant and wild-type mitochondrial genomes [27]. In fact he assessed whether the phenomenon observed by Yoneda et al. would be reproduced in a different cellular background. Temporal analysis of the same mutant mtDNA type (A3243G point mutation in the mitochondrial $tRNA^{Leu(UUR)}$ gene) in lung and bone cell lines revealed a quite distinct outcome. Heteroplasmic lung cybrid clones shifted toward higher levels of wild-type rather than mutant mtDNA whereas bone cybrids always shifted toward increased mutant mtDNA molecules. These results indicate that the nuclear genetic background of the recipient ($\rho^0$) cell can influence the segregation of mutant and wild-type mitochondrial genomes in cell cybrids.

## 1.3 Complementation

The discovery of a variety of mtDNA mutations associated with diseases in humans and the growing evidence of accumulation of mtDNA mutations with aging in somatic tissues have raised a number of questions about the occurrence and frequency of intermixing of mutant and wild-type mtDNA and/or their products within a cell and the role that complementation between these products play in determining the cell phenotype.

Studying complementation of mutant and wild-type mitochondrial genomes in human cells, Yoneda et al. [28] observed that a small minority of wild-type

mtDNA (4%) can protect the cell against the phenotypic effects of the mtDNA mutation. However, these experiments did not clarify how this protection occurs: or the wild-type mtDNA minority provides the sufficient energy for the cellular needs in a complete segregate status from the mutant mtDNA or, alternatively, there is an intermixing cooperation between wild-type and mutant gene products, in presence of mitochondrial fusion, a necessary condition to exert the protective effect of wild-type molecules.

The results show that interaction of the mutant and wild-type genomes occurs if the two genomes coexist in the same organelles. It is very reasonable to think that cells in which this intramitochondrial heteroplasmy is maintained will have a selective advantage because of the possibility of complementation that this situation allows. While it was observed the failure of interaction in the case of intermitochondrial heteroplasmy [28].

An in vivo inter-mitochondrial complementation between $COX^-$ mitochondria carrying ΔmtDNA4696 and $COX^+$ mitochondria carrying wild-type mtDNA was indeed observed by Nakada et al. [29].

In vivo inter-mitochondrial complementation could prevent human subjects from phenotypic expression of respiration defects caused by various pathogenic mutant mtDNAs created in somatic tissues with age. This result opens the possibility of gene therapy by introduction of mitochondria possessing DNA with wild-type sequence. However, no effective procedures are yet available for in vivo introduction of mitochondria into mammalian cells.

## 1.4 Mitochondrial fission and fusion

While in the past mitochondria were depicted as sausage-shaped organelles floating in the cytoplasm, now we know that mitochondria have complex morphologies. The morphology of mitochondria is dynamic, often changing within a cell and from one cell to the next. Their shapes vary from small spherical fragments in rapidly dividing cells, to elaborate branched networks in quiescent cells. They move rapidly along other cellular structures, such as the actin and microtubule cytoskeletons. Mitochondria also undergo frequent divisions and fuse with other mitochondria, in fact mitochondrial division antagonizes fusion, and together these events create a compartment that is connected and thus functional [30].

A number of proteins that affect mitochondrial division and fusion were recently discovered. Mitofusins and OPA1 are essential for mitochondrial fusion, whereas

Fis1 and Drp1 are essential for mitochondrial fission. The overall morphology of the mitochondrial population depends on the relative activities of these two sets of proteins [31, 32].

### 1.4.1 Mitochondrial fission

#### 1.4.1.1 Drp1

Genetic approaches in flies and yeast have identified proteins directly required for mitochondrial division and fusion. Remarkably, among these are several highly conserved dynamin-related proteins (DRPs), which are large self assembling GTPases that regulate membrane dynamics in a variety of cellular processes [30].
The dynamins are a family of structurally similar but functionally diverse GTP-binding proteins with sizes ranging from 70 to 100 kD. The best characterized class of dynamin family members functions in membrane traffic.
There is a growing number of other dynamin-related proteins with novel membrane functions.
X-ray structures of DRP GTPase domains indicate that they posses the core fold common to all regulatory GTPases and establish them as members of the GTPase superfamily [33, 34]. However their relatively large mass as well as kinetic and structural properties make them unique among other classes of GTPases.
In addition to a highly conserved $NH_2$-terminal GTPase domain, DRPs possess two less conserved hallmark domains that contain predicted coiled-coil regions: a middle region of ~250 amino acids and a C-terminal assembly or GTPase effector domain (GED) [35, 36].
In addition, most family members have divergent segments. It seems likely that these divergent inserts help determine the specific functions of the different dynamin family members [37].
In yeast, there are three essential mitochondrial division proteins: Dnm1, Fis1, and Mdv1 and an Mdv1 paralog Caf4 that may play a regulatory role in division. Dnm1 and Fis1 are highly conserved, and their human orthologs are termed “Drp1” and “hFis1”, respectively. In contrast a structural ortholog of Mdv1 has not yet been identified in higher eukaryotes.
Dnm1/Drp1 is the dynamin-related GTPase that is essential for noncytokinetic mitochondrial division [38-40]. A majority of Drp1 is diffusely distributed in the cytosol, although a fraction of the protein is found in mitochondrial-associated assemblies. Such as for Dnm1, not all mitochondrial-associated Drp1 sites undergo division. Importantly, however, Drp1, like Dnm1, is present at sites of mitochondrial division [38].

The GTP-bound state of Drp1 may regulate interactions with other division components, such as hFis1 that in turn likely modulates the self-assembly and nucleotide hydrolysis activities of Drp1 that drive mitochondrial division. The energy generated by GTP hydrolysis is believed to provide the mechanical force required to execute fission [41, 42].

Actually, new regulatory mechanisms that control mitochondrial fission in response to a variety of cellular events, including cell division, metabolic flux and cell differentiation, have been uncovered. Most of these processes seem to regulate the localization, dynamics and activity of Drp1 or Dnm1.

Recent experiments using cultured human cells revealed a direct link between the cell-cycle and the mitochondrial division machinery. This burst of mitochondrial division is correlated with the cyclinB-cyclin-dependent kinase (CDK1-dependent) phosphorylation of Drp1. In vitro assays using purified proteins coupled with cell-culture experiments indicate that the most potent mitotic phosphorylation event occurs on a serine residue in the carboxyl-terminal GTP-ase-effector domain (GED) of Drp1. Another recent study showed that cyclic-AMP-kinase-dependent phosphorylation of a different serine in the GED can decrease the GTPase activity of Drp1. It is likely that Drp1 phosphorylation at different sites might have different physiological consequences. Although these initial studies indicate that Drp1 phosphorylation can modulate the frequency of mitochondrial division, it remains to be determined if fission-competent Drp1 is always phosphorylated or if this is a mechanism exploited only during the cell cycle [43, 44].

It was also uncovered that ubiquitinylation of Drp1 regulates mitochondrial division. A recent work suggests that MARCH-V ubiquitinylates Drp1 and Drp1 ubiquitinylation seems to regulate the kinetics of Drp1 binding to the mitochondrial surface [45].

Drp1 can also be sumoylated. Unlike ubiquitinylation, which often leads to degradation of substrates, sumoylation usually alters the subcellular localization of target proteins or protects them from ubiquitin-mediated destruction. Drp1 pull-down experiments identified SUMO-1 and its conjugating enzyme Ubc9 as Drp1-binding partners [46]. Similar to the cyclinB-CDK1 dependent phosphorylation of Drp1, the interactions among Drp1, SUMO and SENP5, the protease that removes SUMO from Drp1, might help to coordinate mitochondrial division and the cell cycle to insure even segregation of mitochondria [47]. Sumoylation of Drp1 also appears to influence the integration of pro-apoptotic signals and mitochondrial division. Recent experiments illustrate that normal cycling of Drp1 on and off the organelle surface is arrested during apoptosis, such that Drp1 accumulates on the

mitochondria and mitochondria undergo extensive fragmentation and ultimately caspase-indipendent elimination through a process known as mitoptosis [48, 49]. In this scenario, Drp1 is recruited to the mitochondrial membrane independent of its well characterized membrane anchor, hFis1.

#### 1.4.1.2 hFis1

In mammalian cells, Drp1-dependent mitochondrial division requires hFis1, such as in yeast, Dnm1-dependent mitochondrial division requires Fis1 [50-52].

hFis1 and Fis1 are a 18-kDa protein, anchored to the mitochondrial outer membrane via a C-terminal transmembrane domain and with its N-terminal domain exposed to the cytosol. The NMR structure of Fis1, along with the NMR and crystal structures of hFis1, reveals that the cytosolic portion of the protein is composed of six α-helices that adopt a superhelical tetratricopeptide repeat (TPR) fold; specifically α2- α3 and α4- α5 form two TPR motifs. The TPR-like fold of Fis1/hFis1 forms a concave hydrophobic surface that, based on similarity to other TPR-containing proteins, is proposed to serve as a platform for protein-protein interactions. The structure of Fis1 and hFis1 are strikingly similar with exceptions of the α1-helix, which is shorter in yeast, and the presence of an N-terminal arm that precedes the α1-helix of Fis1 but is missing in hFis1 [53-56].

In addition to Fis1, Mdv1 is also required for mitochondrial division in yeast. Mdv1 is an 80-kDa protein that contains at least three regions that mediate various protein-protein interactions required for division: an N-terminal extension (NTE) of unknown structure that interacts with Fis1, a central coiled-coil region that mediates homooligomerization, and a C-terminal WD repeat region predicted to form a seven-bladed propeller that interacts with Dnm1 [57-59]. In vivo Mdv1 is peripherically associated with the mitochondrial outer membrane and colocalizes specifically with mitochondrial-associated Dnm1 puncta [60]. Importantly, time-lapse microscopy of Dnm1 and Mdv1 indicates that both proteins are present in the division complex during fission. Neither a structural nor a functional homolog of Mdv1 has been identified in higher eukaryotes.

In addition to the proteins essential for mitochondrial division in yeast, Caf4, a paralog of Mdv1, has been identified as a nonessential component of the mitochondrial division machine [61].

In yeast, Fis1, which is uniformly distributed along the mitochondrial outer membrane, is required for the mitochondrial targeting of the cytosolic division proteins, Dnm1, Mdv1 and Caf4 [51, 57, 58, 61]. In absence of Fis1, targeting of Dnm1, Mdv1 and Caf4 to mitochondria is severely compromised, suggesting that

Fis1 functions as a membrane receptor for these proteins. Although interactions between Fis1 and both Mdv1 and Caf4 have been detected, an interaction between Fis1 and Dnm1 has not, suggesting that Fis1-dependent targeting of Dnm1 to mitochondria proceeds through Mdv1 and/or Caf4 [55, 58, 59, 61].

The interactions between Fis1 and the adaptors are mediated through the TPR-like fold of Fis1. Mutations in this region of Fis1 interfere with division complex assembly and consequently division itself [54, 55, 59]. The exact structural basis for the Fis1 –Mdv1/Caf4 interaction is unknown; however, TPR folds in other proteins mediate interactions by binding to short amino acid structures. A single point mutation in the NTE of Mdv1 abolishes Fis1 binding. If such a small region is sufficient for binding to Fis1, it may in part explain the lack of a structural homolog of Mdv1 in higher eukaryotes.

Although the bulk of Dnm1 targeting to the mitochondrial outer membrane in yeast is Fis1 dependent, a role for hFis1 in the mitochondrial targeting of Drp1 is less clear.

It seems likely that, as is the case in yeast, the hFis1-Drp1 interaction is bridget by an as of yet unidentified adaptor, the identification of which is eagerly anticipated. Consistent with the yeast model, disruption of the TPR motif of hFis1 abolishes hFis1-induced mitochondrial fragmentation, presumably by interfering with division complex assembly [56].

In mammalian cells, deletion of the α1-helix of hFis1 appears to strengthen the interaction between hFis1 and Drp1 or a Drp1-containing complex. Interestingly, deletion of the α1-helix abolishes the ability of hFis1 to promote mitochondrial division, suggesting that a labile/dynamic interaction between hFis1 and Drp1 is required for mitochondrial division. These observations suggest that Fis1/hFis1 may play additional regulatory roles in division down-stream of targeting, such as in constriction and fission.

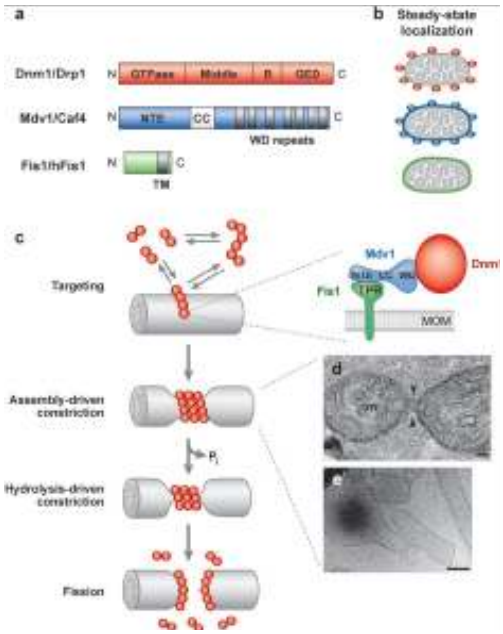


**Figure 1.4:** mitochondrial division. a) the mitochondrial division proteins are shown with functional domains represented as boxes. b) a schematic of the steady-state localization of the mitochondrial division proteins in wild-type cells. c) a model of the mechanism of mitochondrial division. Also shown, a thin section electron microscopy (EM) analysis of yeast cells, showing mitochondrial constriction intermediates (panel d). Electron microscopy analysis showing that purified Dnm1 assembles on and constricts liposomes in vitro (panel e). The bars are 100nm. Panel d and e are reproduced from The Journal of Cell Biology [42]. Abbreviations: arrowheads, electron-dense structures that are found in association with mitochondrial constriction sites that may represent Dnm1 spirals; B, insert B; CC, coiled-coil; GED, GTPase effector domain; GTPase, GTPase domain; M, matrices of the mitochondria; middle, middle domain; NTE, N-terminal extension; TM, transmembrane domain [30].

### 1.4.1.3 Nonessential regulators of mitochondrial division

Studies in mammalian cells have identified additional regulators of mitochondrial dynamics. Endophilin B1 was found to act downstream of Drp1 in the maintenance of mitochondrial morphology [62]. Endophilin B1 is a member of the endophilin family of proteins that self-assemble to form filaments that remodel membranes. Like other endophilins, endophilin B1 possesses an N-BAR domain; such domains are though to sense and/or induce membrane curvature. The cellular distribution of endophilin B1 is similar to that of Drp1, in that it is predominately cytosolic with a fraction of the protein colocalized with mitochondria. Upon treatment of cells with apoptotic stimuli, endophilin B1, like Drp1, translocates to and coalesces into punctate structures on the mitochondria surface; however, neither colocalization of or an interaction between endophilin B1 and Drp1 has been reported. Probably endophilin B1 has a role in the remodeling of the mitochondrial outer membrane during fission.

GDAP1, ganglioside-induced differentiation associated protein 1, has also been implicated as a regulator of mitochondrial division [63]. Interestingly, mutations

in GDAP1, an integral protein of the mitochondrial outer membrane, are associated with Charcot-Marie-Tooth disease, a peripheral neuropathy that is also caused by mutations in the mitochondrial fusion protein, Mfn2.

All known components of the mitochondrial division machine associate with the mitochondrial outer membrane, raising the questions of how is fission of the inner and outer membranes coordinated and how do these two membranes remain separate?

In human cells mitochondrial inner membrane constriction/fission occurs independently to that of the mitochondrial outer membrane in the absence of Drp1 or endophilin B1 function, suggesting that a separate inner membrane division machine exists.

The molecular machine driving mitochondrial inner membrane constriction and/or scission is unknown. One possible candidate in yeast is Mdm33, which lacks a homolog in higher eukaryotes. Mdm33 is an integral mitochondrial inner membrane protein that self-interacts, likely via an extensive coiled-coil domain that is exposed to the matrix compartment [64].

In mammalian cells, MTP18 has been postulated as a mediator of mitochondrial inner membrane fission owing to its proposed residence in the inner membrane space, coupled with the findings that depletion and overexperession of MTP18 promote mitochondrial elongation and fragmentation, respectively [65].

### 1.4.2 Mitochondrial fusion

Mitochondria fuse using mechanism distinct, or at least more complex, from those of other membrane-bound organelles. This might reflect the endosymbiotic origin of these organelles, which have two membranes, an outer (OM) and an inner (IM), that have distinct lipid and protein compositions. Like other membrane-fusion events, mitochondria are first tethered together before their OM and then IM bilayers mix. Two evolutionarily conserved large GTPases, Mitofusins (called Fzo1p in yeast) and OPA1 (named Mgm1p in yeast), have central roles in OM and IM fusion, respectively [66, 67].

#### 1.4.2.1 Mitofusin 1 and 2

Mitofusins are anchored in the mitochondrial OM by a bipartite transmembrane domain, such that both N-terminal GTPase and carboxyl-terminal coiled-coil domains face the cytosol.

Mitofusins are related distantly to dynamin, the large GTPase required for vesicle endocytosis, and, like dynamin, these proteins oligomerize and hydrolyze GTP to

catalyze the membrane rearrangements that leads to mitochondrial fusion. The understanding of mammalian mitochondrial fusion is complicated by the existence of two ubiquitously expressed vertebrate-specific mitofusin isofoms, Mfn1 and Mfn2, which can assemble into homo- and hetero-holigomers. Although evidence suggests that Mfn1 and Mfn2 both function in mitochondrial fusion, many observations indicate that Mfn2 is less active and/or may function differently than Mfn1 in tethering and fusion [68]. Thus, the most basic form of regulation in mammalian cells is likely the relative level of Mfn1 and Mfn2 expression. Indeed, it has been shown that Mfn1 expression is higher in brain tissues, whereas Mfn2 predominates in the testes and heart. This type of regulation may in part explain the tissue specificity of the neurodegenerative diseases linked to mutations in Mfn2. In addition, Mfn1, but not Mfn2, is required for OPA1 function, whereas mutations in Mfn2 cause CMT2A [69-71].

Detailed analysis of the mutations that cause CMT2A has provided insight into the role of Mfn1-Mfn2 interactions. CMT2A is a progressive neurodegenerative disease characterized by the deterioration of long sensory and motor neuron axons. The specific peripheral neuropathies characteristic of CTM2A might be explained, at least in part, by the ratio of Mfn1 and Mfn2 in different cell types. For instance, cells with high levels of Mfn1, such as cardiomyocytes, might be protected from the disease-causing Mfn2 protein because Mfn1 can form a functional complex with the mutant molecule. This functional complementation occurs in trans between Mfn1 and Mfn2 on opposite mitochondria. However, cells that have low levels of Mfn1 or that require higher levels of mitochondrial fusion, such as the long peripheral neurons most affected in CMT2A, might be particularly vulnerable to point mutations in Mfn2 [72].

On apoptotic stimulation, the balance between fusion and division is disrupted and the mitochondria fragment. Two pro-apoptotic Bcl-2 family members, Bax and Bak, have been implicated in mitochondrial dynamic during programmed cell death. Interestingly, Bax and Bak also affect mitochondrial fusion in non-apoptotic cells by regulating the assembly of Mfn2 into high molecular-weigh complexes. In addition to a role for pro-apoptotic proteins in mitochondrial fusion, two anti-apoptotic Bcl-2 family members also promote mitochondrial fusion in mammalian cells by interacting physically with Mfn2. These findings reveal unexpected non-apoptotic functions for both pro- and anti- death Bcl-2 family members and hint that these proteins might exert their reciprocal control over programmed cell death by regulating the assembly of mitochondrial fusion proteins [73-75].

Recent biochemical studies using mammalian cells have identified two additional Mfn partners, mitofusin-binding protein (MIB) and Stoml2. MIB was isolated as a cytosolic Mfn-1 binding protein that associates with the mitochondrial OM. It is a member of the medium-chain dehydrogenase and reductase protein superfamily and it contains a conserved coenzyme-binding domain that might bind and hydrolyze nucleotides. Stoml2 is a stomatin-like protein localized to the mitochondrial IMS where it binds Mfn2. Although knockdown of Stoml2 reduces mitochondrial-membrane potential, this treatment does not alter mitochondrial morphology dramatically [76, 77].

#### 1.4.2.2 OPA1

Yeast Mgm1p and its mammalian counterpart OPA1 are required for mitochondrial fusion and IM cristae morphology [78, 79]. OPA1 (Mgm1p) proteins are found in the intermembrane space (IMS) where they associate with both the IM and OM.

Mgm1p is processed proteolytically into long (i-Mgm1p) and short forms(s-Mgm1p) inside mitochondria. l-Mgm1p is integrated into the IM through its N-terminal transmembrane segment and its mitochondria-targeting presequence is cleaved by the matrix-processing protease. By contrast, s-Mgm1p is processed proteolytically in the IM and then released into the IMS. s-Mgm1p is generated when Mgm1p is cleaved by the rhomboid-related protease Pcp1p in the IM. The levels of Pcp1p, in addition to the concentration of matrix ATP, regulate the production of s-Mgm1p [80, 81]. Ups1p is an evolutionarily conserved IMS protein that regulates the relative amounts of long and short forms of Mgm1p by controlling the insertion of Mgm1p's Pcp1p-sensitive rhomboid-cleavage site into the IM [82].

Both biochemical and cytological data indicate that Mgm1 tethers inner membranes via the formation of trans inner membrane complexes.

The human homolog, OPA1, is also proteolytically processed, albeit by different mechanisms, to generate presumably functionally important isoforms with topologies similar to their yeast counterparts. However, in human cells, the generation of OPA1 isoforms is made more complex because there are many tissue-selective splice variants. These splice variants are generated by alternative splicing of three exons that encode small regions of OPA1 preceding the GTPase domain, indicating that there is additional functional variation among OPA1 isoforms. Current evidence suggests that there are multiple proteases involved in OPA1 processing and that alternate spliced products may influence the efficiency

of proteolytic processing.

The exact mechanism of OPA1 processing remains outstanding. To date, two different proteases have been implicated: PARL (presenilin-associated rhomboid-like protein) and paraplegin. Mouse cells lacking PARL, which is the Pcp1 mammalian rhomboid ortholog, have a reduced amount of the short, more soluble form of OPA1. It is possible that the cell type dictates the contribution of each protease or that they are influenced by other unidentified factors [83-85].

Dissipation of membrane potential stimulates the production of OPA1 short in mammalian cells, pointing to a difference from yeast in the regulation of processing, where loss of mitochondrial energetics inhibits Mgm1 processing. In mammalian cells, however, this regulation likely serves to connect cellular energetics with other mitochondrial functions, such as apoptosis [86].

Biochemical fractionation and careful cytological studies indicate that cristae is a separate mitochondrial inner membrane compartment that connects to the IMS though small, relatively uniform tubular segments called cristae junctions [87].

Interestingly, OPA1's role in cristae regulation can be uncoupled from its role in mitochondrial fusion. However, the extent to which inner membrane fusion and cristae maintenance functions of Mgm1/OPA1 overlap remains an unresolved question.

How outer and inner membrane fusion events are coordinated is currently not understood. In yeast, the best candidate for this role is the protein Ugo1, which is a member of the mitochondrial transporter family localized to the outer membrane. Although Ugo1 is present only in yeasts, it is likely that a functional homolog exists in other organisms.

In contrast to the mitochondrial division machinery, mitochondrial fusion proteins appear to protect the cells from apoptosis, as an increase in mitochondrial fusion delays/inhibits apoptosis, whereas a decrease in fusion makes cells spontaneously undergo apoptosis or become more sensitive to apoptotic stimuli [88]. OPA1 appears at least in part to exert an antiapoptotic effect through its role in cristae morphology maintenance. In apoptotic cells, prior to cytochrome c release, the oligomeric state of OPA1 changes, and this change correlates with increased cristae junction size [83, 84].

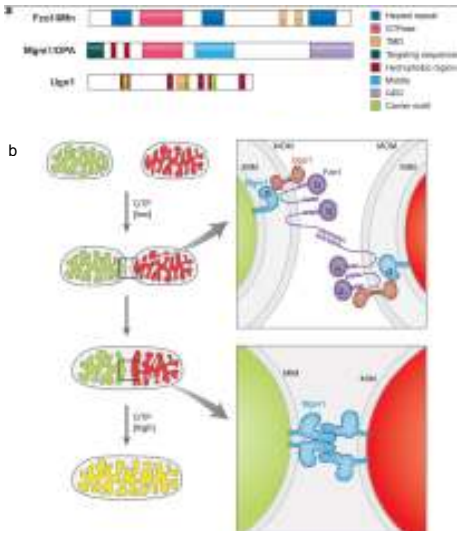

**Figure 1.5:** The mitochondrial fusion machine. a) The mitochondrial fusion proteins are shown with functional domains represented as colour-coded boxes. b) Model of the mechanism of mitochondrial fusion. Mitochondrial fusion requires the sequential interaction of the outer mitochondrial membranes and the inner mitochondrial membranes. Fusion of the outer membranes requires GTP and a proton gradient. Fusion of the inner membrane requires exogenously added GTP and the electrical component of the inner membrane potential. The upper box presents a model of mitochondrial outer membrane fusion. The outer membrane GTPase Fzo1 forms an oligomeric complex in cis and in trans via interactions of the GTPase domain and helical region domains to tether mitochondria. The possible role of the fusion complex containing Fzo1, Ugo1 and Mgm1 in the formation of the tethering complex or in the subsequent fusion reaction is not known. The lower box presents a model for mitochondrial inner membrane fusion. The inner membrane GTPase Mgm1/OPA forms oligomeric complexes in cis and in trans to tether the inner membranes [30].

## 1.5 Mitochondrial disorders

Mitochondrial disorders are clinical phenotypes associated with abnormalities of oxidative phosphorylation (OXPHOS), the terminal component of mitochondrial energy metabolism. They affect at least 1 in 5000 of general population, making them the most common inherited metabolic disease [19, 89].

The variability in clinical manifestations of mtDNA stems from a number of factors, including the nature of the mutation, i.e. its intrinsic pathogenicity, and the gene specifically affected, the mutation load and the tissue distribution, and the relative reliance of each organ system on the mitochondrial energy supply. In general, the visual and auditory systems, the CNS and PNS, the heart, muscle, endocrine pancreas, kidney and liver are, in that order, the organs most sensitive to OXPHOS failure [8, 89, 90].

### 1.5.1 Nuclear genes in mitochondrial disorders

With the exception of complex II, which is entirely encoded by nuclear DNA, the remaining OXPHOS enzymatic complexes are composed of a variable number of subunits, encoded by either nuclear or mitochondrial DNA. As a result, OXPHOS disorders can be determined by mutations in each of these genomes.

Although the number of nuclear OXPHOS-related genes that have been proven to be associated with mitochondrial syndromes is still rather small, a clinical-genetic classification can be proposed for these defects, as follows [91]:

1. genes encoding structural components of OXPHOS complexes.
2. genes encoding assembly factors of OXPHOS complexes.
3. genes altering the stability of mtDNA.
4. genes encoding factors involved in the biogenesis of mitochondria, including OXPHOS.
5. mitochondrial protein synthesis genes.
6. genes encoding biosynthetic enzymes for lipids or cofactors [89].

OXPHOS disorders associated to nuclear genes mutations are increasing every year, demostrating that this field may deserve novel important finding in the future.

### 1.5.2 Mitochondrial DNA mutations

Mutations in mtDNA include either large-scale rearrangements (i.e. partial deletions or duplications), which are usually sporadic, and inherited point mutations, which are usually transmitted through the maternal lineage. Whereas large-scale rearrangements are invariably heteroplasmic, point mutations may be either heteroplasmic or homoplasmic, and can affect structural genes or genes encoding the RNA apparatus involved in mtDNA translation [90, 91].

Point mutations are responsible for a tremendous number of different clinical phenotypes. This variability has been related to the peculiarities of mitochondrial genetics: random segregation of a given mutation within the human body; heteroplasmy and thresholds effects.

Several different pathomechanism at different levels of cellular function have been identified: point mutations may reduce the steady state levels of the corresponding tRNA; may interfere with the level of aminoacylation with the corresponding aminoacid; induce an atypical base-modification pattern; and may result in quantitative and/or qualitative alterations of protein synthesis and respiratory chain (RC) function [92].

### 1.5.2.1 Large-scale rearrangements of mtDNA

Single, large-scale rearrangements of mtDNA can be single partial deletions, or partial duplications.

Three main clinical phenotypes are associated with these mutations: Kearns-Sayre syndrome (KSS), sporadic external ophthalmoplegia (PEO) and Pearson's syndrome.

KSS is a sporadic disorder characterized by the triad of: chronic progressive external ophthalmoplegia; onset before age of 20 years; pigmentary retinopathy. Cerebellar syndrome, heart block, diabetes and short stature are also part of the syndrome. Patients with this disease invariably show RRFs in muscle biopsy [93, 94].

Single deletions/duplications can also result in milder phenotypes as PEO, characterized by late-onset progressive external ophthalmoplegia, proximal myopathy and exercise intolerance. In both KSS and PEO, diabetes mellitus and hearing loss are frequent additional features, that may occasionally precede, by years, the onset of neuromuscular symptoms [95].

Large-scale single deletions/duplications of mtDNA may cause Pearson's bone-marrow-pancreas syndrome, a rare disorder of early infancy characterized by connatal sideroblastic pancytopenia and, less frequently, severe exocrine pancreatic insufficiency with malabsorption. Infants surviving into childhood or adolescence may develop the clinical features of KSS [96].

The majority of single large-scale rearrangements of mtDNA are sporadic and are therefore believed to be the result of the clonal amplification of a single mutational event, occurring in the maternal oocyte or early during the development of the embryo [97].

### 1.5.2.2 Point mutations of mtDNA

mtDNA point mutations are usually maternally inherited. Marked reductions of both mitochondrial protein synthesis and respiration have been documented for some mutations, when a threshold of 80-90% of mutant mtDNA is reached. It is worth mentioning that the clinical and biochemical variability of many mtDNA mutations may be due to different mitochondrial and/or nuclear 'gene backgrounds'.

Point mutations can be homoplasmic and heteroplasmic.

#### 1.5.2.2.1 Heteroplasmic point mutations

##### 1.5.2.2.1.1 MELAS

The acronym MELAS for Mitochondrial encephalomyopathy with lactic acidosis and stroke-like episodes was first coined by Pavlakis et al. [98]. MELAS is the commonest of the mitochondrial disorders. Onset ranges between childhood and adulthood. MELAS is defined by the presence of stroke-like episodes due to focal brain lesions, often localized in the parieto-occipital lobes, lactic acidosis and/or Ragged Red Fibers. Multisystemic organ involvement is seen, including the central nervous system (CNS), skeletal muscle, eye, cardiac muscle, and, more rarely, the gastrointestinal and renal systems. Other signs of CNS involvement include dementia, recurrent headache and vomiting, focal or generalized seizures, pigmentary retinopathy and deafness. Ataxia can be observed in some patients. The first stroke episode usually occurs in childhood between the ages of 4 and 15 years, but it may occur in infants or in young adults. Prior to the first stroke, the child may be slow to grow and develop.

MELAS was first associated with a heteroplasmic point mutation in the $tRNA^{Leu(UUR)}$, an A→G transition at position 3243. Approximately 80% of the MELAS patients carry the A3243G mutation. Many other MELAS-associated point mutations were later reported in the $tRNA^{Phe}$, $tRNA^{Val}$, $tRNA^{Lys}$, COXIII, ND1, ND5 or rRNA genes or small-scale mtDNA deletions in the cytb gene and also in the same $tRNA^{Leu(UUR)}$ other point mutations were detected (3244 G→A, 3258 T→C, 3271 T→C, and 3291 T→C) [98-104].

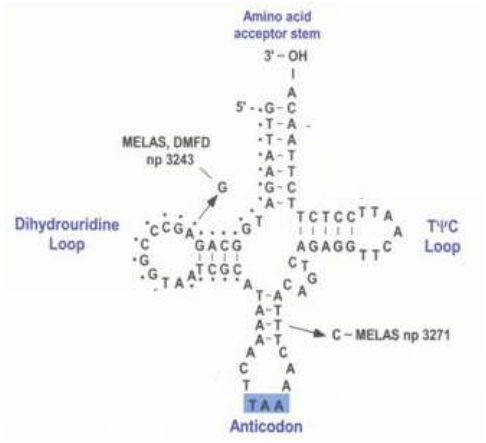


**Figure 1.6:** secondary structure of the human mitochondrial $tRNA^{Leu(UUR)}$. The mutations A3243G and T3271C associated with MELAS are indicated with arrows.

The 3243A>G mutation has also been detected in several patients with maternally

inherited PEO, isolated myopathy alone, cardiomyopathy, maternally inherited diabetes mellitus and deafness [98, 99].

Mitochondrial dysfunctions such as MELAS could have multiple causes, including, decreased tRNA stability, decreased aminoacylation, or abnormal conformations, which would lead to decreased steady-state levels of the normal aminoacylated tRNAs and result in reduced mitochondrial protein synthesis. The reduction in the levels of leucyl-$tRNA^{Leu(UUR)}$ may not be the only factor contributing to decrease in the rates of mitochondrial protein synthesis [105-108]. In fact, it was also observed that several disease-associated mitochondrial tRNA gene mutations are associated with a lack of taurine wobble base-modification in the mutant tRNAs. In HeLa cybrids cells homoplasmic for the pathogenic point mutation, the taurine-containing modified uridine ($\tau m^5 s^2 U$; 5-taurinomethyluridine), which normally occurs at the anticodon wobble position of mt $tRNA^{Leu(UUR)}$, remains unmodified in mt $tRNA^{Leu(UUR)}$ bearing either the A3243G or T3271C MELAS mutation. This indicates that the RNA-modifying enzyme responsible for the 5-taurinomethyl group, which has not been identified, is a class of enzyme that recognizes the whole tertiary structure of tRNA, because the np 3243 is far from the wobble position. It is known that uridine modification at the wobble position is responsible for precise and efficient codon recognition [109-111].

In MELAS syndrome, the 3243A>G mutation was demonstrated to be the direct cause of reductions in oxygen consumption and mitochondrial protein synthesis using a cybrid cell system in which mutant mtDNA derived from patients were intercellularly transferred into recipient cells lacking mtDNA ($\rho^0$ cells).

In the MELAS syndrome, as in all the mitochondrial diseases, segregation and threshold effect play a primary role on respiration and biogenetic function of cells. Using a cybrid cell model, it was observed that below 70% mutant mtDNA cells are apparently normal. Between 70% and 90% of mutant mtDNA a mild complex I deficit is evident. Above 90% mutant mtDNA there is a general impairment of respiration, with lower ATP/ADP ratios, declined energy charge and increased oxidative stress, but only at 95% or more mutant mtDNA there is a severe drop in mitochondrial protein synthesis [112, 113].

Also measurements of respiratory enzyme activities in intact mitochondria have revealed that more than one half of the patients with MELAS may have complex I or complex I + IV deficiency. A close relationship appears to exist between MELAS and complex I deficiency. The mt $tRNA^{Leu(UUR)}$ lacking the taurine-modification showed severely reduced UUG translation. This result could explain

the defective translation of UUG-rich genes such as ND6 (component of complex I) that leads to the observed decrease in respiratory chain activity [109].
Unfortunately there is as yet no treatment to stop the damage done by MELAS syndrome, and the outcome for individuals with the syndrome is usually poor. Moderate treadmill training can help improve the endurance of individuals with myopathy. Metabolic therapies, including dietary supplements, have shown benefits for some individuals. These treatments include coenzyme Q10, phylloquinone, menadione, ascorbate, riboflavin, nicotinamide, creatine monohydrate, idebenone, succinate, and dichloroacetate. Whether these supplements will help all individuals with MELAS syndrome is still being studied [8].

**1.5.2.2.2 Other heteroplasmic point mutations syndromes**

Myoclonic epilepsy with ragged red fibres (MERRF) is a maternally inherited neuromuscular disorder characterized by myoclonus, epilepsy, muscle weakness and wasting with RRFs, cerebellar ataxia, deafness and dementia [114].
The most commonly observed mutation of mtDNA associated with MERRF is an A→G transition at nt 8344 in the $tRNA^{Lys}$ gene [115]. As described for A3243G or T3271C MELAS mutations, A8344G mutation doesn't allow a correct taurine wobble base-modification in the tRNAs [109]. Complex IV deficiency is the most prominent biochemical finding in 8344A>G-positive MERRF muscle, although complex I can be affected too. COX-depleted RRFs are invariably detected in the muscle biopsy.
A8344G transition has also been reported in phenotypes as different as Leigh's syndrome, isolated myoclonus, familial lipomatosis, isolated myopathy and a variant neurological syndrome characterized by ataxia, myopathy, hearing loss and neuropathy [116].
Neurogenic weakness, ataxia and retinitis pigmentosa (NARP) is another maternally inherited syndrome in which the cardinal manifestations include ataxia, pigmentary retinopathy and peripheral neuropathy [117].
NARP is associated with a heteroplasmic T→G transversion at position 8993 in the ATPase 6 subunit gene. The degree of heteroplasmy is correlated with the severity of the disease. When the percentage of mutant mtDNA is >95%, patients show the clinical findings of maternally inherited Leigh's syndrome. NARP/ maternally inherited Leigh's syndrome phenotypes have been described in association with other mutations of the ATPase 6 gene, for example mutation 9176T→C. Impairment of ATP synthesis has been reported in cell cultures

harbouring the T8993G mutation [118, 119].
7472insC is responsible of hearing loss-ataxia-myoclonus. This mutation affects the $tRNA^{Ser(UCN)}$. Clinical manifestations go from isolated hearing loss, to epilepsia partialis continua and ataxia, to overt MERRF [120, 121].

#### 1.5.2.2.3 Homoplasmic point mutations

In contrast to many heteroplasmic mutations, the clinical expression of disorders associated with homoplasmic mutations is mainly restricted to a single tissue. In this group of disorders, the presence of a pathogenic mtDNA mutation is necessary but not sufficient to induce disease. As a consequence, penetrance is incomplete and possibly controlled by environmental factors, additional mitochondrial polymorphism, or the effect of nuclear genes [122].
Leber's hereditary optic neuropathy (LHON) was the first maternally inherited disease to be associated with a mtDNA point mutation [123]. LHON typically affects young adults, more often males. Visual acuity deteriorates over a period of days/weeks as a consequence of rapid, painless loss of central vision in one eye, usually followed by the other eye.
The three most frequent mtDNA mutations associated with LHON are the 11778G>A, 3460A>G and 14484T>C mutations [123, 124]. All the LHON mutations which have been proved to be pathogenic affect different mtDNA-encoded subunits of complex I. Mutations are usually homoplasmic, although heteroplasmy can occasionally be found in some families or singleton cases.
Non-syndromic and aminoglycoside-induced sensorineural hearing loss (SNHL) has been both associated with a unique, maternally inherited point mutation at position 1555 (A→G) of the 12S rRNAgene [125].

| Type | Mutation | Clinical | LA | RRF | BIOCHEMISTRY |
|---|---|---|---|---|---|
| Mutations affecting mitochondrial protein synthesis *in toto* | Single deletions | KSS | + | + (COX-) | ↓ I, III, IV |
| | | PEO | + | + (COX-) | ↓ I,III,IV |
| | | PS | - | - | |
| | | MELAS | + | + (COX+) | ↓I, III, IV |
| | tRNA mutations | MERRF & other multisystemic | + | + (COX-) | ↓ I, III, IV |
| | | myopathy | + | + (COX-) | ↓ I, III, IV |
| Mutations in protein-coding genes | | LHON | - | - | ↓ I (+/-) |
| | ND genes | MELAS, LS | + | +/- (COX+) | ↓ I |
| | | myopathy | +/- | + (COX+) | ↓ I |
| | Cyt b | multisystemic | +/- | + (COX+) | ↓ III |
| | | myopathy | + | + (COX+) | ↓ III |
| | COX genes | multisystemic | +/- | +/- (COX-) | ↓ IV |
| | | myopathy | + | + (COX-) | ↓ IV |
| | ATPase 6 gene | NARP/MILS | +/- | - | ↓ V |

**Table 1.1:** clinical, morphological and biochemical features of mtDNA-related disorders [126]. LA= Lactic Acidosis, RRF= Ragged Red Fibers.

### 1.6 Cybrids

No procedures are available to generate disease models by direct introduction of mutated mtDNA into cells or mouse embryos. The only procedures to introduce exogenous mtDNA are microinjection of mitochondria or cell-fusion techniques.

Cytoplasmic hybrids (cybrids) are created by fusion of enucleated cells (cytoplast) with mtDNA depleted cells ($\rho^0$ cells).

King and Attardi succeeded in deplete human cell line of endogenous mtDNA. These authors first reported creation of human osteosarcoma $\rho^0$ lines, which they named 143B101 and 143B206 [127]. These lines were generated through chronic exposure of the parental cell line to ethidium bromide. Ethidium bromide exposure results in pyrimidine auxotrophy, which can be overcome by supplementing cells with uridine. Pyrimidine auxotrophy is likely a consequence of the fact that dihydroorotate dehydrogenase enzyme activity is coupled to activity of the electron transport chain. Dihydroorotate dehydrogenase, which is localized within mitochondria, catalyzes the conversion of dihydroorotic acid to orotic acid. Uridine is a pyrimidine pathway metabolite generated downstream of this synthetic step and therefore bypasses the pyrimidine synthesis block that results from elimination of electron transport chain activity.

It is important to note that although these cells no longer contained detectable mitochondrial DNA, mitochondrial organelles nevertheless persisted.

In addition to showing uridine auxotrophy, both 143B osteosarcoma $\rho^0$ lines were also auxotrophic for pyruvate [128]. The leading explanation for pyruvate auxotrophy relates to issue of anaerobic cell redox modulation. An absence of oxidative phosphorylation deprives cells of a major NADH oxidation pathway. Theoretically, overreliance on glycolysis could shift cell NADH to $NAD^+$ ratio excessively towards NADH. Supplying excess pyruvate should promote regeneration of $NAD^+$ by inducing metabolism of pyruvate to lactate by lactate dehydrogenase.

King and Attardi [127] also demonstrated repopulation of their osteosarcoma $\rho^0$ lines with exogenous mtDNA. Two approaches were identified to repopulate $\rho^0$ cells with mtDNA. One approach utilized PEG-mediated fusion of enucleated cytoplast with $\rho^0$ cells. The other approach involved direct microinjection of isolated mitochondria into $\rho^0$ cells. The use of platelets in place of enucleated cells is a variation of the PEG fusion method [129]. This modification capitalized on the fact that platelets do not contain nuclei but do contain mitochondria and therefore mtDNA. For this approach, platelets are essential treated as prepackaged cytoplast.

During the early 1990s, the cybrids technique was applied to the study of mitochondrial encephalomyopathy diseases. Examples include MELAS and MERRF syndromes.

The cybrids approach was used to assess the impact of these mutations on oxidative phosphorylation and to address the threshold of mutational burden needed to cause an abnormal biochemical phenotype. Cybrids approaches have also proven useful in studies of mtDNA-nuclear DNA compatibility [130].

In our work we created heteroplasmic MELAS A3243G mutant mtDNA cybrids by fusing rhabdomyosarcoma (RD) $\rho^0$ cells with cytoplasts derived from osteosarcoma (206) cybrids [131]. These osteosarcoma cybrids had 74% MELAS A3243G mutation (206 MELAS 74%).

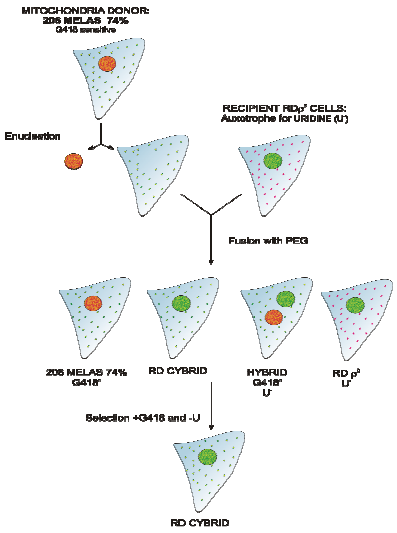


**Figure 1.7:** cybrids production. Host $\rho^0$ cells receive mtDNA from cytoplasts. Selection for 20 days with G418 and without uridine allows to isolate RD cybrids.

Cybrids were selected by adding G418 to the culture medium and by removing uridine from the culture medium. G418 is an aminoglycoside antibiotic similar to gentamicin, neomycin and kanamycin, which blocks polypeptide synthesis by inhibiting phospholipase D (PLD) and consequently the entire protein elongation. G418 resistance stably integrated gene was only present in mitochondria recipient cells (in this work RD $\rho^0$ cells) and so it permitted to select against the not enucleated 206 MELAS 74% cells and against those hybrids containing both nuclei. While, since $\rho^0$ cells are auxotroph for uridine, the lack of uridine in the culture medium allowed to eliminate $\rho^0$ cells that didn't fuse with cytoplasts.

## 1.7 ROS

Reactive oxygen species (ROS) is a collective term that describes the chemical species that are formed upon incomplete reduction of oxygen and includes the superoxide anion $O^{\cdot-}_2$ , hydrogen peroxide $H_2O_2$, the hydroxyl radical $HO^{\cdot}$, $^1O_2$ (singlet oxygen), and perhydroxyl radical ($HO_2^{\cdot}$, the protonated form of superoxide). ROS are thought to mediate the toxicity of oxygen because of their greater chemical reactivity with regard to oxygen. They also operate as intracellular signalling molecules, a function that has been widely documented but is still controversial [132].

The complete reduction of $O_2$ via the mitochondrial electron transport chain involves the transfer of four electrons to $O_2$ generating two equivalents of water. Incomplete reduction of $O_2$ will result in the formation of $O^{\cdot-}_2$ (one-electron reduction), and $H_2O_2$ (two-electron reduction) [133].

Oxygen radicals can be produced into mitochondria by the respiratory chain [134], in the endoplasmatic reticulum by the cytochrome P450 oxido-reductase [135], in the plasmatic membrane where is localized a respiratory electron chain with not known functions [136], in the cytosol by different enzymes such as xanthine oxidase, NADPH oxidase or monoaminooxidase [137].

The mitochondrial electron transport chain is remarkably efficient at reducing $O_2$ to $H_2O$. However, during electron transport in the respiratory chain, electrons can "leak" from the respiratory complexes and be passed one at a time to molecular oxygen ($O_2$) to form low amounts of superoxide anion $O^{\cdot-}_2$. Under normal conditions only ~1% of $O_2$ acting as the terminal electron acceptor in this system is though to be converted to the side products $O^{\cdot-}_2$ and $H_2O_2$.

Reactive species are produced not only from $O_2$, but also from small molecules containing oxygen together with nitrogen. These compounds are often referred to as reactive nitrogen-containing species (RNS). A biologically important RNS is the signalling molecule nitric oxide ($^{\cdot}NO$), synthesized by nitric oxide synthase isozymes. Another biologically important RNS is peroxynitrite ($ONOO^-$) generated by the rapid reaction of $^{\cdot}NO$ with $O^{\cdot-}_2$. Peroxynitrite is unstable and either rapidly rearranges to the much more stable nitrate ($NO_3^-$) or loses O to form the relatively stable nitrite ($NO_2^-$). Peroxynitrite also reacts rapidly with ambient $CO_2$ to form carbonate radical ($CO_3^{\cdot-}$) and nitrogen dioxide ($NO_2^{\cdot}$). The $NO_2^{\cdot}$ reacts with $O^{\cdot-}_2$ at the diffusion-controlled rate to form the strong oxidant peroxynitrate ($O_2NOO^-$). $NO_2^{\cdot}$ can nitrate protein tyrosine residues (P-Tyr) with subsequent formation of nitrotyrosine residues. Nitration of brain proteins is a consistent feature of neurodegenerative disease [133, 138].

Oxidative stress is caused by an imbalance between the production of reactive oxygen and a biological system's ability to readily detoxify the reactive intermediates or easily repair the resulting damage. Generally, harmful effects of reactive oxygen species on the cell are most often: damage of DNA; oxidations of polydesaturated fatty acids in lipids; oxidations of amino acids in proteins.

In normal conditions cells have mechanisms for protection against radicals. These protective systems can be enzymatic and non enzymatic antioxidants. Three groups of enzymes play significant roles in protecting cells from oxidant stress: superoxide dismutase (SOD), catalase (CAT), glutathione peroxidase (GPx), glutathione reductase (GR).

SODs catalyze the conversion of two superoxides into hydrogen peroxide and oxygen. SOD accelerates this detoxifying reaction roughly 10,000-fold over the non-catalyzed reaction.

$$O^{\cdot -}_2 + O^{\cdot -}_2 \xrightarrow{SOD} O_2 + H_2O_2$$

SODs are metal-containing enzymes that depend on a bound manganese, copper or zinc for their antioxidant activity. In mammals, the manganese-containing enzyme is most abundant in mitochondria, while the zinc or copper forms predominant in cytoplasm [139, 140]. The hydrogen peroxide is substantially less toxic that superoxide but is dangerous in the cell because it can easily transform into a hydroxyl radical (via reaction with $Fe^{2+}$: Fenton chemistry), one of the most destructive free radicals.

Catalase, degrades hydrogen peroxide to water and oxygen, and hence finishes the detoxification reaction started by SOD.

Glutathione peroxidase, like catalase, reduces hydrogen peroxide by transferring the energy of the reactive peroxides to a very small sulfur containing protein called glutathione. The selenium contained in these enzymes acts as the reactive center, carrying reactive electrons from the peroxide to the glutathione. Some GPx have also the function of detoxification from hydroperoxide lipids produced by ROS on the membrane. Glutathione reductase (GR) regenerates reduced glutathione [139].

Non-enzymatic antioxidants of particular importance are vitamin E, Vitamin C or ascorbic acid, Glutathione. Vitamin E is the major lipid-soluble antioxidant, and plays a vital role in protecting membranes from oxidative damage. Its primary activity is to trap peroxy radicals in cellular membranes. Vitamin C is a water-soluble antioxidant that can reduce radicals from a variety of sources. It also appears to participate in recycling vitamine E radicals. Interestingly, vitamin C also functions as a pro-oxidant under certain circumstances. Glutathione may well

be the most important intracellular defence against damage by reactive oxygen species. It is a tripeptide (glutamyl-cysteinyl-glycine). The cysteine provides an exposed free sulphydryl group (SH) that is very reactive, providing an abundant target for radical attack. Reaction with radicals oxidizes glutathione, but the reduced form is regenerated in a redox cycle involving glutathione reductase and the electron acceptor NADPH [141].
Other molecules that function as antioxidants are bilirubin, uric acid, flavonoids and carotenoids.
Growing evidence suggests that ROS, especially $H_2O_2$, contribute to cell signalling. Indeed, far from being a noxious waste product of aerobic existence, $H_2O_2$ (a "much misunderstood and maligned molecule") is now regarded as crucial in signaling of redox-sensitive proteins [142]. For example it leads to the activation of protein tyrosine kinases followed by the stimulation of downstream signalling systems including MAP kinase and PLC-γ.

**1.8 Uridine**

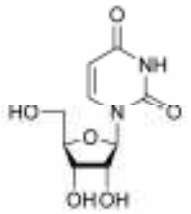


Uridine, a pyrimidine nucleoside essential for the synthesis of RNA and biomembrane, is a crucial element in the regulation of normal physiological processes as well as pathological states [143]. Pyrimidines are synthesized de novo in mammalian cells through a multistep process starting from glutamine and carbon dioxide to form, the pyrimidine ring in the second to last intermediate, orotic acid, which is then converted to its nucleotide form in the presence on 5-Phosphorylribose 1-pyrophosphate (PRPP). From the degradation of the nucleic acids and nucleotides a large portion of the pyrimidines are salvaged. The relative contribution of de novo synthesis and salvage pathway to the maintenance of the nucleotide pools varies in different cells and tissues. A crucial difference between purine and pyrimidine metabolism is that purines are recycled from their bases while pyrimidines are salvaged from their nucleosides, particularly uridine [143].
Besides the critical role of uridine in the synthesis of RNA and bio-membranes, through the formation of pyrimidine-sugar conjugates, experimental and clinical evidence suggests a role for uridine in regulating a series of biological functions [144]. For example in the area of the peripheral nervous system, uridine appears to have a modulatory role. It has been shown to hyperpolarize amphibian ganglia

and rat superior cervicalganglia at submillimolar concentrations, possibly resulting in an inhibitory activity. Several clinical observations indicate the crucial function of pyrimidine nucleoside salvage in maintenance of normal CNS activity [145]. Deficiencies in the catabolism of pyrimidines due to impaired activity of one of the steps in the catabolic pathway, such as dihydropyrimidine dehydrogenase or β-ureidopropionase, have resulted in autism, convulsions, mental retardation and decreased motor coordination [145].

Aside from the 'physiological' effects that we have just briefly outlined, uridine appears to have remarkable functions in tissues under stress or pathological situations and in the clinical setting. In hearts subjected to ischemia, perfusion with uridine rapidly restored myocardial ATP levels, glycogen and UDPG [146]. Similarly, uridine perfusion resulted in the maintenance of brain metabolism during ischemia or severe hypoglycemia. Furthermore, uridine induced recovery from neuronal degeneration produced by diabetic neuropathy [143].

### 1.9 Creatine

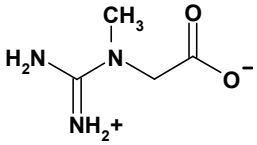


Creatine is nitrogenous organic acid which naturally occurs in vertebrates and helps to supply energy to muscle and nerve cells. Creatine was identified in 1832 when Michel Eugène Chevreul discovered it as a component of skeletal muscle. Creatine by way of conversion to and from phosphocreatine is present and functions in all vertebrates, as well as some invertebrates, in conjunction with the enzyme creatine kinase. The phosphocreatine/creatine kinase system also acts as an intracellular energy transport system from those places where ATP is generated (mitochondria and glycolysis) to those places where energy is needed and utilized, e.g. at the myofibrils for muscle contraction, at the sarcoplasmic reticulum (SR) for calcium pumping and many more biological processes which depend on ATP.

In the human body, approximately half of the daily creatine is biosynthesized by the use of parts from three different aminoacids: arginine, glycine and methionine. The rest is taken in by alimentary sources mainly from fresh fish and meat. 95% of it is later stored in the skeletal muscles, with the rest in the brain, heart and testes. Since vegetables do not contain creatine, vegetarians clearly show lower levels of muscle creatine which rise upon creatine supplementation more than meat-eaters [147].

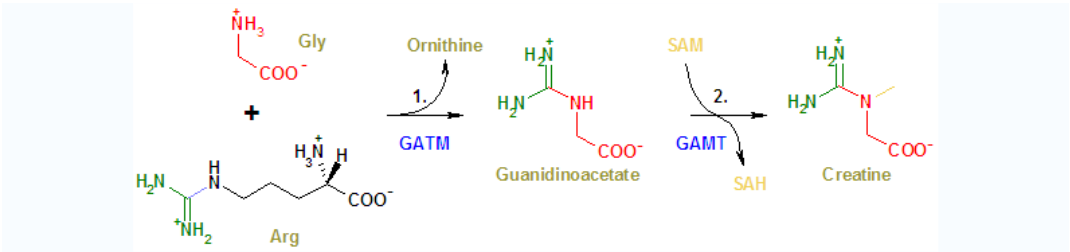


**Figure 1.8:** pathway for the synthesis of creatine Arg - Arginine; GAMT - Guanidinoacetate N-methyltransferase; GATM - Glycine amidinotransferase; Gly - Glycine; Met - Methionine; SAH - S-adenosyl homocysteine; SAM - S-adenosyl methionine.

Creatine supplementation has been, and continues to be, investigated as a possible therapeutic approach for the treatment of muscular, neurological and neuromuscular diseases (arthritis, congestive heart failure, disuse atrophy, gyrate atrophy, McArdle's disease Huntington's disease, miscellaneous neuromuscular diseases, mitochondrial diseases, muscular dystrophy, neuroprotection).

Two studies have indicated that creatine may be beneficial for neuromuscular disorders. First, a study demonstrated that creatine was twice as effective as the prescription drug riluzole in extending the lives of mice with the degenerative neural disease amyotrophic lateral sclerosis (ALS, or Lou Gehrig's disease). The neuroprotective effects of creatine in the mouse model of ALS may be due either to an increased availability of energy to injured nerve cells or to a blocking of the chemical pathway which leads to cell death. Secondly, creatine has been demonstrated to cause modest increases in strength in people with a variety of neuromuscular disorders [148].

### 1.10 N-acetylcysteine (NAC)

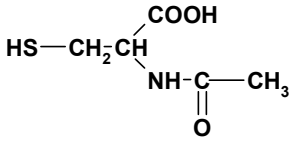

N-acetylcysteine (NAC) is the acetylated precursor of the amino acid L-cysteine. Historically it has been used as a mucolytic agent in chronic respiratory illness. Recently, animal and human studies of NAC have shown it to be a powerful antioxidant and a potential therapeutic agent in the treatment of cancer, heart disease, HIV infection, heavy metal toxicity and other diseases characterized by free radicals and oxidant damage.

NAC's effectiveness is primarily attributed to its ability to act intracellularly as a source of sulfhydryl groups. As a source of sulfhydryl groups, NAC stimulates glutathione (GSH) synthesis, enhances glutathione S-transferase activity, promotes liver detoxification by inhibiting xenobiotic biotransformation, and is a powerful nucleophile capable of scavenging free radicals [149].

### 1.11 RNA interference (RNAi)

RNA interference (RNAi) is a powerful, naturally occurring biologic mechanism of post-transcriptional gene silencing mediated by either degradation or translation arrest of target RNA. The discovery that 21-23 nucleotide RNA duplexes (small-interfering RNAs [siRNAi]) mediate RNAi in mammalian cells has revolutionized functional genomics, as well as drug target identification and validation.

Molecular mechanisms of RNAi action have been investigated intensively in a variety of organisms including fungi, hydra, plants and amphibians. The unique feature of RNAi is its exquisite sequence specificity; introduction of a single base mismatch in the siRNA structure abrogates its RNAi effect [150].

There are two types of naturally occurring small RNAs that can act as gene silencers: short, interfering RNA (siRNA) and microRNA (miRNA) [151].

**siRNA.** The pathways of RNA interference can be broken down into 2 main phases. In the first phase, long, double-stranded RNA (dsRNA) is recognized and processed by Dicer, an Rnase III enzyme, into duplexes of siRNA of 21 to 24 nucleotides (nt) in length. Exogenous synthetic siRNAs or endogenous expressed siRNAs can also be incorporated into the RNA-induced silencing complex (RISC), thereby bypassing the requirement for dsRNA processing by Dicer. The most ubiquitous siRNA consists of a 19-29 nt dsRNA molecule or short hairpin dsRNA (shRNA) that, when transfected into cells, can mediate transient gene silencing. In the second phase, siRNAs are incorporated into the multiprotein RISC. A helicase in RISC unwinds the duplex siRNA, which then pairs by means of its unwound antisense strand to messenger RNAs (mRNAs) that bear a high degree of sequence complementarity to the siRNA. Within the RISC, an unidentified Rnase (Slicer) proceeds to degrade the mRNA at sites not bound by the siRNA. Cleavage of the target mRNA begins at single site 10 nt upstream of the most 5' residue of the siRNA-target mRNA duplex [150].

**miRNA.** miRNAs represent a class of noncoding, small RNAs 21-25 nucleotides in length thought to function in translational control or other undefined mechanisms of genetic regulation [152]. miRNA processed sequentially from primary miRNA precursor transcripts regulate gene expression at the post-transcriptional level. The precursor of primary miRNAs is transcribed in the nucleus. The dsRNA-specific ribonuclease Drosha digests the primary miRNA in the nucleus to form another precursor miRNA before being exported to the cytoplasm. Exportin-5 (Exp5) is responsible for export of precursor miRNAs from the nucleus to the cytoplasm. Like siRNAs, miRNAs are processed by Dicer.

Further processing by the Dicer protein creates the mature miRNA, a strand of which is incorporated into a ribonucleoprotein complex, known as the miRNP, which is similar, if not identical, to the RISC. Base pairing between the miRNA and its target directs RISC to either destroy the mRNA or attenuate its translation into protein [150].

# 2 AIMS

This project aimed to gain insights into the mechanism of mitochondrial segregation occurring in mitochondrial diseases using an in vitro model of mitochondrial myopathy. The study aimed to obtain a clear understanding of mitochondrial dynamic and its impact on mtDNA segregation, with the final aim to develop rational therapies for mitochondrial disease.

Clinical status of human mitochondrial disorders associated with heteroplasmic mtDNA mutations is greatly dependent on the residual amount of wild-type mtDNA molecules. No clinical symptoms or biochemical respiratory chain defects are detected above a relatively low threshold of wild-type mtDNA proportion [101]. Therapeutic approaches to human disorders are therefore trying to modify the relative proportion of wild-type and mutant mtDNA [153]. In that prospect a better understanding of conditions and mechanisms by which cells modify their mtDNA mutant amount by a segregation from heteroplasmic to homoplasmic status or by increasing proportion of wild-type mtDNA molecules, could help us better understand the pathogenesis of mitochondrial diseases and could deserve potential consequences regarding therapeutic approaches to human diseases associated with heteroplasmic mtDNA mutations.

The transition A to G at nt 3243 of mtDNA, was originally described in MELAS syndrome, and later reported in association with other distinct maternally inherited phenotypes, including PEO, diabetes with or without deafness and hypertrophic cardiomyopathy. Although the mechanism at the basis of the MELAS pathology has been the subject of intensive analysis, the essential pathophysiological pathways that determinate the differential distribution of mutant and wild-type mtDNA molecules at cellular level, that affect the derangement of individual tissue and the differences in clinical phenotype remain elusive.

To study the mechanism of mutant mtDNA segregation we used an in vitro model of mitochondrial myopathy: the rhabdomyosarcoma transmitochondrial hybrids (cybrids) harbourig A3243G mtDNA mutation.

Heteroplasmic RD cybrids were established by fusing human rho0 cell lines with human muscle nuclear background and enucleated cells harbouring 74% mutant mtDNA in the gene encoding $tRNA^{Leu\ (UUR)}$: MELAS mutation.

The research work can be divided in three parts corresponding to the three years of the study.

## 2.1 First part

**Generation and characterization of heteroplasmic cybrids in muscle nuclear background (RD-cybrids)**

14 RD cybrids clones harbouring heteroplasmic MELAS A3243G mtDNA mutation were generated from enucleation of 74% MELAS 206 cybrids cells. Their following characterizations were performed: percentage of mutant mtDNA molecule by hot-PCR, that was set up to better evaluate the proportion of mutant mtDNA; nuclear polymorphism analysis to confirm the nuclear background; myogenic capacity; $O_2$ consumption.

**Functional and molecular responses to energetic stress in homoplasmic and heteroplasmic RD cybrids**

To verify if reduced glucose content in the medium might influence percentage of mutant mtDNA content, growth regimes with normal glucose 25mM (G25) and decreased glucose 10mM (G10), 5mM (G5) were applied to undifferentiated 0% (wt), 92% and 83% mutant MELAS RD cybrids cells. Everyone of these subgroups included four different conditions: plus uridine, plus creatine (100μM) and plus both uridine (50μg/ml) and creatine (100μM). The cells cultured in these growth regimes were tested for the following parameters: growth rate; oxygen consumption; ROS production; percentage of mtDNA mutation; mtDNA amount.

## 2.2 Second part

To explain why heteroplasmic MELAS mutant RD cybrids survived better than wild-type cells in low glucose, we hypothesized a compensative induction of energy enzymes, as reported by Heddi [154]. To assess this hypothesis an other set of experiments was performed: 0%, 83%, 92% and 99% RD cybrids were grown in normal (G25) and low (G5) glucose, supplemented or not with uridine for 8-20 days.

The following physiological, biochemical and molecular parameters were tested:

- Growth rate, expressed as duplication time
- Oxygen consumption and respiratory control ratio (RCR) factor
- Activities of phosphofructokinase, lactic dehydrogenase, succinate dehydrogenase (SDH), cytochrome C oxidase (COX), citrate synthase (CS)
- Amount of mtDNA
- Percentage of mutant mtDNA

## 2.3 Third part

Mitochondrial dynamic and fission-fusion events may interfere with mtDNA complementation and may influence the mtDNA segregation toward homoplasmic status. To analyze the impact of proteins involved in mitochondrial fission-fusion on segregation of mtDNA, a set of experiments was performed focused on the modulation of expression levels of OPA1, Drp1 and hFis1 by RNA interference. OPA1, Drp1 and hFis1 genes were permanently silenced by RNAi technique in RD cybrids with 0%, 74%, 83% and 92% MELAS mutant mtDNA. The resulting clones were characterised for physiological, biochemical and molecular analysis .

At the beginning it was hypothesized that an increase in mitochondrial fusion, could favour a shift in mtDNA with an increase in wild-type percentage of mtDNA.

90% and 80% heteroplasmic cybrids were transfected with pSilencer™ 2.1-U6 hygro and pSilencer™ 2.1-U6 hygro OPA1-RNAi (gift of Dr. Luca Scorrano, Venetian Institute of Molecular Medicine, Padua) to obtain control clones and clones with OPA1 down expression respectively, as described in paragraph 3.1.12. 90%, 80% and 70% heteroplasmic cybrids were also transfected with pREP4 hygro, pREP4 hygro Drp1-RNAi and pREP4 hygro hFis1-RNAi (gift of prof. Richard J. Youle, National Institute of Health, Bethesda) to obtain control clones and clones with Drp1 and hFis1 down expression respectively. Table 2.1 resumes the abbreviations used for these clones.

| VECTOR / CLONE | pSilencer™ 2.1-U6 hygro | pSilencer™ 2.1-U6 hygro OPA1-RNAi | pREP4 hygro | pREP4 hygro Drp1-RNAi | pREP4 hygro hFis1-RNAi |
|---|---|---|---|---|---|
| **RD MELAS 90% cybrids** | 90-Sil | 90-OPA | 90-Rep | 90-Drp | 90-Fis |
| **RD MELAS 80% cybrids** | 80-Sil | 80-OPA | 80-Rep | 80-Drp | 80-Fis |
| **RD MELAS 70% cybrids** | | | 70-Rep | 70-Drp | 70-Fis |

**Table 2.1:** abbreviations used to indicate clones transfected with the empty vectors pSilencer™ 2.1-U6 hygro and pREP4 hygro and with pSilencer™ 2.1-U6 hygro OPA1-RNAi, pREP4 hygro Drp1-RNAi and pREP4 hygro hFis1-RNAi.

# 3 MATERIALS AND METHODS

## *3.1 Cell biology*

### 3.1.1 Materials for cell culture

All work has been done under sterile conditions using a sterile hood (SterilGARD®III Advance The Baker Company). Cells were grown in a humidified $CO_2$ incubator (Haereus) at 37°C, and were observed with an inverted microscope (ZEISS IM35). Disposable sterile plastic articles (dishes, flasks, pipettes, tubes and filtered tips) were from Gibco. Glass Pasteur pipettes were sterilized in autoclave for 30 minutes at 121°C under 1 atm steam pressure.

### 3.1.2 Cell lines

Several immortalized cell lines were used for the experiments:

| CELL LINE | NUCLEAR BACKGROUND | MITOCHONDRIAL GENOTYPE | NAME USED IN THIS WORK |
|---|---|---|---|
| ***PARENTAL RD Rho$^{+}$***[a] | Rhabdomyosarcoma | Wild-type mtDNA | ***RD ($\rho^{+}$)*** |
| ***RD Rho$^{0}$***[b] | Rhabdomyosarcoma | w/o mtDNA | ***RD Rho$^{0}$ ($\rho^{0}$)*** |
| ***RD WT CYBRIDS*** | Rhabdomyosarcoma | 100% wild-type mtDNA (from healthy subject's fibroblasts) | ***WT7*** |
| ***206 MELAS 74% CYBRIDS***[d] | Osteosarcoma | 74% MELAS mutant mtDNA | ***206 MELAS 74%*** |
| ***RD MELAS 99% CYBRIDS***[b] | Rhabdomyosarcoma | 99% (homoplasmic) MELAS mutant mtDNA (from 55% mutant fibroblasts of MELAS patient) | ***RD MELAS 99%*** |
| ***HETEROPLASMIC RD CYBRIDS*** | Rhabdomyosarcoma | Heteroplasmic for MELAS (from 206 MELAS 74% cybrids) | ***RD HETEROPLASMIC MELAS*** |

a. Rhabdomyosarcoma (RD Rho$^{+}$) cells were a gift of prof. Salviati (Biomedical Sciences Department, University of Padua).
b. RD $\rho^{0}$ and RD cybrids MELAS 99% were established in our laboratory [131].
c. RD WT cybrids were a gift of prof. J. Poulton (John Radcliff Hospital, University of Oxford).
d. 206 cybrids MELAS 74% were a gift of prof. I.J. Holt (MRC, Dunn Human Nutrition Unit, Cambridge, UK).

## 3.1.3 Media

### 3.1.3.1 Media for cell cultures

Every media has been prepared using sterile filtered cups with a 0.22μm cut-off to avoid bacteria contaminations.

Parental RD and RD $\rho^0$ cells were grown in Dulbecco's modified Eagle medium (DMEM) containing 4.5g/liter glucose, 110mg/liter pyruvate, supplemented with foetal calf serum (FCS) (previously decomplemented by keeping it at 56°C for 30 minutes), penicillin and streptomycin, Amphotericin B, aminoacids, L-glutamine and vitamins.

| | **PARENTAL RD Rho$^+$ MEDIUM** | **RD Rho$^0$ MEDIUM** |
|---|---|---|
| **DMEM** (High glucose 4.5g/l-110mg/ml pyruvate) (Gibco, cat. n. 41966-029) | 90% | 70% |
| **FCS** | 10% (Euroclone, cat. n. ECS0180L) | 30% (Gibco, cat. n. ECS0180L) |
| **PS**[a] (Biochrom, cat. n. A2213) | 1X | 1X |
| **Amphotericin B** (Bristol-Myers-Squibb, 50mg/ml Cat. n. J02AA01) | 3.33μg/ml | 3.33μg/ml |
| **Aminoacids**[b] (Gibco, Cat. n. 51051-019) | 1X | 1X |
| **L-glutamine**[d] (Sigma, cat. n. G-5763) | 0.296mg/ml | 0.296mg/ml |
| **Vitamins**[d] (Seromed, Cat. n. K0373) | 1X | 1X |
| **Uridine**[e] (Sigma, cat. n. U-3003) | - | 50μg/ml |

[a.] PS (Penicillin and Streptomycin) was provided as 100X solution. 1X solution has 100units/ml penicillin and 0.1mg/ml streptomycin.

[b.] Aminoacids were provided as 50X solution (Amioacids 50X contain 6320mg/ml L-Arginine, 1200mg/ml L-Cysteine, 2100mg/ml L-Histidine hydrochloride-$H_2O$, L-Isoleucine, 2260mg/ml L-Leucine, 3625mg/ml L-Lysine, 775mg/ml L-Methionine, 1650mg/ml L-Phenylalanine, 2380mg/ml L-Threonine, 510mg/ml L-Tryptophan, 1880mg/ml L-Tyrosine and 2340mg/ml L-Valine prepared in distilled water).

[c.] Vitamins were provided as 100X solution (Vitamins 100X contain 100mg/ml Choline chloride, 100mg/ml D-Calcium pantothenate, 100mg/ml Folic Acid, 200mg/ml i-Inositol, 100mg/ml Nicotinamide, 100mg/ml Pyridoxal hydrochloride, 10mg/ml Riboflavin, 100mg/ml Thiamine hydrochloride and 8500mg/ml Sodium Chloride).

[d.] L-glutamine solution was prepared dissolving 29.6mg of L-glutamine powder for 1ml of sterile water.

[e.] Uridine was prepared dissolving 50mg of uridine powder in 10ml of sterile water.

### 3.1.3.2 Dyalization of FCS

Dialysis of decomplemented serum is done in order to remove uridine. In this way the growth of $\rho^0$ cells is avoided.

500ml of FCS are inserted into a Spectra/Por® 3 membrane (Spectrum Lab. Inc. cat.132720) with a 3500 Da cut-off and then dialysed for ten cycles of 1 hour each at 4°C in 5 litres of 1X dialysis buffer prepared diluting 1:10 a 10X stock solution (1.5M NaCl, 50mM KCl, 250mM Tris, pH 7.4) in constant agitation.

After this procedure the FCS is aliquoted in 50mL Falcon and stored at -20°C.

The following scheme reports the two principal cybrids media used:

| | CYBRIDS MEDIUM | REACH CYBRIDS MEDIUM |
|---|---|---|
| **DMEM** (high glucose 4.5 g/l-110 mg/ml pyruvate) (Gibco, cat. n. 41966-029) | 85% | 70% |
| **Dialyzed FCS** (Gibco, cat. n. ECS0180L) | 15% | 30% |
| **PS** (Biochrom, cat. n. A2213) | 1X | 1X |
| **Amphotericin B** (Bristol-Myers-Squibb, 50mg/ml Cat. n. J02AA01) | 3.33µg/ml | 3.33µg/ml |
| **Aminoacids** (Gibco, n. 51051-019) | 1X | 1X |
| **L-glutamine**[c] (Sigma, cat. n. G-5763) | 0.296mg/ml | 0.296mg/ml |
| **Vitamin** (Seromed, Cat. n. K0373) | 1.5X | 1.5X |
| **(FGF)** (human FGF-basic) (Pepro Tech EC Ltd Cat. n. 100-18B) | - | 25 ng/mL |
| **(EGF)** (Pepro Tech EC Ltd Cat. n. 100-15) | - | 10ng/mL |

### 3.1.3.3 Differentiation media

Rhabdomyosarcoma cells maintain the capacity to differentiate into myotubes using differentiation medium. Cells differentiate in 6-9 days in presence of TPA (Phorbol 12-Myristate 13-Acetate 2mM in DMSO).

TPA was added in the medium after filtering and the medium was kept protected from light.

| | **PARENTAL RD Rho$^{+}$ DIFFERENTIATION MEDIUM** | **RD Rho$^{0}$ DIFFERENTIATION MEDIUM** |
|---|---|---|
| **DMEM** (Gibco, cat. n. 41966-029) or **HAM'S F14** (Euroclone cat. n. EC M0136L) | 98% | 98% |
| **FCS** (Gibco, cat. n. ECS0180L) | 2% | 2% |
| **PS** (Biochrom, cat. n. A2213) | 1X | 1X |
| **Amphotericin B** (Bristol-Myers-Squibb, 50mg/ml Cat. n. J02AA01) | 3.33µg/ml | 3.33µg/ml |
| **Insulin**[a] (Sigma, cat.n. I 5500) | 10µg/ml | 10µg/ml |
| **Uridine** (Sigma, cat. n. U-3003) | - | 50µg/ml |
| **TPA**[b] (Sigma, cat. n. P8139) | 100nM | 100nM |

[a.] Insulin was prepared mixing in order: 12ml of HCl 1N, 88 ml of milliQ water and 100mg of insulin. The solution was filtered, aliquoted and stored at -20°C.

[b.] TPA was added after filtration

## 3.1.4 Culturing procedures

### 3.1.4.1 Proliferating cells

Parental, Rho$^{0}$ and cybrid RD cells were splitted every 2 days using trypsin-EDTA (Biochrom AG, Cat. n. L2153) and maintained at low confluence. They were seeded at 30-40% confluence.

They must reach maximum 60-70% confluence to avoid spontaneous fusion of cells, that would be lost at the following trypsinisation. The best start concentration is 80.000 cells/cm2.

### 3.1.4.2 Differentiation

For differentiation, cells were seeded according to the following table and differentiation medium was added the day after. Usually RDρ$^{+}$ and WT (0% mutant) RD cybrids differentiated after 5-6 day, whereas RDρ$^{0}$ and MELAS mutant RD-cybrids needed 8-9 days.

| | Cells for Dish 35∅ | Cells for Dish 60∅ | Cells for Dish 100∅ |
|---|---|---|---|
| **RD** | 30-50.000 | 150.000 | 400.000 |
| **RD rho0** | 80-100.000 | 200.000 | 500.000 |
| **WT RD cybrids** | 30-50.000 | 150.000 | 400.000 |
| **Mutated RD cybrids** | 80-100.000 | 200.000 | 500.000 |

## 3.1.5 Cells counting

Cell counting is done using a Burker chamber.

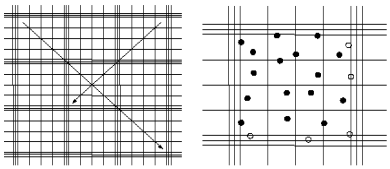

20µl, from cells resuspended in a exact volume of PBS, are loaded on the Burker chamber. Usually cells in 5 of 9 square are counted. The average of cells counted is divided per 64. The value obtained corresponds to millions of cells in 1ml.

i.e. cells resuspended in 10ml of PBS;
cells per square: 30, 35, 29, 32, 34; Average: 32
32/64=0.5 $0.5x10^{6}$=500.000 cells/ml
500.000 cells x 10ml=5.000.000 cells

## 3.1.6 Cell growth rate

In order to calculate the growth rate of the cell lines, cells were seeded and then collected at different times. Cell doubling time was estimated as described in Methods in Enzymol [155] using the following formula:

$$doubling\ time = \frac{\Delta\, time}{log_2(cells\ at\ \ final\ time) - log_2(cells\ at\ initial\ time)}$$

### 3.1.7 Creation and selection of heteroplasmic cybrid cell lines

MATERIALS:

- Sterile 1X PBS
- Sterile 1X tripsyn-EDTA
- Centrifuge tubes with diameter of 6cm (ETO sterilized)
- Beckman Coulter™ AVANTI J-25 centrifuge with rotor JA14
- Enucleation medium (DMEM, 5% dialyzed FCS, PS 1X, L-GLUTAMINE 0.296mg/ml and CYTOCHALASIN B (Sigma, Cat. n.C-6762) 10µg/ml in absolute ethanol added after filtration)
- RD $\rho^0$ medium
- PEG 8000 (PolyEthylene Glycol. Sigma, cat. n. P-2139) previously sterilized by autoclaving.
- PEG solution: 1:1 (W/V) PEG and DMEM + 10% DMSO
- DMEM + 10% DMSO solution
- Selection medium (reach cybrid medium supplemented with G418)
- 50mg/ml G418 Sulfate solution (Inalco S.P.A., cat. n. 345812)

All the procedure has been done according to King's and Attardi's protocol [156].

**Mitochondria donor cells**: 4 days before the experiment, 12 dishes (35mm) were seeded with 80000 206 MELAS 74% cybrids in order to have 450000 cells at the time of enucleation. They were cultured in cybrids medium with 15% dialyzed FCS.

**Recipient $\rho^0$ cells:** RD$\rho^0$ cells were maintained in culture avoiding fusion and differentiation until the day of the experiment using RD $\rho^0$ medium. RD$\rho^0$ were resistant to G418 thanks to a previously transfection with G418 resistance vector.

The day before the experiment the rotor JA14 was cleaned and kept at room temperature over night.

All the experiment has been done under strict sterile conditions to avoid contaminations.

**First day: creation of cytoplasts by enucleation of mitochondria donor cells.**

- 6 centrifuge tubes were numbered and filled with 32ml of enucleation medium.
- Each 35mm dish with 206 MELAS 74% cybrids was emptied, cleaned from the outside with absolute ethanol, numbered and immersed upside-

down into the enucleation medium. Tubes were centrifuged for 20 minutes at 7000 rpm at 34°C.

- In the mean time RDρ$^0$ cells were collected with trypsin-EDTA, counted with a Burker chamber, and resuspended with RDρ$^0$ medium to have 450000 cells/ml.
- After the centrifugation, the dishes with enucleated 206 MELAS 74% were recovered and cleaned with absolute ethanol.
- Enucleation was controlled at microscope, and then 1ml of RDρ$^0$ cells suspension was seeded in each dish and incubated at 37°C. The same procedure was repeated for another set of 6 dishes 35mm.

**Second day: fusion of RDρ$^0$ with cytoplasts.**

- cells were washed twice with DMEM, and incubated for 1 minute with 1ml of PEG-DMEM+10% DMSO solution to fuse cells.
- PEG was washed off 3 times with 1ml of DMEM+10% DMSO and cells were incubated at 37°C with 2ml of RDρ$^0$ medium.

**Third day: selection of RD cybrids.**

To select RD cybrids from RDρ$^0$ and 206 MELAS 74%, the day after, cybrids medium lacking uridine and supplemented with 0.5mg/ml G418 was added. The selection was continued for 20 days.

### 3.1.8 Growth regimes in establishing heteroplasmic RD-clones

MATERIALS:

- 10mM creatine (Sigma, Cat. n. C3630; RT) SOLUTION: 11.3mg/10ml of sterile water. Stored in 500µl aliquots at -20°C
- 50mM NAC (Sigma, Cat. n. A9165; store dry at 4°C): Stored in 500µl aliquots at -20°C, thawed maximum two times.

NAC and creatine were added directly in the dishes.

To verify the influence of different compounds on the segregation of MELAS mutant mtDNA, STANDARD medium, medium with 0.5mM NAC or 100µM CREATINE was used at the beginning of selection.

Three sets of experiments, for a total of 30 dishes, were obtained: 8 grown with STANDARD medium, 11 with medium supplemented with 0.5mM NAC and 11 with medium supplemented with 100µM CREATINE.

After about 15 days, clones were picked up scraping the bottom of dishes with pipette's tips and grown in 24 well Corning plates in reach cybrids medium, until obtaining stable cultures in 100mm dishes.
Each clone was then cultivated with cybrids medium. Periodically cells were collected, part was stored frozen in criovials, part seeded and part used to extract DNA to characterize heteroplasmy and nuclear background by PCR.

### 3.1.9 Differentiation assay

Differentiation assays were operated seeding cells in 13mm microscopy glasses (10000 each) with cybrids medium. The following day, cybrids medium was replaced by differentiation medium. Glasses were then used to obtain fluorescence microscopy images by MitoTracker staining or Anti-merosin immunostaining.
To verify differentiation competence in presence of different compounds, clones were seeded in 6 wells Corning plates for cell culture (80000 cells/well) using cybrids medium and the following day, cybrids medium was substituted by differentiation medium. For each plate 2 wells were supplemented with 0.5mM NAC, 100µM creatine or nothing.
Cells were then collected at different times to extract DNA and to verify nuclear background and heteroplasmy by PCR.

### 3.1.10 Growth regimes

MATERIALS:

- 10mM creatine (Sigma, Cat. n. C3630) SOLUTION*:* 11.3mg/10ml of sterile water. Stored in 500µl aliquots at -20°C
- 5mg/ml uridine solution.

Heteroplasmic RD cybrids clones were grown until obtaining a sufficient number to seed 12 dishes 100mm with 500000 cells each. For each kind of medium 2 dishes were used: one supplemented with 100µM creatine and the other with no addition.

| | N (25mM glc) | G 10mM | G 5mM |
|---|---|---|---|
| **DMEM**[a] high glucose 4.5 g/l-110 mg/ml pyruvate (GIBCO, cat. n. 41966-029) | 90% | - | - |
| **DMEM** w/o glucose and pyruvate[b] (Sigma, cat. n. D5030) | - | 90% | 90% |
| **FCS**[c] | 10% | 10% | 10% |
| **PS** | 1X | 1X | 1X |
| **Amphotericin B** | 3.33µg/ml | 3.33µg/ml | 3.33µg/ml |
| **Glutamine** | 0.296mg/ml | 0.296mg/ml | 0.296mg/ml |
| **Glucose**[d] | - | 10mM | 5mM |
| **Pyruvate** (Sigma P2256 100mM) | - | 1mM | 1mM |
| **Final glucose concentration** | 25 mM | 10mM | 5mM |

a. DMEM (GIBCO, cat. n. 41966-029) containing high glucose (4.5g/l) and 110mg/ml pyruvate.
b. For 10ml solution: 83mg of DMEM BASE powder (Sigma, cat. n. D5030), 37mg of $NaHCO_3$ (Merck, cat. n. E06329), 0.1ml of 100X glutamine solution (29.6mg/ml).
c. Dialyzed FCS was used for media w/o uridine, while standard FCS was used when 50µg/ml uridine was added.
d. Glucose 1M 100X solution.

Obtained feeding combinations are resumed below:

| | NORMAL | 10mM GLUCOSE | 5mM GLUCOSE |
|---|---|---|---|
| NORMAL | **N** | **G10** | **G5** |
| 100µM CREATINE[a] | **N+CR** | **G10+CR** | **G5+CR** |
| 50µg/ml URIDINE[b] | **N+U** | **G10+U** | **G5+U** |
| 100µM CREATINE + 50µg/ml URIDINE | **N+U+CR** | **G10+U+CR** | **G5+U+CR** |

a. Creatine (Sigma, cat. n. C3630-100G) 10mM solution (100X) was prepared dissolving 11.3mg of powder in 10ml of sterile water and filtering it with MILLEX® VV 0.1µm filter unit. Creatine was aliquoted in sterile Eppendorfs and stored at –20°C.
b. Uridine (Sigma, cat. n. U-3003) was prepared dissolving 50mg of powder in 10ml of sterile water and filtering it with MILLEX® VV 0.1µm filter unit. It was aliquoted in sterile Eppendorfs and stored at –20°C.

RD cybrids (WT7, A5N and AP4) were grown using these different media up to 25 days. For each set, 12 dishes 100mm were seeded with 500000 cells each.
During the period of the experiment, oxygen consumption, mutation rate and ROS production were measured.

## 3.1.11 Bacteria

### 3.1.11.1 Bacterial culture

Bacteria used during these work were TOP 10 competent bacteria.

Bacteria grew in liquid media Luria Bertani (LB) (Bacto-tryptone 10g/l, extract Bacto yeast 5g/l, Ampicilin 100mg/l pH7) or on agar plate (150g agar/l media) at 37°C (unless differently specified).

Bacteria inoculation and plate was done in semi-sterile conditions, using a Bunsen. Different bacteria stock were preserved at -70°C in 15% glycerol.

### 3.1.11.2 Bacteria transformation for thermal shock

Competent bacteria were thawed out on ice at 4°C. 1-2µl of DNA were added at 50µl of competent bacteria. The thermal shock was gotten thanks to the following different temperatures: 20 minutes on ice at 4°C, 45 seconds at 42°C, 2 minutes on ice at 4°C. Then, 500µl of LB were added and the mix was shaked at 37°C for 1 hour. After shaking, 100µl of mix were plated using a scrape and the plate was incubated over night at 37°C.

## 3.1.12 Transfection

Wild-type and heteroplasmic cybrids were transfected with pSilencer™ 2.1-U6 hygro, pSilencer™ 2.1-U6 hygro OPA1-RNAi (gift of Dr. Luca Scorrano, Venetian Institute of Molecular Medicine, Padua), pREP4 hygro, pREP4 hygro Drp1-RNAi, pREP4 hygro hFis1-RNAi (gift of prof. Richard J. Youle, National Institute of Health, Bethesda).

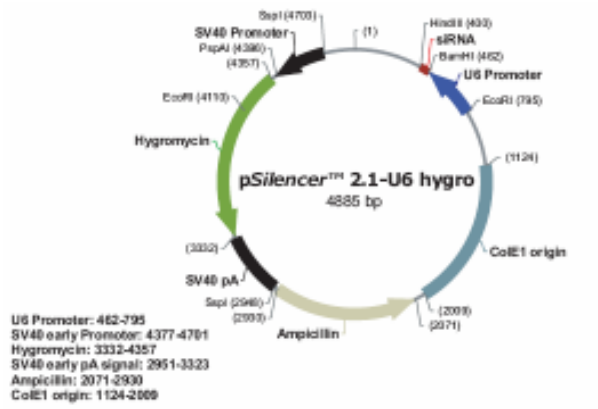


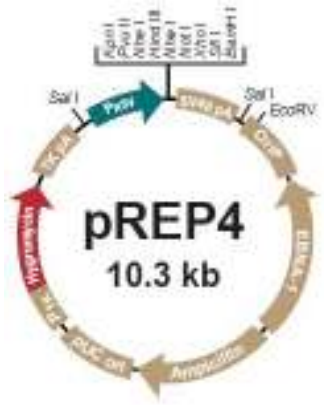


**Comments for pREP4:**
**10349 nucleotides**
RSV LTR promoter: bases 1-571
Multiple cloning site: bases 575-632
SV40 polyadenylation signal: bases 641-882
OriP: bases 1332-3306
EBNA-1 gene (complementary strand): bases 3607-5532
Ampicillin resistance gene: bases 6158-7018
pUC origin: bases 7027-7802
TK promoter: bases 8524-8686
Hygromycin resistance gene: bases 8750-9892
TK polyadenylation signal: bases 9893-10054

The transfection was performed using Lipofectamine™ 2000 from Invitrogen (Cat.No. 11668-027). One day before transfection, $10^5$ cells were seeded in a 6-well format in 2ml of growth medium per well so that they were 90-95% confluent at the time of transfection. DNA-Lipofectamine™ 2000 complexes were prepared as follows: 2µg of DNA were diluted in 250µl of DMEM and 5µl of Lipofectamine™ 2000 were diluted in 250µl of DMEM. The mixtures were incubated for 5 minutes at room temperature. After this incubation, the diluted DNA was combined with the diluted Lipofectamine™ 2000 (total volume was 500µl). The mixture was mixed gently and incubated for 20 minutes at room temperature, to allow the DNA-Lipofectamine™ 2000 complexes to form. 500µl of DNA-Lipofectamine™ 2000 complexes were added to each well containing cells and 2ml of DMEM. 6-well plate was incubated at 37°C in a $CO_2$ incubator and the medium was changed after 4-6 hours. 24 hours after transfection cells were passed into 60mm plates and the following day, the selective medium with 0.5mg/ml hygromycin was added.

## *3.2 Biochemistry*

### 3.2.1 ROS quantification by Amplex method

#### 3.2.1.1 Amplex® ROS assay

MATERIALS:

- Medium without Amphotericin B and phenol red (both of them interfere with Amplex assay): DMEM BASE powder (Sigma, cat. n. D5030) plus glucose (25mM, 10mM or 5mM). For the detailed composition refer to paragraph 3.1.10.
- 100X AMPLEX®RED reagent (10-acetyl-3,7-dihydroxyphenoxazine by Molecular Probes, cat. n. A12222): 20mM solution with DMSO, stored at -20°C protected from light.
- 100X POD (Horseradish Peroxidase, Sigma cat. n. P8250): 1000U/ml working solution from 5000U/ml stock solution. Stored at -20°C.
- 100X OPERATING MIX (protected from light): PBS, 200µM Amplex, 10U/ml POD (i.e. 200µl of PBS, 25µl of Amplex Red and 25µl of POD). 10µl were put in 1ml of medium.

- 2000X APOCYNIN (Sigma, cat. n. A10809): fresh prepared just before the experiment by dissolving 3.32mg in 1ml DMSO. Final concentration is 10µM. 6.5µl were put in 13ml of medium.
- PBS
- 10µM $H_2O_2$

$H_2O_2$ formation was measured by fluorimetric method using Amplex red reagent. In presence of horseradish peroxidase (POD), the Amplex Red reagent reacts with $H_2O_2$ in a 1:1 stoichiometry to produce a stable highly fluorescent product, resorufin ($\lambda_{exc}$ 530nm, $\lambda_{em}$ 585nm).
Fluorescence was measured using a plate reader (FLUOROSCAN ASCENT FL2.5 – LABSYSTEM).
The assay was conducted using undifferentiated cells (seeded 40000 in 12 wells Corning plates 2 days before).
Medium was then substituted with 1ml of medium without phenol red and Amphotericin B.
Each cell sample was analyzed in four wells, two with and two without 10µM apocynin in the medium.
Apocynin (4′-Hydroxy-3′-methoxyacetophenone or acetovanillone) is an inhibitor of plasmatic NADPH oxidase and therefore blocks hydrogen peroxide production at plasma membrane level.
Adding of apocynin requires an incubation of 20 minutes at 37°C.
After the incubation 10µl of operating mix were added to each well and the first measure was suddenly taken (T=0).
Fluorescent signal of the central area of each well was operated every 30 minutes for 90 minutes.
An internal standard curve was made each time by adding to wells different amounts of 10µM $H_2O_2$ and measuring readily the fluorescence. By this measure, transmittance of 1pMol of $H_2O_2$ ($T_{1pM}$) was calculated.
After this assay, cells were controlled at microscope, washed with PBS and prepared for the protein quantization.

### 3.2.1.2 Protein quantization by Bradford assay

MATERIALS:

- BRADFORD 5X solution: (Sigma): diluted 1:5 from stock solution and used 5ml/sample
- 1mg/ml BSA

Comassie® Brilliant Blue G-250 was used for this assay. Reacting with amino and carbossilic groups of proteins its absorbance maximum shifts from 465 (red) to 595nm (blue) in acid solutions. Since colour intensity is not linear with a vast amount of protein concentration, it's necessary to prepare a standard BSA curve for each test. The standard curve is made using increasing quantity of BSA from 0 to 100µg.

Cells in each well were lysed using 300µl of 0.1M NaOH and kept in agitation for 5 minutes.

All the suspension of undifferentiated cells was added to Bradford solution.

The assay is up to be read at the spectrophotometer after 5 minutes since the sample have been added and is stable until 1 hour.

From the standard BSA curve 1µg of proteins' Optical Density ($O.D._{1\mu g}$) was obtained and protein concentration of each sample was calculated using the following equation:

$$mg\ of\ proteins = O.D._{,sample} \div O.D._{,1mg} \div used\ sample\ ml \times total\ sample\ ml$$

### 3.2.1.3 Data analysis

The rate of $H_2O_2$ production by cells was expressed as nMol/min/mg of proteins. The following formula was used:

$$\frac{T_X - T_0}{\mu g\ of\ proteins} \div X \div T_{1\,pM_{H_2O_2}} =$$

$$= \frac{pMoles_{H_2O_2}}{\mu g\ of\ proteins} \times min =$$

$$= \frac{nMoles_{H_2O_2}}{mg\ of\ proteins} \times min \times 1000 =$$

$$= \frac{pMoles_{H_2O_2}}{mg\ of\ proteins} \times min$$

where $X$ is time expressed in minutes, $T_X$ is the transmittance at $X$ time and $T_0$ is the transmittance at the starting point.

## 3.2.2 Determination of oxygen consumption

MATERIALS:

- non sterile PBS and PBS-EDTA
- non sterile trypsin and NCS
- IMP: 100X solution containing 80mM L-isoleucin, 20mM L-methionine, 103.5mM $NaHPO_4$, 1.1% Na-pyruvate. Stored at -20°C.
- 4% $CaCl_2$ solution
- dialyzed FCS

Oxygraphy medium was prepared according to the following protocol:

| OXIGRAPHY MEDIUM | |
|---|---|
| DMEM solution w/o glucose[a] | 9.4 ml |
| Dialyzed FCS | 450 µl |
| IMP | 100 µl |
| 4% $CaCl_2$ | 50 µl |

[a.] DMEM solution containing 83mg of DMEM BASE (Sigma, cat. n. D5030) powder and 37mg $NaHCO_3$ dissolved in 10ml of sterile water.

700000 cells in 100mm dishes (9000/$cm^2$) were seeded 2 days before the experiment in order to obtain at least 1x$10^6$ cells for the experiment, but without having confluence.

To measure oxygen consumption HANSATECH OXYGRAPH PLUS instrument associated to a recording software was used. All the procedure was performed in warmed chamber at 37°C.

The instrument was set up by determining 100% $O_2$ concentration in water at 37°C (corresponding to maximum $O_2$ content) and 0% of $O_2$ content removing all $O_2$ by gurgling $N_2$.

The first record was done only with the medium to measure basal $O_2$ consumption. Cells were trypsinized in non sterile conditions, counted and centrifuged for 5 minutes at 1000g. The pellet was then resuspended in oxygraphy medium at a final concentration of 1x$10^6$ cells/ml. Cell suspension was inserted into the oxygraph chamber to measure oxygen consumption at 37°C with a stirrer speed of 20rpm for 3-5 minutes. Then 10µl of 100µM FCCP were added to measure the maximum respiratory capacity of cells (decoupled state). FCCP was routinely added for 3 times and then 10µl of 100mM KCN were added for 3 times to block mitochondrial respiration chain.

After the experiment cells were recovered into 1.5ml sterile Eppendorfs for DNA extraction.
Recorded data were analyzed using the same recording HANSATECH OXYGRAPH PLUS program. $O_2$ consumption was expressed as nMol/minute/1x$10^6$ cells. Since $O_2$ consumption values can be influenced by the number of cells, Respiratory Control Ratio (RCR), dependent only on the conditions of cells, was calculated as:

$$RCR = \frac{FCCP\ O_2\ consumption}{BASAL\ O_2\ consumption}$$

RCR indicates the part of the total respiratory potentiality used by the cell. It is an index of bioenergeting conditions: high values, around 2, indicate good bioenergetic conditions; low values, around 1, indicate bioenergetic stress conditions.

## 3.2.3 Measure of OXPHOS and glycolytic activity

The enzymatic activities of three complexes of mitochondrial respiratory chain (Complex I, II and IV) and of two enzyme of glycolytic metabolism (Phosphofructokinase and Lactic Dehydrogenase) were measured. The analysis of Citrate synthase activity was also performed because Citrate synthase is a marker for mitochondrial matrix. Measuring Citrate synthase activity, it is possible to assess the mitochondrial enrichment after sonication. So the value obtained, testing the activity of the three complex of mitochondrial chain, was then normalized for the value of Citrate synthase activity.

### 3.2.3.1 Sample preparation

Cells were tripsinized in non sterile conditions and counted using a Burker chamber (see paragraph 3.1.5). Then, cells were centrifuged at 1000g for 5 minutes and the pellet obtained was resuspended in a volume of 50mM Tris-HCl, 150mM KCl pH 7,4 so as to have 500000 cells in 100µl of buffer.
To analyse the activity of the glycolytic enzyme PFK, as described in Method in Enzymology [157], samples were resuspended in 30mM KF - 1mM EDTA. This buffer preserves both activity and stability of the enzyme more than the one with Tris-HCl and KCl. Then, cells, resuspended in the appropriate buffer, were collected in eppendorf and sonicated for three times at 60W for 5 seconds on ice. After sonication, the homogenate was centrifuged at 2000g for 4 minutes at 4°C to

pellet remainings of membranes. So the cytosolic material, ready for the assay, was transferred to a fresh tube.

### 3.2.3.2 Phosphofructokinase (PFK)

PFK activity was measured using the reaction catalyzed by phosphofructokinase:

fructose-6-phosphate + ATP → fructose 1,6-diphosphate + ADP

and the reactions catalyzed by aldolase:

fructose 1,6-diphosphate → dihydroxyacetone phosphate + glyceraldehyde-3-phosphate

by triose phosphate isomerase:

glyceraldehyde-3-phosphate → dihydroxyacetone-phosphate (TPI)

by α-glycerophosphate dehydrogenase:

dihydroxyacetone-phosphate → α-glycerophosphate (α-GDH).

| **PFK** | **Blank** | **Sample** |
|---|---|---|
| Tris-HCl 200mM, pH 8.0 | 200µl | 200µl |
| $MgCl_2$ 60mM | 100µl | 100µl |
| NADH 1M (fresly prepared) | 100µl | 100µl |
| ATP 20mM (fresly prepared) | 100µl | 100µl |
| F6P 30mM | 100µl | 100µl |
| Wait for 5 minutes | | |
| aldolase (Fluka, cat. n. 05520) | 5µl | 5µ |
| α-GDH-TPI (Sigma, cat. n. G1881) | 5µl | 5µl |
| sample | / | 20µl |
| $H_2O$ | 390µl | 370µl |
| Lecture at 30°C at λ=340nm for 5 minutes | | |

Also in this assay to measure the PFK enzymatic activity the extinction factor of the Cofactor NADH ($\varepsilon_{340}$=6,2$mM^{-1}cm^{-1}$) was used.

### 3.2.3.3 Lactate dehydrogenase (LDH)

The assay was based on Kornberg method [158]. LDH catalyzes the oxidation of NADH. The reaction is the following:

PYRUVATE + NADH → LACTATE + $NAD^+$
(homolactic fermentation)

| Lactate dehydrogenase (LDH) | | |
|---|---|---|
| | **Blank** | **Sample** |
| 150mM K-phosphate, pH 7.4 (30mM final) | 200µl | 200µl |
| 3mM Pyruvate (0.3mM final) | 100µl | 100µl |
| 2mM NADH fresh solution (0.2mM final) | 100µl | 100µl |
| 10mM NaCl (1mM final) | 100µl | 100µl |
| Sample | / | 5µl |
| $H_2O$ | 500µl | 495µl |
| Lecture at 30°C at λ=340nm for 3 minutes | | |

The enzyme activity was calculated using the extinction factor of the Cofactor NADH ($\varepsilon_{340}$=6,2mM$^{-1}$cm$^{-1}$). The activity was expressed as nmoles/min/mg proteins.

$$Activity = \frac{\Delta OD}{\min} \times \frac{1}{6.2} \times \frac{1}{mg.protein}$$

### 3.2.3.4 Complex I: NADH Dehydrogenase

The activity of complex I of the respiratory chain was measured following the NADH oxidation at 340nm. The following reagents were used [159]:

| NADH-DH | Blank | Sample |
|---|---|---|
| K-phosphate 0.1M, pH 7.5 | 340µl | 340µl |
| Ferricyanide 10mM | 170µl | 170µl |
| NADH 2mM (freshly prepared) | 100µl | 100µl |
| sample | / | 20µl |
| $H_2O$ | 390µl | 370µl |
| Lecture at 30°C at λ=340nm; $\varepsilon_{340}$=6,2mM$^{-1}$cm$^{-1}$ | | |

### 3.2.3.5 Complex II: Succinate Dehydrogenase (SDH)

In this assay the reduction of 2,6-dichlorophenolindophenol (DCPIP) was followed at 600nm (extinction factor 19.1 $mM^{-1}cm^{-1}$) [159]. Since all the subunits of the Complex II are codified by nuclear genome, the SDH activity is not impaired by mtDNA mutations.

| SDH | Blank | Sample |
|---|---|---|
| K-phosphate 0.1M, pH 7.0 | 500µl | 500µl |
| Succinate 400mM | 40µl | 40µl |
| DCPIP 0.015% | 200µl | 200µl |
| KCN 15mM (freshly prepared) | 100µl | 100µl |
| sample | / | 25µl |
| $H_2O$ | 160µl | 135µl |
| Lecture at 30°C at λ=600nm for 10 minutes | | |

To calculate the activity of complex II the following formula was used:

$$Activity = \frac{\Delta OD}{\min} \times \frac{1}{19.1} \times \frac{1}{mg.protein}$$

### 3.2.3.6 Complex IV: Cytochrome c oxidase (COX)

The activity of COX was measured following the oxidation of cytochrome c [160]. *Cytochrome c, freshly prepared, was reduced with sodium dithionite (using a few grams, get orange-pink colour).

| COX | Blank | Sample |
|---|---|---|
| 0.1M K-phosphate, pH 7.0 | 100µl | 100µl |
| 1% reduced Cyt c* (freshly prepared) (in 0.1M K-phosphate, pH 7.0 ) | 100µl | 100µl |
| sample | / | 25µl |
| $H_2O$ | 800µl | 775µl |
| Lecture at 30°C at λ=550nm | | |

The activity was expressed as nmoles/min/mg proteins using the extinction factor of reduced cytochrome c ($\varepsilon_{550}$=6,2$mM^{-1}cm^{-1}$):

$$Activity = \frac{\Delta OD}{\min} \times \frac{1}{18.5} \times \frac{1}{mg.protein}$$

### 3.2.3.7 Citrate synthase activity

The assay is a spectrophotometric method based on reduction of 5,5'-Dithiobis(2-nitrobenzoic acid) (DTNB) absorbance. In fact in presence of Oxalacetic acid (OAA), DTNB and AcetylCoA are transformed in 5-thio-2-nitrobenzoate [161]. The absorbance is recordered at 412nm for 5 minutes at 30°C.

| **Citrate synthase (CS)** | | |
|---|---|---|
| | **Blank** | **Sample** |
| 10mM AcetylCoA | 30µl | 30µl |
| 10mM Oxalacetic acid (OAA) (in 0.1M Tris-HCl pH=8.1) | 50µl | 50µl |
| 10mM DTNB (in 0.1M Tris-HCl pH=8.1) | 100µl | 100µl |
| Sample (mitochondria) | / | 5µl |
| $H_2O$ | 820µl | 815µl |
| Lecture at 30°C at λ=412nm for 5 minutes | | |

The enzyme activity was calculated using the extinction factor of DTNB ($\varepsilon_{412}$=13.6$mM^{-1}cm^{-1}$). Activity was expressed as nmoles/min/mg proteins.

$$Activity = \frac{\Delta OD}{\min} \times \frac{1}{13.6} \times \frac{1}{mg.protein}$$

## *3.3 Molecular biology*

### 3.3.1 DNA extraction from cells

MATERIALS:

- 75mM NaCl + 50mM EDTA (pH=8.0) solution
- 0.5% SDS solution (25µl per ml from 20% stock solution)
- 10mg/ml Proteinase K, recombinant, PCR grade (Roche, cat. n. 0.115836001. Aliquots stored at -20°C)
- Isopropanol
- 70% Ethanol
- TE solution pH=8.0: 10mM Tris-HCl and 1mM EDTA

All the solutions were filtered using sterile cups with a 0.22 µm cut-off.
To extract DNA, cells were collected into sterile Eppendorfs and centrifuged for 5 minutes at 1000g. The supernatant was removed. 500µl of NaCl-EDTA solution, 25µl of 20% SDS and 10µl of 10mg/ml proteinase K were added. The suspension was rinsed with pipette until it became viscose and then left overnight at 37°C (bath or incubator).
The next day, 500µl of isopropanol were added and the suspension was inverted until a sort of medusa could be seen. Eppendorfs were then centrifuged for 1 minute at 13000 rpm and the supernatant was removed. The pellet was rinsed with 500µl 70% ethanol and centrifuged again for 1 minute at 13000 rpm. Ethanol was removed and the pellet was left to air dry at room temperature for some hours.
DNA was then resuspended in an adequate volume of TE buffer (or water) according to its amount and incubated for 30 minutes at 37°C to solubilise. Samples were stored at -20°C until use.

### 3.3.2 Measure of DNA concentration

DNA concentration is measured by spectrophotometer at 260nm. It is obtained multiplying $OD_{260}$ per conversion factor 50µl/ml per dilution factor. Ratio $OD_{260nm}/OD_{280nm}$ indicates the purity of DNA preparation. When the ratio is in a range between 1.7 and 2, the DNA has no contaminations.

### 3.3.3 PCR

MATERIALS:

- Sterile water
- GeneAmp 10X PCR Buffer II (Sigma, cat. n. N808-0010)
- GeneAmp 25mM $MgCl_2$ buffer (provided with 10X PCR Buffer II)
- 5U/µl AmpliTaq GOLD (provided with 10X PCR Buffer II)
- 2mM dNTP (prepared from 100mM stock solutions of dATP, dCTP, dGTP, dTTP diluted with sterile water)
- Forward (F) and Reverse (R) 10µM primers (Sigma, from 100µM stock solutions)
- Sterile tubes for PCR (Eppendorf)
- Sterile pipette tips

Polymerase Chain Reaction (PCR), originally developed by Kerry Mullis, allows to amplify specific DNA sequences starting from complex DNA such as genomic DNA.

To amplify a sequence, two short complementary oligonucleotides (primers) are attached to 3'-ends of denatured DNA using hybridization conditions that assure maximum binding specificity (annealing).

Primers are then extended by a thermostable TAQ polymerase, an enzyme isolated from Thermus Aquaticus, a bacterium living in thermal smoke-holes or in hot sources at 90-100°C. This enzyme uses dNTP (dATP, dCTP, dGTP, dTTP) to lengthen the copied DNA strand.

Using AmpliTaq GOLD DNA polymerase a pre-PCR step at 95° is requested in order to activate the enzyme. Then three steps are repeated for a number of cycles that depends on samples, enzyme and primers chosen. The steps are denaturation, annealing and extension.

The annealing temperature (Ta) depends on primers chosen. It can be estimate with the following formula:

$$Ta=69.3 + (0.41 \times \%GC) - 650/n$$

n=nucleotide numbers

A typical protocol for one sample mix is shown in the following scheme:

| **PCR** | |
|---|---|
| Sterile water | 7.7 µl |
| 10X PCR Buffer II | 2 µl |
| 50 mM $MgCl_2$ | 1.2 µl |
| 2mM dNTP | 2 µl |
| 10 µM F primers | 1 µl |
| 10 µM R primers | 1 µl |
| AmpliTaq GOLD 5U/µl | 0.1 µl |
| DNA | 5 µl |
| **Final volume** | **20 µl** |

All the PCR reagents were stored at -20°C, thawed just before the use and kept in ice during the experiment.
The entire procedure must be done maintaining sterility to avoid contaminations of PCR products.
To verify possible contaminations, in each PCR a negative control, containing no DNA, was included.

### 3.3.3.1 Nuclear polymorphism PCR

To verify if cybrids had RD or 206 nuclear background, polymorphic locus D11S533 on chromosome 11 was amplified by PCR. The sequence of primers is:

Forward 5'- GGT GTG GTC AAT CGC TTT CT –3'
Reverse 3'- CAT GTC CCC AGT GGATAA GG -3'

PCR PROGRAM:

- Taq GOLD activation 95°C 10'
- 3 steps for 40 cycles:
  - Denaturation 95°C 30''
  - Annealing 60°C 30''
  - Polymerase 72°C 30''
- Elongation 72°C 7'
- Stop 4°C ∞

Positive controls were represented by RD MELAS and 206 MELAS.

### 3.3.3.2 Mitochondrial gene amplification PCR

In order to verify the presence of mtDNA or the percentage of mutant mtDNA, the region 3033-3361 bp of mtDNA containing the site of the point mutation A3243G causing MELAS syndrome was amplified using primers with the following sequences:

Forward 5'- GTT CGT TTG TTC AAC GAT T -3'
Reverse 3'– GCC ATT GCC ATT AGA ATG G –5'

PCR PROGRAM:

- Taq GOLD activation 95°C 10'
- 3 steps for 40 cycles:
  - Denaturation 95°C 30''
  - Annealing 50°C 1'
  - Polymerase 72°C 2'
- Elongation 72°C 7'
- Stop 4°C ∞

In this case WT7, RD MELAS 99% and 206 MELAS 74% were used as controls.

## 3.3.4 Apa I digestion

MATERIALS:

- Sterile water
- Sterile tubes and tips (Eppendorf)
- APA I KIT (Invitrogen, cat. n. 15440-019, stored at -20°C) containing:
  - React® 4 10X buffer: concentrate assay buffer with 200µg/ml BSA supplied to be dilute 1 part in 10 in final reaction mixture.
  - 10U/µl APA I

To verify the presence of A3243G mutation, amplified DNA from MELAS PCR was used.

*Wild Type:* *GGACCC* / *CCTGGG* *Melas (A → G):* *GG⎜GCCC* / *CCCG⎜GG*

This point mutation introduces a restriction site for APAI in amplified mtDNA (328 bp). APAI cuts a GGGCCC sequence generating two fragments of 214 and 114 bp. Digestion was performed over night at 25°C.
The mix used for each sample was:

| **APA I DIGESTION MIX** | |
|---|---|
| Sterile water | 3.8 µl |
| REact® 4 10X buffer | 1 µl |
| APA I | 0.2 µl |
| SAMPLE | 5 µl |
| **Final volume** | 10 µl |

## 3.3.5 Agarose gel electrophoresis

MATERIALS:

- 2% Agarose (Invitrogen cat. n. 15510-027) solution
- 1X TAE solution: 40mM Tris-acetate, 1mM EDTA
- 6X Loading Dye: 0.25% Bromophenol Blue, 0.25% Xylen cyanol FF, 30% glycerol
- Ethidium bromide (EtBr): final concentration 0.5µg/ml

Agarose is a linear polymer useful to separate DNA of different sizes. It generates a matrix with variable density according to its starting solution's concentration. DNA will then migrate differently depending on his dimensions and spatial conformation.
Usually, DNA is detected by staining with planar aromatic cations like Ethidium Bromide, which intercalates between bases and emits fluorescence when irradiated by UV light. With EtBr up to 50ng DNA can be detected.
To pour a gel, agarose powder is mixed with electrophoresis buffer (1X TAE) to the desired concentration, and then heated in a microwave oven until completely melted. Ethidium bromide (final concentration 0.5µg/ml) is added to the gel at this point. The solution is poured into a casting tray containing a sample comb and allowed to solidify at room temperature.
After the gel has solidified, the comb is removed, using care not to rip the bottom of the wells. The gel, still in its plastic tray, is inserted horizontally into the electrophoresis chamber and covered with 1X TAE. Samples containing DNA

mixed with 6X loading buffer are then pipeted into the sample wells, the lid and power leads are placed on the apparatus, and a 80-90V current is applied. The distance DNA has migrated in the gel can be judged by visually monitoring migration of the tracking dyes.
To visualize DNA, the gel is placed on a ultraviolet transilluminator and then a digital image is taken using IMAGE MASTER TOTAL LAB PRO instrument.

## 3.3.6 Last Cycle Hot PCR (LC-PCR) and phosphor-imaging

### 3.3.6.1 LC-PCR

LC-PCR permits to quantify restriction bands with great precision by following a normal PCR protocol modified by the addition of a radioactive step. In fact, PCR mix is the same given in section 3.3.3, but the program involves a pause in correspondence of the last but one annealing step to insert radioactive material to the reaction mix.
Radioactive material used was cytidine 5'-[α-$^{32}$P] triphosphate (GE Healthcare, cat. n°AA0005. 9.25 MBq/ml, 250 μCi, 25μl).

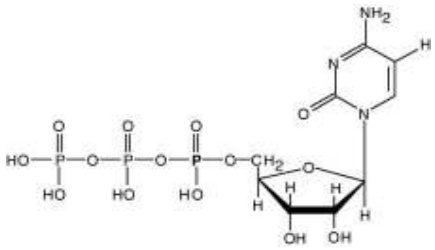

**Figure 3.1:** chemical structure of cytidine 5'-[α-$^{32}$P] triphosphate ($^{32}$P-dCTP)

This protocol was used to quantify Apa I restriction bands and so the PCR program was similar to that of MELAS standard PCR:

PCR PROGRAM:

- Taq GOLD activation 95°C 10’
- 3 steps for 39 cycles:
  - Denaturation 95°C 30’’
  - Annealing 50°C 1’
  - Polymerase 72°C 2’
- Single radioactive cycle:
  - Denaturation 95°C 30’’

- Pause at 50°C
- Addition of 1 µl of diluted radioactive solution in each tube
- Annealing 50°C 1'
- Polymerase 72°C 2'

– Elongation 72°C 7'
– Stop 4°C ∞

$^{32}P$ radioactivity decays in 26 days, so for the first experiments a 1:20 diluted solution was used while, after a week 1:10 solution was employed.
When the PCR was completed, Apa I digestion was performed using the same PCR machine to incubate the mix at 25°C for at least 4 hours. Apa I digestion was performed according with the protocol described at section 3.3.4, but using a final volume of 20µl instead of 10µl.

### 3.3.6.2 Acrylamide gel electrophoresis

MATERIALS:

- 10X TBE: 108g of tris hydroxymetyl aminomethane, 55g of boric acid, 40ml of 0.5M EDTA pH 8. Taken up to 1L with milliQ water
- 10% Acrylamide solution: 16.67ml of acrylamide/bis-acrylamide 29:1 (30%) solution (Sigma, cat. n. A3574), 5ml of 10X TBE, 28.3ml of milliQ water.
- 10% Ammonium persulfate (APS) solution
- TEMED (Bio-Rad, cat. n. 161 0801)
- Hoeffer mini electrophoresis instrument
- 6X loading dye

Glass plates and 0.75mm spacers were thoroughly cleaned. The plates were rinsed with deionised water and ethanol. The glass plates must be free of grease spots to prevent formation of air bubbles in the gel. The glass plates were assembled with spacers in the gel caster.
For a single minigel 6ml of 10% acrylamide solution were used adding, just before pouring the gel, 24µl of APS 10% and 12µl of TEMED. The solution was then quickly poured with a pipette into the gel apparatus having care not to create bubbles. An appropriated comb was suddenly inserted and the gel was left to polymerize for one hour (a small aliquot of gel was kept in a falcon to control the

polymerization). After the gel had polymerized the plates were assembled into the electrophoretic apparatus filled with 1X TBE buffer. The wells were rinsed with 1X TBE buffer using a syringe.
The DNA samples were prepared to be run adding 10µl of 6X loading dye for 20µl of PCR product. In each gel, control samples of RD MELAS 99% and WT7 0% MELAS DNA were loaded. 15µl of the solution were loaded into the wells using a micropipette with drawn-out plastic tips.
The electrophoretic chamber was then closed and the electrodes were connected to a power supply.
The run was performed at 100V for one hour and half, until the loading dye front reached the end of the gel.

### 3.3.6.3 Detection of bands with phosphor-imaging

After the run, 10% acrylamide minigels were dried between Amersham plastic sheets using a gel drier at 55°C for 1 hour.
Dried gels were then put into phosphor-imaging chambers in order to impress slabs (previously cancelled with the specific lamp) for different times (e.g. 30 minutes, 1, 2 or 3 hours and overnight).
Phosphor-imaging slabs were then scanned by the Amersham phosphor-image scanner system.
Obtained images were then analyzed by Gel-Pro Analyzer 4 in order to quantify bands intensity and to obtain the MELAS mutated percentage.

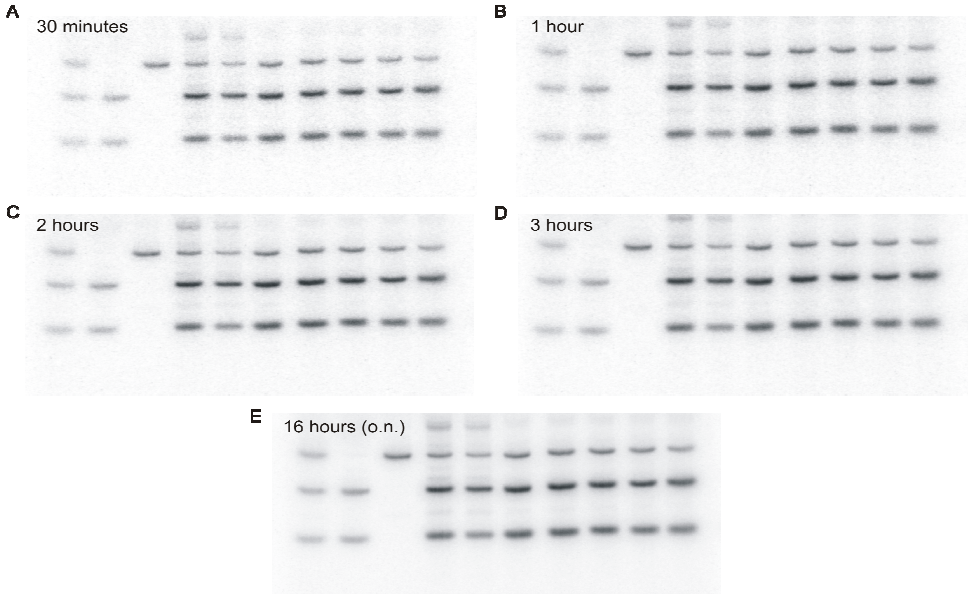


**Figure 3.2:** phosphor imaging of the same LC-PCR products at different exposure times.

## 3.3.7 Molecular analysis of cells

### 3.3.7.1 Nuclear polymorphism

To estimate the nuclear background of RD cybrids and quantify contamination by osteosarcoma cells, amplification of nuclear polymorphic region D11S533 on chromosome 11 was performed. A standard curve was created mixing different ratios of RD and 206 DNAs and amplifying them by PCR (see paragraph 3.3.3.1). RD presents a 500bp band different from the one of osteosarcoma cells (206) having a band of 450bp.

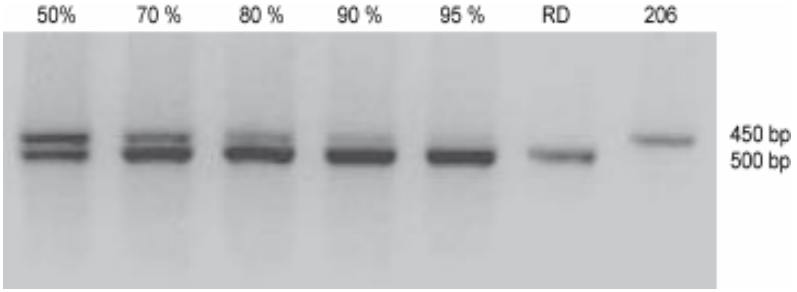


**Figure 3.3:** DNA from RD MELAS and 206 MELAS was mixed and amplified by PCR (see paragraph 3.3.3.1) to obtain a standard nuclear polymorphism curve. RD nuclear background corresponds to a 500bp band (the lower), while 206 amplified DNA gives a 450bp band (the upper). The showed values represent the % abundance of RD nuclear DNA in comparison to that of 206.

### 3.3.7.2 MELAS mutation detection and quantification

To detect and quantify MELAS point mutation in mtDNA of cells, PCR products (see 3.3.3.2) were digested by Apa I (see 3.3.4) and run in 2% agarose gel with EtBr. Bands were analyzed using specific programs (ImageJ, TotalLab, Gel-Pro Analyzer 4).

Heteroduplexes of wild-type and mutant mtDNA, formed during the final steps of PCR amplification, may be resistant to APA I digestion. To correct this possibility, a mixed template standard curve was constructed by PCR amplification of a DNA sample containing ~99% mutated mtDNA, and one containing 100% wild-type mtDNA. Different ratio mixtures of the mutant and wild-type were prepared.

Figure 3.4 compares the mixed template standard curve (T) thus constructed with the mixed product standard curve (P), obtained by mixing the PCR products independently amplified from RD MELAS 99%-derived and WT7-derived PCR products in different ratios and then subjecting the mixtures to Apa I digestion [26].

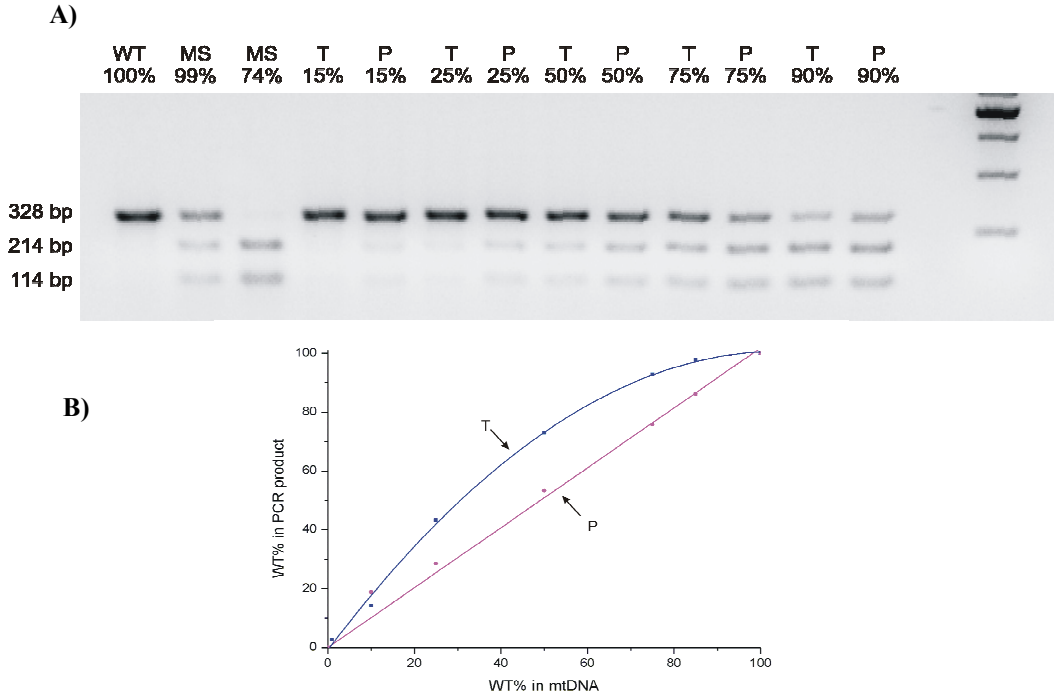


**Figure 3.4:** MELAS standard curve with EtBr construction of standard curves for the quantification of the MELAS mutation in mtDNA. A) MELAS PCR and Apa I restriction were performed. The product was run in 2% agarose gel and coloured by EtBr. MS stands for MELAS. For each sample the % of WT is given. B) Curves: T, mixed template standard curve; P, mixed-product standard curve. The equation for curve T is $y = -0.0091x^2 + 1.9146x$ and $R^2 = 0.9985$. MS: MELAS.

Heteroplasmy ratio was calculated considering intensities of the 328 bp ($B_{328}$) and 214 bp ($B_{214}$) bands of each sample. A correction factor (CF), calculated as $B_{328}(WT)/B_{214}(MS)$, was needed to normalize bands intensities to the intensity of WT $B_{328}$.

The WT % was so obtained as following:

$$WT\% = \frac{B_{328}}{B_{328} + (B_{214} \times CF)} \times 100$$

WT% were then plotted obtaining curves of Figure 3.4 (B). The equation of the T curve was then used to correct all quantization then made.

Heteroplasmy % was calculated as *100-WT%.*

Quantification of the MELAS mutant percentage by LC-PCR was done following the same procedure of the previously described method.

In last cycle hot PCR, there are no digestion problems caused by the presence of heteroduplexes [162], so the construction of a standard curve was done only to confirm that bands intensities reflect the real amount of cut or uncut mtDNA.

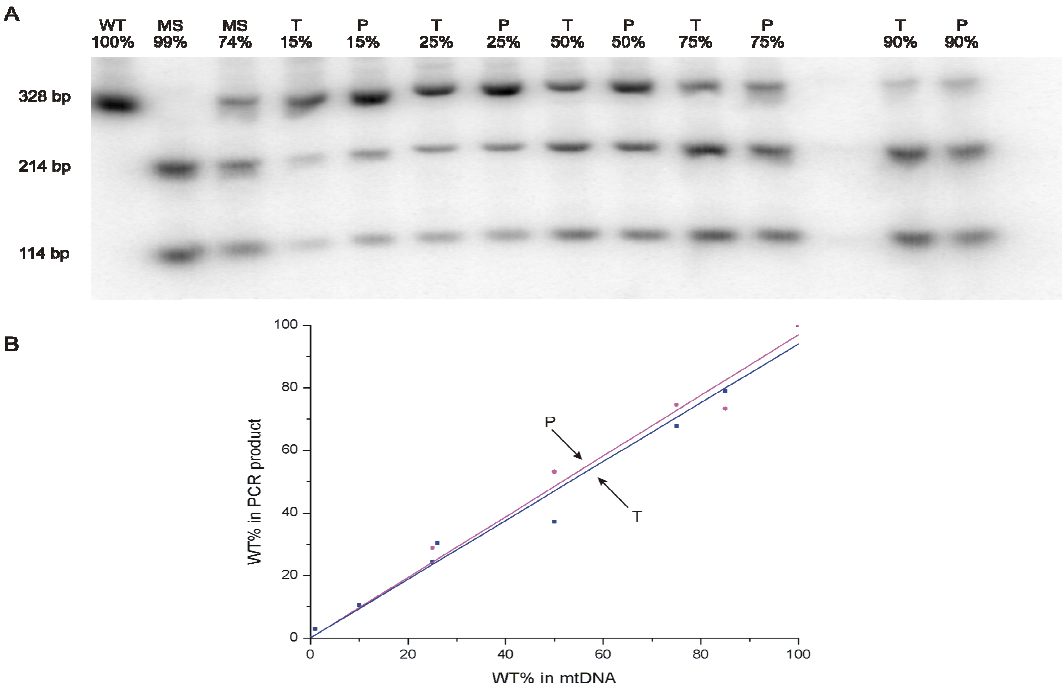


**Figure 3.5: MELAS** standard curve with LC-PCR**.** Construction of standard curves for the quantification of MELAS mutation percentage in mtDNA. The used procedure is the same described for Figure 3.4. Equation for curve T is y = 0.9405x and $R^2$ = 0.9906; equation for curve P is y =0.9699x and $R^2$ = 0.9903.

The equation of standard T curve showed in figure 3.5 confirmed the previous affirmation, because T and P curves were almost identical, above all for the range of WT% presence that we considered (from 0% to 50%). Consequently, the calculation of mutant percentages was done without correcting final values with T curve's equation.

## 3.3.8 RNA extraction

RNA extraction is performed using TRIzol Reagent (Invitrogen, life technologies). Cells are lysed directly in a culture dish adding 0.5ml of TRIzol to a 6cm diameter dish. PHASE SEPARATION: the homogenized samples are incubated for 5 minutes at room temperature to permit the complete dissociation of nucleoprotein complexes. 0.1ml of chloroform per 0.5ml of TRIzol are added. The tubes are shaked vigorously by hand for 15 seconds and incubated for 2-3 minutes at room temperature. The samples are centrifuged at 12000g for 15 minutes at 4°C. After the centrifugation, the mixture separates into a lower red, phenol-chloroform phase, an interphase and a colorless upper aqueous phase. RNA remains exclusively in the aqueous phase. The volume of the aqueous phase

is about 60% of the volume of TRIzol used for homogenization. RNA PRECIPITATION: the aqueous phase is transferred to a fresh tube and the RNA is precipitated from the aqueous phase by mixing with isopropyl alcohol. 0.25ml of isopropyl alcohol is used per 0.5ml of TRIzol used for the inizial homogenization. Samples are incubated at room temperature for 10 minutes and centrifuged at 12000g for 10 minutes at 4°C. RNA WASH: the supernatant is removed and the RNA pellet is washed adding 0.5ml of 75% ethanol. The samples are vortexed and centrifuged at 7500g for 5 minutes at 4°C. REDISSOLVING THE RNA: RNA pellet is briefly dried at room temperature, then dissolved in Rnase-free water and stored at -70°C.

### 3.3.9 Measure of RNA concentration

RNA concentration is measured by spectrophotometer at 260nm. It is obtained multipling $OD_{260}$ per conversion factor 40µl/ml per diluition factor. The purity of RNA preparation is obtained such as written for DNA (see paragraph 3.3.2).

### 3.3.10 Reverse transcription

First-Strand cDNA synthesis was performed using SuperScript™ II Reverse Transcriptase from Invitrogen.
The following components were added to a nuclease-free microcentrifuge tube:

| | |
|---|---|
| Random primers | 1µl |
| 1ng to 5µg total RNA | xµl |
| dNTP Mix (10µM each) | 1µl |
| Sterile, distilled water | to 12µl |

The mixture was heated to 65°C for 5 minutes and then the following reagents were added:

| | |
|---|---|
| 5X First-Strand Buffer | 4µl |
| 0.1M DTT | 2µl |

The mixture was incubated for 2 minutes at 42°C and then, 1µl (200 units) of SuperScript™ II RT was added plus 1µl of distilled water to a 20µl final volume. The mixture was first incubated at 25°C for 10 minutes and then at 42°C for 50 minutes. In the end the reaction was inactivated by heating at 70°C for 10 minutes.

## 3.3.11 qReal Time PCR

### 3.3.11.1 Experimental procedure

MATERIALS:

- Platinum SYBR green qPCR SuperMix-UDG (Invitrogen, cat. n° 11733-038)
- ROX reference Dye
- Sterile water
- Forward and reverse 40 μM primers (Sigma)
- Sterile 96 wells optical reaction plates with barcode (code 128) for RT-qPCR (Applied Biosystems, cat. n° 4306737)
- Sterile filtered pipette tips
- ABI PRISM 7000 REAL TIME PCR

Real-time Polymerase Chain Reaction (PCR) is a system permitting to monitor the progress of the PCR as it occurs (in real time). This quantitative assay measures the amount of a nucleic acid target during each amplification cycle of the PCR. The target may be DNA, cDNA or RNA.

For our studies we used the Syber Green I Dye chemistry. The Syber Green I Dye detects polymerase chain reaction products by binding to double-stranded DNA formed during PCR. As the PCR progresses, more amplicons are created. Since the Syber Green I Dye binds to all double-stranded DNA, the result is an increase in fluorescence intensity proportionate to the amount of PCR product produced. The higher the starting copy number of the nucleic acid target, the sooner a significant increase in fluorescence is observed. Real-time PCR follows the kinetic of the amplification reaction during the initial exponential phase. The initial cycle of PCR, in which there is little change in fluorescence signal, defines the baseline for the amplification plot. An increase in fluorescence above the baseline indicates the detection of accumulated target. A fixed fluorescence threshold can be set above the baseline. The parameter $C_T$ (threshold cycle) is defined as the fractional cycle number at which the fluorescence passes the fixed threshold. When SYBR Green I Dye is in solution, it generates low fluorescence levels, but during the extension phase it augments its signal, since increasing amounts of staining bind the newly synthesized DNA. During denaturation phase, SYBR Green binding the DNA comes back in solution and its emission levels returns at background levels. Consequently, to monitor the increase of the reaction

products amount, fluorescence is measured at the end of the extension phase, when maximal SYBER Green quantity binds DNA.
RT-PCR was used in this work to quantify the expression levels of the following transcripts: OPA1, Drp1, hFis1, Mfn1, Mfn2, CK. A ribosomal gene 36B4 (acidic ribosomal phosphoprotein PO) was used as housekeeping gene.
Also mtDNA levels were quantified using RT-PCR. The mitochondrial gene analysed was cytochrome b, while the housekeeping was a nuclear gene, the APP (Amyloid Precursor Protein). In this case the RT-PCR was done on DNA and not on cDNA such as done for the other analyses.
To quantify OPA1, Drp1, hFis1, the following mix was prepared for one sample:

| **REAL-TIME PCR** | |
|---|---|
| Supermix buffer | 6.25µl |
| Forward 10µM primers | 0.5µl |
| Reverse 10µM primers | 0.5µl |
| ROX | 0.25µl |
| STERILE WATER | 12.5µl |
| DNA SAMPLE | 5µl |
| **Final volume** | **25µl** |

To quantify 36B4, Mfn1, Mfn2 was used 1µl of 10 µM primers; to quantify CK 0.375µl of 10 µM primers were used; to quantify cyt b and APP, 0.125µl of 40µM primers were used.
The primers used have the following sequences:

APP: Forward 5'-TTT TTG TGT GCT CTC CCA GGT CT-3'
Reverse 5'-TGG TCA CTG GTT GGT TGG C-3'

Cyt b: Forward 5'-GCC TGC CTG ATC CTC CAA AT-3'
Reverse 5'-AAG GTA GCG GAT GAT TCA GCC-3'

OPA1: Forward 5'- GGA AAA GGG AAC AGC TCT GA-3'
Reverse 5'- CAC TTG GTG TGC CTT TAG CA-3'

Drp1: Forward 5'- CTG ACG CTT GTG GAT TTA CC-3'
Reverse 5'- CCC TTC CCA TCA ATA CAT CC-3'

hFis1: Forward 5'- GGAGGACCTGCTGAAGTTTG-3'
Reverse 5'- ACGATGCCTTTACGGATGTC-3'

Mfn1: Forward 5'- TGT TTT GGT CGC AAA CTC TG-3'
Reverse 5'- CTG TCT GCG TAC GTC TTC CA-3'

Mfn2: Forward 5'- ATG CAT CCC CAC TTA AGC AC-3'
Reverse 5'- CCA GAG GGC AGA ACT TTG TC-3'

CK: Forvard 5'- CAA GGA ACT CTT TGA CCC CA-3'
Reverse 5'- CCA CAG AGA GCT TCT CCA CC-3'

36B4: Forward 5'-GTG ATG TGC AGC TGA TCA AGA CT-3'
Reverse 5'-GAT GAC CAG CCC AAA GGA GA-3'

Before to start a relative quantification for OPA1, Drp1, hFis1, Mfn1, Mfn2, a standard curve was made using cDNA to set the working conditions. 1:2 dilutions were used starting from 100ng/5µl to 1.56ng/5µl. Each sample was diluted to work with 25ng/5µl.

**3.3.11.2 Data analysis**

Two types of quantitation are possible with the SYBER Green reagents: relative quantitation and absolute quantitation. Relative quantitation was used for OPA1, Drp1, hFis1, Mnf1, Mfn2, CK expression measurements. Gene expression was measured by the quantification of cDNA converted from a messenger RNA relative to a calibrator sample serving as a physiological reference. We used wild type cells as calibrator sample. All quantifications were also normalized to an endogenous control to account for variability in the initial concentration and quality of the total RNA and in the conversion efficiency of the reverse transcription reaction. Our endogenous control was a ribosomal gene, acidic ribosomal phosphoprotein PO (36B4).

Instead, mtDNA was quantified by an absolute quantitation. In this case, the $C_T$ of an unknown sample was compared to a standard curve with known copy numbers. The standard curve was made using WT 0% MELAS cybrids DNA. The dilutions started from a concentration of 50ng/5µl to 0.08ng/5µl using 1:5 dilutions. Each DNA sample's concentration was quantified before the experiment and then diluted in order to obtain 1ng/µl and 0.2ng/µl working solutions. Both working solutions were used to make 2 samples each.

### 3.3.12 Proteins extraction, SDS-Poliacrilamide gel electrophoresis (SDS-PAGE) and western blot

Proteins extraction: 700.000 cells were plated in 100mm dishes, tripsinized after 48 hours and washed with PBS. The pellet obtained was lysated remaining for 30 minutes on ice with 200µl of RIPA buffer (65mM Tris, 150mM NaCl, 1% NP-40, 0.25% Na-DOC, 1mM EDTA, pH 7.4) and 7µl of a cocktail of protease inhibitor (PIC-Sigma P8340). The cell lysate was centrifuged at 14.000g for 15 minutes at 4°C and the supernatant stored at –80°C until used.

SDS-Poliacrilamide gel electrophoresis (SDS-PAGE): SDS-poliacrilamide gel electrophoresis is performed in vertical gels constituted by two parts, stacking gel and running (or resolving) gel.

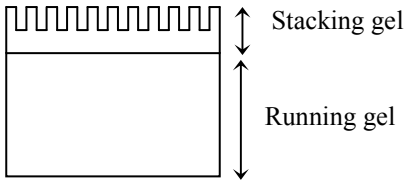


The Laemmli system [163] is a discontinuous SDS system in which the peptides are stacked in a stacking gel before entering the separating gel. The migration of the peptides depends only on the molecular weight because SDS, an anionic detergent, denatures proteins by wrapping around the polypeptide backbone and it confers a negative charge to the polypeptide in proportion to its length. In this way each polypeptide shows a negative charge for unit length.
Equal amount of proteins for each sample was loaded on the gel.

| **Mix for one mini-gel 1.5mm thick** | | | |
|---|---|---|---|
| **Reagent** | **Running gel 12%** | **Running gel 8%** | **Stacking gel** |
| 30% Acrylamide- bisacrylamide (Sigma Cat. n. A3574) | 3ml | 2ml | 0.415ml |
| $H_2O$ bd | 2.5ml | 3.5ml | 1.75ml |
| 1.5M Tris pH=8.8 | 1.875ml | 1.875ml | / |
| 0.5M Tris pH=6.8 | / | / | 0.34ml |
| 10% SDS | 75µl | 75µl | 25µl |
| TEMED | 7.5µl | 7.5µl | 2.5µl |
| 10% APS | 75µl | 75µl | 25µl |

Extracted proteins were prepared with 5X loading buffer and denaturated for 5 minutes at 99°C.

| LOADING BUFFER 5X | | |
|---|---|---|
| **Reagent** | **Final concentration** | **Quantity** |
| 0.5M Tris pH=6.8 | 125mM | 1ml |
| SDS | 10% | 0.4g |
| Glycerol | 50% | 2ml |
| Bromophenol blue | 0.2% | 8mg |
| β-mercaptoethanol | 25% | 1ml |

Samples were loaded into the gel with a molecular weights indicator (BIORAD prestained SDS-PAGE standards), this allows to control the separation of interest proteins. The electrophoresis is performed in buffer SDS/Tris-Glycine (0.1% SDS, 3g Tris-HCl, 14.4g Glycina), at 120V constant for 1 hour and 30 minutes.

Western Blot: After the separation of samples in acrylamide gel, proteins were transferred into a nitrocellulose membrane (Schleicher&Schuell Bioscience PROTRAN BA85 0.45µm) for 4 hours at 1.5A constant in transfer buffer (3g Tris-HCl, 14.4g Glycine, pH=8.3 and 10% methanol). The trasfer efficiency was controlled using red ponceau [0.1% w/v Ponceau S solution (Sigma Cat.n. P7170), 5% v/v acetic acid (Carlo Erba Cat. n. 401391)] on the membrane. The gel was stained with stain solution (0.125% comassie blue, 50% methanol, 10% acetic acid) and decoloring with a destaining solution (50% methanol, 10% acetic acid) to see if there were any remaining proteins on the gel. The membrane was blocked in 5% non-fat dry milk in TTBS (0.02 M Tris-HCl pH 7.5, 0.137 M NaCl, and 0.1% Tween 20) for 1 hour at room temperature and incubated overnight at 4°C with primary antibodies. To control that in each lane the same quantity was loaded, the signal of the protein of interest was normalized for the actin value or for the VDAC/porin value.

The primary antibodies used in our study were diluted in blocking solution. They are: anti-OPA1 monoclonal antibody (BD Biosciences, Cat. N° 612607, 1:1000); anti-DLP1 monoclonal antibody (BD Biosciences Pharmingen, Cat. N° 611112, 1:1000); anti-actin monoclonal antibody (Chemicon International, Cat. N° MAB1501, 1:4000); anti-hFis1 polyclonal antibody (Alexis, ALX-210-907-R100, 1:1000); anti-VDAC/porin monoclonal antibody (Sigma, Cat. N° V2139, 1:1000). Then, the membrane was probed with appropriated horseradish peroxidase-conjugates secondary antibody (Amersham Biosciences) diluted 1:2500 in

blocking solution: anti-mouse for OPA1, Drp1, actin; anti-rabbit for hFis1, VDAC. Bounded antibody was visualized using an ECL reagent (Amersham Biosciences). The reaction is based on oxidation of the substrate luminol by the peroxidase conjugated to secondary-Ig. The luminol in excited state decays to ground state via a light emitting pathway with a maximum after 5-20 minutes that can be detected by an exposure to autoradiography film for the necessary time. The signals were quantified using Gel-Pro Analyzer program.

## *3.4 Other techniques*

### 3.4.1 Aldehyde-based fixation

MATERIALS:

- 4% paraformaldehyde (PFA) or glutaraldehyde solution
- PBS
- PBS + 0.02% BSA + Na-azyde

This method allows fixation of cells.
The entire procedure was performed at room temperature.
Cells, cultured in dishes or glasses, were washed three times with PBS and then fixed with PFA or glutaraldehyde for 10 minutes. Three washes with PBS-0.02% BSA were done to remove fixative. Cells were used immediately or preserved with PBS-0.02% BSA and Na-azyde at 4°C.

### 3.4.2 Eosin and hematoxylin staining

MATERIALS:

- Harris' hematoxylin solution (according to Papanicolau. Merck, cat.n.109253)
- 1% Yellow Eosin (Merck, cat. n. 115935)
- glacial acetic acid
- MilliQ water
- Absolute ethanol
- 70 and 80% ethanol solutions

This staining protocol was used to control enucleation efficiency during the creation of cybrids.
Hematoxylin-eosin stain is a simple method for general histology.
Cells, adhered to dishes, were fixed with PFA (see 3.4.1) and air dried for at least

10 minutes. Harris' hematoxylin was filtered with paper to remove oxidized particles.
Cells were stained with hematoxylin for 3-4 minutes at room temperature, washed three times with water and incubated for 1 minute with 1% yellow eosin (acidified by adding 2-3 drops of glacial acetic acid). Cells were then washed three times with water, quickly dehydrated with 70%, 80% and 100% ethanol and covered with glycerol.

### 3.4.3 MitoTracker® Red staining

MATERIALS:

- 125nM DMSO MitoTracker® Red CMXRos (Molecular Probes, cat. n. M7512) solution (from 1mM stock solution stored at -20°C protected from light)
- PBS (Oxoid, cat. n. BR0014G)

MitoTracker Red CMXRos is a lipofilic red-fluorescent dye that stains mitochondria in live cells and its accumulation is dependent upon membrane potential.
To label mitochondria, cells were incubated with 125nM MitoTracker Red probe, which passively diffuses across the plasma membrane and accumulates into active mitochondria. Once mitochondria were labelled, the slide with cells was assembled on a holder and observed with confocal microscope (LEICA TCS SP5) or fluorescence microscope (Olympus IX81).

## *3.5 Statistical analysis*

Data were expressed as mean ± SD. Statistical analysis of group differences was examined using Student's t-test. The differences were considered significant at the 95% confidence level ($P<0.05$).

# 4 RESULTS

## FIRST PART

### *4.1 Creation and characterization of heteroplasmic MELAS A3243G RD cybrids*

### 4.1.1 Creation

Three sets of experiments were performed to generate heteroplasmic MELAS A3243G RD cybrids, according to the procedure described in paragraph 3.1.7. After the fusion of enucleated cells (cytoplasts) and $\rho^0$ cells, the selection was started to cut off fused cells (cybrids). The selection was performed growing the cells for 19-20 days in a selective medium with G418 and without uridine.
Every set of experiments was subdivided in three groups. One group of cells was treated with standard medium, another group with medium supplemented with 0.5mM NAC and the last one group of cells was treated with medium supplemented with 100μM creatine.
The conditions of the three sets of experiments are summarized in the following scheme:

| CYBRIDS SET | A | B | C |
|---|---|---|---|
| DATE | 27/04 | 06/05 | 12/05 |
| G418 START | 29/04 | 08/05 | 14/05 |
| G418 END | 18/05 | 27/05 | 03/06 |
| DAYS OF SELECTION | 19 | 19 | 20 |
| STANDARD DISHES | 4 | 2 | 2 |
| 0.5 mM NAC DISHES (N) | 4 | 4 | 3 |
| 100 μM CREATINE DISHES (C) | 4 | 4 | 3 |

**Table 4.1.1:** Summary of the three sets of experiments performed to create heteroplasmic RD cybrids.

From each set of experiments, more clones were collected:

- Set A: 21 clones with standard conditions, 17 clones with NAC, 26 clones with creatine
- Set B: 7 clones with NAC, 6 clones with creatine
- Set C: 3 clones with standard conditions, 2 clones with NAC, 41 clones with creatine

Stable proliferating clones or pool of cybrids were then expanded, stored at -80°C and characterized. For each clone an acronym was created based on:

- Data of experiment (A, B or C)
- Modality to obtain the clones (a single clone, a pool of single clones (P) or a collection of cells in a dish (R))
- Used treatment (NAC (N) or creatine (C))

For example, A5N is the fifth clone obtained from the first set of experiment (A) and grown in presence of 0.5mM NAC.

During their growth, some clones showed a drastic decrease in proliferation. To help their growth, they were treated with 50μg/ml uridine and this supplementation was indicated as "+U".

## 4.1.2 Characterization

### 4.1.2.1 Molecular characterization

Obtained cybrids were routinely analyzed to check nuclear background and percentage of mutant A3243G mtDNA. To make these analyses DNA from different clones was extracted.

#### 4.1.2.1.1 Nuclear polymorphism analysis

Nuclear polymorphism of obtained cybrids was analysed to check if these cells had a muscular nuclear background or they showed some traces of bone nuclear background coming from mitochondrial donor cells.

Figure 4.1.1 shows that nuclear background of cybrid clones was exclusively the muscular background coming from rhabdomysarcoma cells.

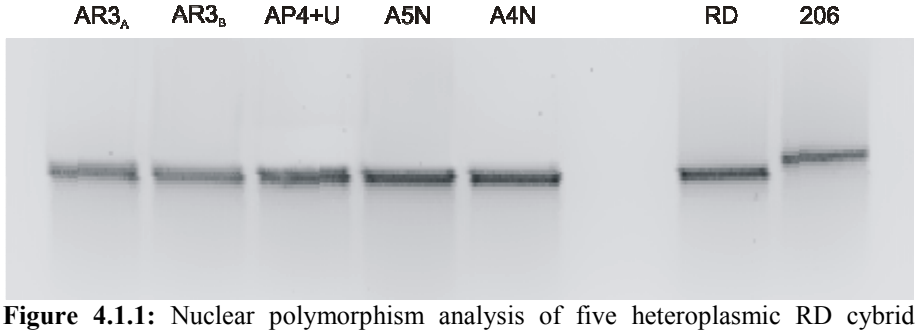


**Figure 4.1.1:** Nuclear polymorphism analysis of five heteroplasmic RD cybrid clones. PCR products were run on 2% agarose gel and stained with EtBr. All the examined clones had 100% muscular nuclear background.

#### 4.1.2.1.2 Quantification of MELAS mutant mtDNA

Quantification of MELAS mutant mtDNA percentage was analysed by PCR and APAI digestion as described in paragraph 3.3.7.2. For each clone the product of digestion was run on 2% agarose gel in presence of EtBr. The ones with only a nuclear muscular background were also analysed by LC-PCR (see paragraph 3.3.6.1). LC-PCR gives an estimation of the percentage of mutant mtDNA more precise than the RFLP-ethidium bromide gel analysis. The error is 3% for LC-PCR and 5-10% for RFLP-ethidium bromide gel analysis. Figure 4.1.2 is an example of quantification of MELAS mutation both with LC-RFLP-Hot PCR and EtBr RFLP-PCR.

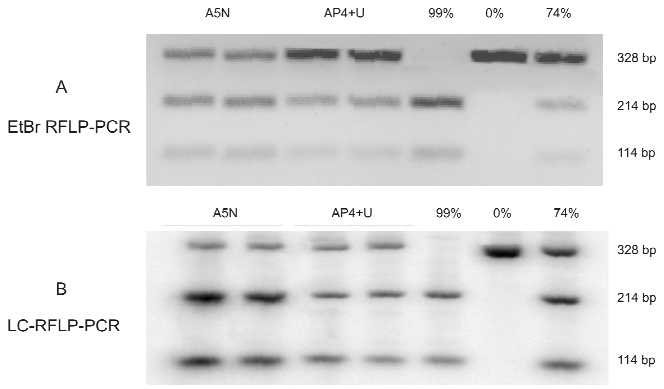


**Figure 4.1.2:** percentage of MELAS mutation in A5N and AP4+U. MELAS mutation percentage was obtained by both (A) RFLP-PCR run in 2% agarose with EtBr and (B) Last Cycle Hot PCR (LC-RFLP-PCR) using $^{32}P$ and running PCR products in 10% acrylamide gels. In the same analysis are present as internal standard samples of 0%, 99% and 74% mutant clones.

| | 2% AGAROSE + EtBr | | LC-PCR |
|---|---|---|---|
| **CLONES** | **RD %** | **MELAS FINAL%** | **MELAS FINAL%** |
| **A1** | 90% | 80% | 83% |
| **A1+U** | 90% | 70% | |
| **A4N** | 100% | 90% | 90,2% |
| **A5N** | 100% | 94% | 92% |
| **AP1** | 90% | 70% | 82,7% |
| **AP2** | 95% | 75% | 78,8% |
| **AP3** | 95% | 72% | 77,4% |
| **AP4** | 100% | 84% | 83% |
| **AR1** | 70% | 70% | 77,6% |
| **AR2** | 70% | 70% | |
| **$AR3_A$** | 100% | 88% | 75,5% |
| **$AR3_B$** | 100% | 70% | 74% |
| **B1N** | 50% | 70% | |
| **BR1N** | 50% | 70% | |

**Table 4.1.2:** Summary of molecular characterization of 14 heteroplasmic RD-cybrids clones**.**

### 4.1.2.2 Differentiation

In the obtained heteroplasmic cybrids, the capacity to differentiate in myotubes was tested. Cells were grown in differentiation medium for 15 days (see paragraph 3.1.4.2).

As summarised in table 4.1.3, a lot of clones showed a good differentiation, measured as myotubes' amount, size and nuclei content. The best result was observed in clones with 100% RD nuclear background, such as A5N, AP2+U, AP4+U, $AR3_A$, $AR3_B$.

| CLONES | MYOGENIC CAPACITY | PELLET DNA |
|---|---|---|
| **A1** | + | 5 and 12 days |
| **A1+U** | ++ | 5 and 12 days |
| **A4N** | - | 6, 9, 12 and 15 days |
| **A5N** | +++ | 6, 8, 13 and 15 days |
| **AP1** | + | 9 and 15 days |
| **AP2** | ++ | 8 and 14 days |
| **AP3** | - | 6, 10, 12 and 14 days |
| **AP4** | ++ | 6, 9, 12 and 16 days |
| **AR1** | | |
| **AR2** | - | 7, 9, 12 and 15 days |
| **$AR3_A$** | +++ | 6, 9, 12 and 15 days |
| **$AR3_B$** | +++ | 6, 9, 12 and 15 days |
| **B1N** | | |
| **BR1N** | | |

**Table 4.1.3:** Differentiation assays. One or more + symbols denote a good degree of differentiation, while – means no signs of myotubes. The last column reports the days at which cells were collected to extract DNA.

In differentiated clones, mitochondrial shape and distribution were observed with the mitochondrial target fluorescence probe MitoTraker Red and images were taken at fluorescence microscope. Figure 4.1.3 shows a normal mitochondrial distribution in myotubes of heteroplasmic RD-cybrids.

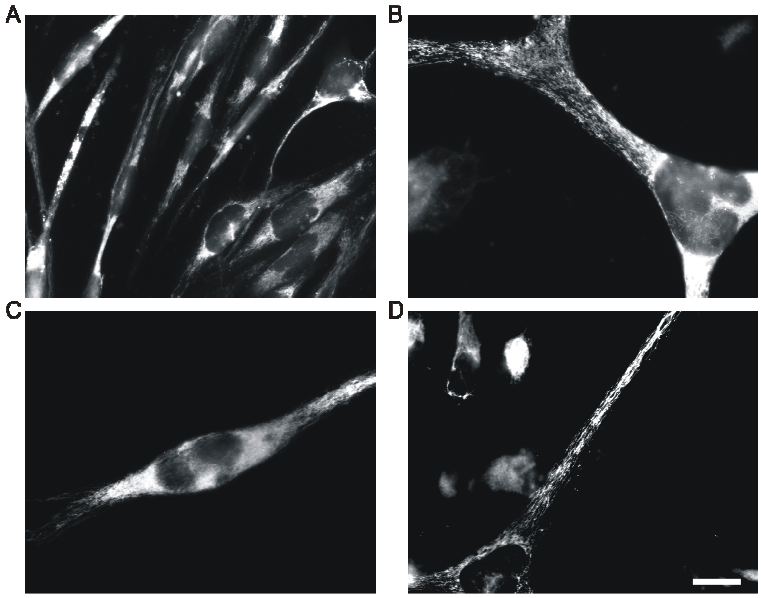


**Figure 4.1.3:** mitochondrial distribution in myotubes of 92% mutant RD-cybrids (A5N) at 13 days of differentiation. MitoTracker Red was used to stain mitochondria. Scale bar: 20μm.

To study if differentiation could influence the proportion of mutant mtDNA, heteroplasmic RD cybrids were induced to differentiate in the following growth regimes: standard medium, medium with 0.5mM NAC and medium with 100μM creatine. Cells were collected after different days of differentiation (see table 4.3) to extract DNA. DNA was used to analyze nuclear background and percentage of mutant mtDNA.

Figure 4.1.4 shows myotubes obtained in clone A5N.

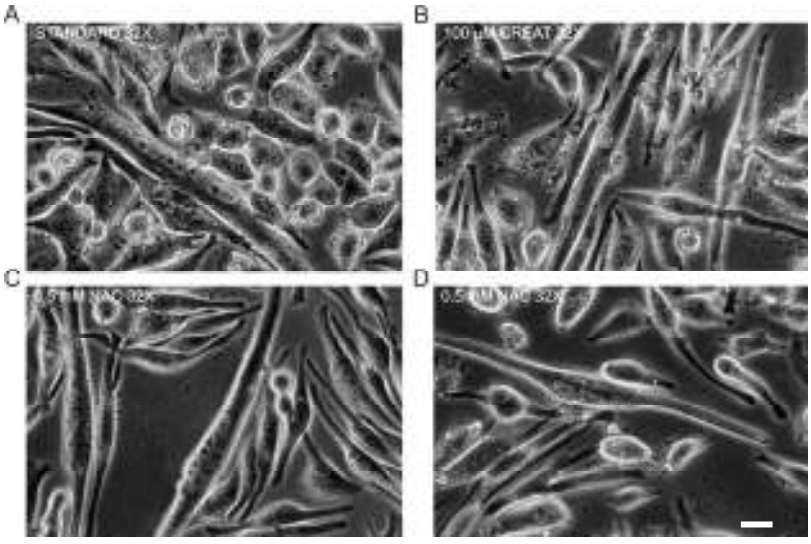


**Figure 4.1.4:** contrast phase images of myotubes from 92% mutant RD-cybrids (A5N) at 15 days differentiation in different treatments: standard differentiation medium (**A**), 100μM creatine (**B**) and 0.5mM NAC (**C** and **D**). Scale bar: 20μm.

Figure 4.1.5A confirms that differentiation carried out only in cells with pure RD nuclear background. Addition of NAC or creatine during differentiation didn't change percentage of mutant mtDNA in A5N (figure 4.5B)

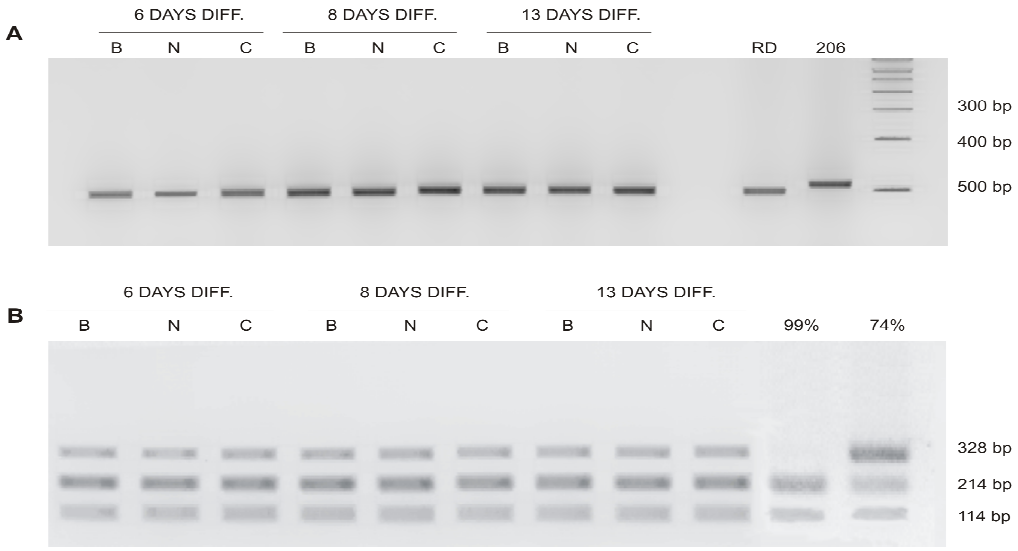


**Figure 4.1.5**: polymorphism analysis (A) and MELAS RFLP-PCR (B) of A5N cybrids (92% MELAS mutant) differentiated in standard conditions, or in presence of 0.5mM NAC (N) or 100μM creatine (C). PCR products were run in 2% agarose gel with EtBr.

### 4.1.2.3 Oxygen consumption

Basal oxygen consumption was measured in each clone as described in paragraph 3.2.2. Functionality of respiratory chain in each clone was compared to the one of parental RD cells.

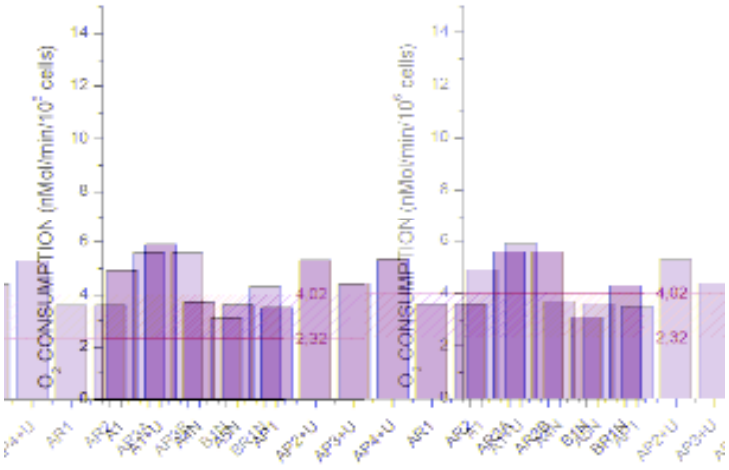


**Figure 4.1.6:** basal $O_2$ consumption of RD heteroplasmic cybrids. Values are referred to a range of values of oxygen consumption representing the normal respiratory activity.

As showed in figure 4.1.6, the obtained heteroplasmic RD cybrids had a normal $O_2$ consumption. In fact in each clone the mutant mtDNA percentage doesn't reach the threshold value corresponding to the appearance of the pathological phenotype. Some clones (A1, A1+U, AP2+U, AP4+U, $AR3_A$ and $AR3_B$) showed oxygen consumption superior to the one of parental RD cells. This could be due to an increased mitochondrial biogenesis in uridine treated cells.

### *4.1.3 Growth regimes with decreased glucose content*

Two RD heteroplasmic cybrid clones, previously obtained, were chosen to test the effect of reduced glucose content in the medium on percentage of mutant mtDNA. The study was performed on A5N and AP4+U. Both of them were chosen because they had 100% muscular nuclear background and a good ability to differentiate. Moreover A5N had 92% of mutant mtDNA, a value that is close to the cellular 95-98% threshold for phenotypic expression of MELAS, while AP4+U had an 83% of mutant mtDNA.

A control cell line, represented by 0% mutant mtDNA (WT) was studied in parallel.

The three different clones were treated with three different glucose concentrations, 25mM (standard condition), 10mM (G10) and 5mM (G5). In each condition the effects of 100μM creatine, 50μg/ml uridine and together 100μM creatine and 50μg/ml uridine were then analysed.

Table 4.1.4 resumes the experiment performed on these three clones for a period of 54 days.

Every 8 days cells were collected and counted to calculate the growth rate and one million of cells were used to measure $O_2$ consumption. After the oxygraphies, cells were collected and used to extract DNA. The DNA was used to quantify mtDNA content by RT-PCR and to calculate mutant mtDNA percentage to verify possible effects of growth regimes on mutant mtDNA segregation.

After 15 and 30 days of treatment, ROS production was quantified by AMPLEX method (see paragraph 3.2.1).

#### 4.1.3.1 Growth rate

Doubling time (DT), expressed in hours, was calculated for each clone in each condition. Cells, collected for the oxygraphies, were counted and the obtained values were used to calculate the doubling time.

Since the presence of 100μM creatine gave no different effects compared to the respective glucose medium, data obtained with creatine were not considered in this work.

Surprisingly 0% mutant control line resulted the most sensitive to reduced energy supply compared to 83% and 92% heteroplasmic mutant RD cybrids, in fact 0% cybrids died after 3-4 days of treatment. Consistent with this null tolerance to decreased energy supply, 0% mutant RD clones stopped to grow and died after 4 days of treatment with G5 and G10. At 4 days all the cells were found floating in the medium. Whereas 92% and 83% mutant cells grew in low glucose (G5) till 29 and 34 days.

Uridine preserved all the cells from death.

No significant variation in the percentage of mutant mtDNA was found in all the cells treated either with decreased glucose and plus or minus creatine and uridine.

Oxygen consumption was unaffected by growth regimes but was increased by uridine treatment, in association with an increased mtDNA amount, probably index of mitochondrial biogenesis.

ROS production was reduced in all the cells in presence of uridine in normal and low glucose.

CONCLUTIONS: RD cybrids with a higher proportion of mutant mtDNA are more prone to compensate energy deprivation in vitro than wild-type cybrids. We can say that no other mutations were present in wild-type clone, since their entire mtDNA was sequenced [149].

Uridine always helps the cells to survive in energetic stress, promoting mechanisms of compensation such as mtDNA synthesis and probably mitochondrial biogenesis.

The characterization of 0%, 80%, 90% and 99% cybrids was performed in triplicate.

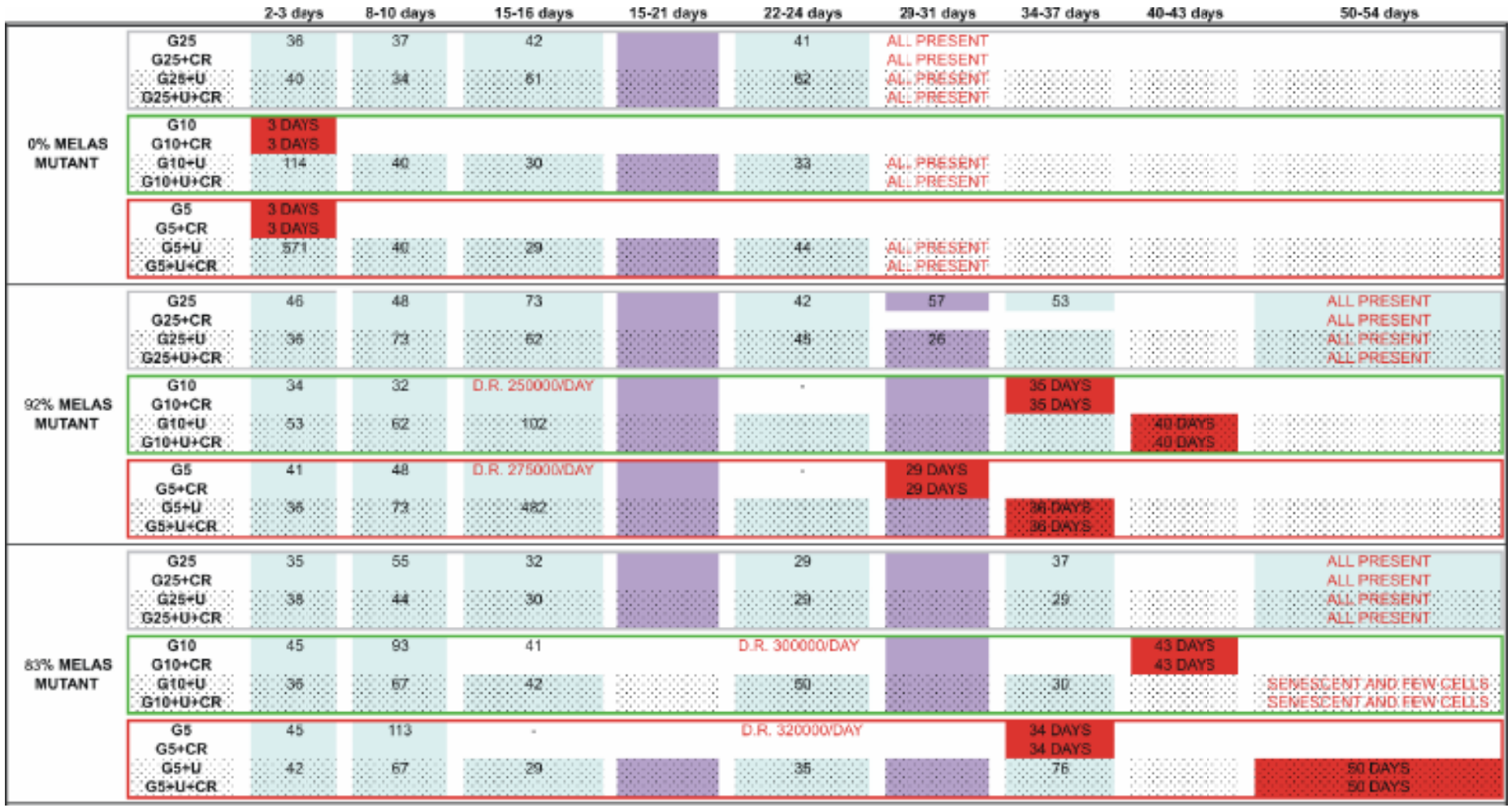


**Table 4.1.4:** plan of experiments done with MELAS RD cybrids in growth regimes up to 54 days of treatment. Different glucose concentrations are represented by different border lines. Uridine addition is represented by punctuate zone. Different shaded coloured zones are used to indicate different experiments: cyan for oxygen consumption measurement, growth rate calculation and DNA extraction; violet for ROS Amplex assay. Red boxes show death of the cell population and the day in which it occurred. Duplication times (in hours), and death rates (number of cells dyed/day) are reported into boxes.

## SECOND PART

To explain why heteroplasmic MELAS mutant RD cybrids survived better than wild-type cells in low glucose, we hypothesized a compensative induction of energy enzymes, as reported by Heddi [154]. To assess this hypothesis another set of experiments was performed: 0%, 83%, 92% and 99% RD cybrids were grown in normal (G25) and low (G5) glucose, supplemented or not with uridine for 8-20 days. Since the more interesting effects were in the first days of treatment, all the set of the second experimental plan was repeated focusing on the first 8 days.
The following physiological, biochemical and molecular parameters were tested:

- Growth rate, expressed as duplication time
- Oxygen consumption and respiratory control ratio (RCR) factor
- Activities of phosphofructokinase, lactic dehydrogenase, succinate dehydrogenase (SDH), cytochrome C oxidase (COX), citrate synthase (CS)
- Amount of mtDNA
- Percentage of mutant mtDNA

## *4.2 Functional and molecular responses to energetic stress in homoplasmic and heteroplasmic RD cybrids*

### 4.2.1 Growth rate

Growth rate, expressed as duplication time (DT) was calculated in cybrids with different percentage of mutant mtDNA in different growth regimes. So 0%, 83%, 92% and 99% RD cybrids were grown in normal (G25) and low (G5) glucose, supplemented or not with uridine 50µg/ml. For a week cells were collected and counted (see paragraph 3.1.5). The duplication time was calculated as described in paragraph 3.1.6.

Table 4.2.1 shows the mean values of counted cells. Measures were performed in triplicate. These values are represented in figure 4.2.1.

| %Melas | days | 0 | 1 | 2 | 3 | 4 | 6/7 |
|---|---|---|---|---|---|---|---|
| 0% | G25 | 104000 | 142600 | | 550000 | | $3,47x10^6$ |
| | G25+U | 93000 | 160000 | | 619000 | | $4,20x10^6$ |
| | G5 | 93500 | 178000 | 170000 | 658000 | $1,0x10^6$ | $2,38x10^6$ |
| | G5+U | 83000 | 174000 | | 591000 | | $5,14x10^6$ |
| 99% | G25 | 89300 | 94000 | | 391800 | | $1,26x10^6$ |
| | G25+U | 89300 | 135200 | | 275000 | | $1,18x10^6$ |
| | G5 | 94200 | 165000 | 153000 | 240600 | | 416600 |
| | G5+U | 80200 | 84800 | | 215600 | | 487500 |
| 92% | G25 | 75400 | 119000 | | 237500 | | 821000 |
| | G25+U | 56400 | 96200 | | 280000 | | $3,05x10^6$ |
| | G5 | 69000 | 99300 | 149000 | 247500 | 490400 | 548400 |
| | G5+U | 53100 | 120400 | | 328000 | | $3,8x10^6$ |
| 83% | G25 | 58500 | 108200 | | 339000 | | $2,15x10^6$ |
| | G25+U | 50900 | 86600 | | 440000 | | $4,22x10^6$ |
| | G5 | 48500 | 96700 | 142000 | 343700 | | $1,02x10^6$ |
| | G5+U | 37700 | 89100 | | 522500 | | $2,25x10^6$ |

**Table 4.2.1:** mean values of counted 0%, 83%, 92% and 99% cybrids in different growth regimes (G25, G5, G25+U, G5+U). Cells dying at the 8$^{th}$ day of treatment are reported in red. Measures were done in triplicate. These values were used to determinate the duplication time.

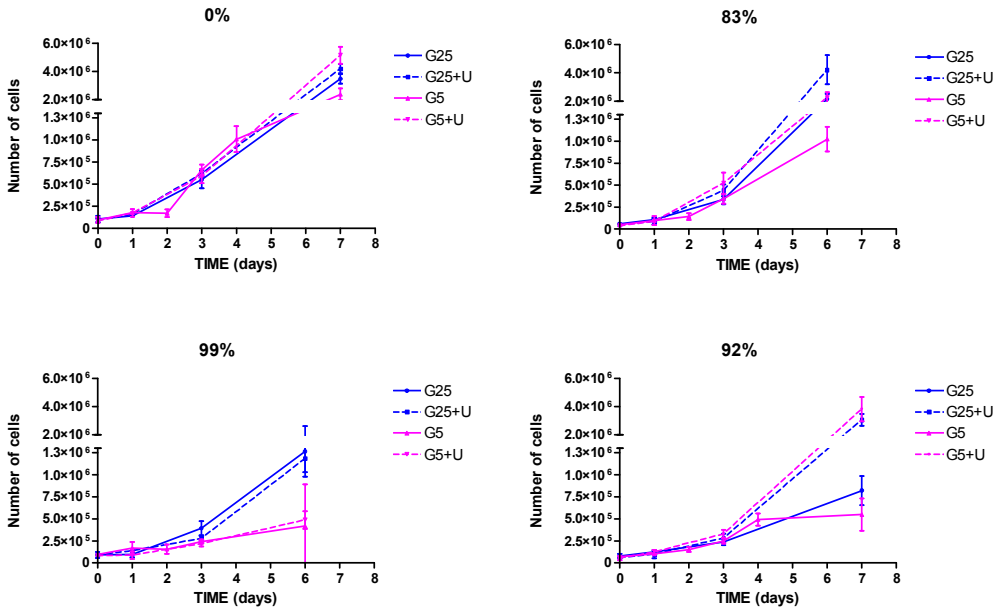


**Figure 4.2.1**: growth curves for 0%, 99%, 92% and 83% RD cybrids in different growth regimes (G25, G5, G25+U, G5+U). Each point is the mean value of three measurements.

We observed again that both heteroplasmic MELAS 83% and 92% RD cybrids were more adapted to survive in reduced glucose concentration (G5) than homoplasmic 0% and 99% cybrids. G5 medium was changed each day in dishes with 0% cybrids to avoid their death after 3-4 days of treatment (tab. 4.1.4). 0% and 99% cybrids had a block in proliferation after two days of treatment in G5. Table 4.2.2 in fact shows that 0% and 99% cybrids had negative growth rate in G5: DT: -353 and DT: -220 respectively, while duplication time of heteroplasmic 83% and 92% cells was unaffected by G5 treatment. Duplication time in heteroplasmic 83% and 92% cybrids in G5 was the same observed in normal condition (G25): DT: 46-41 and DT: 33 hours respectively. Uridine seems to help growth in all homoplasmic and heteroplasmic cybrids.

| DUPLICATION TIME AFTER 2 DAYS OF TREATMENT | | | | |
|---|---|---|---|---|
| **GROWTH REGIMES** | PERCENTAGE OF MUTATION | | | |
| | **O%** | **99%** | **92%** | **83%** |
| **G 25** | 24 | 36 | 46 | 33 |
| **G 25+U** | 24 | 36 | 31 | 24 |
| **G 5** | **-353** | **-220** | 41 | 33 |
| **G5+U** | 25 | 36 | 33 | 19 |

**Table 4.2.2**: duplication time (hours) in 0%, 83% 92% and 99% RD MELAS cybrids after 2 days of treatment in growth regimes (G25, G5, G25+U, G5+U).

### 4.2.3 Oxygen consumption and RCR

In all the cybrids 0%, 83%, 92% and 99% in different growth regimes, oxygen consumption was measured and the respiratory control ratio (RCR) was calculated as ratio between the maximum $O_2$ consumption (in presence of FCCP) and basal $O_2$ consumption. RCR factor indicates the part of the total respiratory potentiality used by the cell. It is an index of bioenergetic conditions: high values, around 2, indicate good bioenergetic conditions; low values, around 1, indicate bioenergetic stress conditions.

The $O_2$ consumption data are summarized in table 4.2.3 and in figure 4.2.2, while figure 4.2.3 shows the values of RCR factor.

| Percentage of mutant mtDNA | Growth Regime | BASAL MEAN VALUE (nmol $O_2$/min/$10^6$cells) | FCCP MEAN VALUE (nmol $O_2$/min/$10^6$cells) | *RCR (FCCP/basal)* |
|---|---|---|---|---|
| **0%** | **G25** | 2,9±0,98 | 5,05±2,06 | *1,74* |
| | **G5** | 3,99±0,61 | 5,26±0,65 | *1,32* |
| | **G25+U** | 3,02±0,69 | 4,84±1,4 | *1,6* |
| | **G5+U** | 3,69±0,43 | 4,75±0,63 | *1,29* |
| **99%** | **G25** | 1,04±0,33 | 1,67±0,22 | *1,61* |
| | **G5** | 1,09±0,61 | 1,31±0,32 | *1,2* |
| | **G25+U** | 0,78±0,21 | 1,81±0,32 | *2,32* |
| | **G5+U** | 0,65 | 1,61 | *2,48* |
| **92%** | **G25** | 3,92±0,59 | 5,38±0,48 | *1,37* |
| | **G5** | 4,31±0,16 | 5,37±0,47 | *1,25* |
| | **G25+U** | 3,48±0,38 | 5,35±0,92 | *1,54* |
| | **G5+U** | 3,57±1,05 | 4,42±1,06 | *1,24* |
| **83%** | **G25** | 4,45±1,14 | 6,14±1,31 | *1,38* |
| | **G5** | 4,09±0,58 | 5,83±1,07 | *1,43* |
| | **G25+U** | 4,12±0,93 | 6,01±0,99 | *1,46* |
| | **G5+U** | 4,28±0,17 | 5,45±0,27 | *1,27* |

**Table 4.2.3:** oxygen consumption values in 0%, 83%, 92% and 99% RD cybrids in different growth regimes (G25, G5, G25+U, G5+U). Basal values and maximal values (in presence of FCCP) are expressed as nmol/min/$10^6$cells. In italics are reported the RCR values. Measurements were done in triplicate.

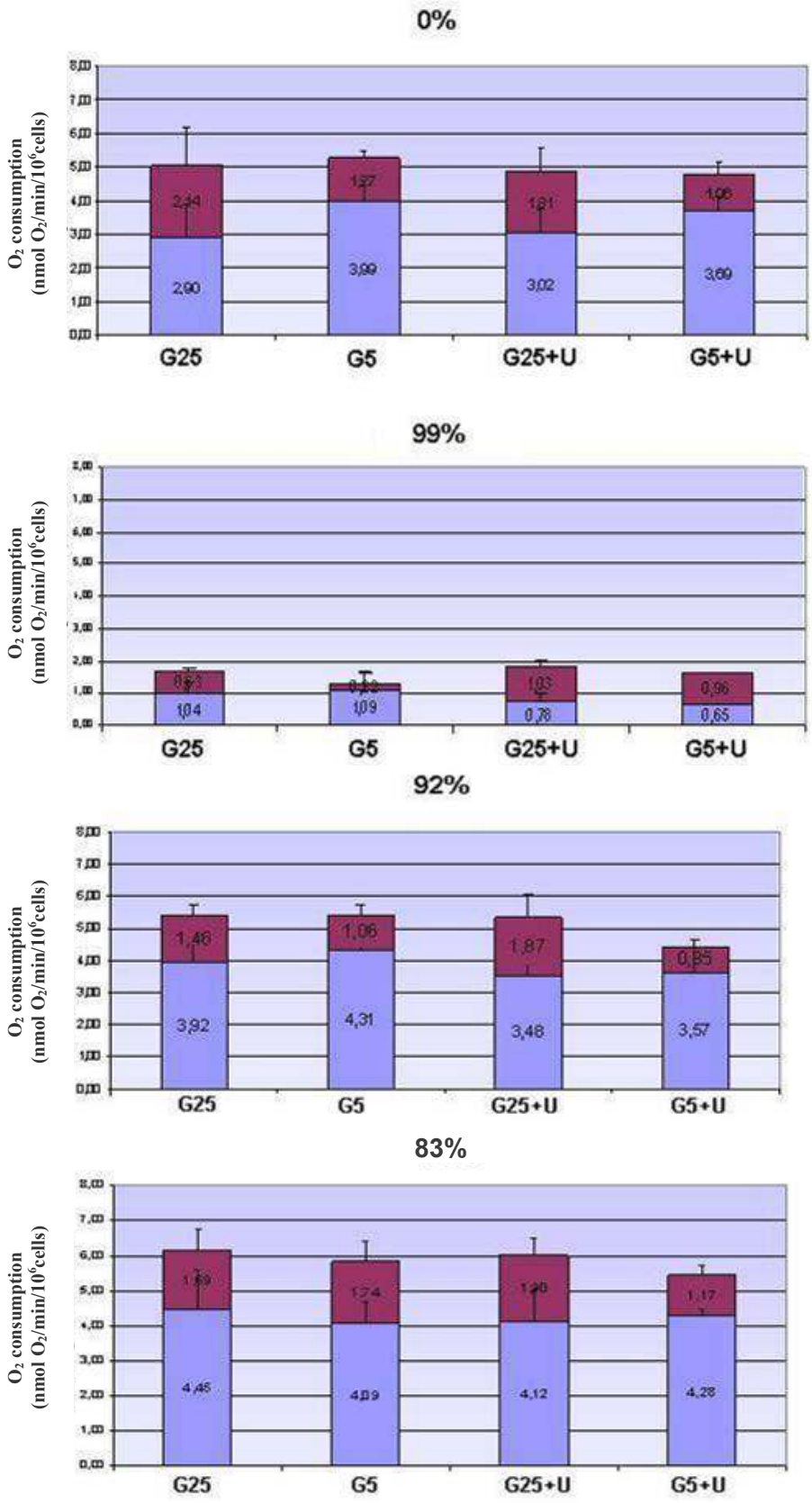


**Figure 4.2.2:** oxygen consumption values in 0%, 83%, 92% and 99% RD cybrids in different growth regimes (G25, G5, G25+U, G5+U). Basal values (blue) and maximal values (in presence of FCCP) (violet) are expressed as nmol/min/$10^6$cells. Measurements were done in triplicate.

In wild-type and heteroplasmic cybrids there wasn't a significant difference in the basal value of $O_2$ consumption that is between 3,4 and 4,2 nmol $O_2$/min/$10^6$cells. These heteroplasmic cybrids in fact didn't overcome the threshold value of mutant mtDNA, so they have a normal respiration.

It's really interesting to see that in G5, RCR factor was significantly reduced in both 0% and 99% cybrids, but not in 83% and 92% (fig. 4.2.3). This finding was indicative of a bioenergetic stress of 0% and 99% cells in low glucose.

Although uridine helps the growth in heteroplasmic cybrids, it didn't give any variation in oxygen consumption values or in RCR factor (fig. 4.2.2 and 4.2.3).

As we expected, RD MELAS 99% cybrids had a reduced $O_2$ consumption. The basal value was around 1nmol$O_2$/min/$10^6$cells. It was significantly reduced compared to the other cybrids ($P<0,05$) (fig. 4.2.2).

Uridine increased significantly the RCR factor in 99% cybrids in both G25 and G5, index of a reduced respiratory stress.

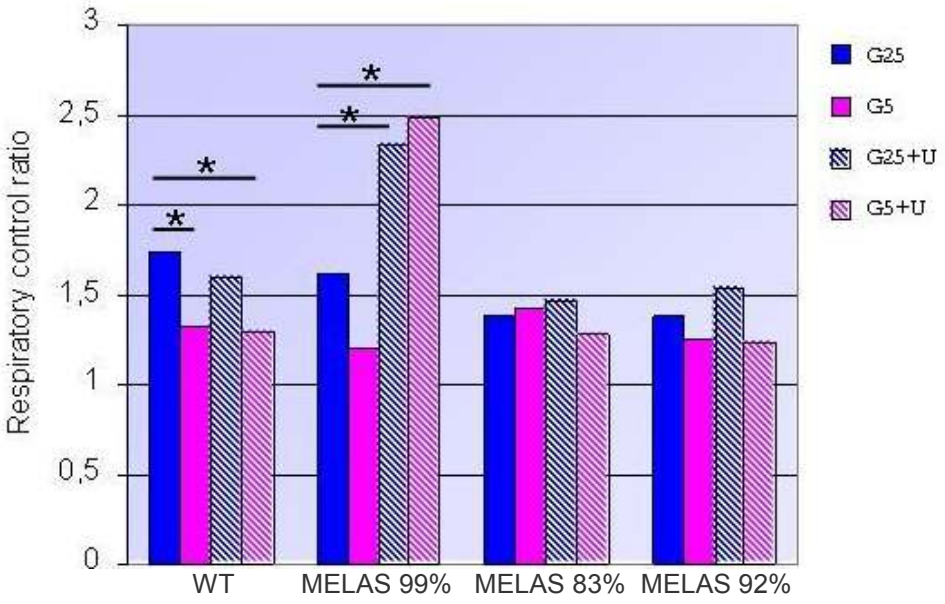


**Figure 4.2.3:** RCR factor in 0%, 83%, 92% and 99% cybrids in different growth regimes. Values are ratio of three different measurements. *($P<0,05$).

### 4.2.4 ROS production

ROS production was measured by Amplex red method in 0%, 83%, 92% and 99% cybrids in different growth regimes (G25, G25+U, G5, G5+U).

Figure 4.2.4 resumes the results of ROS production.

In G25 ROS generation from heteroplasmic 92% and 83% cybrids was significantly lower compared to 0% cybrids ($P<0.05$ and $P<0.01$ respectively).

The stress caused by low glucose concentration (G5mM) didn't increase ROS generation in all the cells. In G25, heteroplasmic cybrids were more protected from oxidative stress than control cells. In G5, 0% and 99% RD cybrids were not subjected to oxidative stress.

Uridine reduced ROS production only in wild-type cells growing in G25, but it didn't cause any variation in ROS production in the other clones and in the other growth regimes.

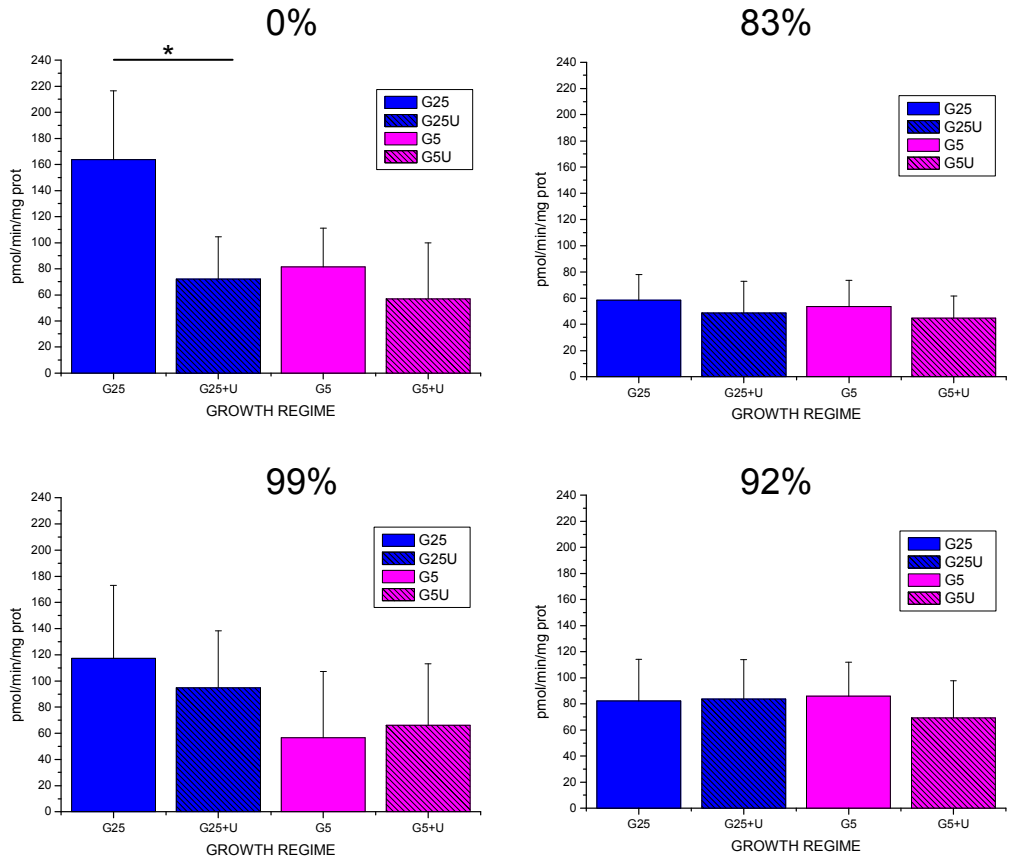


**Figure 4.2.4:** ROS production measured by Amplex red method in 0%, 83%, 92% and 99% cybrids in different growth regimes (G25, G25+U, G5, G5+U). ROS production was measured as pmol/min/mg prot. *p<0.05

| Percentage of mutant mtDNA | Growth regimes | ROS PRODUCTION (pmol/min/mg prot) |
|---|---|---|
| 0% | G25 | 163,67±52,75 |
| | G25+U | 72,07±32,38 |
| | G5 | 81,43±29,62 |
| | G5+U | 57,01±42,93 |
| 99% | G25 | 117,34±55,57 |
| | G25+U | 94,63±43,61 |
| | G5 | 56,63±50,69 |
| | G5+U | 66,18±46,92 |
| 92% | G25 | 82,28±31,82 |
| | G25+U | 83,60±30,18 |
| | G5 | 85,91±26,11 |
| | G5+U | 69,38±28,21 |
| 83% | G25 | 58,42±19,44 |
| | G25+U | 48,79±24,11 |
| | G5 | 53,47±20,04 |
| | G5+U | 44,74±16,79 |

**Table 4.2.4:** ROS production in 0%, 83%, 92% and 99% cybrids in different growth regimes (G25, G25+U, G5, G5+U) expressed as pmol $H_2O_2$/min/mg protein. Measurements were performed in triplicate.

### 4.2.5 Enzymatic activities

To understand the biochemical and molecular bases of the better survival of heteroplasmic MELAS mutant RD cybrids in low glucose rather than wild-type cells, enzymatic activities of complexes of respiratory chain and of some glycolytic enzymes were assessed.

Table 4.2.5 and the first part of table 4.2.6 summarize mean values of activities of complexes I, II, IV of respiratory chain and of citrate synthase, obtained in the different cell lines after different days of treatment in growth regimes.

Table 4.2.6 shows mean values of two glycolytic enzymes activities, phosphofructokinase, the rate limiting step of glycolysis, and lactate dehydrogenase, obtained in the different cell lines after different days of treatment in growth regimes.

| | 2 days | | 4 days | | 8 days | | 20 days | |
|---|---|---|---|---|---|---|---|---|
| **NADH DH** | **nmol/min/mg** | ***(NADH/CS)*** | **nmol/min/mg** | ***(NADH/CS)*** | **nmol/min/mg** | ***(NADH/CS)*** | **nmol/min/mg** | ***(NADH/CS)*** |
| WT G25 | 491,3±50,7 | *3,5±0,18* | 535,0±145,2 | *3,4±0,47* | 601,1±21,9 | *3,0±0,26* | 549,3±45,41 | *2,5±0,07* |
| WT G25+U | 495,0±46,8 | *3,4±0,33* | 477,9±66,3 | *3,2±0,25* | 595,7±91,3 | *3,2±0,31* | 539,6±34,25 | *3,0±0,15* |
| WT G5 | 566,4±56,0 | *3,7±0,32* | 344,6±72,02 | *2,7±0,64* | 531,3±33,3 | *4,4±0,57* | 555,2±11,36 | *2,8±0,009* |
| WT G5+U | 520,7±81,1 | *3,4±0,26* | 378,8±50,01 | *2,9±0,58* | 573,2±54,8 | *4,0±0,25* | 591,9±33,88 | *3,6±0,34* |
| 99% G25 | 464,0±24,56 | *3,4±0,08* | 414,2±74,05 | *3,2±0,68* | 436,0±23,11 | *3,0±0,41* | 784,7±101,3 | *3,6±0,64* |
| 99% G25+U | 402,6±4,25 | *3,2± 0,2* | 427,5±70,01 | *3,2±0,49* | 443,0±9,87 | *2,6±0,09* | 727,2±48,61 | *3,4±0,23* |
| 99% G5 | 601,8±117,3 | *3,4± 0,45* | 504,1±76,3 | *3,1±0,17* | 509,1±12,36 | *3,0±0,15* | 583,3±11,44 | *2,9±0,2* |
| 99% G5+U | 627,1±164,7 | *3,2±0,16* | 494,4± 30,82 | *3,2±0,07* | 495,6±25,13 | *3,2±0,43* | 659,0±54,09 | *3,2±0,48* |
| 92% G25 | 350,1± 7,41 | *3,3± 0,7* | 598,4± 18,91 | *5,1±0,9* | 523,3±42,77 | *4,7±0,83* | 527,2±34,37 | *3,5±0,15* |
| 92% G25+U | 424,7± 1,32 | *3,2± 0,1* | 687,2± 50,43 | *5,4±0,8* | 526,2±27,54 | *4,6±0,41* | 600,8±74,07 | *5,1±0,6* |
| 92% G5 | 419,6± 17,53 | *3,2± 0,3* | 788,7± 16,24 | *4,5±0,21* | 503,9±32,12 | *3,3±0,39* | 575,0±42,46 | *4,1±0,18* |
| 92% G5+U | 503,5± 84,79 | *3,6±0,58* | 649,0± 75,08 | *3,9±0,21* | 558,7±22,91 | *3,4±0,23* | 617,8±9,61 | *5,3±0,18* |
| 83% G25 | 330,4± 6,16 | *3,8±0,58* | 572,6± 20,85 | *5,7±1,37* | 424,3±19,38 | *5,0±0,28* | 422,9±47,92 | *4,2±0,96* |
| 83% G25+U | 326,6± 0,86 | *3,2± 0,1* | 564,7± 16,31 | *4,9±0,06* | 427,1±12,74 | *4,9±0,28* | 447,9±43,77 | *5,3±1,7* |
| 83% G5 | 380,5± 21,88 | *3,4±0,57* | 554,0± 48,43 | *3,7±0,33* | 478,6±17,28 | *3,9±0,68* | 461,1±28,8 | *4,8±0,33* |
| 83% G5+U | 376,2± 103,13 | *3,2± 0,99* | 531,3±43,61 | *3,2±0,06* | 451,6±39,5 | *4,2±0,39* | 438,4±5,21 | *5,2±0,36* |

| **SDH** | nmol/min/mg | *(SUCC/CS)* | nmol/min/mg | *(SUCC/CS)* | nmol/min/mg | *(SUCC/CS)* | nmol/min/mg | *(SUCC/CS)* |
|---|---|---|---|---|---|---|---|---|
| WT G25 | 5,2±1,24 | *3,3±1,45* | 6,1±1,13 | *4,0±0,85* | 5,7±1,35 | *3,3±0,44* | 6,1±0,16 | *2,8±0,25* |
| WT G25+U | 5,9±0,62 | *3,3±0,67* | 5,8±0,35 | *3,9±0,67* | 6,6±0,91 | *3,6±0,05* | 6,7±0,52 | *3,7±0,36* |
| WT G5 | 6,6±1,53 | *4,3±0,89* | 4,8±1,84 | *3,5±0,15* | 6,6±1,46 | *5,2±1,2* | 7,0±1,14 | *3,6±0,69* |
| WT G5+U | 6,3±0,97 | *4,2±0,86* | 5,4±1,29 | *4,0±0,52* | 6,5±0,34 | *5,0±0,25* | 6,6±0,36 | *4,1±0,25* |
| 99% G25 | 6±0,37 | *4±0,5* | 6,9±0,5 | *5,3±0,4* | 6±0,39 | *4,1±0,39* | 7,5±0,8 | *3,5±0,44* |
| 99% G25+U | 6,3±0,81 | *4,1±0,5* | 4,8±0,6 | *3,6±0,5* | 6,3±0,13 | *3,7±0,13* | 7,1±1,22 | *3,9±0,56* |
| 99% G5 | 8,6±2,56 | *4,8±0,91* | 6,2±1,23 | *3,8±0,61* | 7,2±0,64 | *4,3±0,32* | 7,9±0,9 | *4±0,69* |
| 99% G5+U | 8,9±2,65 | *4,5±0,48* | 6,6±0,34 | *4,3±0,31* | 6,7±0,25 | *4,3±0,4* | 9,1±0,29 | *4,4±0,43* |
| 92% G25 | 5,3±0,84 | *5,1±1,76* | 7,8±2,05 | *7±3,27* | 6,3±0,56 | *5,7±1,05* | 6,2±0,23 | *0,57* |
| 92% G25+U | 5,9±0,41 | *4,4±0,32* | 8±0,06 | *6,3±0,45* | 6,6±1,02 | *5,8±0,32* | 7±0,47 | *5,9±0,44* |
| 92% G5 | 6,3±0,78 | *4,8±0,89* | 7,1±1,64 | *4±0,89* | 7,2±0,54 | *4,8±0,33* | 5,8±0,1 | *4,1±0,49* |
| 92% G5+U | 5,1±1,22 | *3,7±1,67* | 7,9±1,85 | *4,9±1,52* | 7,3±0,89 | *4,4±0,62* | 6,5±0,86 | *5,6±0,76* |
| 83% G25 | 6±0,47 | *6,8±1,12* | 7,1±0,53 | *7,1±1,97* | 5,2±0,36 | *6,1±0,54* | 4,8±0,6 | *4,8±1,6* |
| 83% G25+U | 5±0,76 | *5,0±0,77* | 8,7±1,13 | *7,6±0,93* | 5,7±0,7 | *6,5±0,47* | 5,7±0,72 | *6,7±2,38* |
| 83% G5 | 5,7±0,54 | *5,1±0,71* | 7,5±3,02 | *5±1,93* | 6,8±0,42 | *5,5±1,02* | 6,1±0,69 | *6,3±0,56* |
| 83% G5+U | 5,4±0,53 | *4,6±0,92* | 7,7±1,44 | *4,7±1,15* | 7,7±0,53 | *7,1±0,58* | 6,2±0,15 | *7,3±0,66* |

| **COX** | nmol/min/mg | *(COX/CS)* | nmol/min/mg | *(COX/CS)* | nmol/min/mg | *(COX/CS)* | nmol/min/mg | *(COX/CS)* |
|---|---|---|---|---|---|---|---|---|
| WT G25 | 19,8±3,65 | *11,7±1,27* | 20±5,65 | *13,8±6,43* | 22±0,69 | *11,1±0,96* | 11,5±0,62 | *5,3±0,17* |
| WT G25+U | 19,9±2,55 | *12,4±2,04* | 23,7±6,18 | *16,3±6,24* | 25,6±1,48 | *14±1,25* | 10,8±0,52 | *6±0,3* |
| WT G5 | 17,8±7,82 | *11,8±5,13* | 16,4±7,84 | *11,5±1,67* | 10,8±2,02 | *8,9±2,16* | 11±0,71 | *5,6±0,14* |
| WT G5+U | 19,6±6,96 | *12,6±2,59* | 23±8,57 | *15,4±4,12* | 11,4±2,15 | *8,1±1,15* | 14±1,42 | *8,5±0,81* |
| 99% G25 | 5,4±0,48 | *3,6±0,24* | 4,6±1,92 | *3,6±1,54* | 4,6±0,69 | *3,1±0,4* | 10,1±2,32 | *4,7±1,25* |
| 99% G25+U | 5,85±1,53 | *3,79±0,73* | 3,95±0,52 | *2,96±0,35* | 5,08±0,73 | *2,95±0,43* | 10,43±1,63 | *5,72±0,81* |
| 99% G5 | 7,4±2,28 | *4,1±0,82* | 5,1±1,74 | *3,3±1,33* | 6,4±0,19 | *3,8±0,15* | 6,1±1,6 | *3,1±1,03* |
| 99% G5+U | 7,2±2,02 | *3,7±0,21* | 5,8±2,16 | *3,8±1,55* | 6,2±0,4 | *4±0,51* | 7,8±0,82 | *3,8±0,66* |
| 92% G25 | 30,4±0,63 | *29,2±5,72* | 34,3±2,46 | *29,7±4,19* | 67,7±4,28 | *61±10,62* | 71,5±4,37 | *47,8±2,32* |
| 92% G25+U | 37,6±0,91 | *28,4±0,95* | 44,8±2,67 | *35,5±4,92* | 60,1±3,8 | *53±5,44* | 81,1±3 | *69,2±6,87* |
| 92% G5 | 34,4±1,93 | *26,2±1,49* | 47,2±1,36 | *26,8±2,28* | 54±4,66 | *35,8±1,71* | 67,7±10,57 | *48,9±12,77* |
| 92% G5+U | 44,3±8,49 | *31,3±5,15* | 57,1±5,21 | *34,7±2,92* | 65,8±4,23 | *40±3,67* | 86±2,28 | *73,7±0,64* |
| 83% G25 | 35,3±8,01 | *40,7±13,03* | 44,5±3,48 | *44,3±11,37* | 63,6±0,7 | *74,6±7,96* | 22,7±1,01 | *23,1±7,54* |
| 83% G25+U | 31,6±7,99 | *31,1±7,55* | 57,4±5,55 | *50±4,58* | 56,9±8,26 | *66,2±13,56* | 31,5±0,56 | *36,9±9,88* |
| 83% G5 | 45,2±4,51 | *40,9±8,84* | 62,2±5,49 | *41,5±5,5* | 66,2±1,68 | *54,4±12,61* | 43,1±1,29 | *44,5±2,51* |
| 83% G5+U | 45,3±2,73 | *38,7±5,96* | 73,6±9,41 | *44,9±7* | 72,4±4,49 | *68,1±14,61* | 50,5±5,34 | *60,2±11,26* |

**Table 4.2.5:** mean values of activities of complexes I (NADHDH), II (SDH) and IV (COX) of respiratory chain in RD cybrids 0%, 99%, 92% and 83% obtained in the different cellular cell lines after different days of treatment in growth regimes G25, G25+U, G5 and G5+U. Measurements were performed in triplicate and expressed as nmoles/min/mg protein. The activities of the complexes are normalized for activity of citrate synthase (italics values).

| | 2 days | 4 days | 8 days | 20 days |
|---|---|---|---|---|
| **CS** | **nmol/min/mg** | **nmol/min/mg** | **nmol/min/mg** | **nmol/min/mg** |
| WT G25 | 170,7±37,76 | 157,9±37,19 | 199,9±18,14 | 216,6±18,61 |
| WT G25+U | 187,5±62,28 | 152,7±27,46 | 184,6±28,06 | 180±5,79 |
| WT G5 | 153,4±9,8 | 137,2±56,03 | 122,2±7,51 | 196,6±8,21 |
| WT G5+U | 152±32,2 | 137,2±41 | 140,9±5,52 | 164,3±10,93 |
| 99% G25 | 151,6±21,02 | 131,3±13,6 | 146,7±24,3 | 219,2±46,47 |
| 99% G25+U | 154,4±31 | 133,6±13,4 | 172,6±2,75 | 182,3±5,06 |
| 99% G5 | 177,5±25,46 | 162,4±17,84 | 167,1±4,3 | 198,4±14,16 |
| 99% G5+U | 197,7±52,65 | 154,1±7,88 | 157,6±16,7 | 207,7±13,41 |
| 92% G25 | 106,2±18,63 | 117,5±24,33 | 112,6±16,08 | 150±16,23 |
| 92% G25+U | 132,2±2,74 | 126,8±10,32 | 114±10,98 | 117,9±9,13 |
| 92% G5 | 131,7±10,09 | 176,7±11 | 151,2±18,08 | 141±14,8 |
| 92% G5+U | 143±26,11 | 164,7±11,52 | 164,9±4,6 | 116,7±3,31 |
| 83% G25 | 88,9±16,14 | 103,1±20,25 | 85,8±8,44 | 105,2±31,51 |
| 83% G25+U | 101,3±1,71 | 114,2±1,18 | 86,7±6,42 | 89,2±21,1 |
| 83% G5 | 112,1±11,75 | 150,7±7,32 | 125,7±26,64 | 97,2±8,17 |
| 83% G5+U | 118,2±10,95 | 164,5±12,94 | 108,6±16,15 | 84,7±6,3 |

| **PFK** | **nmol/min/mg** | **nmol/min/mg** | **nmol/min/mg** | **nmol/min/mg** |
|---|---|---|---|---|
| WT G25 | 131,1±44,21 | 147,8±45,99 | 127,6±5,02 | 161,7±25,25 |
| WT G25+U | 113,7±23,53 | 113,1±24,16 | 123,6±5,79 | 141,5±5,92 |
| WT G5 | 113,6±20,56 | 125,2±12,72 | 108,3±16,09 | 145,4±10,1 |
| WT G5+U | 111,4±14,91 | 106,9±17,25 | 98,3±5,1 | 116,6±17,76 |
| 99% G25 | 169,8±7,89 | 147,5±14,69 | 97,2±52,13 | 184,9±40,82 |
| 99% G25+U | 186,4±13,76 | 135,5±20,45 | 97,1±10,74 | 185,2±16,4 |
| 99% G5 | 236,8±84,48 | 74,8±30,73 | 195,9±9,12 | 128±20,36 |
| 99% G5+U | 215±143,02 | 87±38,27 | 207,6±19,04 | 141,7±59,13 |
| 92% G25 | 234±23,27 | 274,1±12,78 | 238±22,54 | 291,5±22,51 |
| 92% G25+U | 260,7±22,6 | 270,8±14,24 | 239,2±14,38 | 284,4±16,58 |
| 92% G5 | 258,2±52,43 | 308,4±59,14 | 245,8±27,36 | 405,7±113,3 |
| 92% G5+U | 277,1±34,04 | 304,2±10,6 | 270,6±7,61 | 276,1±6,38 |
| 83% G25 | 210,6±16,38 | 279,8±45,25 | 177,5±1,46 | 203,5±17,72 |
| 83% G25+U | 190,7±24,53 | 268,2±22,23 | 184,5±5,94 | 177,2±32,59 |
| 83% G5 | 219,4±41,15 | 268,1±27,7 | 185,9±38,56 | 233,9±20,51 |
| 83% G5+U | 236,1±42,88 | 256,3±15,02 | 204,5±13,63 | 196,8±29,32 |

| **LDH** | **nmol/min/mg** | **nmol/min/mg** | **nmol/min/mg** | **nmol/min/mg** |
|---|---|---|---|---|
| WT G25 | 1723,1±452,7 | 1629,3±389 | 1673,4±140,1 | 1722,7±87,9 |
| WT G25+U | 1917,7±735,4 | 1615±250,66 | 1895,4±147,95 | 1748,3±140,8 |
| WT G5 | 1759,5±75,17 | 1332,7±493,0 | 1389±24,87 | 1682,6±72,35 |
| WT G5+U | 1713,3±313,8 | 1431,2±380,6 | 1262,3±962,8 | 1827,5±71,53 |
| 99% G25 | 1668,2±187,2 | 1539,9±179,92 | 1986±150,78 | 2227,1±270,7 |
| 99% G25+U | 1717±283,96 | 1589,3±235,4 | 1971,4±303,5 | 1971,2±175,7 |
| 99% G5 | 2159,4±406,11 | 1767,9±255,6 | 2187,7±108,02 | 1932±107,12 |
| 99% G5+U | 2284±437,6 | 1822,7±70,04 | 2282,7±67,13 | 2016,1±56,63 |
| 92% G25 | 1231,7±75,71 | 1515,6±125,0 | 1297,3±69,11 | 1372,6±154,6 |
| 92% G25+U | 1448,6±36,97 | 1340,8±550,8 | 1255,3±25,19 | 1392,6±11,27 |
| 92% G5 | 1177,4±87,19 | 1738,1±70,05 | 1203±33,96 | 1540,4±26,55 |
| 92% G5+U | 1542,9±127,1 | 1665±61,62 | 1250,4±68,72 | 1518,4±78,26 |
| 83% G25 | 993,4±83,12 | 2246,8±66,36 | 1625,6±191,91 | 1542,4±379,1 |
| 83% G25+U | 1087±121,01 | 2145,7±72,18 | 1763±69,23 | 2062,2±188,5 |
| 83% G5 | 2154,4±150,6 | 2466,5±65,38 | 1693,4±175,83 | 1847,5±152,12 |
| 83% G5+U | 2170,6±125,64 | 2588,1±99,77 | 1748,1±154,69 | 1912,5±103,63 |

**Table 4.2.6:** mean values of activities of citrate synthase (CS) and glycolytic enzymes phosphofructokinase (PFK) and lactate dehydrogenase (LDH), in RD cybrids 0%, 99%, 92% and 83% obtained in the different cellular lines after different days of treatment in growth regimes G25, G25+U, G5 and G5+U. Measurements were performed in triplicate and expressed in nmol/min/mg protein.

### 4.2.5.1 Complex II: Succinate dehydrogenase

Succinate dehydrogenase, the complex II of respiratory chain, is only encoded by the nuclear genome, so its activity is not impaired in mitochondrial diseases. This consideration was confirmed by our results, in fact as showed in figure 4.2.5 the succinate dehydrogenase activity, normalized to the activity of citrate synthase (SDH/CS), had a value that is about 5 in cybrids with mutant mtDNA and in wild-type cybrids. This value was obtained in all the growth regimes.

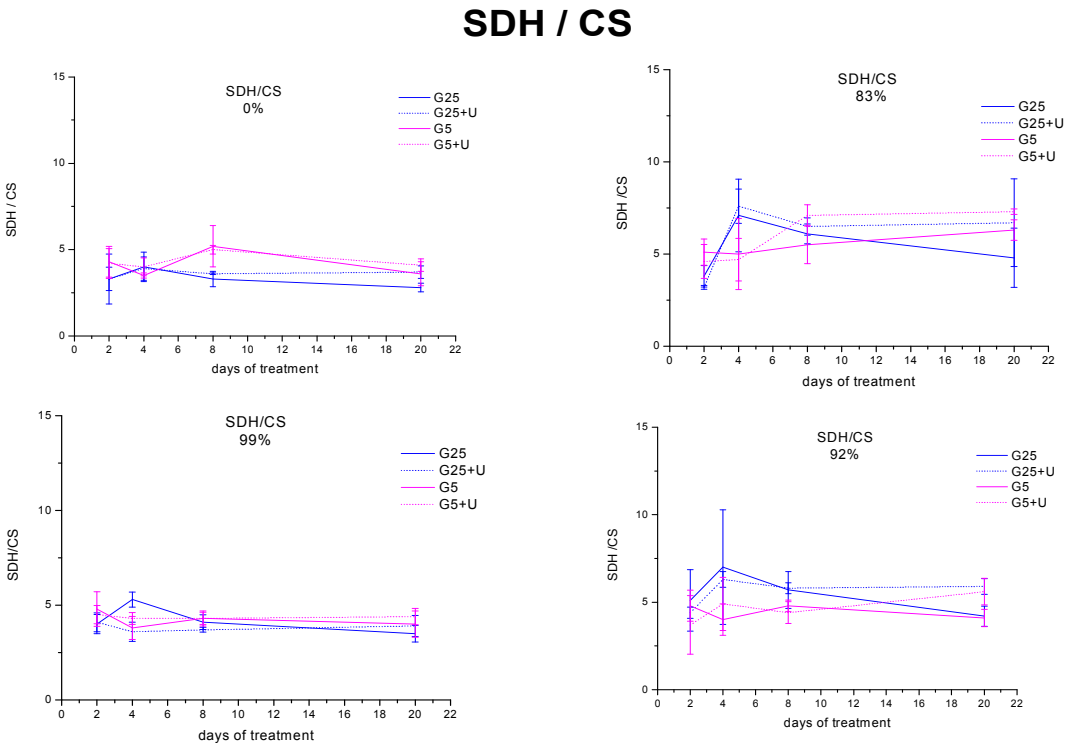


**Figure 4.2.5:** mean value of activity of complex II of respiratory chain, succinate dehydrogenase, normalized for the activity of citrate synthase, a mitochondrial matrix enzyme. The activity was measured in homoplasmic (0% and 99%) and heteroplasmic (92% and 83%) RD MELAS cybrids after different days of treatment in growth regimes (G25, G5, G25+U, G5+U). Measurements were performed in triplicate.

### 4.2.5.2 Complex IV: Cytochrome c oxidase (COX)

The COX assay highlighted great differences between heteroplasmic and homoplasmic cells. In normal conditions COX activity, expressed as ratio with CS, was 12 in wild-type cybrids (see figure 4.2.6 and table 4.2.5). RD MELAS cybrids 99% showed a clear reduction of COX activity, that was 30% of wild-type value (as showed in figure 4.2.6). This result corroborates the validity of enzymatic COX assay as test to verify the activity of respiratory chain.

Heteroplasmic cybrids (83%-92%), showed a significant and interesting increase of COX activity. 92% mutant cells had an increase of COX activity of 2,6-4,7-fold compared to wild-type cybrids and 83% mutant cells had an increase of COX activity of 3,6-6,7-fold compared to wild-type cybrids. In cybrids MELAS 83% at 20 days of treatment with G25, the ratio COX/CS was significantly reduced if compared to the values obtained in G5 and G5+U. During the first days of treatment, there were no significant differences among different growth regimes, because of the high standard deviations. In cybrids MELAS 92% after 8 days of treatment, the activity ratio COX/CS was significantly reduced in G5 and G5+U compared to G25. No significant differences were showed during the first days of treatment and after addition of uridine. After 20 days of treatment instead, COX activity was significantly increased when uridine was added: COX activity was higher in G25+U compared to G25 and in G5+U compared to G5.

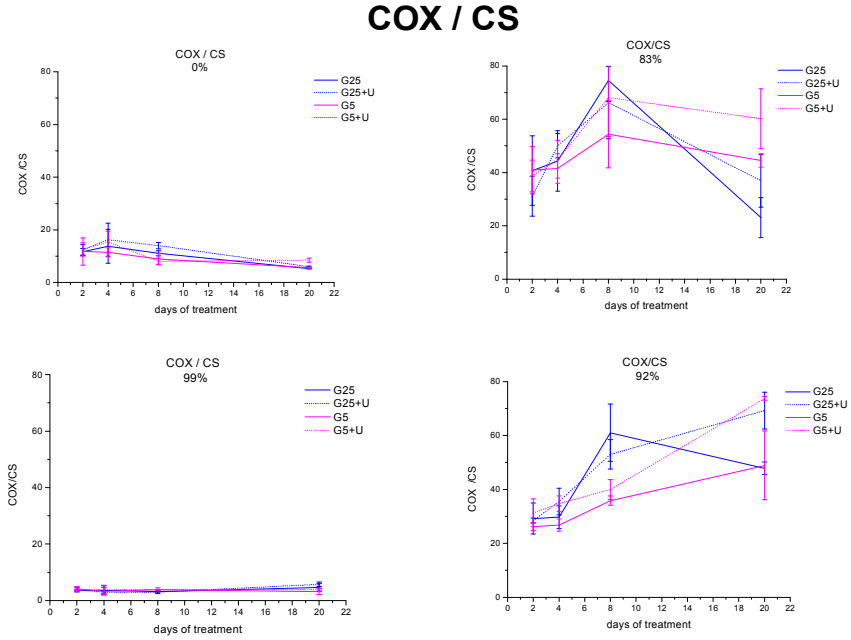


**Figure 4.2.6** mean value of activity of complex IV of respiratory chain, Cytochrome c oxidase, normalized for the activity of citrate synthase, a mitochondrial matrix enzyme. The activity was measured in homoplasmic (0% and 99%) and heteroplasmic (92% and 83%) RD MELAS cybrids after different days of treatment in growth regimes (G25, G5, G25+U, G5+U). Measurements were performed in triplicate.

### 4.2.5.3 Phosphofructokinase (PFK)

PFK activity, like COX activity, in heteroplasmic MELAS 92% and 83% cybrids, in normal condition (G25), was significantly increased compared to homoplasmic 0% and 99% MELAS cybrids, 1,6-1,78-fold (see figure 4.2.7 and table 4.2.6).

There were no significant differences in PFK activity in the different growth regimes and along the time.

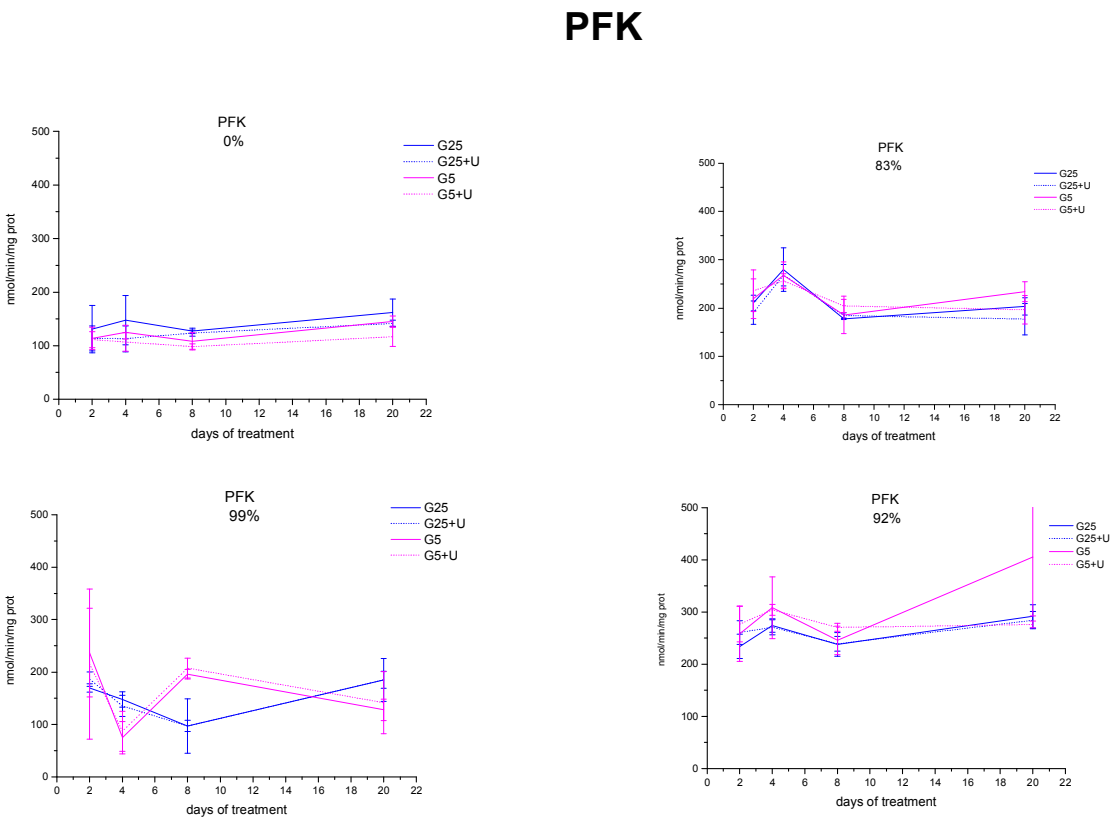


**Figure 4.2.7:** mean values of activity of the glycolytic enzyme phosphofructokinase, the step limiting enzyme of glycolysis. The activity was measured in homoplasmic (0% and 99%) and heteroplasmic (92% and 83%) RD MELAS cybrids after different days of treatment in growth regimes (G25, G5, G25+U, G5+U). Measurements were performed in triplicate.

### 4.2.5.5 Lactate dehydrogenase

There were no significant differences of LDH activity among different cell lines and different growth regimes (see figure 4.2.8 and table 4.2.6). The values obtained had a range between 1500 and 2000 nmoles/minute/milligrams of protein. The only exception was observed in 83% MELAS cybrids after 2 days of treatment with low glucose concentration (G5). In this condition these cells had a double LDH activity compared to the value obtained in normal condition (G25).

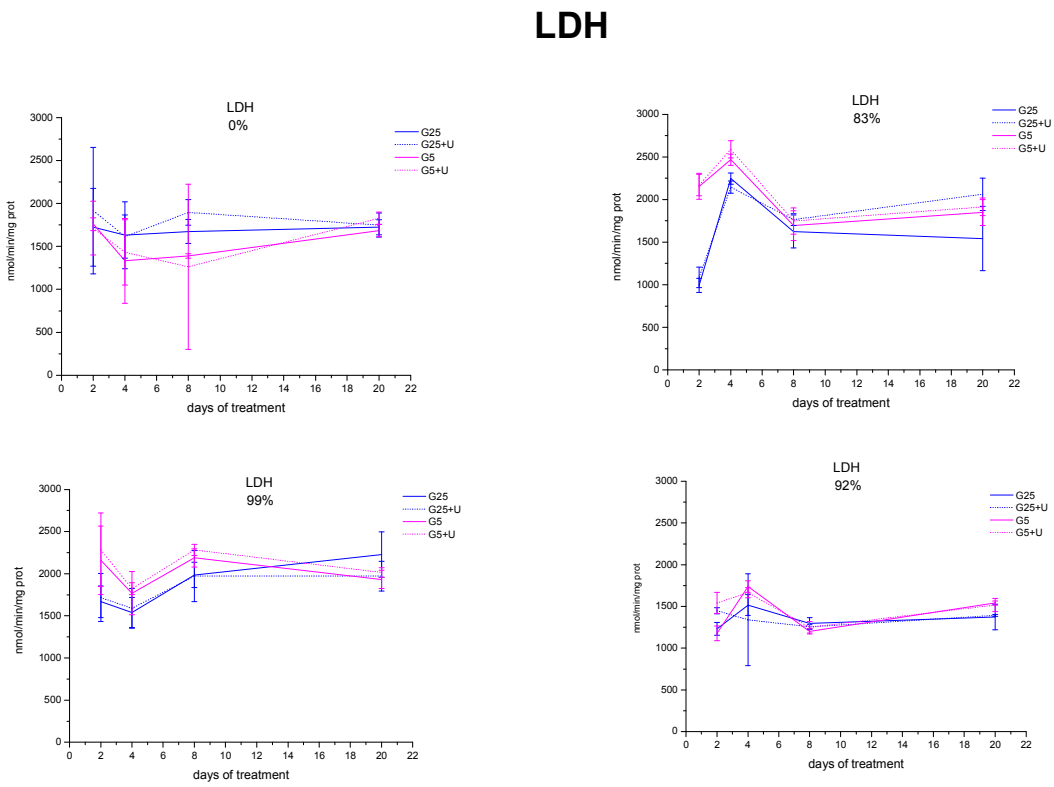


**Figure 4.2.8:** mean values of activity of the glycolytic enzyme lactate dehydrogenase. The activity was measured in homoplasmic (0% and 99%) and heteroplasmic (92% and 83%) RD MELAS cybrids after different days of treatment in growth regimes (G25, G5, G25+U, G5+U). Measurements were performed in triplicate.

### 4.2.5.5 Complex I : NADH-dehydrogenase

The NADH-dehydrogenase activity, the first enzyme of respiratory chain, showed a range of value that was about 4. There were no significant differences among cybrids with different heteroplasmy and in different growth regimes (fig. 4.2.9). Since also 99% mutant RD cybrids had activity of NADH-dehydrogenase similar to wild-type cells, it means that this assay is not believable. Probably the activity of both cytosolic and mitochondrial NADH-dehydrogenase is measured, since for this assay the total cellular extract is used.

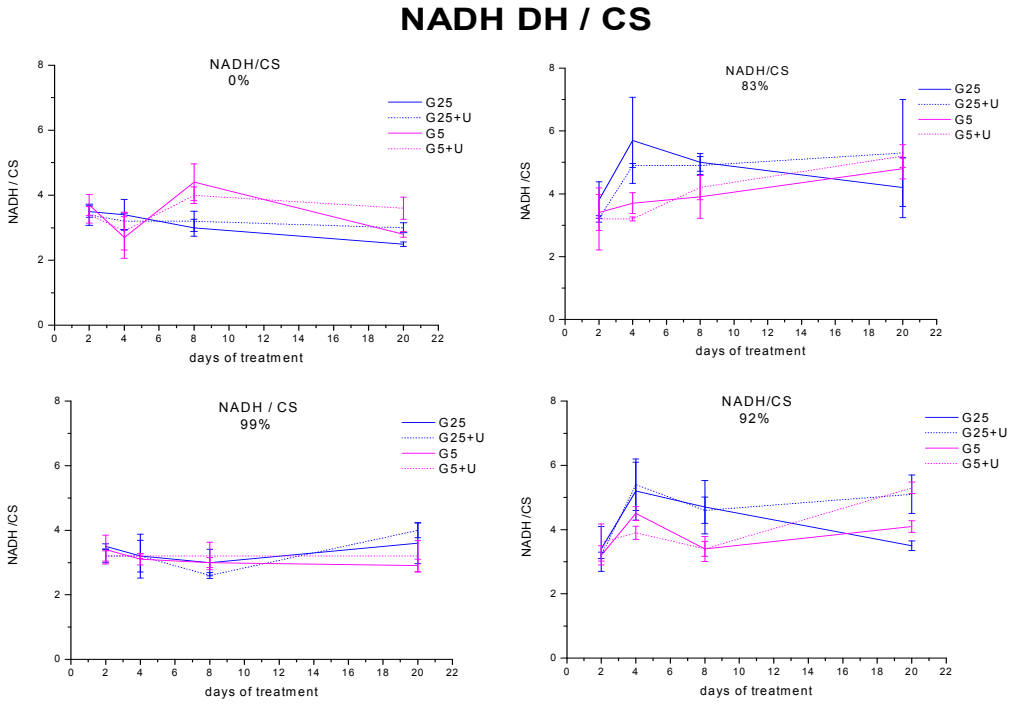


**Figure 4.2.9:** mean value of activity of complex I of respiratory chain, NADH-dehydrogenase, normalized for the activity of citrate synthase, a mitochondrial matrix enzyme. The activity was measured in homoplasmic (0% and 99%) and heteroplasmic (92% and 83%) RD MELAS cybrids after different days of treatment in growth regimes (G25, G5, G25+U, G5+U). Measurements were performed in triplicate.

#### 4.2.5.6 Summary of glycolytic and OXPHOS activities

Figure 4.2.10 resumes the enzymatic activity measured in four different wild-type clones, three different 80% mutant clones, two 90% mutant clones, four 99% mutant clones, parental RD and 143B (bone) cells.

**SDH:** cells with a bone nuclear background (143B) had a 2,6-fold increase activity of complex II of respiratory chain, the complex all encoded by the nuclear genome, compared to muscular nuclear background cells

**COX:** in heteroplasmic 92% and 83% cybrids COX activity (expressed as ratio with citrate synthase: COX/CS) was significantly increased to 1,6- and 1,7-fold compared to wild-type cybrids. 143B cells had a 1,6-fold reduction in COX activity compared to parental RD cells.

**CS:** CS activity was 1,6- 2-fold increased in muscular nuclear background cells compared to bone nuclear background cells. These results indicate that muscle cells had more mitochondria than bone cells.

**PFK:** such as observed for COX activity, heteroplasmic 92% and 83% cybrids had also a 2,1-fold increase in PFK activity compared to wild-type cybrids. Parental bone cells (143B) had a 2,3-fold increase in PFK activity compared to RD parental cells. These results indicated that bone cells were more glycolytic than muscular cells.

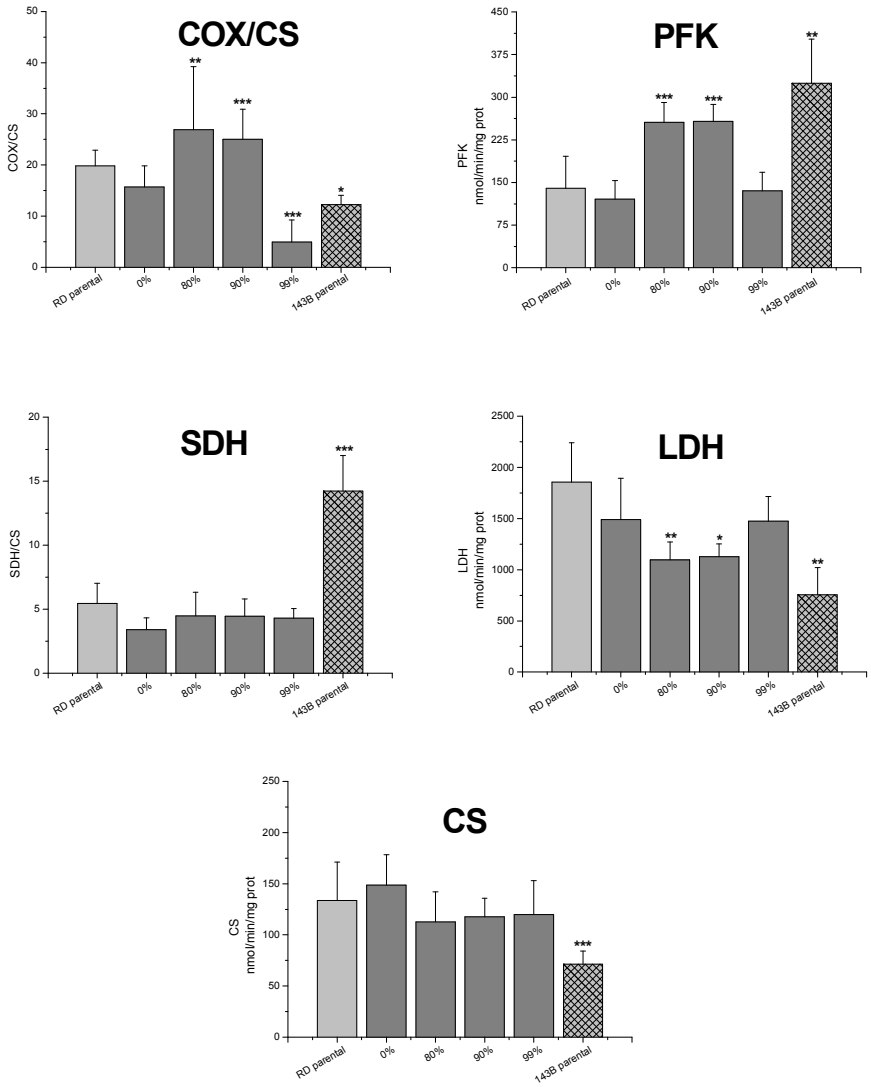


**Figure 4.2.10:** Enzymatic activities of COX, SDH, PFK, LDH and CS in muscular RD cybrid clones, parental RD and 143B cells were measured by spectrophotometric assay in triplicate. Cytochrome c oxidase (COX) and Succinate dehydrogenase (SDH) are expressed as ratio to CS activity (COX/CS and SDH/CS). COX but not SDH activity was significantly increased in heteroplasmic cells compared to wild type. Phosphofructokinase (PFK) activity was significantly increased in heteroplasmic (83% and 92%) RD cybrids compared to wild-type. Statistical analysis: heteroplasmic 83% and 92% mutant cells vs. wild-type, 143B bone cells vs. RD parental cells significantly different for: *p<0.05; **p<0.01; ***p<0.001

## 4.2.6 Molecular analysis

Mitochondrial DNA (mtDNA) is a multycopy genome. A cell contains hundreds of mitochondria, and each mitochondrion contains five to ten copies of mtDNA [15]. Dependent to the tissue and energy demand, each cell contains between 500 and 10000 mtDNA molecules.

The greater resistance of heteroplasmic cybrids compared to homoplasmic cells to acute energetic stress and the increase of COX activity, could be explained by an increase in mtDNA amount in heteroplasmic cybrids.

To asses this hypothesis we measured mtDNA amount in heteroplasmic and homoplasmic cybrids.

### 4.2.6.1 mtDNA amount

mtDNA amount was measured by qReal-Time PCR (see paragraph 3.3.11). Figure 4.2.11 shows the results obtained in homoplasmic 0% and 99% and heteroplasmic 83% and 92% after 2 and 8 days of treatment in different growth regimes (G25, G5, G25+U, G5+U).

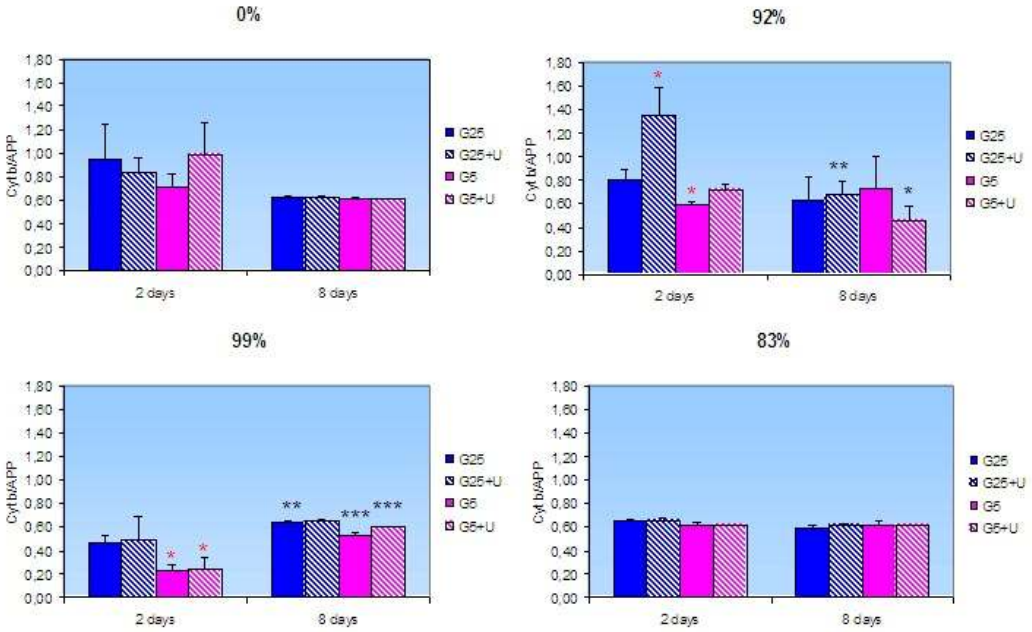


**Figure 4.2.11:** mtDNA quantification by qReal-Time PCR in 0%, 83%, 92% and 99% cybrids after 2 and 8 days of treatment in different growth regimes (G25, G5, G25+U, G5+U). '*' indicates significant differences comparing the value to normal condition (G25). '* ** ***' indicate significant differences between 8 days and 2 day of treatment in different growth regimes. Measurements were performed in triplicate.

There wasn't an increase of mtDNA amount in heteroplasmic cybrids compared to wild-type either if they grew in G25 and in G5 medium.

In 92% cybrids at 2 days of treatment, uridine caused a significant increase of

mtDNA amount in G25 while low glucose concentration (G5) caused a 30% reduction compared to normal condition (G25).
The homoplasmic 99% cybrids have half amount of mtDNA compared to wild-type; low glucose concentration halved the mtDNA amount compared to normal condition (G25); at 8 days of treatment in each growth regime there was a significant increase of mtDNA amount compared to the value observed at the second day.
There wasn't a variation in mtDNA amount that could explain the increased COX activity in heteroplasmic cybrids. This increase could be due to trascriptional-traductional variations (increase of transcriptional activity; more stability of mRNA; increased traductional activity).

CONCLUTIONS: All the data indicate that cells with an intermediate mutant load presented an increase of their bioenergetic anaerobic and aerobic pathways, that helps the cells to better survive in energetic stress as shown by growth rate and RCR value, concomitant to a reduced ROS generation.

# THIRD PART

Mitochondrial dynamic and fission-fusion events may interfere with mtDNA complementation and may influence the mtDNA segregation. To analyze the impact of proteins involved in mitochondrial fission-fusion on segregation of mtDNA, a set of experiments was performed focused on the modulation of the expression levels of OPA1, Drp1 and hFis1 by RNA interference.

## *4.3 Creation and characterization of heteroplasmic MELAS A3243G RD cybrids with OPA1 down expression*

### 4.3.1 RD MELAS 92% cybrids

#### 4.3.1.1 Clones collection

RD MELAS 92% were transfected with pSilencer™ 2.1-U6 hygro and pSilencer™ 2.1-U6 hygro OPA1-RNAi to obtain control clones and clones with OPA1 down regulation respectively.

12 control clones were collected, three of them were chosen for the study and called C90-1, C90-2 and C90-3.

15 clones were collected after transfection with pSilencer™ 2.1-U6 hygro OPA1-RNAi. All of them were tested by western blotting to check the OPA1 expression and five of them were chosen for the study. In these five clones OPA1 expression was less than 60% compared to the controls. These clones were called O90-1, O90-2, O90-3, O90-4 and O90-5.

Figure 4.3.1 shows the OPA1 expression levels in the chosen clones.

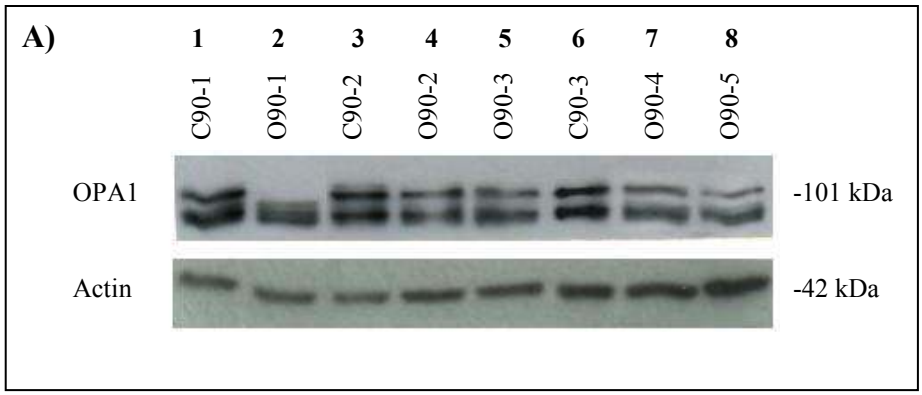


**Figure 4.3.1: A)** Western blot analysis of OPA1 expression in 90-Sil (lines 1-3-6) and 90-OPA (lines 2-4-5-7-8). OPA1 expression was detected using anti-OPA1 monoclonal antibody (Biosciences); the signal was normalized to actin expression. Actin was detected using anti-actin monoclonal antibody (Chemicon). 15μg of proteins were loaded on each well. For each clone at least 2 quantitations were performed.

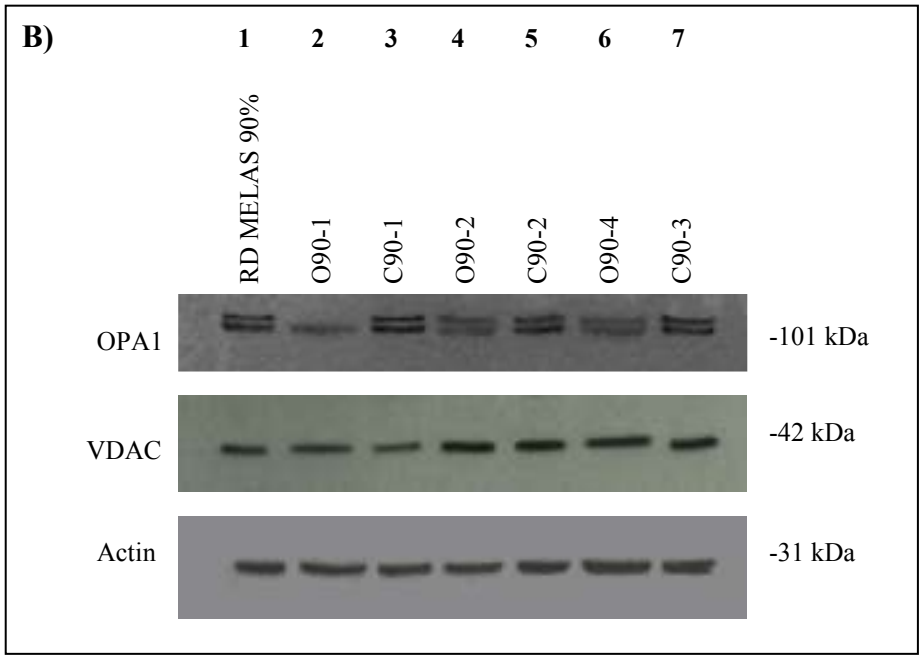


**Figure 4.3.1: B)** OPA1 expression in untransfected RD MELAS 92% cybrids (line 1), 90-Sil cybrids (lines 3-5-7) and in 90-OPA cybrids (lines 2-4-6). OPA1 expression was normalized to VDAC/porin expression. VDAC/porin expression was detected using anti-VDAC/porin monoclonal antibody (Sigma). 15µg of proteins were loaded on each well. For each clone at least 2 quantitations were performed.

The intensity of the bands was quantified by Gel-Pro Analyzer 3 software. To obtain the percentage of expression, the mean value obtained for the three controls was considered 100% of expression and the value obtained for the other clones was compared to the mean value of the control clones. The obtained values are summarized in table 4.3.1 and in figure 4.3.2.

In a first moment the OPA1 signal was normalized to actin (fig. 4.3.1 A) and afterwards, to verify that OPA1 reduction wasn't linked to a mitochondria reduction, in three clones OPA1 expression was normalized to a mitochondrial protein, VDAC/porin (fig. 4.3.1 B). In both the case the OPA1 down expression showed similar values (table 4.3.1).

| Clone | OPA1 expression/ ACTIN | | | OPA1 expression/ VDAC |
|---|---|---|---|---|
| | I value | II value | mean±st.dev. | |
| C90-1 | 100% | 100% | 100% | 100% |
| C90-2 | 100% | 100% | 100% | 100% |
| C90-3 | 100% | 100% | 100% | 100% |
| O90-1 | 3% | 100% | 51%±45 | 100% |
| O90-2 | 42% | 40% | 41%±1,4 | 60% |
| O90-3 | 47,0% | 57,8% | 52,4%±7,6 | |
| O90-4 | 49,0% | 68,7% | 58,9%±13,9 | |
| O90-5 | 57,0% | 37,8% | 47,4%±13,6 | 51% |

**Table 4.3.1:** western blot quantification of OPA1, as percentage of OPA1 presence in 90-OPA clones compared to the control clones (90-Sil). The signal was normalized to both actin and VDAC/porin.

.

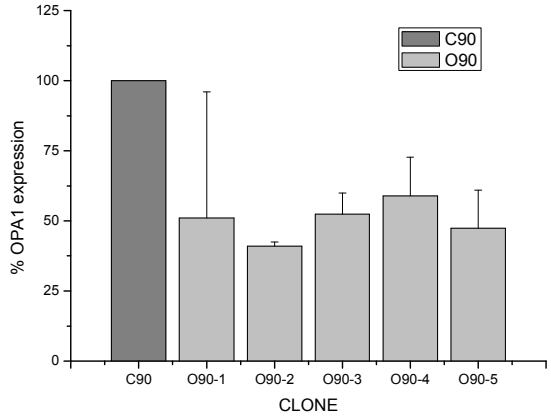


**Figure 4.3.2:** western blot quantification of OPA1, as percentage of OPA1 presence in 90-OPA cybrids compared to the control clones (90-Sil). The signal was normalized to actin.

#### 4.3.1.2 qReal-Time PCR

To confirm the data on OPA1 down expression, obtained by western blot analysis, OPA1 mRNA levels were quantified by qReal-Time PCR (see paragraph 3.3.11). The OPA1 mRNA levels were normalized to the house-keeping gene RPLPO (acidic ribosomal phosphoprotein PO). The mean value obtained for the three controls was considered 100% of expression and the values obtained in the other clones were compared to the control mean value. The results are summarized in the table 4.3.2. Figure 4.3.3 compares the results obtained by western blot analysis and qReal-Time PCR.

| Clone | OPA1 expression |
|---|---|
| C90-1 | 100% |
| C90-2 | 100% |
| C90-3 | 100% |
| O90-1 | 44% |
| O90-2 | 55% |
| O90-3 | 77% |
| O90-4 | 94% |
| O90-5 | 59% |

**Table 4.3.2:** Real-Time PCR quantification of OPA1, as percentage of expression in 90-OPA cybrids compared to the control clones (90-Sil). The samples were analysed in triplicate.

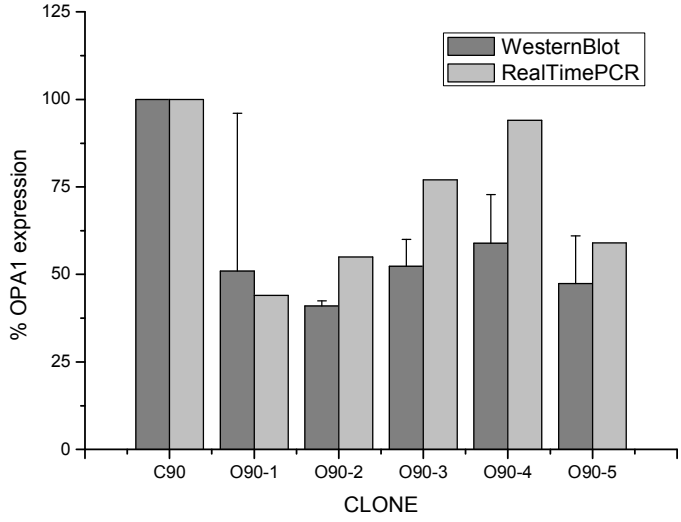


**Figure 4.3.3:** western blot and Real-Time PCR quantification of OPA1, as percentage of expression in 90-OPA clones compared to 90-Sil clones.

#### 4.3.1.3 Quantification of mutant mtDNA

To check if the OPA1 down expression influenced the segregation of mutant and wild-type mtDNA, the percentage of mutation was quantified by Last-cycle Hot-PCR (see paragraph 3.3.6). Figure 4.3.4 shows the result of LC Hot PCR after APAI digestion.

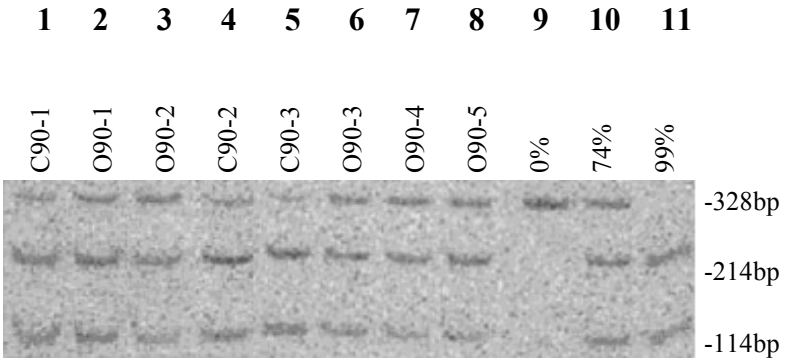


**Figure 4.3.4:** phosphor-image analysis of samples after LC-Hot PCR and APAI digestion. Lines 1-4-5 are the control clones (90-Sil); lines 2-3-6-7-8 are 90-OPA clones; lines 9-10-11 are internal standards.

The bands were analysed by Gel-Pro Analyzer software and the percentage of mutant mtDNA in each clone is summarized in the table 4.3.3.

| Clone | % mutant mtDNA |
|---|---|
| C90-1 | 92,1%±1,46 |
| C90-2 | 92,0%±2,08 |
| C90-3 | 92,2%±1,90 |
| O90-1 | 80,8%±5,16 |
| O90-2 | 83,9%±3,61 |
| O90-3 | 83,5%±8,41 |
| O90-4 | 82,0%±12,66 |
| O90-5 | 87,8%±5,59 |

**Table 4.3.3:** percentage of mutant mtDNA in 90-Sil cybrids and in 90-OPA cybrids. Each value is the mean ± sd of at least two determinations.

The mean value of percentage of mutant mtDNA was 92,1%±0,11 for the control clones and 83,6%±2,65 for the clones with OPA1 down expression. These results show a reduction in mutant mtDNA in the clones with OPA1 down expression. This reduction was analysed by Student's t test and it resulted statistically significant: $P<0.001$.

Figure 4.3.5 resumes these results.

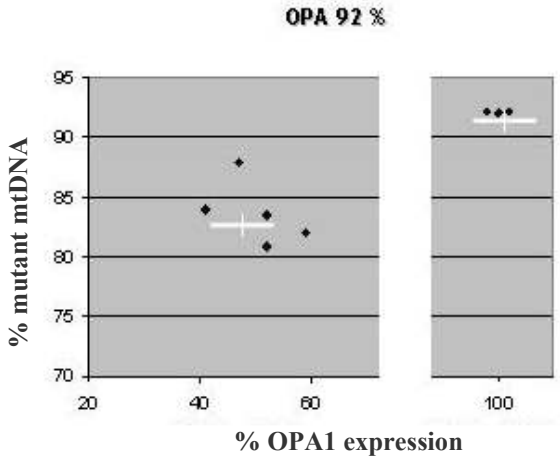


**83,6%±2,65** **92,1%0,11**

**Figure 4.3.5:** relation between OPA1 expression and percentage of mutant mtDNA in control clones (90-Sil) and in 90-OPA clones.

### 4.3.2 RD MELAS 83% cybrids

#### 4.3.2.1 Clones collection

Similarly to RD MELAS 92%, also RD MELAS 83% cybrids were transfected with pSilencer™ 2.1-U6 hygro and pSilencer™ 2.1-U6 hygro OPA1-RNAi to obtain control clones and clones with OPA1 down expression respectively.

After selection in medium with hygromycin, 11 clones from both the transfections were collected. All of them were analysed to check the OPA1 expression levels. Three control clones (80-Sil) from cells transfected with the empty vector were chosen and called C80-1, C80-2, C80-3 and four clones in which OPA1 expression was less than 50% compared to the controls were chosen for the study. These clones were called O80-1, O80-2, O80-3 and O80-4.

The OPA1 down expression was tested by western blot analysis. Figure 4.3.6 shows the result obtained loading on the gel 15μg of protein for each sample.

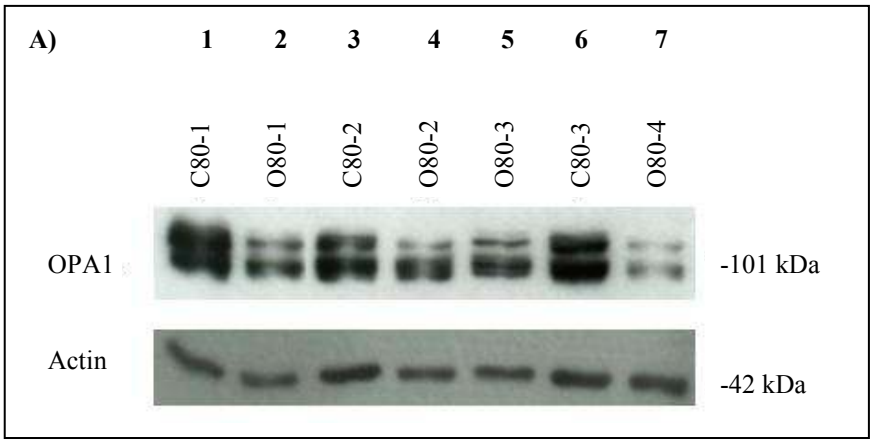


**Figure 4.3.6: A)** western blotting analysis of OPA1 expression in 80-Sil cybrids (lines 1-3-6) and in 80-OPA cybrids (lines 2-4-5-7). OPA1 expression was detected using anti-OPA1 monoclonal antibody (Biosciences); the signal was normalized to actin expression. Actin expression was detected using anti-actin monoclonal antibody (Chemicon). 15μg of proteins were loaded on each well. For each clone at least 2 quantitations were performed.

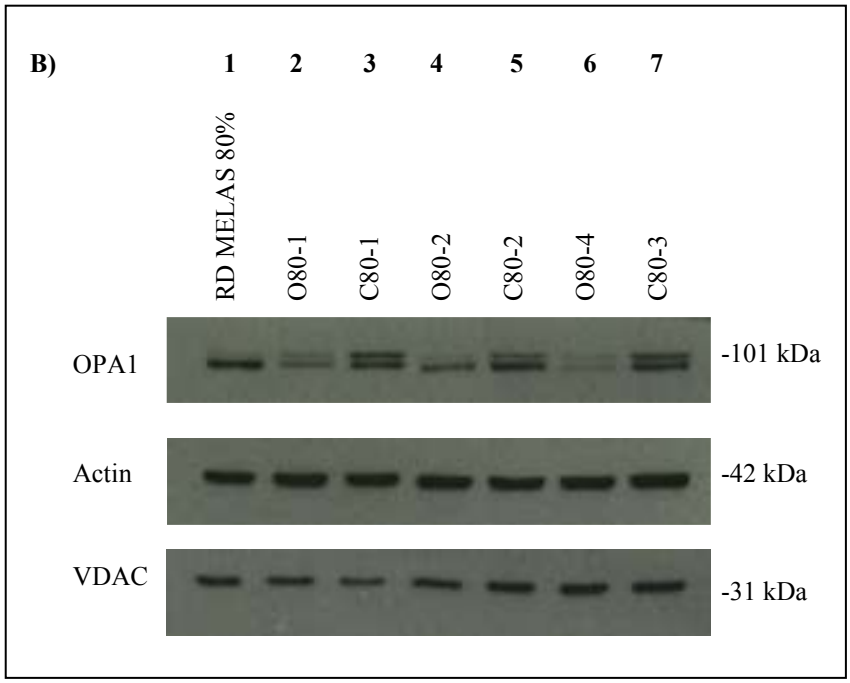


**Figure 4.3.6: B)** OPA1 expression in untransfected RD MELAS 83% cybrids (line 1), in 80-Sil cybrids (lines 3-5-7) and in 80-OPA cybrids (lines 2-4-6). OPA1 expression was normalized to VDAC/porin expression. VDAC/porin expression was detected using anti-VDAC/porin monoclonal antibody (Sigma). 15µg of proteins were loaded in each well. For each clone at least 2 quantitations were performed.

As done for the 92% cybrids, the intensity of the bands was quantified by Gel-Pro Analyzer 3 software. To obtain the percentage of expression (see table 4.3.4 and figures 4.3.6A-B), the mean value obtained for the three controls was considered 100% of expression and the value obtained for the other clones was compared to the mean value of the control clones.

Also in this case in a first moment the OPA1 signal was normalized to actin (fig. 4.3.6 A). Afterwards, to verify that OPA1 reduction wasn't linked to a mitochondria reduction, in three clones OPA1 expression was normalized to a mitochondrial protein, VDAC/porin (fig. 4.3.6 B). In both the case the OPA1 down expression was similar (table 4.3.4).

| Clone | OPA1 expression/ ACTIN | | | OPA1 expression/ VDAC |
|---|---|---|---|---|
| | I value | II value | mean±st.dev. | |
| C80-1 | 100% | 100% | 100% | 100% |
| C80-2 | 100% | 100% | 100% | 100% |
| C80-3 | 100% | 100% | 100% | 100% |
| O80-1 | 25% | 65% | 45%±28,3 | 41% |
| O80-2 | 37% | 47% | 42%±7,1 | 51% |
| O80-3 | 38% | 49% | 44%±7,8 | |
| O80-4 | 44% | 10% | 27%±24,3 | 15% |

**Table 4.3.4:** western blot quantification of OPA1, as percentage of presence in 80-OPA cybrids compared to the control clones (80-Sil). The signal was normalized to both actin and VDAC/porin.

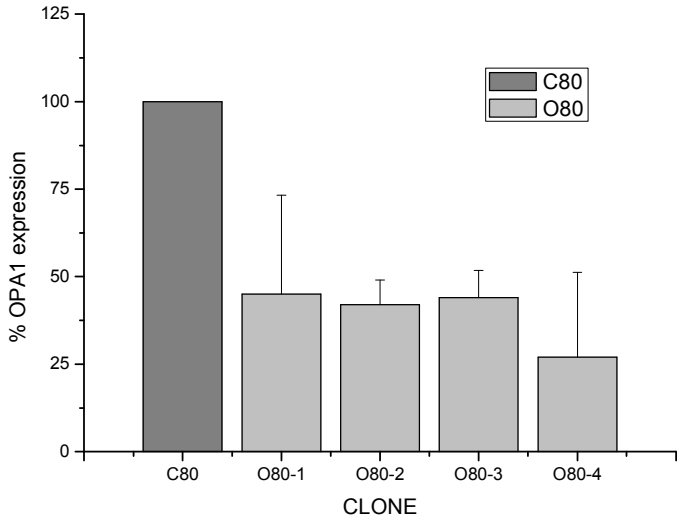


**Figure 4.3.7:** western blot quantification of OPA1, as percentage of presence in 80-OPA cybrids compared to the control clones. The signal was normalized to actin.

### 4.3.2.2 Quantification of mutant mtDNA

Also in RD MELAS 83% the percentage of mutant mtDNA was quantified by Last-cycle Hot PCR to verify the influence of OPA1 down expression on the segregation of mutant and wild-type mtDNA. Figure 4.3.8 shows the result of LC Hot PCR after APAI digestion.

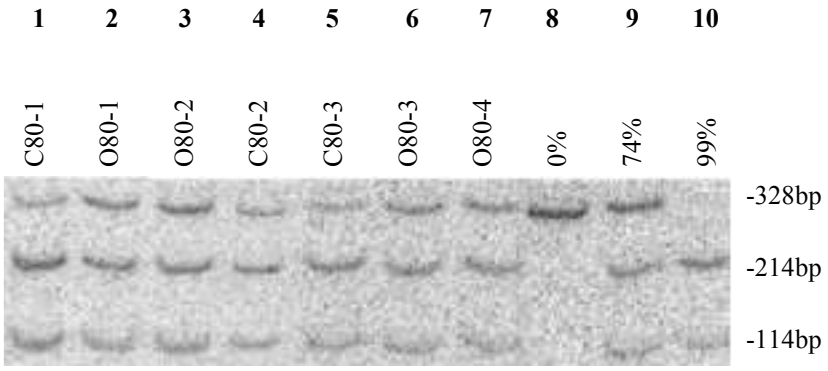


**Figure 4.3.8:** phosphor-image analysis of samples after LC-Hot PCR and APAI digestion. Lines 1-4-5 are the control clones (80-Sil); lines 2-3-6-7 are 80-OPA clones; lines 8-9-10 are internal standards.

The bands were analysed by Gel-Pro Analyzer software and the percentage of mutant mtDNA in each clone is summarized in the table 4.3.5.

| Clone | % mutant mtDNA |
|---|---|
| C80-1 | 84,9%±1,56 |
| C80-2 | 83,4%±3,05 |
| C80-3 | 82,5%±2,40 |
| O80-1 | 76,0%±1,06 |
| O80-2 | 74,9%±3,11 |
| O80-3 | 76,0%±2,34 |
| O80-4 | 78,5%±1,84 |

**Table 4.3.5:** percentage of mutant mtDNA in 80-Sil cybrids and in 80-OPA cybrids. Each value is the mean ± sd of at least two determinations.

In the control clones the mean value of percentage of mutant mtDNA was 83,6±1,19, while in the clones with OPA1 down expression the mean value of percentage of mutant mtDNA was 76,2±1,72. These results show a reduction in mutant mtDNA in the clones with OPA1 down expression. This reduction was analysed by Student's t test and it resulted statistically significant: $P<0.001$.
Figure 4.3.9 resumes these results.

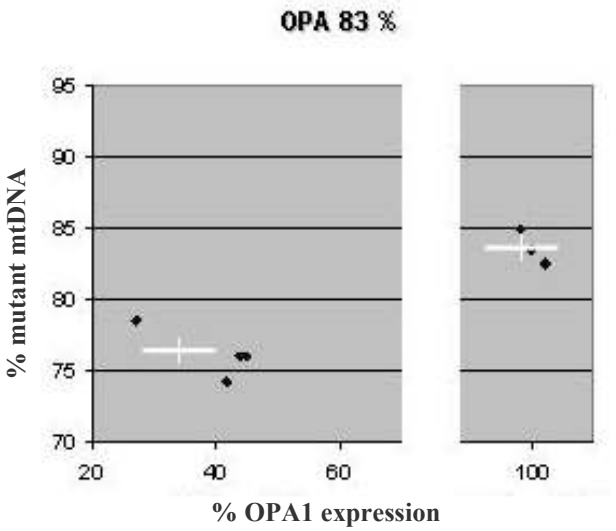


**76,2%±1,76** **83,6%±1,19**

**Figure 4.3.9:** relation between OPA1 expression and percentage of mutant mtDNA in 80-Sil cybrids and in 80-OPA cybrids.

#### 4.3.2.3 Mitochondrial morphology

Since OPA1 is a protein involved in mitochondrial fusion, cells with OPA1 down expression should show an increase in mitochondrial fragmentation.

To check mitochondrial morphology in clones with OPA1 down expression, cybrids were treated with the mitochondrial target fluorescence probe MitoTraker Red and images were taken at confocal microscope (see paragraph 3.4.3).

Figure 4.3.10 shows that, as expected, both 80% and 90% cybrids transfected with the empty vector (fig. 4.3.10 C-D) had a mitochondrial shape similar to the untransfected cells (fig 4.3.10 A-B), while cybrids with OPA1 down expression (fig 4.3.10 E-F) had an increased mitochondrial fragmentation.

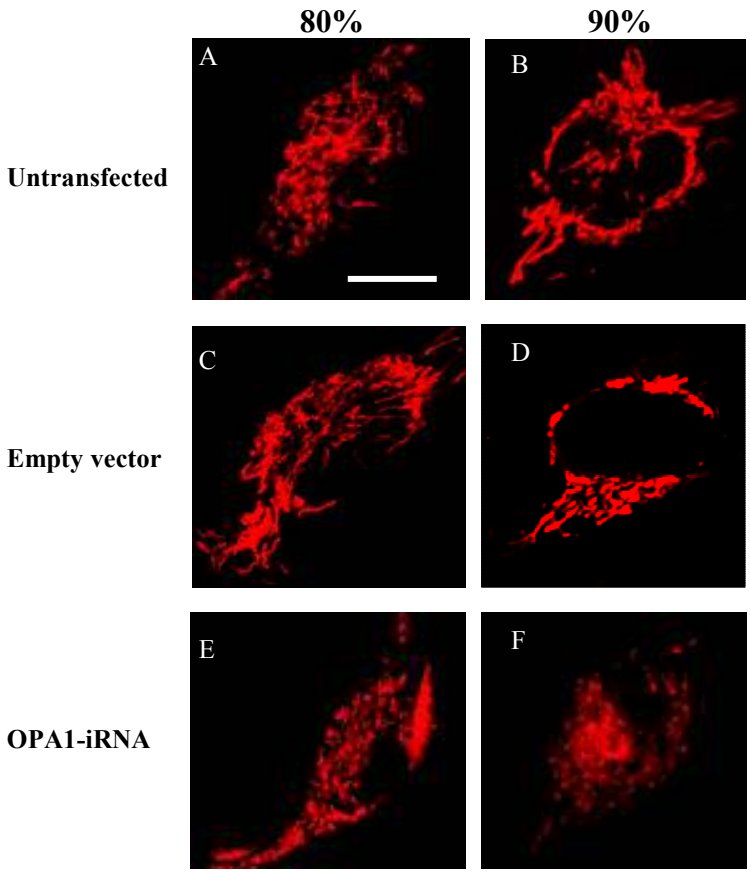


**Figure 4.3.10:** mitochondrial shape and distribution in: A) untransfected RD MELAS 80% cybrids; B) untransfected RD MELAS 92% cybrids; C) 80-Sil cybrids; D) 90-Sil cybrids; E) 80-OPA cybrids; F) 90-OPA cybrids. MitoTracker Red was used to stain mitochondria and images were taken using confocal microscope. Scale bar: 10μm.

## *4.4 Creation and characterization of heteroplasmic MELAS A3243G RD cybrids with Drp1 down expression*

### 4.4.1 RD MELAS 92% cybrids

#### 4.4.1.1 Clones collection

RD MELAS 92% were transfected with pREP4 hygro and pREP4 hygro Drp1-RNAi to obtain control clones and clones with Drp1 down expression respectively. 12 control clones were collected. Three of them were chosen for the study and called C90-1, C90-2 and C90-3.

18 clones were collected after transfection with pREP4 hygro Drp1-RNAi and selection in hygromycin and all of them were analysed by western blot to check the Drp1 levels. Five clones were chosen for the study. In these five clones Drp1 expression was less than 60% compared to the control. These clones were called D90-1, D90-2, D90-3, D90-4 and D90-5.

Figure 4.4.1 shows the Drp1 expression levels in the chosen clones.

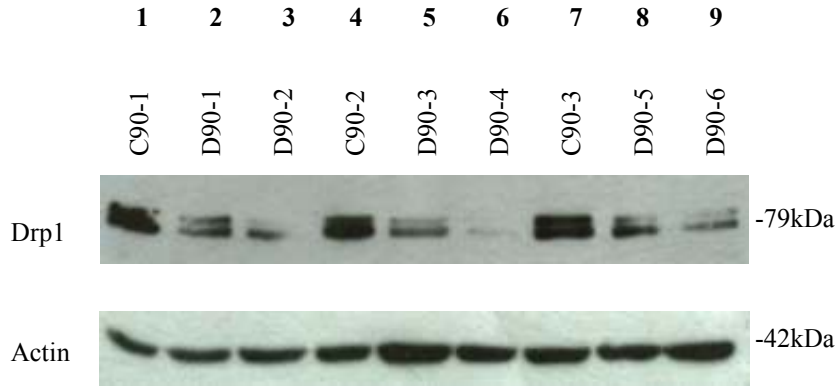


**Figure 4.4.1:** western blot analysis of Drp1 down expression in 90-Rep cybrids (lines 1-4-7) and in 90-Drp cybrids (lines 2-3-5-6-8-9). 30μg of proteins were loaded on a 8% poliacrilamide gel and Drp1 expression was detected using anti-Drp1 monoclonal antibody (Biosciences); the signal was normalized to actin expression. Actin expression was detected using anti-actin monoclonal antibody (Chemicon). For each clone at least 2 quantitations were performed.

The intensity of the bands was quantified by Gel-Pro Analyzer 3 software. The signal of Drp1 expression was normalized to actin intensity bands. To obtain the percentage of expression, the mean value obtained for the three controls was considered 100% of expression and the value obtained for the other clones was compared to the mean value of the control clones. In these clones a Drp1 down expression was observed in a range between 6% and 21%. The obtained values are summarized in table 4.4.1 and in figure 4.4.2.

| Clone | Drp1 expression | | |
|---|---|---|---|
| | I value | II value | mean±st.dev. |
| C90-1 | 100% | 100% | 100% |
| C90-2 | 100% | 100% | 100% |
| C90-3 | 100% | 100% | 100% |
| D90-1 | 3,4% | 25,8% | 14,6%±15,8 |
| D90-2 | 11,0% | 10,3% | 10,7%±0,5 |
| D90-3 | 11,0% | 11,0% | 11,0%±0,0 |
| D90-4 | 12,0% | 1,2% | 6,6%±7,6 |
| D90-5 | 12,5% | 22,5% | 17,5%±7,1 |
| D90-6 | 34,0% | 7,7% | 21,0%±18,6 |

**Table 4.4.1:** western blot quantification of Drp1, as percentage of Drp1 presence in 90-Drp cybrids compared to the control clones (90-Rep).

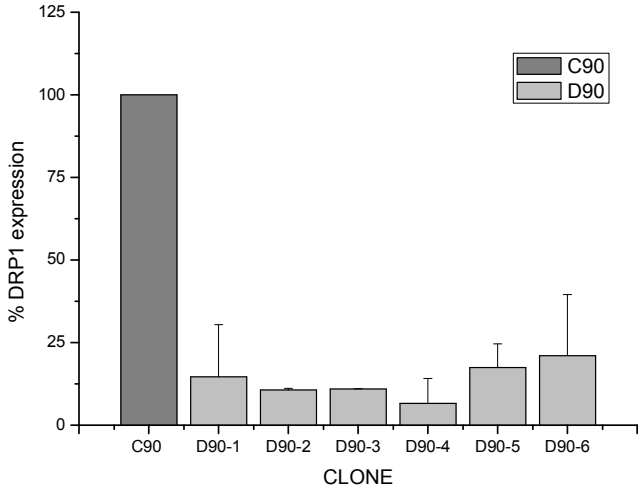


**Figure 4.4.2:** western blot quantification of Drp1, as percentage of Drp1 presence in 90-Drp cybrids compared to the control clones (90-Rep).

### 4.4.1.2 qReal-Time PCR

Data obtained on Drp1 expression levels by western blot analysis, were confirmed quantifying Drp1 mRNA levels by qReal-Time PCR. The Drp1 mRNA levels were normalized to the house-keeping gene RPLPO (acidic ribosomal phosphoprotein PO). The mean value obtained for the three controls was considered 100% of expression and the values obtained in the other clones were compared to the control mean value. The results are summarized in the table 4.4.2. Figure 4.4.3 compares the results obtained by western blot analysis and qReal-Time PCR.

| Clone | Drp1 expression |
|---|---|
| C90-1 | 100% |
| C90-2 | 100% |
| C90-3 | 100% |
| D90-2 | 2% |
| D90-4 | 9,5% |
| D90-5 | 10,4% |
| D90-6 | 15,6% |

**Table 4.4.2:** qReal-Time PCR of Drp1 as percentage of Drp1 expression in 90-Drp cybrids compared to the control clones (90-Rep). The samples were analysed in triplicate.

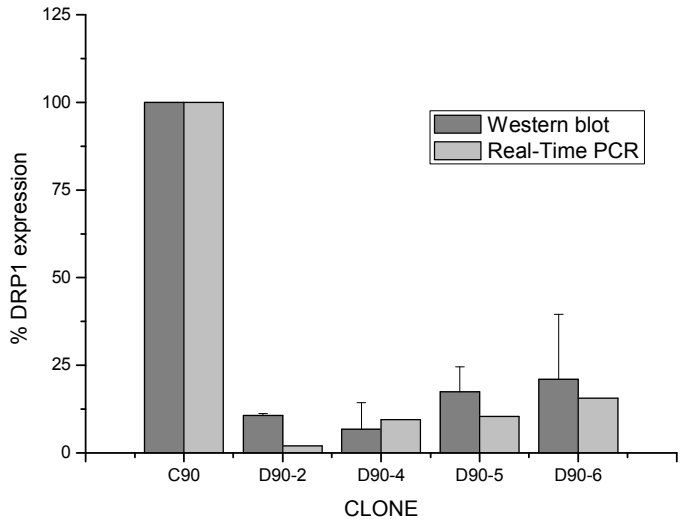


**Figure 4.4.3:** western blot and Real-Time PCR quantification of Drp1, as percentage of Drp1 expression in 90-Drp cybrids compared to the control clones (90-Rep).

#### 4.4.1.3 Quantitation of mutant mtDNA

The percentage of mutant mtDNA was analysed by Last-Cycle Hot PCR in RD MELAS 92% cybrids with Drp1 down expression to verify if a greater mitochondrial fusion could influence mutant or wild-type mtDNA segregation. Figure 4.4.4 shows the result of LC Hot PCR after APAI digestion.

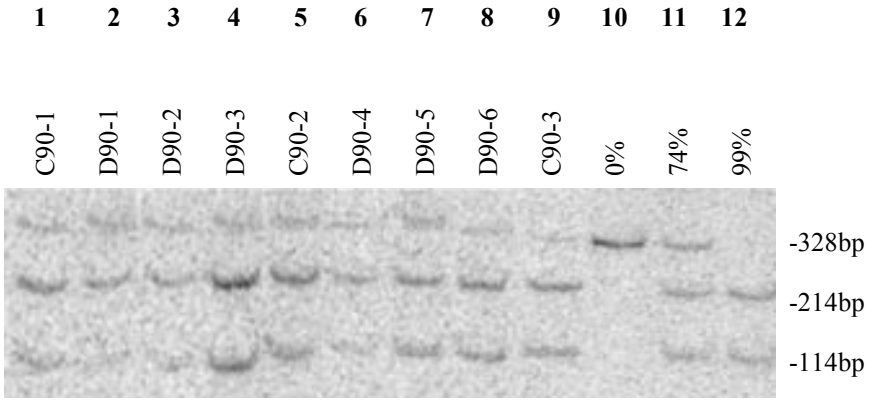


**Figure 4.4.4:** phosphor-image analysis of samples after LC-Hot PCR and APAI digestion. Lines 1-5-9 are the control clones (90-Rep); lines 2-3-4-6-7-8 are 90-Drp clones; lines 10-11-12 are internal standards.

The bands were analysed by Gel-Pro Analyzer software and the percentage of mutant mtDNA in each clone is summarized in the table 4.4.3.

| Clone | % mutant mtDNA |
|---|---|
| C90-1 | 92,1%±1,46 |
| C90-2 | 92,0%±2,08 |
| C90-3 | 92,2%±1,90 |
| D90-1 | 90,4%±4,03 |
| D90-2 | 94,6%±0,07 |
| D90-3 | 90,6%±8,34 |
| D90-4 | 92,2%±12,45 |
| D90-5 | 95,8%±3,96 |
| D90-6 | 93,1%±2,05 |

**Table 4.4.3:** percentage of mutant mtDNA in 90-Rep cybrids and in 90-Drp cybrids. Each value is the mean ± sd of at least two determinations.

The mean value of percentage of mutant mtDNA was 92,1%±0,11 for the control clones and 92,76%±2,16 for the clones with Drp1 down expression. There wasn't a variation in percentage of mutant mtDNA between control clones and clones with Drp1 down expression ($P<0.625$).

Figure 4.4.5 resumes these results.

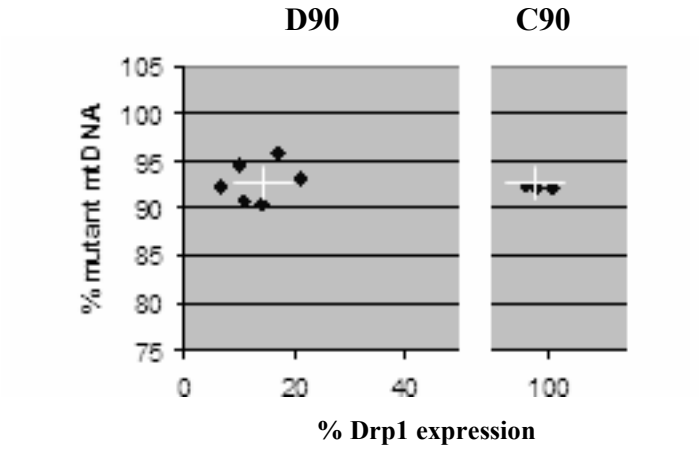


**Figure 4.4.5:** relation between Drp1 expression and percentage of mutant mtDNA in 90-Rep and 90-Drp cybrids.

Although in RD MELAS 92% cybrids the Drp1 down-regulation was really successfully, in fact the Drp1 expression was less than 20% compared to the controls, Drp1 down-expression didn't cause any change in percentage of mutant mtDNA that was constant at 92%.

### 4.4.2 RD MELAS 83% cybrids

#### 4.4.2.1 Clones collection

Such as done for RD MELAS 92%, also RD MELAS 83% cybrids were transfected with pREP4 hygro, pREP4 hygro Drp1-RNAi to obtain control clones (80-Rep) and clones with Drp1 down expression respectively (80-Drp).

After 15 days of selection in medium with hygromycin, 21 80-Drp clones were collected and all of them were processed to check the Drp1 expression levels. Five clones, with less than 70% of Drp1 expression were chosen for the study. These clones were called D80-1, D80-2, D80-3, D80-4 and D80-5.

Alike, 11 control clones were collected, three of them were chosen for the study and called C80-1, C80-2 and C80-3.

Figure 4.4.6 shows the western blot analysis for the chosen clones.

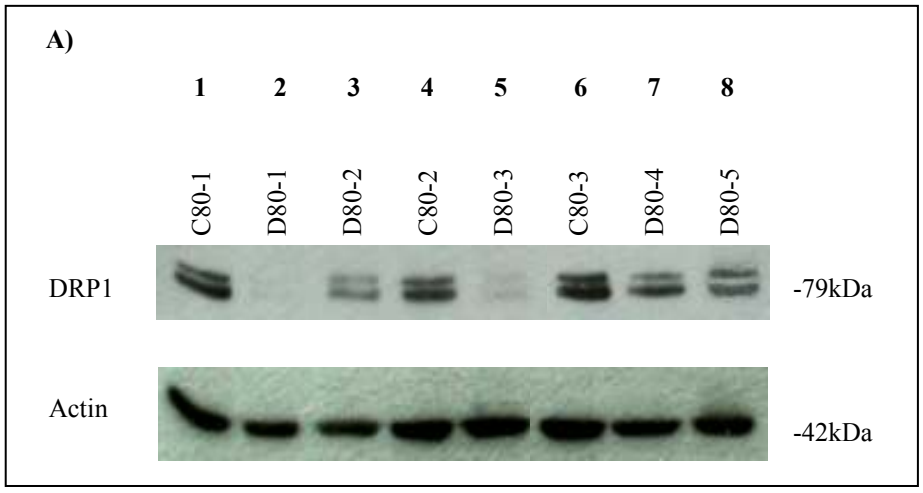


**Figure 4.4.6: A)** western blot analysis of Drp1 expression in 80-Rep cybrids (lines 1-4-6) and in 80-Drp cybrids (lines 2-3-5-7-8). Drp1 expression was detected using anti-Drp1 monoclonal antibody (Biosciences); the signal was normalized to actin expression. Actin expression was detected using anti-actin monoclonal antibody (Chemicon). 30μg of proteins were loaded on a 8% poliacrilamide gel. For each clone at least 2 quantitations were performed.

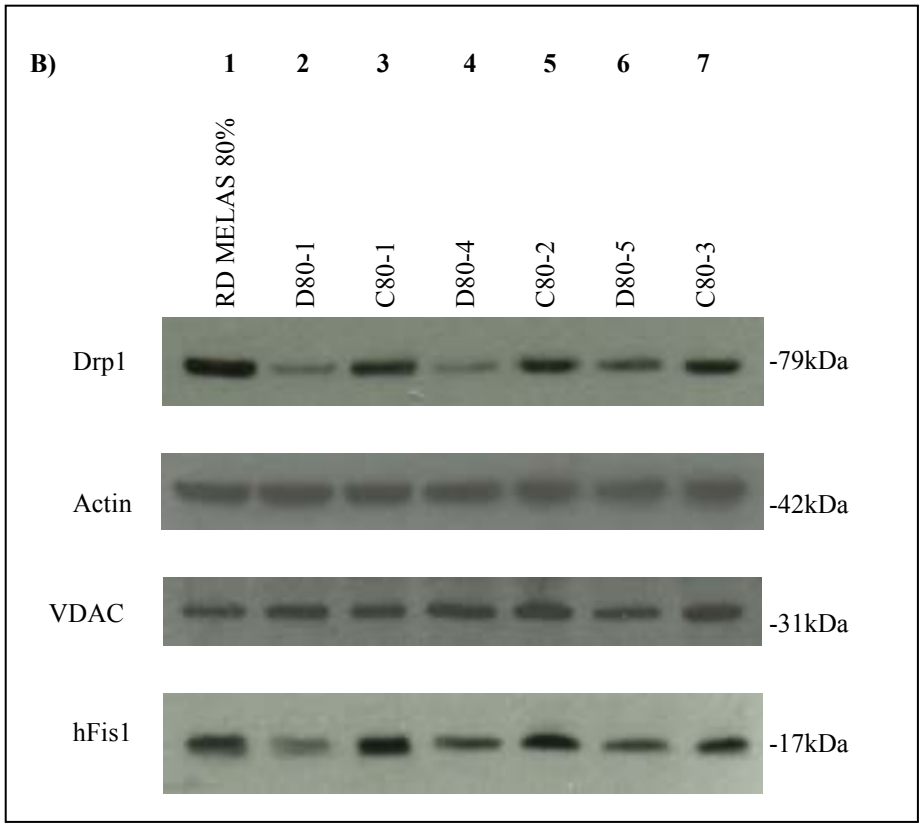


**Figure 4.4.6: B)** Drp1 and hFis1 expression in untransfected RD MELAS 83% cybrids (line 1), in 80-Rep clones (lines 3-5-7) and in 80-Drp clones (lines 2-4-6). Drp1 expression was normalized to VDAC/porin expression. VDAC/porin expression was detected using anti-VDAC/porin monoclonal antibody (Sigma) and hFis1 was detected using anti-hFis1 polyclonal antibody (Alexis ALX-210-907-R100). 30μg of proteins were loaded on a 8% poliacrilamide gel. For each clone at least 2 quantitations were performed.

The intensity of the bands was quantified by Gel-Pro Analyzer 3 software. To obtain the percentage of expression, the mean value obtained for the three controls was considered 100% of expression and the value obtained for the other clones was compared to the mean value of the control clones.

In a first moment the Drp1 signal was normalized to actin (fig. 4.4.6 A). Drp1 expression resulted between 6% and 71%. The obtained values are summarized in table 4.4.4 and in figure 4.4.7. Afterwards, such as done for OPA1 expression, to verify that Drp1 reduction wasn't linked to a mitochondria reduction, in three clones, Drp1 expression was normalized to a mitochondrial protein, VDAC/porin (fig. 4.4.6 B). The Drp1 expression resulted between 19% and 50%. In both the quantifications a Drp1 down expression was observed (table 4.4.4).

In the three clones D80-1, D80-4 and D80-5 also hFis1 levels were detected.

It was observed that Drp1-RNAi not only determined a Drp1 reduction, but also a concomitant secondary hFis1 down expression ranging from 20% to 43%. This result

shows an interesting coordinated down expression of Drp1 and hFis1 in 80-Drp clones.

| Clone | Drp1 expression/ ACTIN | | | Drp1 expression/ VDAC | hFis1 expression/ VDAC |
|---|---|---|---|---|---|
| | I value | II value | mean±st.dev. | | |
| C80-1 | 100% | 100% | 100% | 100% | 100% |
| C80-2 | 100% | 100% | 100% | 100% | 100% |
| C80-3 | 100% | 100% | 100% | 100% | 100% |
| D80-1 | 9,2% | 3,3% | 6,3% ±4,2 | 23% | 20% |
| D80-2 | 23,0% | 42,9% | 33,0%±14,1 | | |
| D80-3 | 52,0% | 4,2% | 28,1%±33,8 | | |
| D80-4 | 60,0% | 71,0% | 65,5% ±7,8 | 19% | 43% |
| D80-5 | 66,0% | 77,0% | 71,5% ±7,8 | 50% | 38% |

**Table 4.4.4:** western blot quantification of Drp1 and hFis1 as percentage of Drp1 and hFis1 presence in five 80-Drp clones compared to the control clones (80-Rep). Drp1 expression is normalized to both actin and VDAC levels. hFis1 expression is normalized to VDAC.

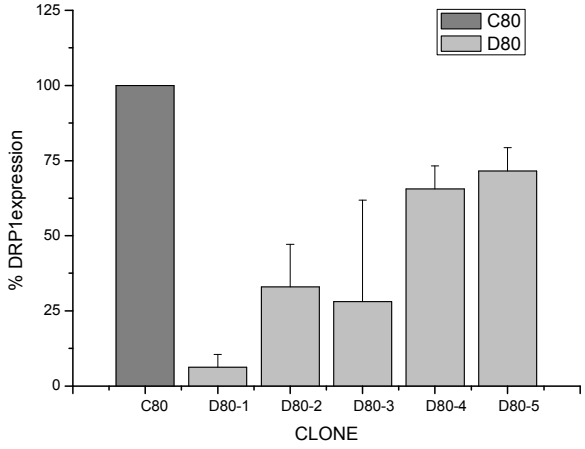


**Figure 4.4.7:** western blot quantification of Drp1 as percentage of Drp1 presence in 80-Drp cybrids compared to the control clones (80-Rep).

### 4.4.2.2 Quantification of mutant mtDNA

Also in RD MELAS 83% the percentage of mutant mtDNA was quantified by Last-cycle Hot PCR to verify if Drp1 down expression had some influence on the segregation of mutant and wild-type mtDNA. Figure 4.4.8 shows the result of LC Hot PCR after APAI digestion.

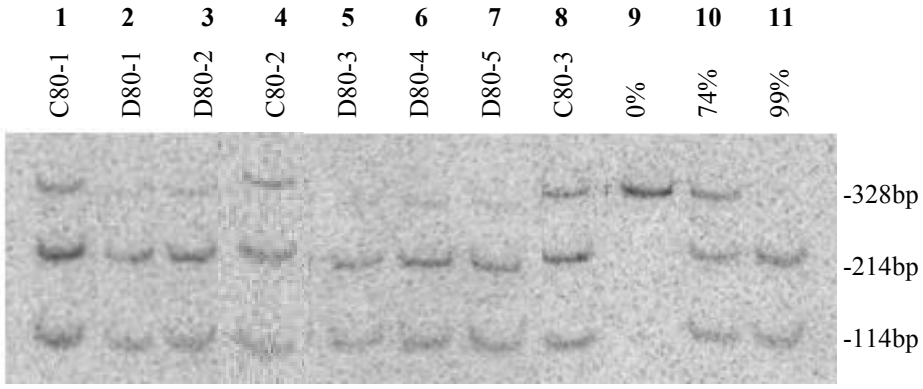


**Figure 4.4.8:** phosphor-image analysis of samples after LC-Hot PCR and APAI digestion. Lines 1-4-8 are the control clones (80-Rep); lines 2-3-5-6-7 are 80-Drp clones; 9-10-11 are internal standards.

The bands were analysed by Gel-Pro Analyzer software and the percentage of mutant mtDNA in each clone is summarized in the table 4.4.5.

| Clone | % mutant mtDNA |
|---|---|
| C80-1 | 81,7%±1,0 |
| C80-2 | 80,0%±1,3 |
| C80-3 | 81,9%±1,4 |
| D80-1 | 93,7%±1,2 |
| D80-2 | 94,3%±2,0 |
| D80-3 | 96,8%±4,5 |
| D80-4 | 99,0%±1,6 |
| D80-5 | 95,0%±3,5 |

**Table 4.4.5:** percentage of mutant mtDNA in 80-Rep cybrids and in 80-Drp cybrids. Each value is the mean ± sd of at least two determinations.

Surprisingly in the clones with down expression of Drp1 the mean value of percentage of mutant mtDNA was 95,8±2,1, while in the control clones it was 81,2±1,1. These results show a 15% of increase in mutant mtDNA in the clones with Drp1 down expression. This reduction was analysed by Student's t test and it resulted statistically significant: $P<0.000$.

Figure 4.4.9 resumes these results.

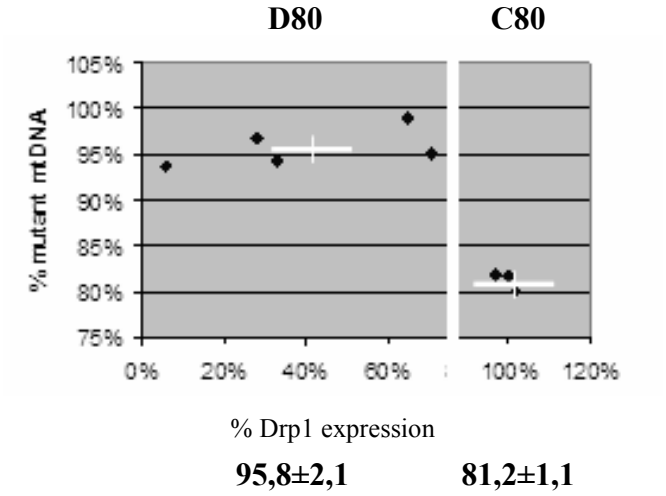


**Figure 4.4.9:** relation between Drp1 expression and percentage of mutant mtDNA in 80-Rep and 80-Drp cybrids.

### 4.4.3 RD MELAS 74% cybrids

#### 4.4.3.1 Clones collection

Such as done for 92% and 83% cybrids, RD MELAS 74% cybrids were transfected with pREP4 hygro (70-Rep) and pREP4 hygro Drp1-RNAi (70-Drp) to obtain control clones and clones with Drp1 down expression respectively.

After selection in hygromycin for 15 days, we collected 6 control clones and 12 clones transfected with pREP4 hygro Drp1-RNAi. All of them were tested by western blot analysis to check the Drp1 and hFis1 expression levels.

Three control clones were chosen for the study and called C70-1, C70-2 and C70-3, but surprisingly no clones had an evident Drp1 down regulation, and only one clone (D70-3) showed low levels of hFis1. In this clone hFis1 presence was half than the controls (70-Rep).

Figure 4.4.10 shows the result of western blot analysis in three control clones and three 70-Drp clones.

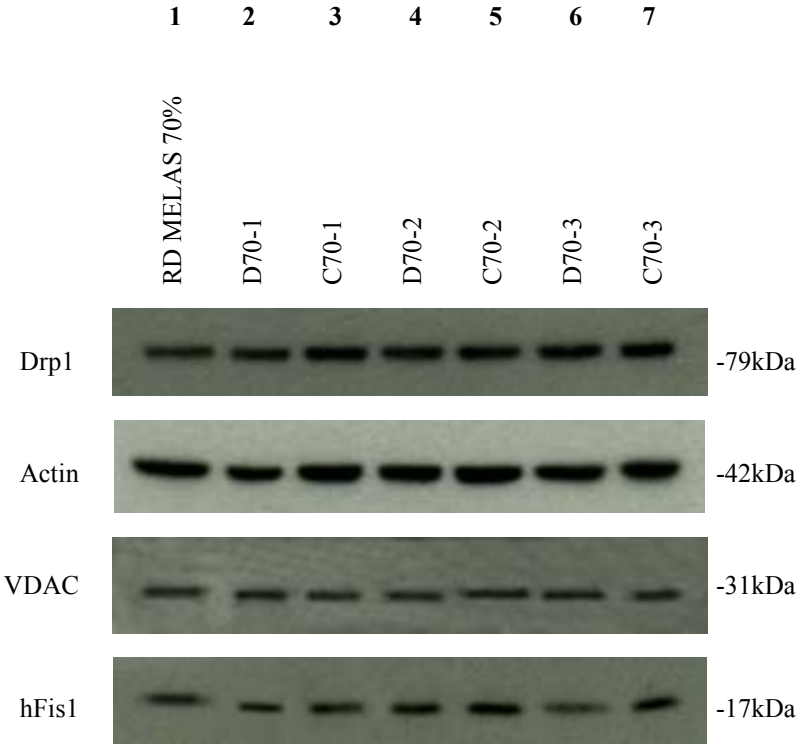


**Figure 4.4.10: A)** western blot analysis of Drp1 and hFis1 expression in RD MELAS 74% cybrids (line 1), in 70-Rep clones (lines 3-5-7) and in 70-Drp clones (lines 2-4-6). 30μg of proteins were loaded on each well and Drp1 expression was detected using anti-Drp1 monoclonal antibody (Biosciences); the signal was normalized to VDAC/porin expression. VDAC/porin expression was detected using anti-VDAC/porin monoclonal antibody (Sigma); hFis1 expression was detected using anti-hFis1 polyclonal antibody (Alexis ALX-210-907-R100); actin expression was detected using anti-actin monoclonal antibody (Chemicon). For each clone at least 2 quantitations were performed.

The intensity of the bands was quantified by Gel-Pro Analyzer 3 software. The signals of Drp1 and hFis1 expression were normalized to VDAC/porin intensity bands. To obtain the percentage of expression, the mean value obtained for the three controls was considered 100% of expression and the value obtained for the other clones was compared to the mean value of the control clones.
The obtained values are summarized in table 4.4.6 and in figure 4.4.11.

| Clone | Drp1 expression/ VDAC | hFis1 expression/ VDAC |
|---|---|---|
| C70-1 | 100% | 100% |
| C70-2 | 100% | 100% |
| C70-3 | 100% | 100% |
| D70-1 | 100% | 100% |
| D70-2 | 100% | 100% |
| D70-3 | 100% | 41,9%±9,9 |

**Table 4.4.6:** western blot quantification of Drp1 and hFis1, as percentage of hFis1 and Drp1 presence in 70-Drp cybrids compared to the control clones (70-Rep).

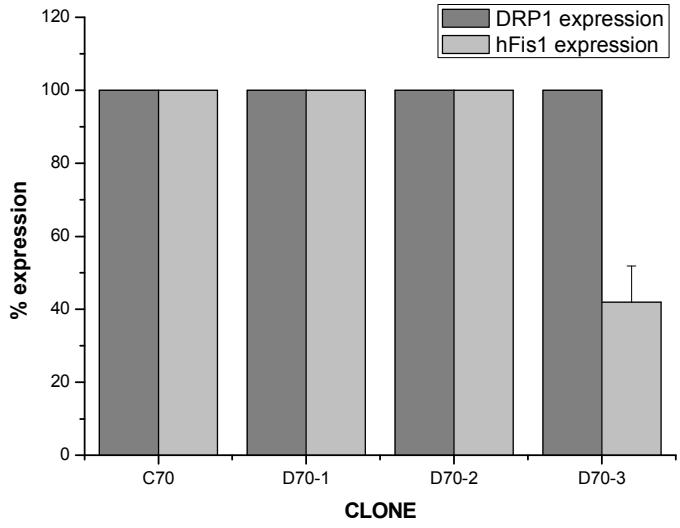


**Figure 4.4.11:** western blot quantification of Drp1 and hFis1, as percentage of Drp1 and hFis1 presence in 70-Drp cybrids compared to the control clones (70-Rep).

### 4.4.3.2 Quantification of mutant mtDNA

The percentage of mutant mtDNA was analysed by Last-Cycle Hot PCR in 70-Drp cybrids even if only one clone (D70-3) got a hFis1 down expression. Figure 4.4.12 shows the result of LC Hot PCR after APAI digestion.

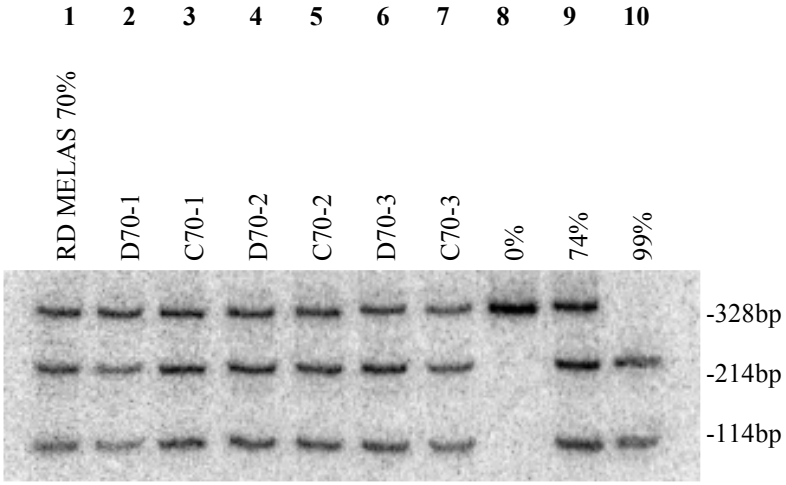


**Figure 4.4.12:** phosphor-image analysis of samples after LC-Hot PCR and APAI digestion. Line 1 are untransfected RD MELAS 74% cybrids; lines 3-5-7 are the control clones (70-Rep); lines 2-4-6 are 70-Drp cybrids; lines 8-9-10 are internal standards

The bands were analysed by Gel-Pro Analyzer software and the percentage of mutant mtDNA in each clone is summarized in the table 4.4.7.

| Clone | % mutant mtDNA |
|---|---|
| C70-1 | 76,2%±2.3 |
| C70-2 | 73,7%±0,7 |
| C70-3 | 74,5%±2,8 |
| D70-1 | 66,5% |
| D70-2 | 76,7% |
| D70-3 | 85,1% |

**Table 4.4.7:** percentage of mutant mtDNA in 70-Rep and 70-Drp cybrids. Data from only one measurement.

As we expected the only clone showing an increase in percentage of mutant mtDNA was D70-3.

In the control clones the mean value of percentage of mutant mtDNA was 74,8±1,25, while in D70-3 it was 85,1%. In D70-1 the percentage of mutation was reduced (66,5%).

Figure 4.4.13 resumes the results.

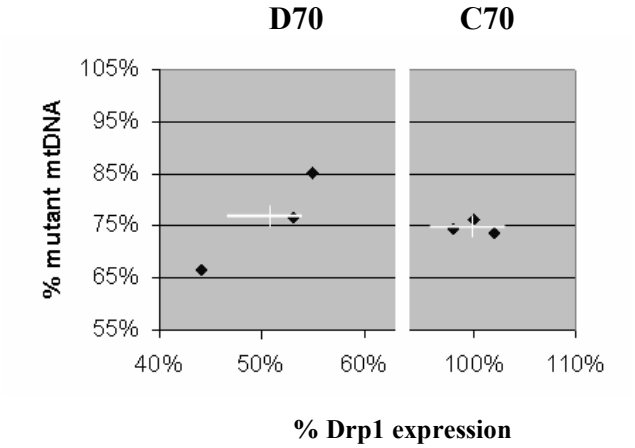


**Figure 4.4.13:** relation between Drp1 expression and percentage of mutant mtDNA in 70-Rep and 70-Drp cybrids.

## *4.5 Creation and characterization of heteroplasmic MELAS A3243G RD cybrids with hFis1 down expression*

### 4.5.1 RD MELAS 92% cybrids

#### 4.5.1.1 Clones collection

In a second set of experiments, the same three clones with 92%, 83% and 74% of mutant A3243G mtDNA, were transfected with pREP4 hygro hFis1-RNAi, in order to obtain clones with hFis1 down expression.

After selection in hygromycin for 15 days, we collected 21 clones transfected with pREP4 hygro hFis1-RNAi. All of them were analysed by western blot to check the hFis1 levels. Three of them, with less than 38% of hFis1 down expression were chosen for the study. These clones were called F90-1, F90-2 and F90-3.

The control clones were the same used to study Drp1 down expression since the empty vector is the same pREP4 hygro.

Figure 4.5.1 shows the western blot analysis for the chosen clones. 30μg of protein were loaded on the gel for each sample.

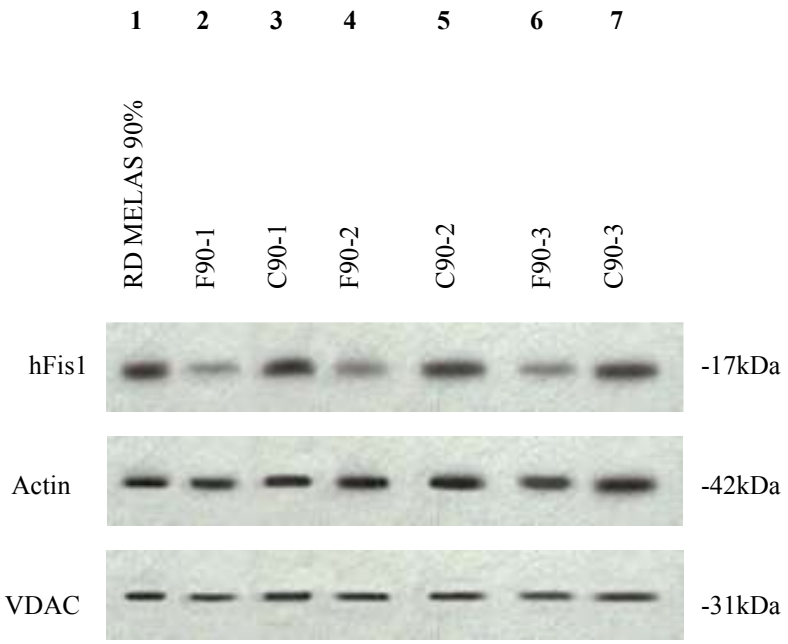


**Figure 4.5.1:** western blot analysis of hFis1 expression in untransfected RD MELAS 92% cybrids (line 1), in 90-Rep cybrids (lines 3-5-7) and in 90-Fis cybrids (lines 2-4-6). 30μg of proteins were loaded on a 12% acrilamide gel. hFis1 expression was detected using anti-hFis1 polyclonal antibody (Alexis ALX-210-907-R100); the signal was normalized to VDAC/porin expression. VDAC/porin expression was detected using anti-VDAC/porin monoclonal antibody (Sigma); actin expression was detected using anti-actin monoclonal antibody (Chemicon). For each clone at least 2 quantitations were performed.

The intensity of the bands was quantified by Gel-Pro Analyzer 3 software. The signal of hFis1 expression was normalized to VDAC/porin intensity bands. To obtain the percentage of expression, the mean value obtained for the three controls was considered 100% of expression and the value obtained for the other clones was compared to the mean value of the control clones. hFis1 down expression resulted between 16% and 38%. The obtained values are summarized in table 4.5.1.

| **Clone** | **hFis1 expression/ VDAC** |
|---|---|
| C90-1 | 100% |
| C90-2 | 100% |
| C90-3 | 100% |
| F90-1 | 16% |
| F90-2 | 38% |
| F90-3 | 30% |

**Table 4.5.1:** western blot quantification of hFis1, as percentage of hFis1 presence in 90-Fis cybrids compared to the control clones (90-Rep).

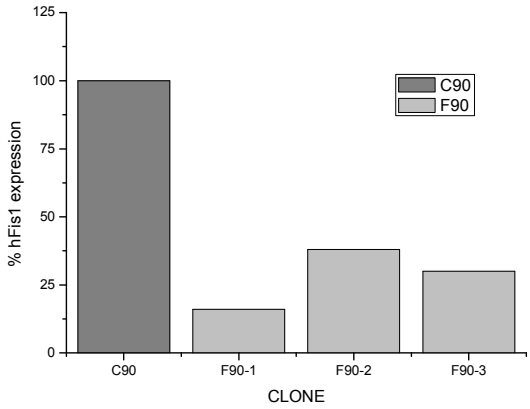


**Figure 4.5.2:** western blot quantification of hFis1, as percentage of hFis1 presence in 90-Fis cybrids compared to the control clones (90-Rep).

### 4.5.1.2 qReal-Time PCR

Data obtained on hFis1 expression level by western blot analysis, were confirmed quantifying hFis1 mRNA levels by qReal-Time PCR. The hFis1 mRNA levels were normalized to the house-keeping gene RPLPO (acidic ribosomal phosphoprotein PO). The mean value obtained for the three controls was considered 100% of expression and the values obtained in the other clones were compared to the control mean value. The results are summarized in the table 4.5.2, while figure 4.5.3 compares the results obtained by western blotting analysis and qReal-Time PCR.

| Clone | hFis1/RPLPO |
|---|---|
| C90-1 | 100% |
| C90-2 | 100% |
| C90-3 | 100% |
| F90-1 | 26,9%±2,83 |
| F90-2 | 48,5%±13,36 |
| F90-3 | 20,7%±2,19 |

**Table 4.5.2:** qReal-Time PCR quantification of hFis1, as percentage of hFis1 down expression in 90-Fis compared to the control clones (90-Rep). The samples were analysed in triplicate.

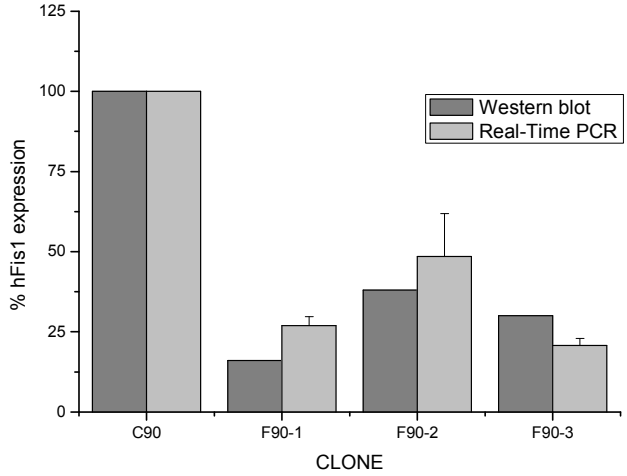


**Figure 4.5.3:** western blot and Real-Time PCR quantification of hFis1, as percentage of hFis1 in 90-Fis cybrids compared to the control clones (90-Rep).

### 4.5.1.3 Quantitation of mutant mtDNA

The percentage of mutant mtDNA was analysed by Last-Cycle Hot PCR in RD MELAS 92% cybrids with hFis1 down expression to verify if hFis1 low levels had some influence on the segregation of mutant and wild-type mtDNA. Figure 4.5.4 shows the result of LC Hot PCR after APAI digestion.

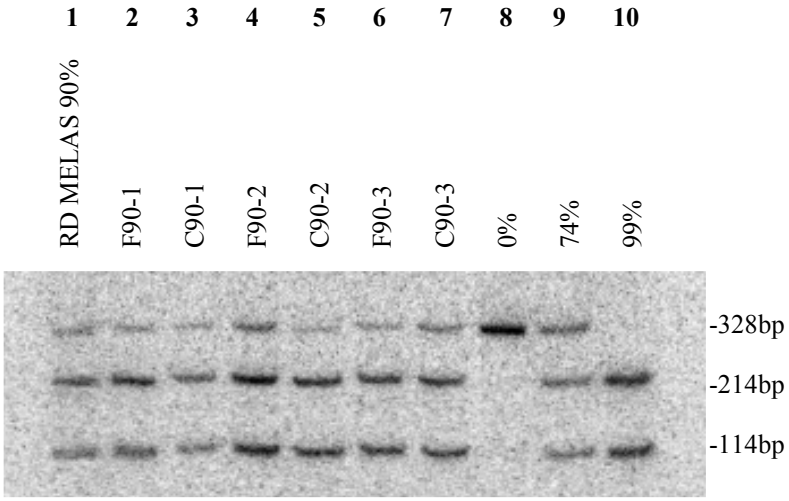


**Figure 4.5.4:** phosphor-image analysis of samples after LC-Hot PCR and APAI digestion. Line 1 are untransfected 92% cybrids; lines 3-5-7 are the control clones (90-Rep); lines 2-4-6 are 90-Fis cybrids; lines 8-9-10 are internal standards

The bands were analysed by Gel-Pro Analyzer software and the percentage of mutant mtDNA in each clone is summarized in the table 4.5.3.

| Clone | % mutant mtDNA |
|---|---|
| C90-1 | 91,7%±0,6 |
| C90-2 | 93,5%±2,1 |
| C90-3 | 90,4%±2,6 |
| F90-1 | 92,6%±2,0 |
| F90-2 | 89,3%±2,1 |
| F90-3 | 92,0%±2,8 |

**Table 4.5.3:** percentage of mutant mtDNA in 90-Rep and 90-Fis cybrids. Each value is the mean ± sd of at least two determinations.

The mean value of percentage of mutant mtDNA was 91,8±1,6 for the control clones and 91,3%±1,8 for the clones with hFis1 down expression. There wasn't a variation in percentage of mutant mtDNA between control clones and clones with hFis1 down expression (NS, P=0.737).
Figure 4.5.5 resumes these results.

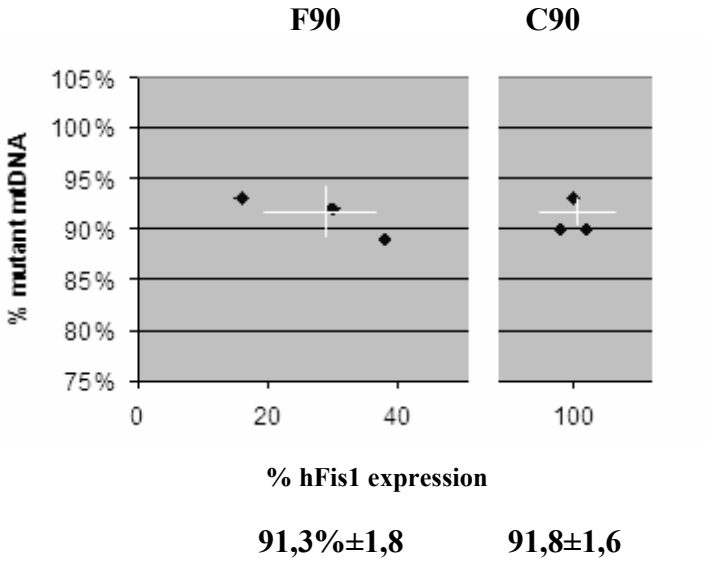


**Figure 4.5.5:** relation between Drp1 expression and percentage of mutant mtDNA in 90-Rep and 90-Fis cybrids.

Such as observed in RD MELAS 92% cybrids with Drp1 down expression, although the hFis1 down expression was successfully, it didn't cause any change in percentage of mutant mtDNA that remained constant.

### 4.5.2 RD MELAS 83% cybrids

#### 4.5.2.1 Clones collection

RD MELAS 83% cybrids were also transfected with pREP4 hygro hFis1-RNAi. After 15 days of selection in medium with hygromycin, 15 clones 80-Fis were collected and all of them were analysed as previously described for hFis1 levels. Three of these clones, with less than 53% of hFis1 down expression were chosen for the study. These clones were called F80-1, F80-2 and F80-3.

The control clones were the 80-Rep, the same used to study Drp1.

Figure 4.5.6 shows the western blotting analysis for the chosen clones. 30μg of protein was loaded on the gel for each sample.

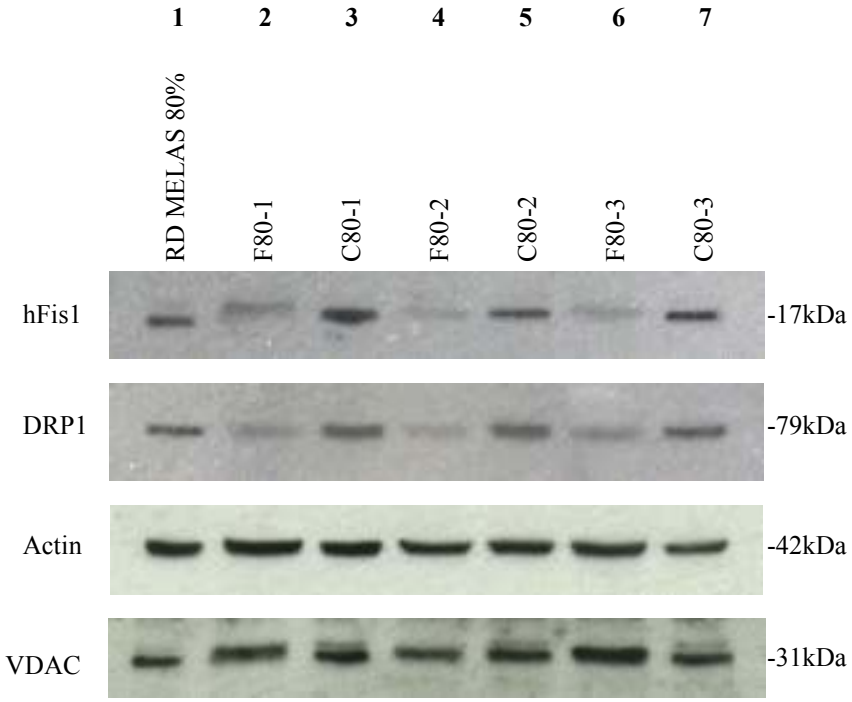


**Figure 4.5.6:** western blot analysis of hFis1 and Drp1 expression in untransfected RD MELAS 83% cybrids (line 1), in 80-Rep cybrids (lines 3-5-7) and in 80-Fis cybrids (lines 2-4-6). 30μg of proteins were loaded on a 12% acrilamide gel. hFis1 expression was detected using anti-hFis1 polyclonal antibody (Alexis ALX-210-907-R100); the signal was normalized to VDAC/porin expression. VDAC/porin expression was detected using anti-VDAC/porin monoclonal antibody (Sigma); Drp1 expression was detected using anti-Drp1 monoclonal antibody (Biosciences); actin expression was detected using anti-actin monoclonal antibody (Chemicon). For each clone at least 2 quantitations were performed.

The intensity of the bands was quantified by Gel-Pro Analyzer 3 software. The signal of hFis1 expression was normalized to VDAC/porin intensity bands. To obtain the percentage of expression, the mean value obtained for the three controls was considered 100% of expression and the value obtained for the other clones was compared to the mean value of the control clones. hFis1 down expression resulted

between 16% and 53%. Such as observed in RD MELAS 83% with Drp1 down expression, in cybrids with hFis1 down expression, a Drp1 down expression was also observed. The obtained values are summarized in table 4.5.4 and in figure 4.5.7.

| Clone | hFis1 expression/ VDAC | | | Drp1 expression/ VDAC |
|---|---|---|---|---|
| | I value | II value | mean±st.dev. | |
| C80-1 | 100% | 100% | 100% | 100% |
| C80-2 | 100% | 100% | 100% | 100% |
| C80-3 | 100% | 100% | 100% | 100% |
| F80-1 | 30,6% | 76,0% | 53,3%±32,10 | 70% |
| F80-2 | 22,6% | 41,0% | 31,8%±13,01 | 47% |
| F80-3 | 12,0% | 20,0% | 16,0%±5,66 | 43% |

**Table 4.5.4:** western blot quantification of hFis1 and Drp1 as percentage of hFis1 and Drp1 presence in 80-Fis cybrids compared to the control clones (80-Rep).

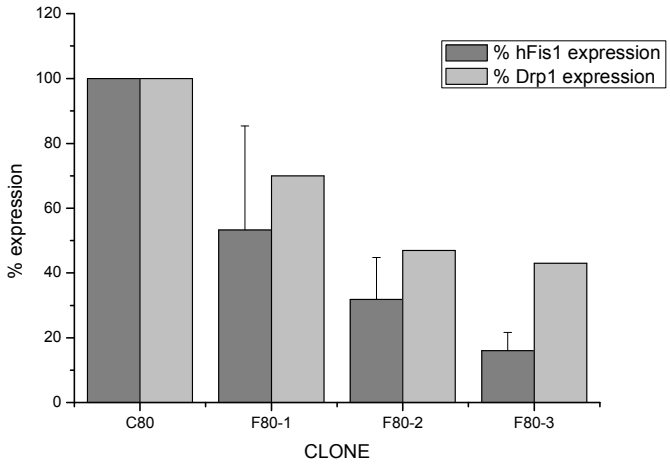


**Figure 4.5.7:** western blot quantification of hFis1 and Drp1 as percentage of hFis1 and Drp1 presence in 80-Fis cybrids compared to the control clones (80-Rep).

### 4.5.2.2 qReal-Time PCR

Data obtained on hFis1 expression level by western blot analysis, were confirmed quantifying hFis1 mRNA levels by qReal-Time PCR. The hFis1 mRNA levels were normalized to the house-keeping gene RPLPO (acidic ribosomal phosphoprotein PO). The mean value obtained for the three controls was considered 100% of expression and the values obtained in the other clones were compared to the control mean value. The results are summarized in the table 4.5.5, while figure 4.5.8 compares the results obtained by western blot analysis and qReal-Time PCR. It is possible to see that the values obtained by qReal-Time PCR are higher than the values obtained by Western blot in all the three clones.

| Clone | hFis1/RPLPO |
|---|---|
| C80-1 | 100% |
| C80-2 | 100% |
| C80-3 | 100% |
| F80-1 | 86,2%±2,1 |
| F80-2 | 53,0%±1,7 |
| F80-3 | 47,8%±0,1 |

**Table 4.5.5:** qReal-Time PCR of hFis1 as percentage of hFis1 expression in 80-Fis cybrids compared to the control clones (80-Rep). The samples were analysed in triplicate.

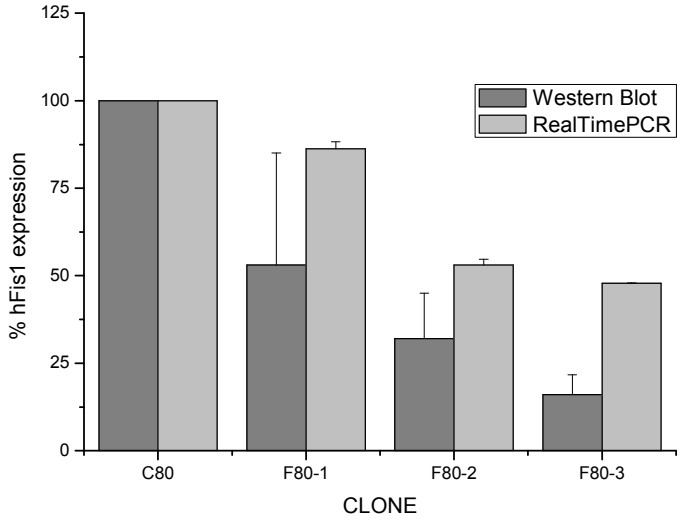


**Figure 4.5.8:** western blot and Real-Time PCR quantification of hFis1, as percentage of hFis1 expression in 80-Fis cybrids compared to the control clones (80-Rep).

### 4.5.2.3 Quantification of mutant mtDNA

The percentage of mutant mtDNA was analysed by Last-Cycle Hot PCR in RD MELAS 83% cybrids with hFis1 down expression to verify if also in this case, a greater mitochondrial fusion could influence mutant mtDNA segregation such as observed in RD MELAS 83% cybrids with Drp1 down expression. Figure 4.5.9 shows the result of LC Hot PCR after APAI digestion.

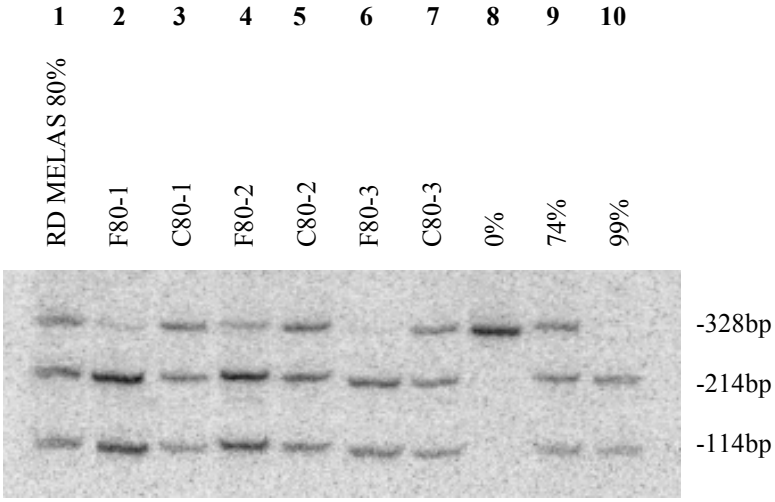


**Figure 4.5.9:** phosphor-image analysis of samples after LC-Hot PCR and APAI digestion. Line 1 are untransfected RD MELAS 83% cybrids; lines 3-5-7 are the control clones (80-Rep); lines 2-4-6 are 80-Fis cybrids; lines 8-9-10 are internal standards.

The bands were analysed by Gel-Pro Analyzer software and the percentage of mutant mtDNA in each clone is summarized in the table 4.5.6.

| Clone | % mutant mtDNA |
|---|---|
| C80-1 | 81,7%±1,0 |
| C80-2 | 80,0%±1,3 |
| C80-3 | 81,9%±1,4 |
| F80-1 | 98,5%±0,1 |
| F80-2 | 92,4%±2,3 |
| F80-3 | 99,7%±0,4 |

**Table 4.5.6:** percentage of mutant mtDNA in 80-Rep and 80-Fis cybrids. Each value is the mean ± sd of at least two determinations.

In the control clones the mean value of percentage of mutant mtDNA was 81,2±1,1, while in the clones with hFis1 down expression the mean value of percentage of mutant mtDNA was 96,8±3,9. These results show a 13% of increase

in mutant mtDNA in the clones with hFis1 down expression. We expected a such result since in clones with hFis1 down expression we also found a Drp1 down expression and vice versa (see paragraph 7.11 and 8.11).
The reduction was analysed by Student's t test and it resulted statistically significant: $P<0.003$.
Figure 4.5.10 resumes these results.

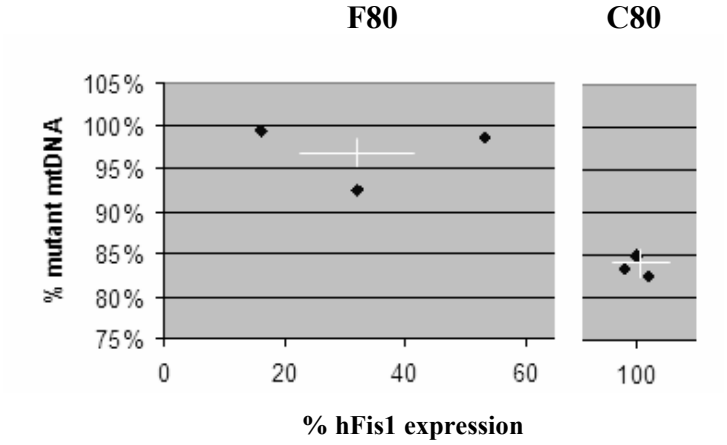


**Figure 4.5.10:** relation between hFis1 expression and percentage of mutant mtDNA in 80-Rep and 80-Fis cybrids.

### 4.5.3 RD MELAS 74% cybrids

#### 4.5.3.1 Clones collection

RD MELAS 74% cybrids were also transfected with pREP4 hygro hFis1-RNAi to obtain clones with hFis1 down expression (70-Fis). After 15 days of selection in medium with hygromycin, 10 clones 70-Fis were collected and all of them were tested by western blot analysis to check the hFis1 and Drp1 expression levels.
Three clones with less than 65% of hFis1 expression were chosen and called F70-1, F70-2 and F70-3.
Also in this case the control clones were the same used to study Drp1 down expression since the empty vector is pREP4 hygro.
Figure 4.5.11 shows the result of western blot analysis.

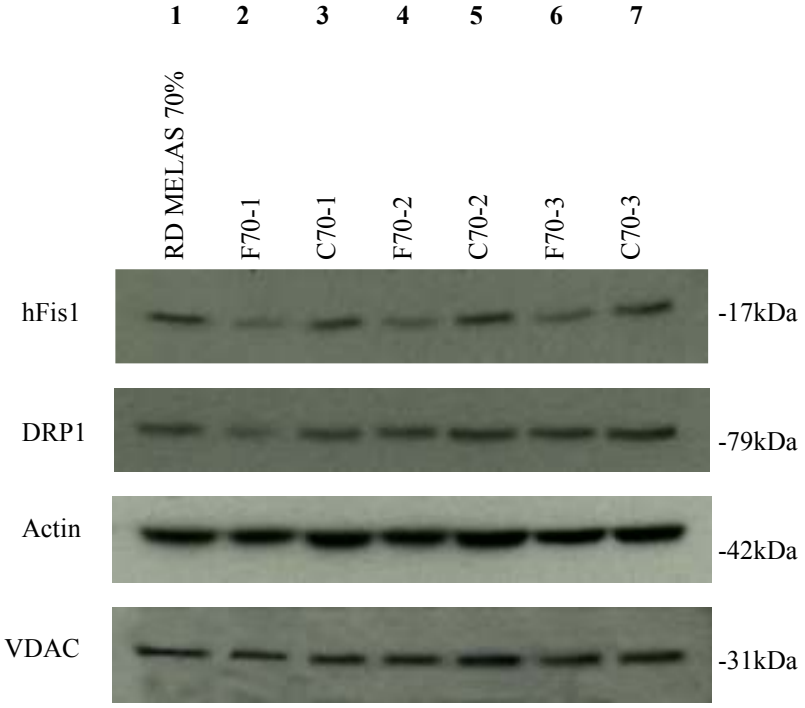


**Figure 4.5.11: A)** western blot analysis of Drp1 and hFis1 expression in untransfected RD MELAS 74% cybrids (line 1), 70-Rep cybrids (lines 3-5-7) and in 70-Fis cybrids (lines 2-4-6). 30μg of proteins were loaded on each well and hFis1 expression was detected using anti-hFis1 polyclonal antibody (Alexis ALX-210-907-R100); the signal was normalized to VDAC/porin expression. VDAC/porin expression was detected using anti-VDAC/porin monoclonal antibody (Sigma); Drp1 expression was detected using anti-Drp1 monoclonal antibody (Biosciences); actin expression was detected using anti-actin monoclonal antibody (Chemicon).

The intensity of the bands was quantified by Gel-Pro Analyzer 3 software. The signal of Drp1 and hFis1 expression was normalized to VDAC/porin intensity bands. To obtain the percentage of expression, the mean value obtained for the three controls

was considered 100% of expression and the value obtained for the other clones was compared to the mean value of the control clones.

hFis1 expression resulted between 41% and 65%, and only in one clone (F70-1) also a down expression of Drp1 was obtained.

The obtained values are summarized in table 4.5.7 and in figure 4.5.12.

| Clone | hFis1 expression/ VDAC | Drp1 expression/ VDAC |
|---|---|---|
| C70-1 | 100% | 100% |
| C70-2 | 100% | 100% |
| C70-3 | 100% | 100% |
| F70-1 | 41,1% | 60,7% |
| F70-2 | 55,9% | 100% |
| F70-3 | 64,6% | 100% |

**Table 4.5.7:** western blot quantification of hFis1 and Drp1, as percentage of hFis1 and Drp1 presence in 70-Fis cybrids compared to the control clones (70-Rep).

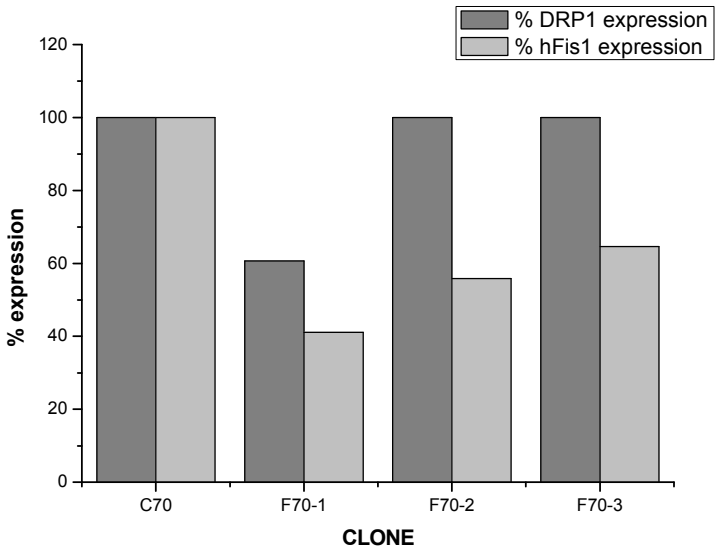


**Figure 4.5.12:** western blot quantification of hFis1 and Drp1, as percentage of hFis1 and Drp1 presence in 70-Fis cybrids compared to the control clones (70-Rep).

### 4.5.3.2 Quantification of mutant mtDNA

Also in RD MELAS 74% cybrids with hFis1 down expression the percentage of mutant mtDNA was analysed by Last-Cycle Hot PCR to verify if a greater mitochondrial fusion could influence mutant mtDNA segregation such as observed in RD MELAS 83% cybrids with Drp1 and hFis1 down expression. Figure 4.5.13 shows the result of LC Hot PCR after APAI digestion.

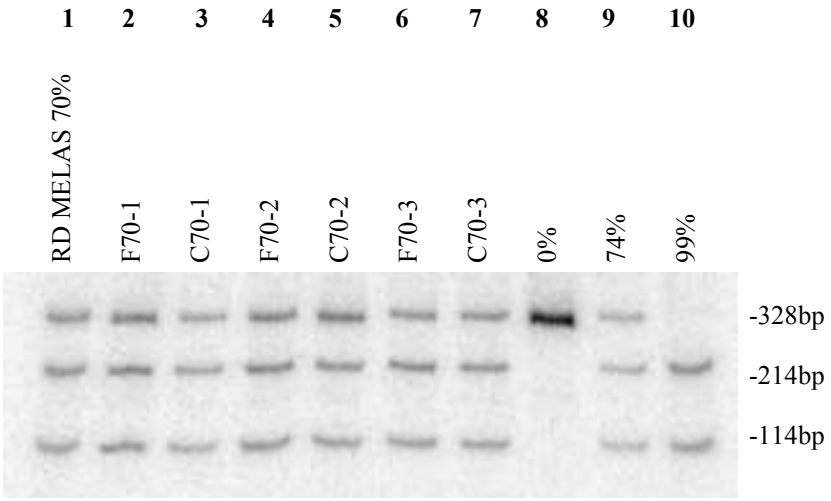


**Figure 4.5.13:** phosphor-image analysis of samples after LC-Hot PCR and APAI digestion. Line 1 are untransfected 74% RD MELAS cybrids; lines 3-5-7 are the control clones (70-Rep); lines 2-4-6 are 70-Fis cybrids; lines 8-9-10 are internal standards.

The bands were analysed by Gel-Pro Analyzer software and the percentage of mutant mtDNA in each clone is summarized in the table 4.5.8.

| Clone | % mutant mtDNA |
|---|---|
| C70-1 | 76,2%±2.3 |
| C70-2 | 73,7%±0,7 |
| C70-3 | 74,5%±2,8 |
| F70-1 | 85,4% |
| F70-2 | 77,2% |
| F70-3 | 77% |

**Table 4.5.8:** percentage of mutant mtDNA in 70-Rep and 70-Fis cybrids.

In the control clones the mean value of percentage of mutant mtDNA was 74,8±1,25, as it was already reported in table 4.4.7 and 4.5.8. In clones with hFis1 down expression the mean value of percentage of mutant mtDNA was 79,9±4,79. These results were analysed by Student's t test and they didn't result statistically significant (P=0,149).

The percentage of mutant mtDNA was increased of 14% compared to 70-Rep clones only in the clone F70-1, in which both hFis1 and Drp1 were down expressed.
Figure 4.5.14 resumes these results.

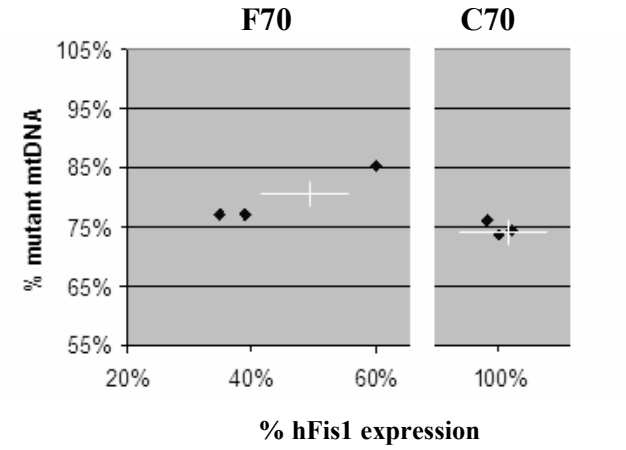


**Figure 4.5.14:** relation between hFis1 expression and percentage of mutant mtDNA in 70-Rep and 70-Fis cybrids.

## 4.6 Mitochondrial morphology

In control clones and clones with Drp1 and hFis1 down expression, mitochondrial shape and distribution were observed using the mitochondrial target fluorescence probe MitoTraker Red and images were taken at confocal microscope (see paragraph 3.4.3). Panel 4.6.1 resumes the results.
Mitochondria of cybrids transfected with the empty vector pREP4 (fig. 4.6.1 D-E-F) were unnoticeable from untransfected clones 70%, 80% and 90% cybrids (fig. 4.6.1 A-B-C).
Cybrids with Drp1 down expression had a characteristic worm-like shape of mitochondria (fig. 4.6.1 G-H-I). They were longer than the mitochondria of control clones, being Drp1 a protein involved in mitochondrial fission.
A similar result was observed in cybrids with hFis1 down expression (fig. 4.6.1 L-M-N).

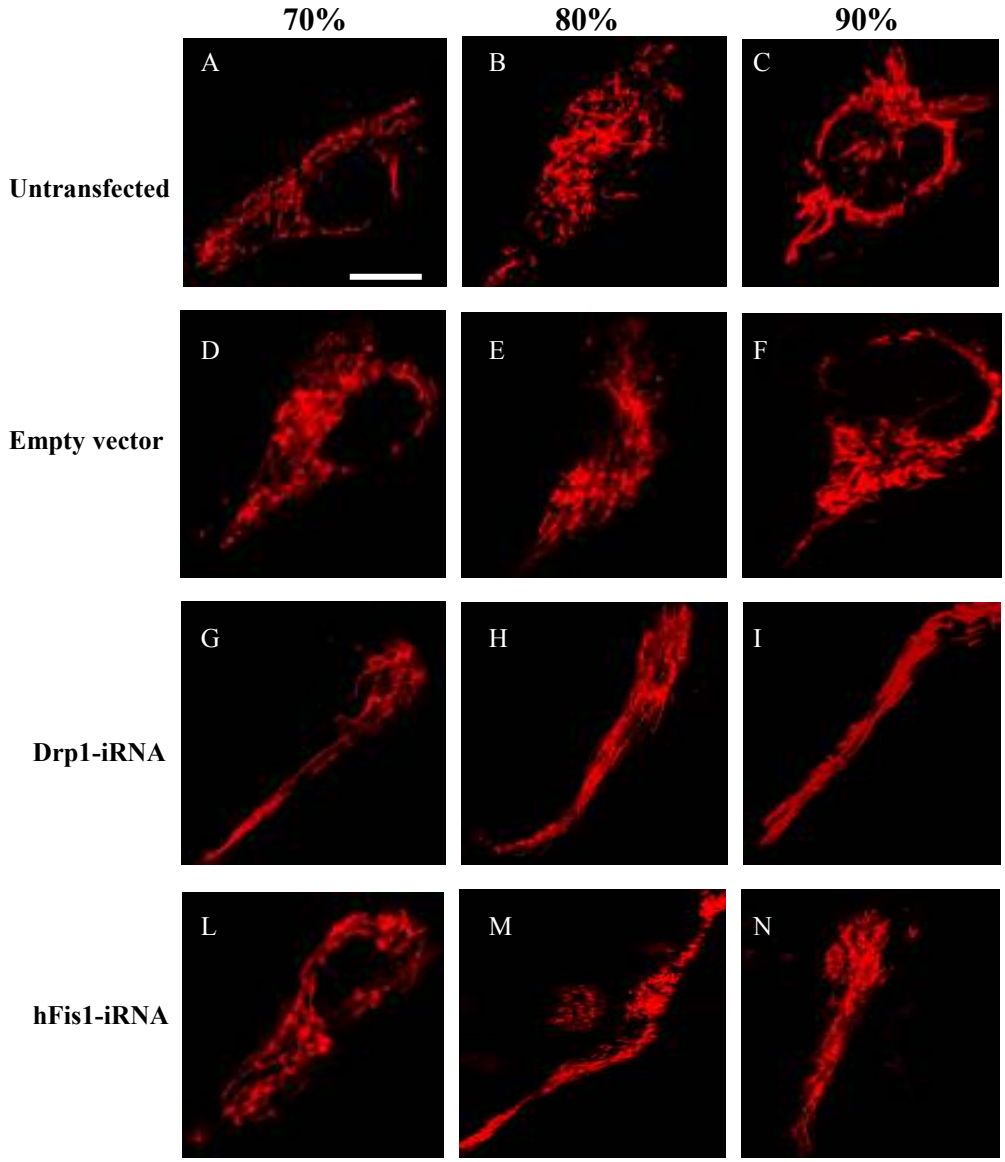


**Figure 4.6.1:** mitochondrial shape and distribution in: untransfected RD MELAS 70% cybrids (A); untransfected RD MELAS 83% cybrids (B); untransfected RD MELAS 92% cybrids (C); 70-Rep cybrids (D); 80-Rep cybrids (E); 90-Rep cybrids (F); 70-Drp cybrids (G); 80-Drp cybrids (H); 90-Drp cybrids (I); 70-Fis cybrids (L); 80-Fis cybrids (M); 90-Fis cybrids (N). MitoTracker Red was used to stain mitochondria and images were taken using confocal microscope. Scale bar: 10μm.

### 4.7 Characterization

We observed that a greater mitochondrial fusion, obtained by down expression of Drp1 and hFis1, caused a shift in percentage on mtDNA in 83% heteroplasmic cybrids.

Three clones: D80-1, D80-5 and D80-4 with respectively 94%, 95% and 99% of mutant mtDNA were characterized for:

- Oxygen consumption and RCR
- Activities of PFK, COX and CS
- mtDNA amount.

Moreover, in three 70-Drp and three 70-Fis clones PFK, COX and CS activities were assayed.

#### 4.7.1 Mitochondrial enzymes

Tables 4.7.1 and 4.7.2 summarize the results of PFK, COX and CS activities found in the previously listed clones.

| **CLONE** | | **COX** | **CS** | ***(COX/CS)*100*** | **PFK** |
|---|---|---|---|---|---|
| clone | % mutant mtDNA | nmol/min/mg prot | nmol/min/mg prot | | nmol/min/mg prot |
| | | | | | |
| WT | 0,0% | 21,5±8,3 | 103,8±24,4 | *21,3±4,2* | 116±14,2 |
| RD MELAS 83% | 83,0% | 32,9±14,0 | 103,6±10,2 | *30,9±12,4* | 216,3±21,9 |
| RD MELAS 99% | 99,0% | 6,2±2,6 | 162,2±39 | *3,75±0,7* | 149,8±38,3 |
| | | | | | |
| C80-1 | 81,7% | 61,9±4,2 | 85,8±10,1 | *72,5±5,5* | 252,4±32,4 |
| C80-2 | 80,0% | 62,0±4,2 | 84,9±8,1 | *73,4±7,2* | 249,1±19,2 |
| C80-3 | 81,9% | 75,5±10 | 96,1±5,9 | *78,5±8,3* | 249,9±20,9 |
| | | | | | |
| D80-1 | 93,7% | 15,8±2,2 | 37,92±7,7 | *42,1±3,3* | 207,7±6,9 |
| D80-5 | 95,0% | 7,6±1,9 | 78,0±3,9 | *9,8±3,0* | 135,9±18,8 |
| D80-4 | 99,0% | 4,75±0,5 | 42,5±5,2 | *11,2±0,9* | 168±14,2 |

**Table 4.7.1:** activities of COX, citrate synthase (CS) and glycolytic enzyme phosphofructokinase (PFK) in untransfected RD 0%, 83% and 99% cybrids, in 80-Rep cybrids and in 80-Drp cybrids. Measurements were performed in triplicate and expressed as mead ± SD. The COX activity was normalized to CS activity (italics values).

| **CLONE** | | **COX** | **CS** | ***(COX/CS)*100*** | **PFK** |
|---|---|---|---|---|---|
| clone | % mutant mtDNA | nmol/min/mg prot | nmol/min/mg prot | | nmol/min/mg prot |
| | | | | | |
| RD MELAS 74% | 74,0% | 30,3 | 65,2 | *46,5* | 300,6 |
| RD MELAS 92% | 92,0% | 51±21,6 | 121,6±19,5 | *41,9±15,4* | 259,3±28 |
| | | | | | |
| C70 (1-2-3) | 74,8% | 33,1±5,3 | 91,5±13,9 | *35,9±10,3* | 233,2±35,3 |
| D70 (1-2-3) | 76,1% | 24,8±13 | 90,9±31,1 | *33,7±28,7* | 240,3±63,1 |
| F70 (1-2-3) | 79,9% | 38,3±5,3 | 58,6±16,5 | *75,2±21,8* | 279,5±4,3 |

**Table 4.7.2:** activities of COX, citrate synthase (CS) and phosphofructokinase (PFK) in untransfected RD 74% and 92% cybrids, in 70-Rep cybrids, in 70-Drp and in 70-Fis cybrids. Measurements were performed in triplicate and expressed as mead ± SD. The COX activity was normalized to CS activity (italics values).

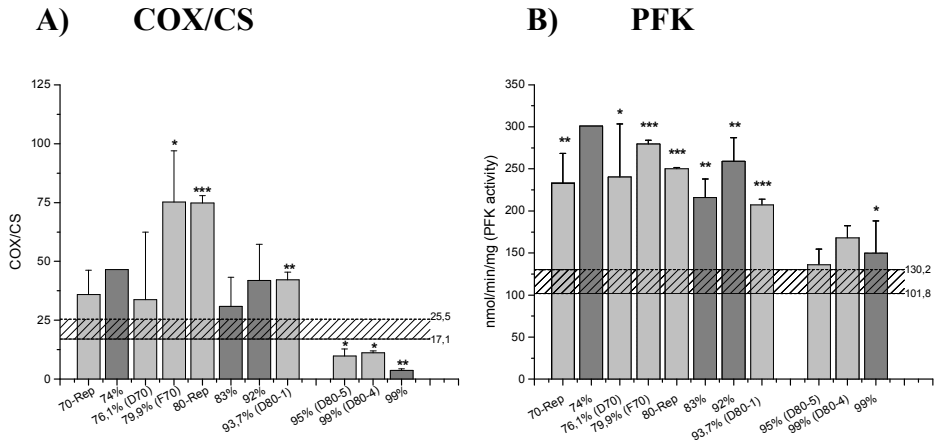


**Figure 4.7.1:** activity of **(A)** COX/CS and **(B)** phosphofructokinase (PFK) in untransfected clones (74%, 83%, 99%), in trasfected control clones (70-Rep, 80-Rep), in clones with dowregulation of Drp1 and hFis1 (70-Drp, 70-Fis, 80-Drp). Sparse pattern indicates a normal range values. Statistical analysis of the different clones is compared to wild-type values: *p<0.05; **p<0.01; ***p<0.001.

Figure 4.7.1 illustrates the greater differences among the tested clones.

It shows that COX and PFK activities were significantly increased in all the clones with an intermediate percentage of heteroplasmy (70%-90%) compared to wild-type cells. COX/CS increased from 1,45 to 2,9-fold ($p<0.05$), while PFK activity increased from 1,86 to 2,4-fold ($P<0.05$).

These results were independent from the down regulation of Drp1 and hFis1, but they were correlable to the percentage of mutant mtDNA. In fact the almost homoplasmic cybrids clones D80-5 and D80-4 had 95% and 99% of mutant mtDNA after downregulation of Drp1. They showed a significant reduction in COX to 13% and 15% respectively compared to control transfected 80-Rep clones (table 4.7.1, fig. 4.7.1), values similar to RD MELAS 99% cybrids. In the same clones PFK activity was reduced to 55% and 67% respectively compared to control 80-Rep clones (table 4.7.1, fig.4.7.1), values again similar to homoplasmic 99% clones.

Moreover there were no significant differences in COX and PFK activities in 70-Fis clones compared to control 70-Rep clones, in line with the unchanged amount of percentage of mutant mtDNA and in spite of downregulation of hFis1.

These results further confirm a direct link between mutant mtDNA and expression of bioenergetic enzymes.

### 4.7.2 Oxygen consumption

In untransfected 0%, 83% and 99% cybrids, in 80-Rep clones and in 80-Drp clones, oxygen consumption and the respiratory control ratio RCR were measured. The $O_2$ consumption data are summarized in table 4.7.3 and in figure 4.7.2.

| CLONE | % mutant mtDNA | BASAL MEAN VALUE (nmol $O_2$/min/$10^6$cells) | FCCP MEAN VALUE (nmol $O_2$/min/$10^6$cells) | *RCR (FCCP/basal)* |
|---|---|---|---|---|
| | | | | |
| **WT** | 0,0% | 2,9±0,9 | 5,1±2,1 | *1,74±0,25* |
| **RD MELAS 83%** | 83,0% | 4,45±1,14 | 6,14±1,31 | *1,38±0,18* |
| | | | | |
| **C80** | 81,2% | 4,59±1,24 | 6,85±2,10 | *1,51±0,09* |
| | | | | |
| **D80-1** | 93,7% | 4,36±1,56 | 5,66±1,15 | *1,39±0,31* |
| **D80-5** | 95,0% | 3,63±1,38 | 3,96±1,45 | *1,09±0,03* |
| **D80-4** | 99,0% | 2,21±0,59 | 3,32±0,54 | *1,57±0,41* |
| | | | | |
| **RD MELAS 99%** | 99,0% | 1,04±0,33 | 1,67±0,22 | *1,61±0,26* |

**Table 4.7.3:** oxygen consumption values in 0%, 83%, and 99% untransfected cybrids, in 80-Rep and in 80-Drp clones. Basal values and maximal values (in presence of FCCP) are expressed as nmol/min/$10^6$cells. In italics are reported the RCR values. Measurements were performed in triplicate.

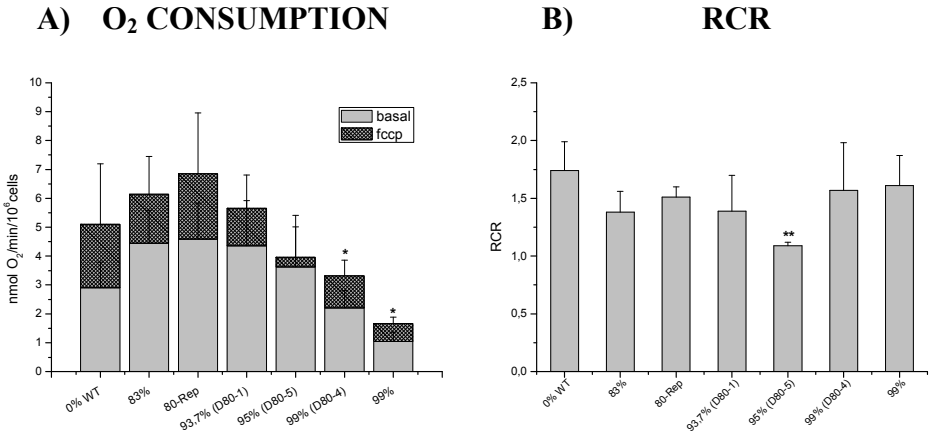


**Figure 4.7.2 A:** oxygen consumption values in untransfected 0%, 83%, 99% RD cybrids, in 80-Rep and in 80-Drp cybrids. Basal values (light gray) and maximal values (in presence of FCCP) (pattern sparse) are expressed as nmol/min/$10^6$cells. Measurements were done in triplicate. Statistical analysis of: 99%D80-4 vs. control clones (83% cybrids, 80-Rep); 99% clone vs. each clone: *p<0.05; **B:** RCR factor in untransfected 0%, 83%, 99% RD cybrids, in 80-Rep and in 80-Drp cybrids. Values come from ratio of three different measurements. Statistical analysis 95%D80-5 vs. control clones 80-Rep: **p<0.01

Table 4.7.3 shows that, as expected, the increase in percentage of mutant mtDNA was correlated to a significant reduction in maximum $O_2$ consumption.

In fact $O_2$ consumption of 99% mutant D80-4 in presence of FCCP was significantly reduced at 48% (table 4.7.3) compared both to 83% 80-Rep cybrids ($p<0.05$) and untransfected 83% cybrids ($P<0.03$).
RCR factor was similar in all the clones except in 95% D80-5 ($P<0.002$) compared to 80-Rep clones (fig 4.7.2 B), indicating a probable condition of stress present in this clone. In fact its percentage of mutation (95%) was near to the probable threshold value (about 96%), that could impair cell bioenergetic homeostasis when exceeded.

### 4.7.3 mtDNA amount

To verify if the heteroplasmic cells increased mitochondrial biogenesis (in particular mtDNA synthesis) to compensate their mitochondrial dysfunction, mtDNA amount was measured by qReal-Time PCR (see paragraph 3.3.11) in 80-Rep, 80-Drp clones and 99% cybrids. In fact the mutant phenotype is close related both to the proportion of mutant mtDNA and to mtDNA copy number. We found that the increase in percentage of mutant mtDNA was not related to a variation in mtDNA amount, that was similar to controls (Fig. 4.7.3).

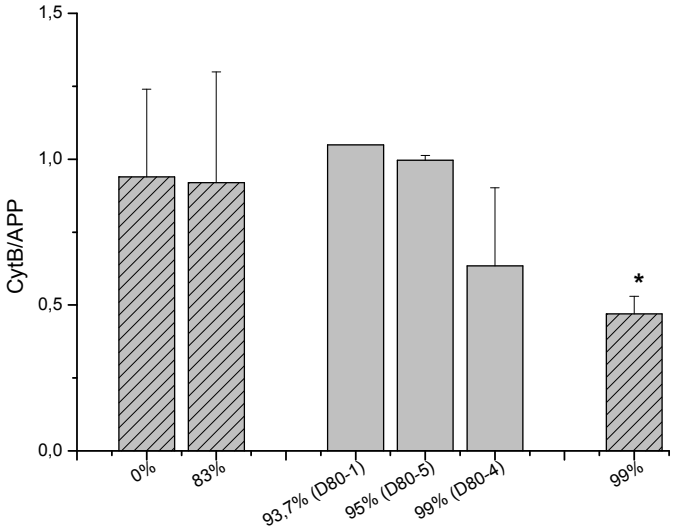


**Figure 4.7.3:** Real-Time PCR quantification of mtDNA in 80-Rep, 80-Drp clones and 99% cybrids. Statistical analysis of 99% clone vs. all the clones with less than 99% mutation: *$p<0.05$

# 5 DISCUSSION

## 5.1 Establishment of heteroplasmic RD cybrids

Muscle nuclear background seems to favour MELAS mutant mtDNA molecules. In fact in all the twelve established new heteroplasmic RD cybrid clones (tab. 4.1.2) the percentage of mutant mtDNA was similar or increased if compared to the donor mitochondrial cells, harbouring 74% mutant mtDNA. Neither adding 0.5mM NAC nor 100μM creatine to the basal selective medium, favoured wild-type mtDNA molecules. These results confirmed previous data obtained in our lab, when four near homoplasmic mutant RD cybrid clones, with 99% MELAS mutant mtDNA molecules, were established from 55% mutant patient's fibroblast [149].
Advantages of mutant mtDNA was also observed by Yoneda et al. [26] in cybrid clones with bone nuclear background, while Dunbar et al. [27] observed that lung nuclear background, on the contrary, favours wild-type mtDNA molecules. The reason why different nuclear backgrounds confer advantages to mutant or wild-type mtDNA, is far from clear.

## 5.2 Growth regimes

Normally in vitro cells have a predominant glycolytic metabolism, and are cultured in medium containing high glucose (25mM-G25) and pyruvate (1mM). To force the use of mitochondrial respiratory chain, wild-type and different heteroplasmic RD cybrids were cultured in reduced glucose medium, i.e. with physiological concentration of glucose: 10mM-G10 and 5mM-G5 in presence of pyruvate.
Surprisingly 0% mutant cells were the most sensitive to reduced energy supply if compared to 83% and 92% heteroplasmic mutant cybrids and died after three-four days of treatment in G5 medium (tab. 4.1.4). Consistent with this null tolerance to decreased energy supply, 0% mutant RD clones stopped to grow and started to die probably for apoptosis at two days when their growth rate was negative, and at 4 days all the cells were found floating in the medium. At two days of growth in 5mM glucose, the bioenergetic stress of homoplasmic normal cells, was confirmed by the RCR factor that was significantly reduced of 25% in 0% cybrids, but not in 83% and 92% cybrids (fig. 4.2.3). In fact both 83% and 92% heteroplasmic mutant RD cybrids revealed a good tolerance to low glucose regime (tab. 4.1.4).
100nM creatine didn't influence both functional and molecular parameters in all the undifferentiated cells, while in reduced energy supply uridine addition always promoted cell growth of all the studied RD cybrid clones (tab. 4.1.4).
To explain why heteroplasmic MELAS mutant RD cybrids survived better than

normal cells in low glucose, a set of biochemical analysis was performed. It demonstrated that bioenergetic anaerobic and aerobic pathways are strengthened in heteroplasmic cybrids. In fact in 92% and 83% cybrids COX activity (expressed as ratio COX/CS) was increased to 1,6-fold and 1,7-fold respectively compared to 0% cybrids, and PFK activity was increased to 2,1-fold compared to 0% cybrids (fig. 4.2.10).

Our result confirms a study conduced by Heddi et al. [154]. He observed that a coordinated increase in expression of genes linked to energetic metabolism such as creatinephosphokinase, glycogen phosphorylase, exokinase, ANT, phosphofructokinase, E1α subunit of pyruvate dehydrogenase was present in different tissues such as heart, muscle, brain of a patient with MELAS mutation and with a clear defect in respiratory chain. This compensative induction was linked to a high grade of heteroplasmy, in fact under 60% of mutation no induction was observed.

**5.3 Down regulation of protein involved in mitochondrial fusion and fission**

Our main objective was to obtain reproducible in vitro conditions of variation of mutated mtDNA amount. Many strategies were adopted: differentiation, low glucose, creatine, uridine, antioxidant (NAC) supplementation, but all failed to succeed. At the end only down regulation of Drp1, hFis1 and OPA1 by RNAi changed mtDNA percentage in heteroplasmic mutant RD cybrids.

Mitochondrial morphology within cells is controlled by precisely regulated rates of fusion and fission. OPA1 is involved in fusion and is localized in the inner mitochondrial membrane, while Drp1 and hFis1 are fission proteins.

We decided to analyse if in 92%, 83% and 74% MELAS RD cybrids, OPA1, Drp1 and hFis1 down regulation could influence mutant mtDNA segregation.

OPA1 down expression was successfully obtained by RNAi methods in both 92% and 83% RD MELAS cybrids, in fact in the clones collected after selection in hygromycin, mitochondria were greatly fragmented (fig. 4.3.10) and OPA1 presence was between 30% and 60% compared to the control clones.

We didn't obtain clones with a complete OPA1 absence, probably because OPA1 absence isn't compatible with cellular survival [83], in fact down regulation of OPA1 leads to a drastic disorganization of the cristae and to the dissipation of $\Delta\mu H^+$. These events are followed by cytochrome c release and apoptotic events.

It's interesting that OPA1 down regulation significantly reduced the percentage of MELAS mutant mtDNA compared to the control cybrids in both the cell lines (fig. 5.1).

The increase in wild-type mtDNA amount that we observed is probably a

consequence of major sensitivity to apoptosis in cells with low OPA1 levels and high mutant mtDNA.

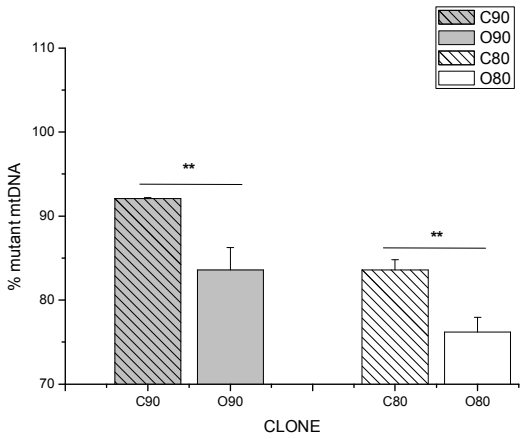


**Figure 5.1:** relation between OPA1 expression and percentage of mutant mtDNA in 80-Sil, 90-Sil clones, 80-OPA and 90-OPA clones. **p<0.01

Also hFis1 down expression was successfully obtained in all the three clones with 92%, 83% and 74% of mutant mtDNA, while Drp1 down expression was successfully in 92% and 83% cybrids, but it was not evident in 74% cybrids.

We got clones with very few levels of Drp1 and hFis1 presence and this was confirmed by the mitochondrial morphology of the clones collected after selection in hygromycin. These clones had a reticular organization of worm-like mitochondria (fig. 4.6.1), that was less evident in cells with low levels of hFis1.

We hypothesized that an increased mitochondrial fusion in heteroplasmic cybrids for A3243G MELAS mutation could increase an inter-mitochondrial complementation. So wild-type mtDNA could have been favoured resulting in a segregation of wild-type mtDNA and in a consequent reduction of mutant mtDNA percentage.

On the contrary to the initial hypothesis, wild-type mtDNA molecules dramatically decreased in 83% RD MELAS cybrids from 17% to 4% or almost 0% (fig. 5.2) and didn't increase in two clones (70% and 90%), where they remained stable.

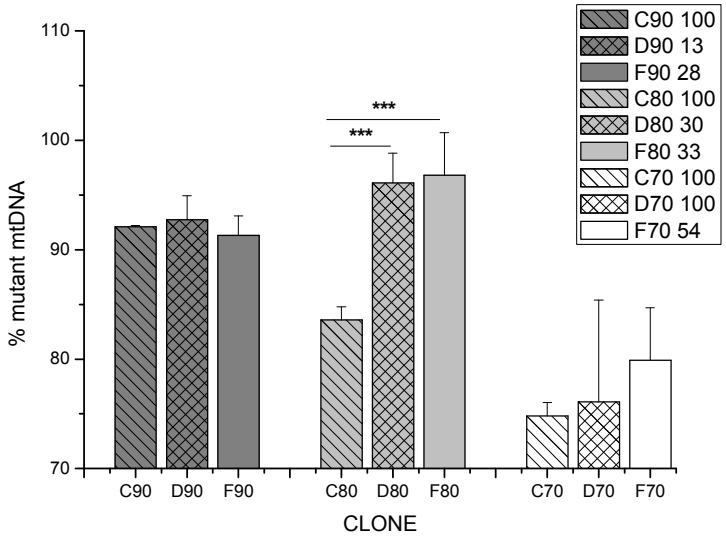


**Figure 5.2:** relation between Drp1 and hFis1 expression and percentage of mutant mtDNA in RD MELAS 92%, 83% and 74% cybrids transfected with the empty vector (C90, C80, C70), pREP4 hygro Drp1-RNAi (D90, D80, D70) and pREP4 hygro hFis1-RNAi (F90, F80, F70). In the insert are listed the % of expression of D (Drp1), F (hFis1) in the different clones. ***p<0.001

In our heteroplasmic RD cybrids $O_2$ consumption, glycolytic and oxidative enzyme activities (PFK and COX activities) were correlated to the increase in percentage of mutant mtDNA, independently to down regulation of Drp1 and hFis1.

These results confirm the previous data, i.e. in heteroplasmic cybrids the increased activity of bioenergetic enzymes is a compensative event that probably helps heteroplasmic cybrids to better survive to stress conditions compared to wild-type cybrids.

The results of RNAi experiments are congruent with the major resistance of heteroplasmic cybrids compared to wild-type. In fact we didn't have problems to get heteroplasmic cybrids with down regulation of OPA1, Drp1 or hFis1, while the transfection of wild-type cybrids was more difficult. We obtained only 3 or 4 wild-type clones with down regulation of fission or fusion proteins and these clones grew very slowly. Lee et al. [164] observed that in HeLa cells the extensive mitochondrial elongation caused by hFis1 depletion induces senescence-associated phenotypic changes. Benard et al. [165] observed that HeLa cells containing siRNA targeting Drp1 showed a slower rate of proliferation in glucose

medium in comparison with control cells. In glucose-deprived medium, these cells were unable to proliferate, and died after three days, in contrast with the controls. This suggests that in HeLa cells with downregulation of Drp1 the OXPHOS system is inefficient. In these Drp1-depleted cells it was also observed a reduction in the endogenous rate of coupled respiration and a strong reduction of mitochondrial ATP synthesis.
It is difficult to explain the reason why mutated mtDNA is dominant. In fact dysfunction of mitochondria has severe cellular consequences, therefore several surveillance strategies have evolved that limit mitochondrial damage and ensure cellular integrity. In line with this observation the positive selection of health mitochondria and the removal of affected mitochondria should be the more probable cellular strategies, in contrast with the observed results. It is therefore difficult to hypothesise the underlying mechanisms for the positive selection of mutated mtDNA. We try to list some hypothesis:

A) One of the surveillance strategies could be the **strengthened of glycolytic pathway and OXPHOS** activities to compensate the mitochondrial dysfunction. Heddi [154]demonstrated an induction and increased expression of genes linked to energetic metabolism in MELAS tissues, we found an increased activity of PFK and COX in heteroplasmic cells.

B) Another possible mechanism is **a major resistance to apoptotic stimuli in heteroplasmic cells.** The advantage could therefore arise from defence to a variety of injuries that prevent the consequent cellular death. The mechanisms involved could be i) sensitivity of PTP; ii) mitophagy; iii) regulation-expression of pro-anti apoptotic proteins.

C) Nucleoid proteins and mtDNA duplication machinery may also determine the positive fate of mutant mtDNA molecules.

Probably the start point is a cross-talk mitochondrion-nucleus, that implies a signal from affected mitochondria direct to nucleus. ROS, Calcium or energy-related signaling could be the possible involved signal molecules. In fact research over the last decade has extended the prevailing view of cell mitochondrial function well beyond its critical bioenergetic role in supplying ATP. Recently it has been recognized that the mitochondria play a critical role in cell regulatory and signaling events, in the responses of cells to a multiplicity of physiological

and genetic stresses, inter-organelle communication, cell proliferation and cell death. The mitochondria act as a dynamic receiver and integrator of numerous translocated signaling proteins (including protein kinases and transcription factors), regulatory $Ca^{2+}$ fluxes and membrane phospholipids as well the transmission of mitochondrial-generated oxidative stress and energy-related signaling.

The nuclear response may be various and determine the downstream activation of heterogeneous signaling cascades. Dissection of the single parts of these steps and their full comprehension may deserve novel strategies to favour selection of normal mtDNA molecules.

The scenario that we try to draw in chronological sequence could be: 1) increased mtDNA mutation, 2) alteration of functional respiratory chain, 3) signaling by mitochondria to nucleus, 4) nuclear activation of signaling cascade, 5) activation of survival strategies.

One hint we got from the present study is that heteroplasmic cells have a metabolic bioenergetic state very similar to the Warburg effect observed in cancer [166]. Therefore we suggest that the mutant mtDNA presents a dominant pattern giving a selective advantage to the cells strengthening the anaerobic glycolysis, reminiscent the well known Warburg effect, observed in cancer cells. Over 50 years ago, Warburg observed that cancer cells frequently exhibit increased anaerobic glycolysis and, even in the presence of oxygen, depend largely on this metabolic pathway for generation of ATP [168]. The Warburg effect has been observed in a wide spectrum of human cancers. Although the biochemical and molecular mechanisms are extremely complex and remain to be defined, mitochondrial malfunction is considered a factor contributing to the Warburg effect. Recently the frequent mtDNA mutations observed in a variety of human cancers are thought to contribute to respiratory malfunction and progressive dependence on glycolysis in cancer cells [167, 169]

When the ability of cells to generate ATP through mitochondrial oxidative phosphorylation is compromised, cells are able to adapt alternative metabolic pathways, such as increasing glycolytic activity, to maintain their energy supply. Mitochondrial respiratory function can be negatively affected by multiple factors, including mutations in mitochondrial DNA, malfunction of the electron transport chain, aberrant expression of enzymes involved in energy metabolism, and insufficient oxygen available in the cellular microenvironment. The constant generation of reactive oxygen species within the mitochondria and the increased free radical stress in cancer cells may cause further damage to both mtDNA and

electron transport chain, thus amplifying respiratory malfunctions and dependency on glycolysis [167].

Mitochondrial defects have long been suspected to play an important role in the development of cancer and recently molecular genetic evidence in favour of a direct implication of mitochondria in oncogenesis has been accumulating.

Another possibility to explain the selective advantage of mutant mtDNA in cells is the activation of a novel mechanism recognised in eukaryotic cells: the autophagy-induced cytoprotection [170]. Similar stress stimuli can induce either apoptosis or autophagy, and in many instances the cell switches between the two responses in mutually exclusive manner. Increased cell autophagy may fuel cells in energy deprivation and preserve them from apoptosis. Therfore when cells are exposed to stress signals, the autophagy, that arise from the inhibition of apoptosis, protects cells from cell death.

In conclusions the reasons of selective advantage of mutant mtDNA molecules is still unclear. This study indicates the following perspectives for the future investigation: A) the metabolic analogy with cancer cells, that could help us to find the activate nuclear signal pathway; B) the presence of the novel mechanism of survival: autophagy in opposition to apoptosis in mutant cells.

# 5 Bibliography


1. Wallace DC (1999) Mitochondrial diseases in man and mouse. Science 283:1482-1488

2. Gray MW, Burger G, Lang BF (1999) Mitochondrial evolution. Science 283:1476-1481

3. Ernster L, Schatz G (1981) Mitochondria: a historical review. J Cell Biol 91:227s-255s

4. Duchen MR (2004) Mitochondria in health and disease: perspectives on a new mitochondrial biology. Mol Aspects Med 25:365-451

5. Chipuk JE, Bouchier-Hayes L, Green DR (2006) Mitochondrial outer membrane permeabilization during apoptosis: the innocent bystander scenario. Cell Death Differ 13:1396-1402

6. Frey TG, Mannella CA (2000) The internal structure of mitochondria. Trends Biochem Sci 25:319-324

7. Scheffler IE (2001) Mitochondria make a come back. Adv Drug Deliv Rev 49:3-26

8. Zeviani M, Di DS (2004) Mitochondrial disorders. Brain 127:2153-2172

9. Smeitink J, van den HL, DiMauro S (2001) The genetics and pathology of oxidative phosphorylation. Nat Rev Genet 2:342-352

10. Carroll J, Fearnley IM, Shannon RJ, Hirst J, Walker JE (2003) Analysis of the subunit composition of complex I from bovine heart mitochondria. Mol Cell Proteomics 2:117-126

11. Saraste M (1999) Oxidative phosphorylation at the fin de siecle. Science 283:1488-1493

12. Di DS (2000) Disorders related to mitochondrial membranes: pathology of the respiratory chain and neurodegeneration. J Inherit Metab Dis 23:247-263

13. Poyton RO, McEwen JE (1996) Crosstalk between nuclear and mitochondrial genomes. Annu Rev Biochem 65:563-607

14. Nass MM (1966) The circularity of mitochondrial DNA. Proc Natl Acad Sci U S A 56:1215-1222

15. Goto Y (2001) Clinical and molecular studies of mitochondrial disease. J Inherit Metab Dis 24:181-188

16. Reynier P, May-Panloup P, Chretien MF, Morgan CJ, Jean M, Savagner F, Barriere P, Malthiery Y (2001) Mitochondrial DNA content affects the fertilizability of human oocytes. Mol Hum Reprod 7:425-429

17. Fernandez-Silva P, Enriquez JA, Montoya J (2003) Replication and transcription of mammalian mitochondrial DNA. Exp Physiol 88:41-56

18. Lightowlers RN, Chinnery PF, Turnbull DM, Howell N (1997) Mammalian mitochondrial genetics: heredity, heteroplasmy and disease. Trends Genet 13:450-455

19. Jacobs LJ, de WG, Geraedts JP, de C, I, Smeets HJ (2006) The transmission of OXPHOS disease and methods to prevent this. Hum Reprod Update 12:119-136

20. Ames BN (1989) Endogenous oxidative DNA damage, aging, and cancer. Free Radic Res Commun 7:121-128

21. Richter C, Park JW, Ames BN (1988) Normal oxidative damage to mitochondrial and nuclear DNA is extensive. Proc Natl Acad Sci U S A 85:6465-6467

22. Shibata T, Ling F (2007) DNA recombination protein-dependent mechanism of homoplasmy and its proposed functions. Mitochondrion 7:17-23

23. Poulton J, Marchington DR (2002) Segregation of mitochondrial DNA (mtDNA) in human oocytes and in animal models of mtDNA disease: clinical implications. Reproduction 123:751-755

24. Sato A, Endo H, Umetsu K, Sone H, Yanagisawa Y, Saigusa A, Aita S, Kagawa Y (2003) Polymorphism, heteroplasmy, mitochondrial fusion and diabetes. Biosci Rep 23:313-337

25. Battersby BJ, Loredo-Osti JC, Shoubridge EA (2003) Nuclear genetic control of mitochondrial DNA segregation. Nat Genet 33:183-186

26. Yoneda M, Chomyn A, Martinuzzi A, Hurko O, Attardi G (1992) Marked replicative advantage of human mtDNA carrying a point mutation that causes the MELAS encephalomyopathy. Proc Natl Acad Sci U S A 89:11164-11168

27. Dunbar DR, Moonie PA, Jacobs HT, Holt IJ (1995) Different cellular backgrounds confer a marked advantage to either mutant or wild-type mitochondrial genomes. Proc Natl Acad Sci U S A 92:6562-6566

28. Yoneda M, Miyatake T, Attardi G (1994) Complementation of mutant and wild-type human mitochondrial DNAs coexisting since the mutation event and lack of complementation of DNAs introduced separately into a cell within distinct organelles. Mol Cell Biol 14:2699-2712

29. Nakada K, Inoue K, Ono T, Isobe K, Ogura A, Goto YI, Nonaka I, Hayashi JI (2001) Inter-mitochondrial complementation: Mitochondria-specific system preventing mice from expression of disease phenotypes by mutant mtDNA. Nat Med 7:934-940

30. Hoppins S, Lackner L, Nunnari J (2007) The machines that divide and fuse mitochondria. Annu Rev Biochem 76:751-780

31. Rube DA, van der Bliek AM (2004) Mitochondrial morphology is dynamic and varied. Mol Cell Biochem 256-257:331-339

32. Chen H, Chan DC (2005) Emerging functions of mammalian mitochondrial fusion and fission. Hum Mol Genet 14 Spec No. 2:R283-R289

33. Praefcke GJ, McMahon HT (2004) The dynamin superfamily: universal membrane tubulation and fission molecules? Nat Rev Mol Cell Biol 5:133-147

34. Klockow B, Tichelaar W, Madden DR, Niemann HH, Akiba T, Hirose K, Manstein DJ (2002) The dynamin A ring complex: molecular organization and nucleotide-dependent conformational changes. EMBO J 21:240-250

35. Hinshaw JE (2000) Dynamin and its role in membrane fission. Annu Rev Cell Dev Biol 16:483-519

36. Muhlberg AB, Warnock DE, Schmid SL (1997) Domain structure and intramolecular regulation of dynamin GTPase. EMBO J 16:6676-6683

37. Smirnova E, Shurland DL, Ryazantsev SN, van der Bliek AM (1998) A human dynamin-related protein controls the distribution of mitochondria. J Cell Biol 143:351-358

38. Smirnova E, Griparic L, Shurland DL, van der Bliek AM (2001) Dynamin-related protein Drp1 is required for mitochondrial division in mammalian cells. Mol Biol Cell 12:2245-2256

39. Yoon Y, Pitts KR, McNiven MA (2001) Mammalian dynamin-like protein DLP1 tubulates membranes. Mol Biol Cell 12:2894-2905

40. Fukushima NH, Brisch E, Keegan BR, Bleazard W, Shaw JM (2001) The GTPase effector domain sequence of the Dnm1p GTPase regulates self-assembly and controls a rate-limiting step in mitochondrial fission. Mol Biol Cell 12:2756-2766

41. Jahani-Asl A, Slack RS (2007) The phosphorylation state of Drp1 determines cell fate. EMBO Rep 8:912-913

42. Ingerman E, Perkins EM, Marino M, Mears JA, McCaffery JM, Hinshaw JE, Nunnari J (2005) Dnm1 forms spirals that are structurally tailored to fit

mitochondria. J Cell Biol 170:1021-1027

43. Cerveny KL, Tamura Y, Zhang Z, Jensen RE, Sesaki H (2007) Regulation of mitochondrial fusion and division. Trends Cell Biol 17:563-569

44. Chang CR, Blackstone C (2007) Cyclic AMP-dependent protein kinase phosphorylation of Drp1 regulates its GTPase activity and mitochondrial morphology. J Biol Chem 282:21583-21587

45. Karbowski M, Neutzner A, Youle RJ (2007) The mitochondrial E3 ubiquitin ligase MARCH5 is required for Drp1 dependent mitochondrial division. J Cell Biol 178:71-84

46. Harder Z, Zunino R, McBride H (2004) Sumo1 conjugates mitochondrial substrates and participates in mitochondrial fission. Curr Biol 14:340-345

47. Di BA, Ouyang J, Lee HY, Catic A, Ploegh H, Gill G (2006) The SUMO-specific protease SENP5 is required for cell division. Mol Cell Biol 26:4489-4498

48. Wasiak S, Zunino R, McBride HM (2007) Bax/Bak promote sumoylation of DRP1 and its stable association with mitochondria during apoptotic cell death. J Cell Biol 177:439-450

49. Arnoult D, Rismanchi N, Grodet A, Roberts RG, Seeburg DP, Estaquier J, Sheng M, Blackstone C (2005) Bax/Bak-dependent release of DDP/TIMM8a promotes Drp1-mediated mitochondrial fission and mitoptosis during programmed cell death. Curr Biol 15:2112-2118

50. Yoon Y, Krueger EW, Oswald BJ, McNiven MA (2003) The mitochondrial protein hFis1 regulates mitochondrial fission in mammalian cells through an interaction with the dynamin-like protein DLP1. Mol Cell Biol 23:5409-5420

51. Mozdy AD, McCaffery JM, Shaw JM (2000) Dnm1p GTPase-mediated mitochondrial fission is a multi-step process requiring the novel integral membrane component Fis1p. J Cell Biol 151:367-380

52. James DI, Parone PA, Mattenberger Y, Martinou JC (2003) hFis1, a novel component of the mammalian mitochondrial fission machinery. J Biol Chem 278:36373-36379

53. Suzuki M, Jeong SY, Karbowski M, Youle RJ, Tjandra N (2003) The solution structure of human mitochondria fission protein Fis1 reveals a novel TPR-like helix bundle. J Mol Biol 334:445-458

54. Suzuki M, Neutzner A, Tjandra N, Youle RJ (2005) Novel structure of the N terminus in yeast Fis1 correlates with a specialized function in mitochondrial fission. J Biol Chem 280:21444-21452

55. Karren MA, Coonrod EM, Anderson TK, Shaw JM (2005) The role of Fis1p-Mdv1p interactions in mitochondrial fission complex assembly. J Cell Biol 171:291-301

56. Yu T, Fox RJ, Burwell LS, Yoon Y (2005) Regulation of mitochondrial fission and apoptosis by the mitochondrial outer membrane protein hFis1. J Cell Sci 118:4141-4151

57. Tieu Q, Nunnari J (2000) Mdv1p is a WD repeat protein that interacts with the dynamin-related GTPase, Dnm1p, to trigger mitochondrial division. J Cell Biol 151:353-366

58. Cerveny KL, Jensen RE (2003) The WD-repeats of Net2p interact with Dnm1p and Fis1p to regulate division of mitochondria. Mol Biol Cell 14:4126-4139

59. Tieu Q, Okreglak V, Naylor K, Nunnari J (2002) The WD repeat protein, Mdv1p, functions as a molecular adaptor by interacting with Dnm1p and Fis1p during mitochondrial fission. J Cell Biol 158:445-452

60. Naylor K, Ingerman E, Okreglak V, Marino M, Hinshaw JE, Nunnari J (2006) Mdv1 interacts with assembled dnm1 to promote mitochondrial division. J Biol Chem 281:2177-2183

61. Griffin EE, Graumann J, Chan DC (2005) The WD40 protein Caf4p is a component of the mitochondrial fission machinery and recruits Dnm1p to mitochondria. J Cell Biol 170:237-248

62. Karbowski M, Jeong SY, Youle RJ (2004) Endophilin B1 is required for the maintenance of mitochondrial morphology. J Cell Biol 166:1027-1039

63. Niemann A, Ruegg M, La P, V, Schenone A, Suter U (2005) Ganglioside-induced differentiation associated protein 1 is a regulator of the mitochondrial network: new implications for Charcot-Marie-Tooth disease. J Cell Biol 170:1067-1078

64. Messerschmitt M, Jakobs S, Vogel F, Fritz S, Dimmer KS, Neupert W, Westermann B (2003) The inner membrane protein Mdm33 controls mitochondrial morphology in yeast. J Cell Biol 160:553-564

65. Tondera D, Czauderna F, Paulick K, Schwarzer R, Kaufmann J, Santel A (2005) The mitochondrial protein MTP18 contributes to mitochondrial fission in mammalian cells. J Cell Sci 118:3049-3059

66. Sesaki H, Southard SM, Yaffe MP, Jensen RE (2003) Mgm1p, a dynamin-related GTPase, is essential for fusion of the mitochondrial outer membrane. Mol Biol Cell 14:2342-2356

67. Santel A, Fuller MT (2001) Control of mitochondrial morphology by a human mitofusin. J Cell Sci 114:867-874

68. Chen H, Detmer SA, Ewald AJ, Griffin EE, Fraser SE, Chan DC (2003) Mitofusins Mfn1 and Mfn2 coordinately regulate mitochondrial fusion and are essential for embryonic development. J Cell Biol 160:189-200

69. Cipolat S, Martins de BO, Dal ZB, Scorrano L (2004) OPA1 requires mitofusin 1 to promote mitochondrial fusion. Proc Natl Acad Sci U S A 101:15927-15932

70. Kijima K, Numakura C, Izumino H, Umetsu K, Nezu A, Shiiki T, Ogawa M, Ishizaki Y, Kitamura T, Shozawa Y, Hayasaka K (2005) Mitochondrial GTPase mitofusin 2 mutation in Charcot-Marie-Tooth neuropathy type 2A. Hum Genet 116:23-27

71. Baloh RH, Schmidt RE, Pestronk A, Milbrandt J (2007) Altered axonal mitochondrial transport in the pathogenesis of Charcot-Marie-Tooth disease from mitofusin 2 mutations. J Neurosci 27:422-430

72. Detmer SA, Chan DC (2007) Complementation between mouse Mfn1 and Mfn2 protects mitochondrial fusion defects caused by CMT2A disease mutations. J Cell Biol 176:405-414

73. Cereghetti GM, Scorrano L (2006) The many shapes of mitochondrial death. Oncogene 25:4717-4724

74. Youle RJ, Karbowski M (2005) Mitochondrial fission in apoptosis. Nat Rev Mol Cell Biol 6:657-663

75. Karbowski M, Lee YJ, Gaume B, Jeong SY, Frank S, Nechushtan A, Santel A, Fuller M, Smith CL, Youle RJ (2002) Spatial and temporal association of Bax with mitochondrial fission sites, Drp1, and Mfn2 during apoptosis. J Cell Biol 159:931-938

76. Eura Y, Ishihara N, Oka T, Mihara K (2006) Identification of a novel protein that regulates mitochondrial fusion by modulating mitofusin (Mfn) protein function. J Cell Sci 119:4913-4925

77. Hajek P, Chomyn A, Attardi G (2007) Identification of a novel mitochondrial complex containing mitofusin 2 and stomatin-like protein 2. J Biol Chem 282:5670-5681

78. Griparic L, van der Wel NN, Orozco IJ, Peters PJ, van der Bliek AM (2004) Loss of the intermembrane space protein Mgm1/OPA1 induces swelling and localized constrictions along the lengths of mitochondria. J Biol Chem 279:18792-18798

79. Meeusen S, DeVay R, Block J, Cassidy-Stone A, Wayson S, McCaffery JM, Nunnari J (2006) Mitochondrial inner-membrane fusion and crista maintenance requires the dynamin-related GTPase Mgm1. Cell 127:383-395

80. McQuibban GA, Saurya S, Freeman M (2003) Mitochondrial membrane remodelling regulated by a conserved rhomboid protease. Nature 423:537-541

81. Herlan M, Vogel F, Bornhovd C, Neupert W, Reichert AS (2003) Processing of Mgm1 by the rhomboid-type protease Pcp1 is required for maintenance of mitochondrial morphology and of mitochondrial DNA. J Biol Chem 278:27781-27788

82. Sesaki H, Dunn CD, Iijima M, Shepard KA, Yaffe MP, Machamer CE, Jensen RE (2006) Ups1p, a conserved intermembrane space protein, regulates mitochondrial shape and alternative topogenesis of Mgm1p. J Cell Biol 173:651-658

83. Frezza C, Cipolat S, Martins de BO, Micaroni M, Beznoussenko GV, Rudka T, Bartoli D, Polishuck RS, Danial NN, De SB, Scorrano L (2006) OPA1 controls apoptotic cristae remodeling independently from mitochondrial fusion. Cell 126:177-189

84. Cipolat S, Rudka T, Hartmann D, Costa V, Serneels L, Craessaerts K, Metzger K, Frezza C, Annaert W, D'Adamio L, Derks C, Dejaegere T, Pellegrini L, D'Hooge R, Scorrano L, De SB (2006) Mitochondrial rhomboid PARL regulates cytochrome c release during apoptosis via OPA1-dependent cristae remodeling. Cell 126:163-175

85. Ishihara N, Fujita Y, Oka T, Mihara K (2006) Regulation of mitochondrial morphology through proteolytic cleavage of OPA1. EMBO J 25:2966-2977

86. Duvezin-Caubet S, Jagasia R, Wagener J, Hofmann S, Trifunovic A, Hansson A, Chomyn A, Bauer MF, Attardi G, Larsson NG, Neupert W, Reichert AS (2006) Proteolytic processing of OPA1 links mitochondrial dysfunction to alterations in mitochondrial morphology. J Biol Chem 281:37972-37979

87. Frey TG, Renken CW, Perkins GA (2002) Insight into mitochondrial structure and function from electron tomography. Biochim Biophys Acta 1555:196-203

88. Olichon A, Baricault L, Gas N, Guillou E, Valette A, Belenguer P, Lenaers G (2003) Loss of OPA1 perturbates the mitochondrial inner membrane structure and integrity, leading to cytochrome c release and apoptosis. J Biol Chem 278:7743-7746

89. Zeviani M, Carelli V (2007) Mitochondrial disorders. Curr Opin Neurol 20:564-571

90. Zeviani M, Spinazzola A, Carelli V (2003) Nuclear genes in mitochondrial disorders. Curr Opin Genet Dev 13:262-270

91. Zeviani M, Carelli V (2003) Mitochondrial disorders. Curr Opin Neurol 16:585-594

92. Mollers M, Maniura-Weber K, Kiseljakovic E, Bust M, Hayrapetyan A, Jaksch M, Helm M, Wiesner RJ, von Kleist-Retzow JC (2005) A new mechanism for mtDNA pathogenesis: impairment of post-transcriptional maturation leads to severe depletion of mitochondrial tRNASer(UCN) caused by T7512C and G7497A point mutations. Nucleic Acids Res 33:5647-5658

93. Mita S, Schmidt B, Schon EA, DiMauro S, Bonilla E (1989) Detection of "deleted" mitochondrial genomes in cytochrome-c oxidase-deficient muscle fibers of a patient with Kearns-Sayre syndrome. Proc Natl Acad Sci U S A 86:9509-9513

94. Barkovich AJ, Good WV, Koch TK, Berg BO (1993) Mitochondrial disorders: analysis of their clinical and imaging characteristics. AJNR Am J Neuroradiol 14:1119-1137

95. Shoffner JM, Lott MT, Voljavec AS, Soueidan SA, Costigan DA, Wallace DC (1989) Spontaneous Kearns-Sayre/chronic external ophthalmoplegia plus syndrome associated with a mitochondrial DNA deletion: a slip-replication model and metabolic therapy. Proc Natl Acad Sci U S A 86:7952-7956

96. Shanske S, Tang Y, Hirano M, Nishigaki Y, Tanji K, Bonilla E, Sue C, Krishna S, Carlo JR, Willner J, Schon EA, DiMauro S (2002) Identical mitochondrial DNA deletion in a woman with ocular myopathy and in her son with pearson syndrome. Am J Hum Genet 71:679-683

97. Chen X, Prosser R, Simonetti S, Sadlock J, Jagiello G, Schon EA (1995) Rearranged mitochondrial genomes are present in human oocytes. Am J Hum Genet 57:239-247

98. Finsterer J (2007) Genetic, pathogenetic, and phenotypic implications of the mitochondrial A3243G tRNALeu(UUR) mutation. Acta Neurol Scand 116:1-14

99. Hirano M, Ricci E, Koenigsberger MR, Defendini R, Pavlakis SG, DeVivo DC, DiMauro S, Rowland LP (1992) Melas: an original case and clinical criteria for diagnosis. Neuromuscul Disord 2:125-135

100. Dubeau F, De SN, Zifkin BG, Arnold DL, Shoubridge EA (2000) Oxidative phosphorylation defect in the brains of carriers of the tRNAleu(UUR) A3243G mutation in a MELAS pedigree. Ann Neurol 47:179-185

101. Chinnery PF, Howell N, Lightowlers RN, Turnbull DM (1997) Molecular pathology of MELAS and MERRF. The relationship between mutation load and clinical phenotypes. Brain 120 ( Pt 10):1713-1721

102. Goto Y, Nonaka I, Horai S (1990) A mutation in the tRNA(Leu)(UUR) gene associated with the MELAS subgroup of mitochondrial encephalomyopathies. Nature 348:651-653

103. DiMauro S (2004) Mitochondrial diseases. Biochim Biophys Acta 1658:80-88

104. Bentlage HA, Attardi G (1996) Relationship of genotype to phenotype in fibroblast-derived transmitochondrial cell lines carrying the 3243 mutation associated with the MELAS encephalomyopathy: shift towards mutant genotype and role of mtDNA copy number. Hum Mol Genet 5:197-205

105. Park H, Davidson E, King MP (2003) The pathogenic A3243G mutation in human mitochondrial tRNALeu(UUR) decreases the efficiency of aminoacylation. Biochemistry 42:958-964

106. Chomyn A, Enriquez JA, Micol V, Fernandez-Silva P, Attardi G (2000) The mitochondrial myopathy, encephalopathy, lactic acidosis, and stroke-like episode syndrome-associated human mitochondrial tRNALeu(UUR) mutation causes aminoacylation deficiency and concomitant reduced association of mRNA with ribosomes. J Biol Chem 275:19198-19209

107. Jacobs HT, Holt IJ (2000) The np 3243 MELAS mutation: damned if you aminoacylate, damned if you don't. Hum Mol Genet 9:463-465

108. Suzuki T, Suzuki T, Wada T, Saigo K, Watanabe K (2002) Taurine as a constituent of mitochondrial tRNAs: new insights into the functions of taurine and human mitochondrial diseases. EMBO J 21:6581-6589

109. Yasukawa T, Kirino Y, Ishii N, Holt IJ, Jacobs HT, Makifuchi T, Fukuhara N, Ohta S, Suzuki T, Watanabe K (2005) Wobble modification deficiency in mutant tRNAs in patients with mitochondrial diseases. FEBS Lett 579:2948-2952

110. Yasukawa T, Suzuki T, Ueda T, Ohta S, Watanabe K (2000) Modification defect at anticodon wobble nucleotide of mitochondrial tRNAs(Leu)(UUR) with pathogenic mutations of mitochondrial myopathy, encephalopathy, lactic acidosis, and stroke-like episodes. J Biol Chem 275:4251-4257

111. Yasukawa T, Suzuki T, Ishii N, Ohta S, Watanabe K (2001) Wobble modification defect in tRNA disturbs codon-anticodon interaction in a mitochondrial disease. EMBO J 20:4794-4802

112. Chomyn A, Martinuzzi A, Yoneda M, Daga A, Hurko O, Johns D, Lai ST, Nonaka I, Angelini C, Attardi G (1992) MELAS mutation in mtDNA binding site for transcription termination factor causes defects in protein synthesis and in respiration but no change in levels of upstream and downstream mature transcripts. Proc Natl Acad Sci U S A 89:4221-4225

113. Lehtinen SK, Hance N, El MA, Juhola MK, Juhola KM, Karhu R,

Spelbrink JN, Holt IJ, Jacobs HT (2000) Genotypic stability, segregation and selection in heteroplasmic human cell lines containing np 3243 mutant mtDNA. Genetics 154:363-380

114. Shoffner JM, Lott MT, Lezza AM, Seibel P, Ballinger SW, Wallace DC (1990) Myoclonic epilepsy and ragged-red fiber disease (MERRF) is associated with a mitochondrial DNA tRNA(Lys) mutation. Cell 61:931-937

115. Wallace DC, Zheng XX, Lott MT, Shoffner JM, Hodge JA, Kelley RI, Epstein CM, Hopkins LC (1988) Familial mitochondrial encephalomyopathy (MERRF): genetic, pathophysiological, and biochemical characterization of a mitochondrial DNA disease. Cell 55:601-610

116. Austin SA, Vriesendorp FJ, Thandroyen FT, Hecht JT, Jones OT, Johns DR (1998) Expanding the phenotype of the 8344 transfer RNAlysine mitochondrial DNA mutation. Neurology 51:1447-1450

117. Holt IJ, Harding AE, Petty RK, Morgan-Hughes JA (1990) A new mitochondrial disease associated with mitochondrial DNA heteroplasmy. Am J Hum Genet 46:428-433

118. onisi-Vici C, Seneca S, Zeviani M, Fariello G, Rimoldi M, Bertini E, De ML (1998) Fulminant Leigh syndrome and sudden unexpected death in a family with the T9176C mutation of the mitochondrial ATPase 6 gene. J Inherit Metab Dis 21:2-8

119. Carelli V, Baracca A, Barogi S, Pallotti F, Valentino ML, Montagna P, Zeviani M, Pini A, Lenaz G, Baruzzi A, Solaini G (2002) Biochemical-clinical correlation in patients with different loads of the mitochondrial DNA T8993G mutation. Arch Neurol 59:264-270

120. Tiranti V, Chariot P, Carella F, Toscano A, Soliveri P, Girlanda P, Carrara F, Fratta GM, Reid FM, Mariotti C, . (1995) Maternally inherited hearing loss, ataxia and myoclonus associated with a novel point mutation in mitochondrial tRNASer(UCN) gene. Hum Mol Genet 4:1421-1427

121. Hutchin TP, Cortopassi GA (2000) Mitochondrial defects and hearing loss. Cell Mol Life Sci 57:1927-1937

122. Howell N, Mackey DA (1998) Low-penetrance branches in matrilineal pedigrees with Leber hereditary optic neuropathy. Am J Hum Genet 63:1220-1224

123. Wallace DC, Singh G, Lott MT, Hodge JA, Schurr TG, Lezza AM, Elsas LJ, Nikoskelainen EK (1988) Mitochondrial DNA mutation associated with Leber's hereditary optic neuropathy. Science 242:1427-1430

124. Chinnery PF, Turnbull DM (2001) Epidemiology and treatment of

mitochondrial disorders. Am J Med Genet 106:94-101

125. Estivill X, Govea N, Barcelo E, Badenas C, Romero E, Moral L, Scozzri R, D'Urbano L, Zeviani M, Torroni A (1998) Familial progressive sensorineural deafness is mainly due to the mtDNA A1555G mutation and is enhanced by treatment of aminoglycosides. Am J Hum Genet 62:27-35

126. DiMauro S, Davidzon G (2005) Mitochondrial DNA and disease. Ann Med 37:222-232

127. King MP, Attardi G (1989) Human cells lacking mtDNA: repopulation with exogenous mitochondria by complementation. Science 246:500-503

128. King MP, Attardi G (1996) Isolation of human cell lines lacking mitochondrial DNA. Methods Enzymol 264:304-313

129. Chomyn A, Lai ST, Shakeley R, Bresolin N, Scarlato G, Attardi G (1994) Platelet-mediated transformation of mtDNA-less human cells: analysis of phenotypic variability among clones from normal individuals--and complementation behavior of the tRNALys mutation causing myoclonic epilepsy and ragged red fibers. Am J Hum Genet 54:966-974

130. Khan SM, Smigrodzki RM, Swerdlow RH (2007) Cell and animal models of mtDNA biology: progress and prospects. Am J Physiol Cell Physiol 292:C658-C669

131. Vergani L, Prescott AR, Holt IJ (2000) Rhabdomyosarcoma rho(0) cells: isolation and characterization of a mitochondrial DNA depleted cell line with 'muscle-like' properties. Neuromuscul Disord 10:454-459

132. D'Autreaux B, Toledano MB (2007) ROS as signalling molecules: mechanisms that generate specificity in ROS homeostasis. Nat Rev Mol Cell Biol 8:813-824

133. Bunik VI, Schloss JV, Pinto JT, Gibson GE, Cooper AJ (2007) Enzyme-catalyzed side reactions with molecular oxygen may contribute to cell signaling and neurodegenerative diseases. Neurochem Res 32:871-891

134. Hansford RG, Hogue BA, Mildaziene V (1997) Dependence of H2O2 formation by rat heart mitochondria on substrate availability and donor age. J Bioenerg Biomembr 29:89-95

135. Cross AR, Jones OT (1991) Enzymic mechanisms of superoxide production. Biochim Biophys Acta 1057:281-298

136. Berridge MV, Tan AS (2000) Cell-surface NAD(P)H-oxidase: relationship to trans-plasma membrane NADH-oxidoreductase and a potential source of circulating NADH-oxidase. Antioxid Redox Signal 2:277-288

137. Morel Y, Barouki R (1999) Repression of gene expression by oxidative

stress. Biochem J 342 Pt 3:481-496

138. Ischiropoulos H, Beckman JS (2003) Oxidative stress and nitration in neurodegeneration: cause, effect, or association? J Clin Invest 111:163-169

139. Mates JM, Sanchez-Jimenez F (1999) Antioxidant enzymes and their implications in pathophysiologic processes. Front Biosci 4:D339-D345

140. Fridovich I (1995) Superoxide radical and superoxide dismutases. Annu Rev Biochem 64:97-112

141. Balendiran GK, Dabur R, Fraser D (2004) The role of glutathione in cancer. Cell Biochem Funct 22:343-352

142. Rhee SG (2006) Cell signaling. H2O2, a necessary evil for cell signaling. Science 312:1882-1883

143. Pizzorno G, Cao D, Leffert JJ, Russell RL, Zhang D, Handschumacher RE (2002) Homeostatic control of uridine and the role of uridine phosphorylase: a biological and clinical update. Biochim Biophys Acta 1587:133-144

144. Connolly GP, Duley JA (1999) Uridine and its nucleotides: biological actions, therapeutic potentials. Trends Pharmacol Sci 20:218-225

145. Connolly GP, Simmonds HA, Duley JA (1996) Pyrimidines and CNS regulation. Trends Pharmacol Sci 17:106-107

146. Aussedat J (1983) Effect of uridine supply on glycogen resynthesis after ischaemia in the isolated perfused rat heart. Cardiovasc Res 17:145-151

147. Hultman E, Soderlund K, Timmons JA, Cederblad G, Greenhaff PL (1996) Muscle creatine loading in men. J Appl Physiol 81:232-237

148. Klivenyi P, Ferrante RJ, Matthews RT, Bogdanov MB, Klein AM, Andreassen OA, Mueller G, Wermer M, Kaddurah-Daouk R, Beal MF (1999) Neuroprotective effects of creatine in a transgenic animal model of amyotrophic lateral sclerosis. Nat Med 5:347-350

149. Vergani L, Malena A, Sabatelli P, Loro E, Cavallini L, Magalhaes P, Valente L, Bragantini F, Carrara F, Leger B, Poulton J, Russell AP, Holt IJ (2007) Cultured muscle cells display defects of mitochondrial myopathy ameliorated by anti-oxidants. Brain 130:2715-2724

150. Rychahou PG, Jackson LN, Farrow BJ, Evers BM (2006) RNA interference: mechanisms of action and therapeutic consideration. Surgery 140:719-725

151. Hannon GJ, Rossi JJ (2004) Unlocking the potential of the human genome

with RNA interference. Nature 431:371-378

152. Bartel DP (2004) MicroRNAs: genomics, biogenesis, mechanism, and function. Cell 116:281-297

153. Taylor RW, Chinnery PF, Turnbull DM, Lightowlers RN (1997) Selective inhibition of mutant human mitochondrial DNA replication in vitro by peptide nucleic acids. Nat Genet 15:212-215

154. Heddi A, Stepien G, Benke PJ, Wallace DC (1999) Coordinate induction of energy gene expression in tissues of mitochondrial disease patients. J Biol Chem 274:22968-22976

155. Patterson MK, Jr. (1979) Measurement of growth and viability of cells in culture. Methods Enzymol 58:141-152

156. King MP, Attadi G (1996) Mitochondria-mediated transformation of human rho(0) cells. Methods Enzymol 264:313-334

157. Ling KH, Lardy H (1959) p 306

158. Kornberg A (1955) Lactic dehydrogenase of muscle. pp 441-443

159. King TE, Howard RL (1967) pp 52-58

160. Angelini C, Bresolin N, Pegolo G, Bet L, Rinaldo P, Trevisan C, Vergani L (1986) Childhood encephalomyopathy with cytochrome c oxidase deficiency, ataxia, muscle wasting, and mental impairment. Neurology 36:1048-1052

161. Srere PA (1969) Citrate synthase. pp 3-5

162. Moraes CT, Ricci E, Bonilla E, DiMauro S, Schon EA (1992) The mitochondrial tRNA(Leu(UUR)) mutation in mitochondrial encephalomyopathy, lactic acidosis, and strokelike episodes (MELAS): genetic, biochemical, and morphological correlations in skeletal muscle. Am J Hum Genet 50:934-949

163. Laemmli UK (1970) Cleavage of structural proteins during the assembly of the head of bacteriophage T4. Nature 227:680-685

164. Lee S, Jeong SY, Lim WC, Kim S, Park YY, Sun X, Youle RJ, Cho H (2007) Mitochondrial fission and fusion mediators, hFis1 and OPA1, modulate cellular senescence. J Biol Chem 282:22977-22983

165. Benard G, Bellance N, James D, Parrone P, Fernandez H, Letellier T, Rossignol R (2007) Mitochondrial bioenergetics and structural network organization. J Cell Sci 120:838-848

166. WARBURG O (1956) On the origin of cancer cells. Science 123:309-314

167. Xu RH, Pelicano H, Zhou Y, Carew JS, Feng L, Bhalla KN, Keating MJ, Huang P (2005) Inhibition of glycolysis in cancer cells: a novel strategy to overcome drug resistance associated with mitochondrial respiratory defect and hypoxia. Cancer Res 65:613-621

168. Galluzzi L, Larochette N, Zamzami N, Kroemer G (2006) Mitochondria as therapeutic targets for cancer chemotherapy. Oncogene 25:4812-4830

169. Carew JS, Huang P (2002) Mitochondrial defects in cancer. Mol Cancer 1:9

170. Maiuri MC, Zalckvar E, Kimchi A, Kroemer G (2007) Self-eating and self-killing: crosstalk between autophagy and apoptosis. Nat Rev Mol Cell Biol 8:741-752